THE
PHYSICAL REVIEW
A Journal of Experimental and Theoretical Physics Established by E. L. Nichols in 1893
VOL. 52, No. 8 OCTOBER 15, 1937 SECOND SERIES

Radioactive Isotopes of Palladium and Silver from Palladium

J. D. KRAUS AND J. M. CORK
University of Michigan, Ann Arbor, Michigan
(Received August 23, 1937)

The bombardment of palladium with 6.3 Mev deuterons yields radioactive periods of 17 min. and 13 hr. (both negative) in palladium and periods of 26 min. (positive) and 180 hours (negative) in silver. The palladium activities are due to neutron capture and are probably attributable to Pd^{111} and Pd^{109}, respectively. Fast neutron bombardment of silver shows that there are undoubtedly two distinct long-period negative activities of about 180 hours half-life in the silver due to Ag^{106} and Ag^{111}. The positive 26 min. silver activity is also associated with Ag^{106}, being an example of the existence of isomeric isotopes. The active Ag^{111} can be formed from Pd^{110} directly by proton capture and indirectly by a chain reaction through Pd^{111}. The two 180-hour silver activities differ in that there is a strong gamma-radiation accompanying the beta-emission from Ag^{106} and little or no gamma-radiation from Ag^{111}. The upper limits of energy for the beta-spectra of the 26-min. (Ag^{106}), 13-hr. (Pd^{109}), and 180-hr. (Ag^{111}) activities are 2.24 Mev, 1.08 Mev, and 0.80 Mev, respectively. The excitation functions for the 13-hr. (Pd^{109}) and 180-hr. (Ag^{111}) activities are determined by bombarding a stack of 25 palladium foils. These results are compared, since the processes involved correspond to the escape of a neutron or a proton from similar excited nuclei.

INTRODUCTION

IN a preliminary report[1] it was noted that palladium bombarded by deuterons (6.3 Mev) yields radioactive isotopes of both palladium and silver. This study has been continued to determine which particular isotope is responsible for each radioactive period and to evaluate the upper limits of the beta-spectra. In addition, the excitation functions for certain of the processes are shown, indicating how certain of the activities vary with the energy of the bombarding deuterons.

The radioactive isotopes in palladium are produced with deuteron bombardment by the capture of a neutron and the ejection or rejection of the proton. The radioactive silver isotopes may be produced either by the capture of a proton with the ejection of a neutron or by a secondary process from a radioactive palladium isotope. There is evidence that both processes are present.

Fermi[2] and his collaborators have observed in palladium, as a result of slow neutron bombardment, radioactive periods whose half-lives are 15 min., 12 hr., and 50 hr. These same periods should be expected also with deuteron bombardment. Actually only the first two, slightly modified (17 min. and 13 hr.), are found in the palladium. The longer (50-hr.) period is due to a radioactive silver isotope built up from the palladium in a chain reaction. Although it was intended to study only the palladium in this work, it became necessary to include silver to understand the processes involved.

[1] J. D. Kraus and J. M. Cork, Phys. Rev. **51**, 383 (1937).

[2] E. Amaldi, D'Agostino, E. Fermi, B. Pontecorvo, F. Rassetti, and E. Segrè, Proc. Roy. Soc. **149**, 522 (1935).

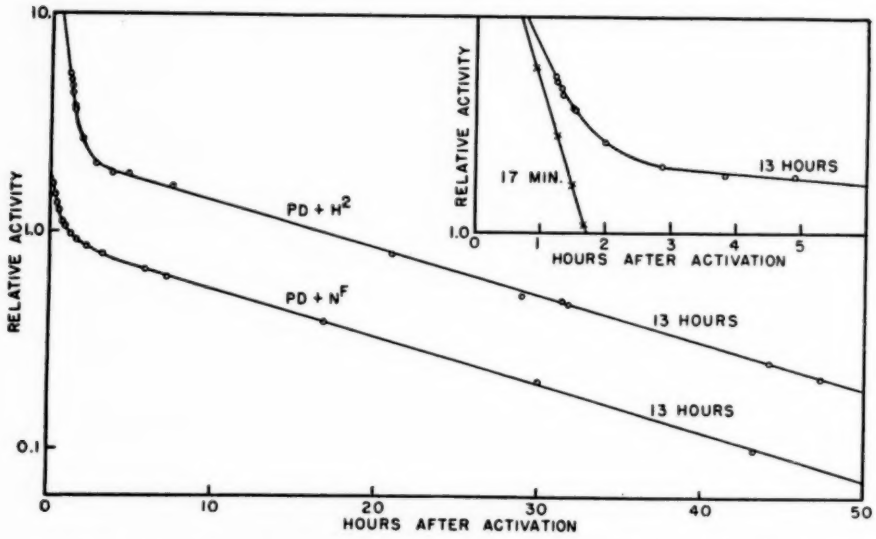

FIG. 1. Decay curves for palladium precipitate following deuteron bombardment (upper) and for palladium following fast neutron bombardment (lower). The inset shows the resolution of the decay curve into the 17-min. and 13-hr. half-life palladium periods.

APPARATUS

In this investigation targets of palladium and silver were bombarded in several ways. Deuterons of energy about 6.3 Mev were produced and allowed to fall directly on the targets in the cyclotron. For slow neutron exposures the palladium or silver specimen was imbedded in a mass of paraffin and placed close to a beryllium target, which in turn was bombarded by the deuteron beam. For fast neutron exposures, the 6.3 Mev deuterons were allowed to fall on a lithium target. The palladium specimen was wrapped so as to exclude any scattered deuterons and was placed close to the lithium.

The intensities of the radioactivities produced were measured with Lauritsen quartz fiber electroscopes and a Wulf string electrometer equipped with ionization chamber. A Wilson cloud chamber was used to determine the sign and energy of the beta-particles.

TABLE I. *Stable and radioactive isotopes of palladium and neighboring elements. Radioactive isotopes with their half-life periods are indicated by circles.*

AT. NO.	AT. WT.	102	103	104	105	106	107	108	109	110	111	112	113
45	RH		100%	4.2 MIN.									
46	PD	.8%		9.3%	22.6%	27.2%		26.8%	13 HR.	13.5%	17 MIN.		
47	AG					16 MIN. 180 45	52.2%	2.3 MIN.	47.5%	22 SEC.	180 HR.		
48	CD					1.5%		1.0%		15.2%	15.2%	21.8%	14.9%

PROCEDURE AND RESULTS

After bombardment, the palladium targets were dissolved and a small quantity of solutions of the neighboring elements, silver, rhodium, and ruthenium, were added. The precipitates were taken down separately and examined. Only the palladium and silver showed radioactivity.

The silver was precipitated from the nitric acid solution as the chloride and then redissolved in ammonium hydroxide and reprecipitated. The palladium was next precipitated by the addition of dimethylglyoxime to the slightly acid solution.

From Table I it appears that radioactive isotopes of palladium corresponding to the addition of a neutron might be expected for the masses 107, 109, and 111. These should be produced by bombardment with deuterons or slow neutrons and in part by very fast neutrons.

The decay curve for the palladium precipitate for deuteron bombardment is shown in Fig. 1 (upper curve and inset). Periods of 13 hr. and 17 min. half-life are apparent. Both are negative active. Similar curves are obtained for slow neutron bombardment. For fast neutron bombardment (lower curve of Fig. 1) the decay curve is similar except the ratio of the initial activities of the 17-min. to the 13-hr. periods is less than it is for slow neutron or deuteron bombardment. Although the fast neutron bom-

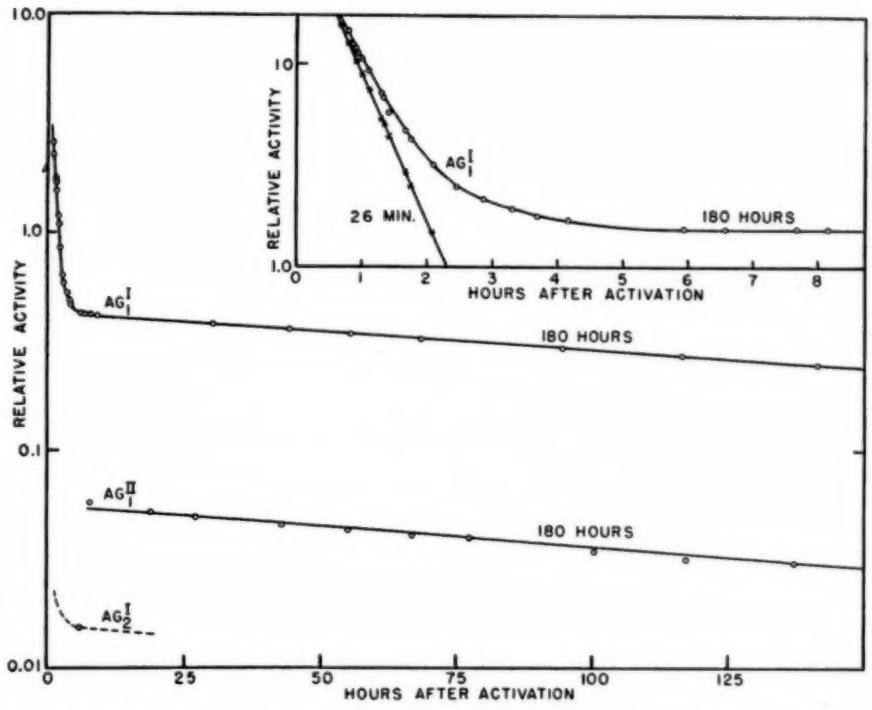

FIG. 2. Decay curves for successive silver precipitates from palladium bombarded by deuterons, showing the production of active silver (Ag^{111}) from active palladium (Pd^{111}). The inset shows the resolution of the silver activity into the 26-min. and 180-hr. half-life periods.

bardment giving the activity shown in Fig. 1 (lower curve) was about twice as long as that with deuterons, giving the activity of the upper curve, the ratio of the 17-min. to the 13-hr. activities is sufficiently smaller in the case of the fast neutron bombardment to indicate a difference in the reactions. The possibility of an additional shorter palladium period is not excluded as several minutes are required for making the chemical separation.

If one of the observed periods is due to the isotope of mass 111 then by beta-decay it should produce a radioactive silver since there is no stable silver of mass 111. Subsequent precipitation of silver from the palladium precipitates proved this to be the case. Moreover, by making these subsequent separations at different times after the original bombardment, it appears to be quite certain that this silver activity (180-hr. half-life) must be built up from the 17-min. palladium and not the 13-hr. palladium. If this assignment is correct, it may seem surprising that this 17-min. activity should appear as strongly as it does by fast neutron bombardment. In the fast neutron reaction a neutron should be ejected and the mass decreased by one, and no activity whatever should be associated with Pd^{111}. Actually the Pd^{111} activity is about half as strong when activated by fast neutrons as by slow neutrons. This may be due to a part of the fast neutron beam being slowed by elastic collisions or to energetic relations existing in the palladium nucleus such that the process of neutron ejection is relatively difficult.

The 13-hr. palladium activity could be due to either isotopes 107 or 109. The assignment to isotope 109 is preferred when one considers the ratio of activities for fast and slow neutrons and the relative abundance of the parent isotopes.

Figure 2 shows the activity of the silver precipitate from palladium bombarded by deuterons. There are two periods evident, one of 26-min. half-life and the other of about 180-hr. The 180-hr. silver activity has been followed for over 500 hours. The 26-min. silver emits positrons, while the 180-hr. silver is negative active. Radioactive silver isotopes of mass numbers 103, 105, 106, and 111 could be made from the stable

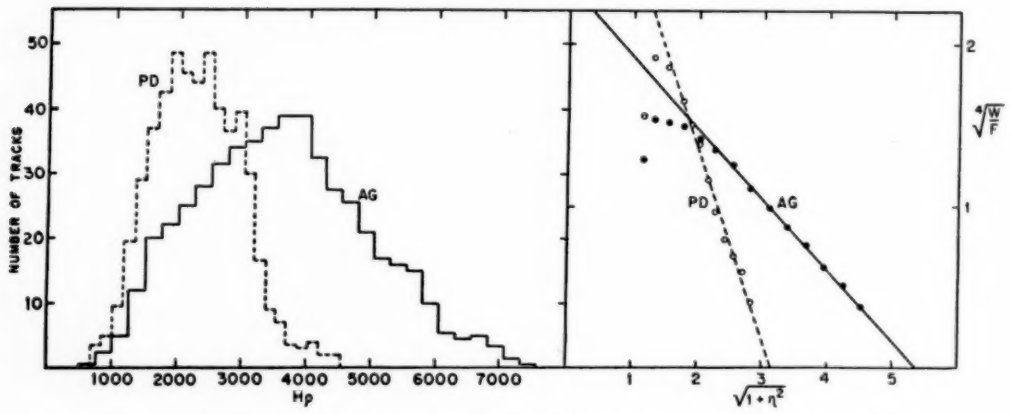

FIG. 3. Beta-ray histograms for the negative 13-hr. Pd^{109} and the positive 26-min. Ag^{106} deuteron induced activities. $H\rho$ in gauss-cm. At the right are the corresponding Kurie plots made according to the Konopinski-Uhlenbeck theory.

palladium isotopes by proton capture. Isotopes 103 and 105 should be radio-positive, 106 either positive or negative, and 111 should be radio-negative. To aid in the correct assignment of the observed activities, silver was bombarded with fast and slow neutrons. The slow neutron bombardment yields the well-known Fermi periods of 22 sec. and 2.3 min. The fast neutron[3] bombardment yields periods of 2.3 min., 26 min., and another period of approximately 180 hr. This fixes the 2.3-min. period as due to isotope 108 and the 26-min. positive activity with isotope 106.

The long negative activity in the silver of half-life 180 hours offers an interesting puzzle. Since it is made by fast neutrons it might be due to either isotopes 106 or 108. Slow neutron bombardment of silver has so far failed to produce this activity, hence it is ascribed to isotope 106. On the other hand, the subsequent separations of silver from the palladium precipitate makes it appear to be due to isotope 111, which could also be formed from palladium by direct proton capture. The activity of this later silver separation from the palladium precipitate is shown in Fig. 2 and is labeled Ag II/1. The first silver precipitate made immediately after bombardment, is called Ag I/1 and this is followed immediately by two additional separations called Ag I/2 and Ag I/3, to make sure that the active silver is completely removed. The separation Ag I/3 was too weak to be indicated in Fig. 2. The separation Ag II/1, made several hours after bombardment, shows many times the activity found in the earlier identical separation Ag I/3, and several times the activity of Ag I/2. A second precipitate, called Ag II/2, made immediately after Ag II/1, shows almost no activity. The half-life of the precipitate Ag II/1 is about 180 hours. It thus appears that there must be two radioactive silver isotopes of approximately the same half-life (180 hr.), both negative active, one being an isomer of mass 106 and the other an isotope of mass 111.

To establish this more definitely, a calculation was made of the ratio of initial activities (immediately after bombardment) for the 26-min. and the 180-hr. periods when fast neutron bombardment of the silver was used and when deuterons were used. For a two and one-half hour exposure, with fast neutrons, the ratio of the initial activities of the 26-min. to the 180-hr. was 990 to 1. When corrected for the periods and length of exposure, the value of the branching ratio for the 26-min. to 180-hr. activities in isotope 106 is about 10 to 1. For the case of proton capture (i.e., the silver precipitate from bombarded palladium), the ratio of the 26-min. to the 180-hr. initial activities for a corresponding exposure is only 60 to 1. It thus appears that the final activity in the silver precipitate from palladium is in large part due to isotope 111 and only slightly due to isotope 106.

That these two periods are quite distinct may

[3] Pool, Cork, and Thornton, Phys. Rev. **52**, 239 (1937).

be shown in still another manner. The activity due to the fast neutron bombardment of silver (isotope 106) is only slightly reduced by placing a one-eighth inch thick aluminum plate between the specimen and the ionization chamber, indicating a very strong gamma-radiation. The activity of the silver precipitate (isotope 111) from palladium bombarded by deuterons was reduced almost to zero when the same aluminum plate was interposed, indicating little or no accompanying gamma-radiation.

The probable reactions are as follows:

$$_{46}Pd^{N}+{}_{1}H^{2}\rightarrow{}_{46}Pd^{N+1}+{}_{1}H^{1}$$

$$_{46}Pd^{N+1}\rightarrow{}_{47}Ag^{N+1}+{}_{-1}e \quad \text{(17 min., 13 hr.)}$$

$$_{46}Pd^{N}+{}_{1}H^{2}\rightarrow{}_{47}Ag^{N+1}+{}_{0}n^{1}$$

$$_{47}Ag^{N+1}\rightarrow{}_{48}Cd^{N+1}+{}_{-1}e \quad \text{(180 hr.)}$$

$$_{47}Ag^{106}\rightarrow{}_{46}Pd^{106}+{}_{+1}e. \quad \text{(26 min.)}$$

Beta-Radiations

Since it was readily possible to isolate certain of the activities, an attempt was made to determine the form and the upper limits of energy for the beta-spectra. For this work tracks were photographed in a hydrogen-filled Wilson cloud chamber using a deflecting magnetic field of about 400 gauss. Only those tracks satisfying arbitrary criteria as to length of visible path and freedom from collisions were measured. The results of these measurements for the positive active 26 min. silver period and for the negative active 13-hr. palladium period are shown in Fig. 3. Over 500 tracks were measured in each case. These data are shown both as histograms, on the left, and as Kurie[4] plots based on the Konopinski-Uhlenbeck[5] theory, on the right. For the higher energies the Kurie plot is linear but for the lower energies the number of tracks is evidently deficient, due probably to the selection criteria. The Kurie plot intercepts indicate an upper energy of 2.24 Mev for the 26-min. Ag^{106} and 1.08 Mev for the 13-hr. Pd^{109}. The upper limits actually observed for the two cases were 1.90 and 1.03 Mev, respectively. Only about 125 tracks were measured for the 180-hr. Ag^{111} activity. The maximum observed energy for this radiation was 0.80 Mev.

[4] F. N. D. Kurie, J. R. Richardson, and H. C. Paxton, Phys. Rev. **49**, 368 (1936).

[5] E. Konopinski and G. Uhlenbeck, Phys. Rev. **48**, 7 (1935).

Excitation Function

In the bombardment of palladium with deuterons two different processes are involved, namely, proton capture and neutron capture, and it is of interest to compare the activation in each case as a function of the bombarding energy. The energy of the deuteron beam in the cyclotron is not perfectly homogeneous, but in this case it seems that any lack of homogeneity would be relatively unimportant since both activities are observed in the same specimens. Accordingly, a stack of 25 foils, each 0.00127 mm thick was exposed to the deuteron beam for 5 hours.

Corrections for the absorption in the platinum foil of the window of the cyclotron and a cover foil over the stack bring the average energy for the top foil to 5.8 Mev. The average energy at the center of each succeeding foil was determined by using a modified value of the stopping power as calculated by Mano.[6] After the bombardment

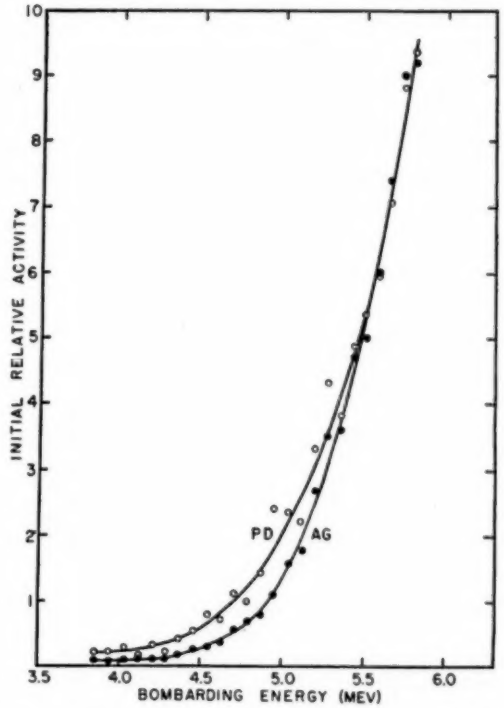

Fig. 4. Excitation curves for the 13-hr. Pd^{109} and the 180-hr. Ag^{111} activities.

[6] J. Mano, J. de phys. et rad. **5**, 628 (1934).

the activity of each foil was followed for over a week and a decay curve plotted for each foil. As explained earlier, the end activity in each foil was quite probably due mainly to the 180-hr. Ag^{111} isotope. The initial activity of the 180-hr. period in each foil was plotted as a function of the bombarding energy. These data for the 180-hr. silver activity are shown by the solid circles in Fig. 4. The curve through these points corresponds to a reaction involving proton capture (i.e., deuteron in, neutron ejected).

By subtracting the 180-hr. activity from the decay curve for each foil, a new family of curves is obtained, each ending in a straight line corresponding to the 13-hr. palladium activity. By extending these curves back to the time at which the bombardment was ended, the relative values of the initial 13-hr. Pd^{109} activities for each foil are obtained. These are shown as open circles in Fig. 4 and the curve through them corresponds to a reaction involving neutron capture (i.e., deuteron in, proton ejected).

While following the activity of the foils, the electrometer was continually calibrated in terms of a known uranium standard. The initial activity of the top foil for the 13-hr. palladium was about 1.70 microcuries and for the 180-hr. silver about 0.092 microcuries.

To facilitate comparison of the two excitation curves, they are arbitrarily adjusted to the same value at an energy of 5.8 Mev. Although too much significance should not be attached to these curves, it seems reasonably certain that as the energy of the incident particle decreases, the activity in the silver falls off somewhat more rapidly than in the palladium. This is contrary to what might be expected from the Bohr model of the nucleus, since it indicates less probability for neutron ejection from the excited nucleus than for proton ejection. It would, however, be more in accord with the Oppenheimer-Phillips[7] consideration, which is concerned with the probabilities of the particles entering the nuclei.

We are greatly indebted to B. R. Curtis for work with the cloud chamber and to D. W. Stewart and E. Rosenbaum for making the many chemical separations.

This investigation was made possible by a grant from the Horace H. Rackham memorial fund.

[7] Oppenheimer and Phillips, Phys. Rev. **48**, 500 (1935).

OCTOBER 15, 1937 PHYSICAL REVIEW VOLUME 52

Neutron-Induced Radioactivity of Long Life in Cobalt

J. R. Risser
*Palmer Physical Laboratory, Princeton University, Princeton, N. J.**
(Received August 28, 1937)

When cobalt is bombarded by neutrons, an activity of long half-life is obtained. The radioactive element has been shown by a chemical analysis to be an isotope of cobalt. The radiations emitted in the disintegration of this element have been investigated, principally by the absorption method. A gamma-ray is observed with a mass absorption coefficient in Pb of about 0.047 cm^2/g, and a spectrum of soft beta-rays with an estimated limiting range of 30 mg/cm^2 of aluminum, representing an energy of 160 kv. A group of more penetrating particles completely absorbed only by about 0.65 g/cm^2 of aluminum is also indicated. This group may represent a relatively infrequent disintegration process, in which the total energy is carried off by the beta-particle and no gamma-ray is emitted. Results of a measurement on the half-life indicate that it is 2.0 ± 0.5 years.

AN activity of half-life over a year was discovered in cobalt bombarded with neutrons by Sampson, Ridenour and Bleakney.[1] Results of activation of only a few weeks with the neutrons of 55 mC of Ra+Be slowed down by water indicated that a very strong activity would be obtained if bombardment were continued for a time comparable to the half-life.

* Now at Purdue University, Lafayette, Indiana.

[1] Sampson, Ridenour and Bleakney, Phys. Rev. **50**, 382 (1936).

The large capture cross section (35×10^{-24} cm^2) found by Dunning and co-workers[2] leads one to expect a strong activity in cobalt bombarded by slow neutrons. The other known activity due to slow neutrons is a weak short-lived one found by Rotblat,[3] the period of which has been given as 11 minutes by Heyn[4] and others.[5, 6] It is probable therefore that the capture process leading to the production of the long-lived radioelement is responsible for the large slow neutron cross section.

Since almost nothing is known about this radioelement, it seemed desirable to measure the period and determine the nature of the radiations emitted by it, as well as to ascertain by chemical test whether it is an isotope of cobalt. Bombardment of about ten weeks with neutrons from the 55 mC source, slowed down by water, produced an activity in a sheet of very pure cobalt metal (about 50 cm^2 in area and 0.4 g/cm^2 thick) great enough to obtain a fairly accurate estimate of the energy of the beta-ray spectrum from its absorption in aluminum as well as to detect the presence of accompanying gamma-radiation and measure the absorption coefficient of the latter in Pb. The activity was not sufficient to use methods of greater precision. To obtain great activity in an element of this half-life, a very large source of neutrons is required unless the bombarding time is made very long.

1. Identity of the Radioelement

For the chemical analysis a solution of cobalt nitrate in water which had been exposed to the neutrons of the 55 mC source for several months, and which showed the long period activity, was used. After adding small quantities of soluble manganese and iron salts, these elements were successively separated by the usual procedures of qualitative analysis.[7] The cobalt itself was then precipitated. The iron and manganese precipitates showed no activity but the cobalt precipitate carried the activity with it. It is therefore concluded that the radioactive element is an isotope of cobalt.

The abundant stable isotope of cobalt is Co^{59}. Co^{57} is also believed to exist, the ratio Co^{57}/Co^{59} being about 1/600.[8] Neutron capture by both Co^{57} and Co^{59} to form radioactive isotopes, Co^{58} and Co^{60}, could be expected. It would seem reasonable to attribute the stronger long period activity to Co^{60}, formed from the more abundant isotope Co^{59}, and the 11-minute activity to Co^{58}. This avoids the necessity of assigning to Co^{57} a cross section about 600 times 35×10^{-24} cm^2. This contingency however is not ruled out because cross sections larger than 21×10^{-21} have been observed.[2] A long period activity due to a cobalt isotope has been observed by Livingood, Fairbrother and Seaborg[6] in Fe bombarded by deuterons, as well as in cobalt bombarded by neutrons. The only way that Co^{60} could be formed by deuteron bombardment of iron is by capture of the whole deuteron by Fe^{58}, the highest mass found in iron, present to less than a percent. The process is regarded as very unlikely, so that this evidence favors the assignment of the 11-minute activity to Co^{60} and the long period to Co^{58}, which could be formed from iron with deuterons by the reaction $Fe^{57}(d, n)Co^{58}$. Evidence favoring this assignment is the failure so far to report the 11-minute period from cobalt bombarded by fast neutrons[4, 9] and by gamma-rays.[10] Both reactions should yield Co^{58}. Less convincing evidence is the failure to find any activity of short half-life in manganese bombarded by 7 Mev alpha-particles in this laboratory.[11] The formation of Co^{58} by the reaction $Mn^{55}(\alpha, n)Co^{58}$ would be expected. A check by the fast neutron reaction $Cu^{63}(n, \alpha)Co^{60}$ [1] is impossible because the 10-minute activity of Cu^{62} from the reaction $Cu^{63}(n, 2n)Cu^{62}$ would obscure the 11-minute period of Co^{60} if it were present. The reaction $Ni(n, p)Co$, which yields the 11-minute period,[3, 4] cannot be used as evidence, because both Co^{58} and Co^{60} can be formed in this way.

[2] Dunning, Pegram, Fink and Mitchell, Phys. Rev. **48**, 265 (1935).
[3] Rotblat, Nature **136**, 515 (1935).
[4] Heyn, Physica **4**, 160 (1937).
[5] Kikuchi, Takeda and Ito, Proc. Phys.-Math. Soc. Japan **19**, 43 (1937).
[6] Livingood, Fairbrother and Seaborg, Phys. Rev. **52**, 135 (1937).
[7] A. A. Noyes, *Qualitative Chemical Analysis.*
[8] Sampson and Bleakney, Phys. Rev. **50**, 732 (1936).
[9] Pool, Cork and Thornton, Phys. Rev. **52**, 239 (1937).
[10] Bothe and Gentner, Zeits. f. Physik **106**, 236 (1937).
[11] Ridenour and Henderson, paper in publication.

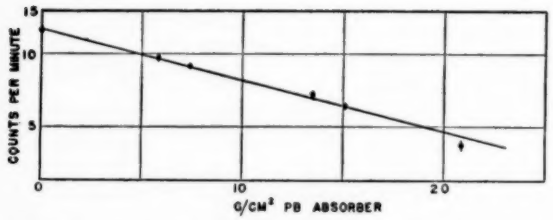

FIG. 1. Absorption in Pb of the gamma-radiation from cobalt. Ordinates represent response of gamma-ray counter in counts per minute above background.

2. GAMMA-RADIATION

For the remaining experiments the activated sheet of cobalt metal was used. When this was placed closely around a gamma-ray tube counter having a wall thickness of about 0.9 g/cm², there was an increase in the counting rate of three times the background. The radiation producing this effect showed an absorption in Pb of exponential character with a mass absorption coefficient of about 0.047 cm²/g. The curve obtained is shown in Fig. 1. A radiation of this penetrating character is doubtless gamma-radiation.

For obtaining the absorption curve of Fig. 1, the cobalt sheet was placed around the counter in the form of a coaxial cylinder, and cylindrical absorbers were inserted between. A large enough number of counts were taken that the estimated statistical errors in the points are as shown by the small vertical lines on the figure. From the value of the absorption coefficient one would attribute to the gamma-ray an energy of 1.5 to 2.0 Mev.[12] A determination of the absorption in copper indicated the correctness of assigning the lower of the two possible energy values associated with this one value of the absorption coefficient. This energy value is not to be taken too seriously, however, because the accurate determination of an absorption coefficient demands a geometry for eliminating scattered radiation from the direct beam which cannot be attained with a low intensity source. For this reason the value 0.047 is probably too low and the estimated energy too high. Nevertheless, the absorption coefficient is given here because a knowledge of the gamma-ray energy would be desirable in connection with an interpretation of the beta-ray spectrum and because it indicates at least that the gamma-ray is fairly hard.

[12] Gentner, J. de phys. et rad. **6**, 274 (1935).

3. THE BETA-RAY SPECTRUM

The principal constituent of the beta-ray spectrum is a group of low energy beta-particles which is completely absorbed by about 30 mg/cm² of aluminum. The wall of the ordinary beta-ray tube counter is of about this thickness, so that for dealing with this group a special experimental arrangement had to be devised to avoid the use of a window that would itself absorb an appreciable fraction of the incident particles. This consisted of a wire screen tube counter mounted axially on the inside and at one end of a glass containing tube, which could be evacuated and filled with dry air at a suitable pressure (8 cm). The cobalt sheet was mounted with a bit of wax to the inside wall of the glass tube so that it completely surrounded the wire screen counter. Cylindrical absorbing foils of aluminum could be inserted between the cobalt and the wire screen, but in the absence of a foil there was no absorber between the cobalt and the sensitive volume of the counter except air of stopping power equivalent to about 1 mm at NTP.

The counter and its containing tube were mounted vertically. By moving iron counterweights in side tubes with a small magnet absorbing foils of three different thicknesses could be lowered into place between cobalt and counter, and removed again, without changing the pressure in the counter. Hence three points on the absorption curve beside that for zero absorber could be taken. The counter then had

TABLE I. *Results of measurements on the absorption of the soft component of the beta-ray spectrum, showing average counting rate of wire screen counter for each absorber thickness and total number of counts taken in determining this average.*

THICKNESS OF Al IN MG/CM²	TOTAL NUMBER OF COUNTS TAKEN	AVERAGE COUNTING RATE IN MIN.⁻¹
No Absorber	53,548	213
2.4	35,096	176
4.6	33,800	155
6.5	30,520	141
10.6	63,188	134
14.7	44,064	129
19.3	35,536	124
29.4	34,484	118
44.1	30,012	112
58.8	22,292	109
221.	10,964	83

to be opened to the air to replace the foils. Once the counter had been opened and refilled with air at its working pressure, its sensitivity at a given working voltage was slightly different. Hence, each time a new set of foils was put in, one of the old set was retained and its absorption was used to fit the new series of readings to the preceding ones.

The results of the absorption measurements taken under these conditions are shown in Table I and Fig. 2. The curve shows a rapid drop for thicknesses up to about 10 mg/cm² after which there is a transition to a portion of more gradual slope. This last gradually sloping portion also has the characteristics of an absorption curve for beta-particles but it does not flatten out until absorber thicknesses of about 0.65 g/cm² of aluminum (Fig. 4) are reached. Absorption curves of beta-ray spectra known to consist of only one component, like that of RaE, do not exhibit the spread out character relative to the half-value thickness of this complete absorption curve. It therefore seems reasonable to attribute the gradually sloping portion of the curve of Fig. 2 to a distinct group of particles of higher energy and to take as the upper limit of the low energy spectrum the point where the first rapid drop merges into it. This point is estimated to be at 30 mg/cm² corresponding to an energy of approximately 160 kv.[13]

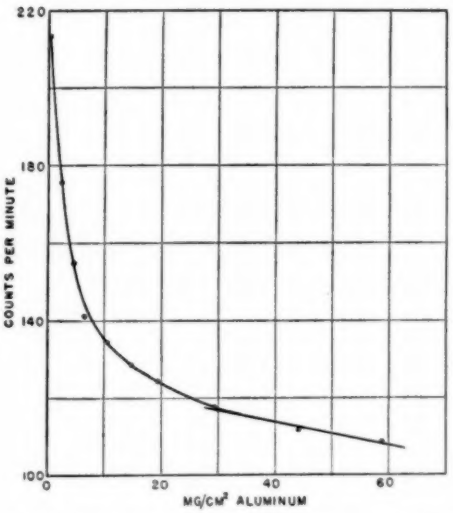

FIG. 2. Absorption in aluminum of the soft component of the beta-ray spectrum. Wire screen counter used as detector.

[13] Results of Madgwick; see Rutherford, Chadwick and Ellis, p. 422.

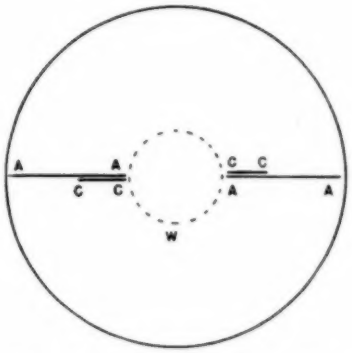

FIG. 3. Schematic diagram of cross section of the magnetic deflection apparatus used in determining the sign of the soft beta-rays. *W*, wire screen tube counter; *CC*, cobalt strips; *AA*, thick Cu supports. Field perpendicular to plane of paper.

It was shown that these low energy particles are negative electrons by a magnetic deflection method. The activity of the source was not great enough to obtain reliable information from a cloud chamber. A modified wire screen counter arrangement which could be placed in the field of a large water-cooled solenoid was used. A cross section of the apparatus perpendicular to the field and to the axis of the wire screen counter is shown in Fig. 3. *W* is the counter; *CC* are strips of cobalt parallel lengthwise to the axis of the counter; *AA* are supporting strips of copper through which the beta-particles could not pass. It can be seen that some particles from the cobalt could enter the counter in the absence of a field but that the number entering could be increased by applying a field of suitable magnitude and sense. The nature of the charge on the particles was then known from the sense of the field causing the increase. For a source of low intensity this simple arrangement was found preferable to ones in which the beam of particles entering the counter was more narrowly defined.

The results showed that the particles were negatively charged. With a counting rate for zero field of about 45 per minute, fields of 800 to 1000 gauss out of the paper on Fig. 3 increased it by 15 to 18 percent, while there was a slight decrease for fields in the opposite direction. Although it is difficult to take into account the disturbing action on the field of the magnetic cobalt strips, the geometry indicates that the radius of curvature for particles leaving the surface of the cobalt normally and entering the

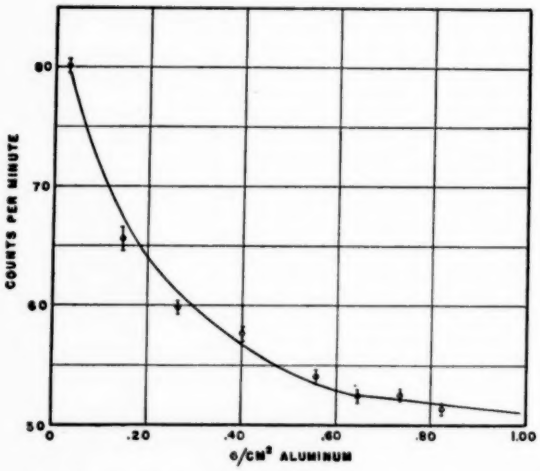

FIG. 4. Absorption in aluminum of the more penetrating beta-rays. Thin-walled counter used as detector.

counter was of the order of a centimeter, giving $H\rho$ values of the order of 1000, corresponding to electron energies in the neighborhood of 100 kv.

The curve of Fig. 4 is a plot of the results obtained by continuing the absorption measurements to greater thicknesses of aluminum, using a beta-ray counter with a thin cylinder of Dow metal. For the first point the wall of the counter acted as absorber. This curve can scarcely represent a tailing-off portion of the curve of Fig. 2, as mentioned before. If, as supposed, it is due to a distinct group of particles, this group is less numerous than that of the soft beta-particles, the ratio being less than 1/30 when the relative absorption of the two groups in the material of the source is considered. (To allow a comparison of Figs. 2 and 4 it should be mentioned that the wire screen counter was somewhat larger than the Dow metal counter, and the natural backgrounds, which were not subtracted here, were about 30 and 25, respectively.) From the curve the upper limit of this higher-energy spectrum is estimated to be 0.65 ± 0.05 g/cm² corresponding to an energy of 1.45 ± 0.10 Mev.[14]

It is difficult to account for the presence of two groups of particles without a more exact knowledge of the gamma-ray energy. Intensity considerations make it seem unlikely that it is a line spectrum due to internal conversion of the gamma-ray. It is suggested that it probably represents a rarer mode of disintegration in which the beta-transition leaves the product nucleus in the ground state and no gamma-radiation is emitted.

[14] Feather, Phys. Rev. **35**, 1559 (1930).

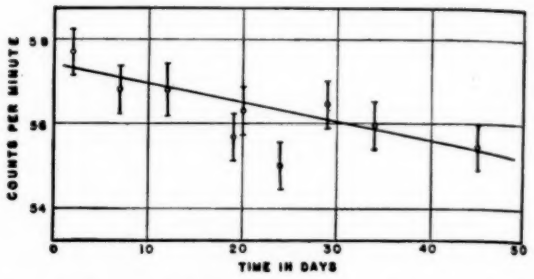

FIG. 5. Decay of the activity of the cobalt sample with time. Ordinates represent response of gamma-ray counter in counts per minute above background.

4. THE HALF-LIFE

Counter measurements of the gamma-ray activity of the cobalt sheet were made over a period of six weeks in an attempt to determine the half-life. A plot of the results is shown in Fig. 5, where the ordinates represent the average counting rate of the counter above background. The ordinate scale is logarithmic. Here, as in the previous cases, the estimated statistical errors, represented by vertical lines through the points, are obtained from the square root of the total number of counts taken in a reading divided by the time, and include the background error. Before each measurement the sensitivity of the counter was checked for constancy against a small source of Ra at a fixed distance. The slope of the decay curve, as drawn in the figure, corresponds to a half-life slightly more than 800 days. It is felt that a half-life value of 2.0 ± 0.5 years represents a conservative estimate consistent with the data.

The writer wishes to take this opportunity to express appreciation to the members of the Princeton faculty for many stimulating discussions during the progress of the investigation. Special acknowledgment is due Professor Walker Bleakney for the suggestion and general supervision of the problem and Professors L. A. Turner and R. Ladenburg, and Dr. L. N. Ridenour for helpful advice and criticism.

The Gamma-Ray Spectrum of B^{10}

P. GERALD KRUGER AND G. K. GREEN
Department of Physics, University of Illinois, Urbana, Illinois

(Received June 21, 1937)

The gamma-rays from B^{10}, produced by bombarding beryllium with 1 Mev deuterons, have been investigated by an examination of the momentum distribution of Compton electrons ejected from a thin mica foil in an expansion chamber. This spectrum consists of six gamma-rays of energies 0.51, 1.07, 1.44, 1.96, 2.81 and 3.21 Mev. These gamma-rays result from all possible transitions between three excited levels and the ground state of B^{10}. The energy levels determined are in agreement with those obtained from a study of the neutron spectrum emitted by the same reaction.

WHEN beryllium is bombarded with deuterons a multienergy spectrum of gamma-rays and neutrons is observed. Bonner and Brubaker[1] have examined the energies of the neutron groups and from them have determined a set of energy levels for the B^{10} nucleus. However, they could not correlate their energy levels and the energies of the gamma-rays reported by Crane, Delsasso, Fowler, and Lauritsen.[2] For this reason, the present investigation sought to determine the gamma-ray energies with sufficient accuracy to fix their origin and their relation to the neutron energies.

In this study the deuteron beam produced by a small cyclotron[3] bombarded a metallic beryllium target. The target was placed in a thin walled brass exposure chamber fixed to the end of the beam outlet tube. A bombarding current of 0.2 microampere of 1 Mev deuterons, which was used throughout the experiment, yielded as large a gamma-ray intensity as could be used in an expansion chamber.

To study the gamma-rays, an air-filled expansion chamber containing alcohol and water vapor was operated at about one atmosphere. The chamber is sylphon actuated and is 13 cm in diameter, with a usable depth of 2 cm. A 96 mg per cm^2 mica conversion foil was cemented to the glass lid of the chamber with water glass and the chamber positioned so that the foil was 40 cm from the target and perpendicular to the line from the foil center to the target.

A magnetic field of the order of 730 oersteds was maintained by a pair of Helmholtz coils whose constant is 18.8 oersteds per ampere. The field strength of these coils was determined with a flux coil and ballistic galvanometer calibrated against a standard solenoid, whose constants are known to 0.2 percent. The same standard ammeter was used to measure the current in the Helmholtz coil during calibration and also during the experiment. The field of the coils varies less than 1.5 percent over the volume in which tracks were measured, and its absolute value is known within 1 percent.

At a current of 40 amperes the Helmholtz coils ran hot even though the current was applied only at the moment of expansion. This required that the expansion chamber be protected from heating with a water-cooled copper shield which was placed between the chamber and Helmholtz coils. A slot in the shield admitted light from a carbon arc. Continuous illumination produced localized heating in the chamber, and consequently poor tracks, so a shutter was arranged to allow the arc to illuminate the chamber only during the time the film was exposed. The tracks were photographed on Super X panchromatic film by a Sept camera (non-stereoscopic) equipped with an f : 3.5 lens.

Gamma-rays from the target eject Compton electrons from the mica foil. Richardson and Kurie[4] have investigated the characteristics of the momentum distribution of such recoil electrons using the Klein-Nishina formula, and have demonstrated the use of this distribution in determining the energy of the gamma-rays pro-

[1] Bonner and Brubaker, Phys. Rev. **50**, 308 (1936).
[2] Crane, Delsasso, Fowler and Lauritsen, Phys. Rev. **47**, 782 (1935).
[3] P. G. Kruger and G. K. Green, Phys. Rev. **51**, 699 (1937).
[4] Richardson and Kurie, Phys. Rev. **50**, 999 (1936).

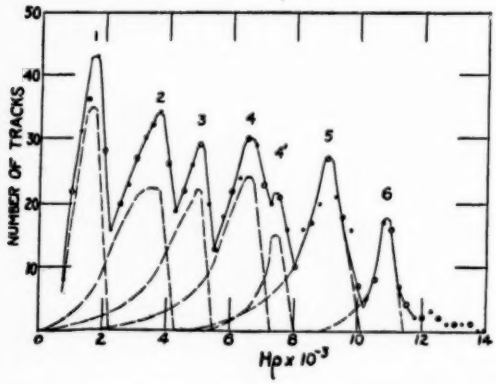

FIG. 1. Momentum distribution of Compton electrons projected by gamma-rays from B^{10}. Solid curve is distribution curve given by experimental data. Dotted curves represent corrected form of each peak.

ducing it. The tracks, reprojected through the same optical systems as was used in the photography, were viewed and measured on a translucent screen.

The tracks selected for measurement satisfied the following criteria. (1) The track must be plainly visible, of uniform curvature and free from any indication of scattering. (2) It must appear to originate in the mica and emerge at an angle of not more than 10° with the direction of the incident gamma-ray. (3) It must be long and of uniform focus so that it does not make an angle of more than 10° with the horizontal. (4) It must not be the negatron of a pair. The curvature of tracks satisfying these criteria was determined by superimposing finely ruled circles on the track image. These circles were ruled on thin celluloid in sets, with successive radii increasing by 2 mm. In practice it is possible to match the track and ruled circle to about ± 2 mm for $\rho < 6$ cm and about ± 4 mm for $\rho > 6$ cm.

Twelve hundred pictures yielded 480 acceptable tracks. During the experiment the magnetic field was not held constant, but varied from 711 to 797 oersteds and was recorded for every expansion. From the values of the magnetic field and ρ, a table of the $H\rho$ products was compiled so that the number of tracks in any $\Delta H\rho$ interval can be found readily. These data can be plotted as a histogram. However, it is preferable to plot the number of tracks occurring in each of a set of $\Delta H\rho$ intervals (i.e., $\Delta H\rho = 500$) as a point at its center and represent the data as a distribution curve drawn through these points. The statistical fluctuations can be smoothed somewhat, and the curve improved, by selecting a second set of $\Delta H\rho$ intervals overlapping the first set by half the interval and plotting the corresponding set of points, which will fall halfway between the first set of points. Distribution curves have been drawn for $\Delta H\rho = 300$, 400, 500, 600, and 700, of which the $\Delta H\rho = 500$ curve is the most satisfactory, since a smaller $\Delta H\rho$ gives rise to larger statistical fluctuations and a larger $\Delta H\rho$ rounds off the peaks too much. The $\Delta H\rho = 500$ curve is shown by the solid line in Fig. 1. The dots represent the number of tracks in one set of intervals, the circles the number of tracks in the overlapping set. The peaks are not completely resolved so that the points of the curve on the high energy sides of all but number 6 include a considerable number of tracks due to the straggling from the peaks of higher energy. For this reason a straight line extrapolated down the high energy side of each peak would give too high a value for the maximum energies of the electrons ejected by the various gamma-rays. In order to correct the curve, the shape of the straggling for peak number 6 was calculated from the data given by White and Millington,[5] and the "tail" of number 6 subtracted from peak 5. This process was continued until all the peaks were corrected. The final form of the peaks is shown by the dotted lines in Fig. 1. The intercepts of the high energy sides of these corrected peaks with the momentum axis are 2250, 4250, 5500, 7250, 8000, 10,100, 11,500 $H\rho$. It will be noted that these intercepts coincide with the abscissae of the points at which the "tail" of each peak cuts the high energy side of the preceding one. After adding the energy of the recoil photon to the electron energies calculated from the above values of $H\rho$, the gamma-ray energies are found to be 0.51, 1.07, 1.44, 1.96, 2.17, 2.81 and 3.21 Mev.

The reality of peak number 4′ might be questioned if the 500 $H\rho$ interval plot of Fig. 1 were considered alone. However, curves similar to those in Fig. 1 but having $\Delta H\rho = 300$, 400 and 600 show peak number 4′ equally prominent and give it the same energy of 2.17 Mev so that it is considered a real peak. Its presence can be

[5] White and Millington, Proc. Roy. Soc. **A120**, 701 (1928).

explained from the fact that the spectrum of gamma-rays from beryllium bombarded by protons has an intense line at 2.2 Mev, but no other strong lines in the region below 3.5 Mev.[2] A small molecular hydrogen contamination of the deuteron beam from the cyclotron will produce protons of 0.5 Mev energy, which is sufficient to excite this 2.2 Mev line. Thus the 2.17 Mev gamma-ray is probably due to proton bombardment of the beryllium target and will not fit in the energy level scheme discussed below. For these reasons it is not included in the data given in Table I, column *C*, which gives the observed gamma-ray energies.

Though it is not shown in Fig. 1, because it would unduly complicate the figure, the effects of probable statistical fluctuations have been studied graphically by replacing each point by a vertical line of length $2\sqrt{N}$, where N is the ordinate of the point. Lines drawn within the envelopes of these vertical lines intersect the momentum axis in a region, the size of which gives an estimate of the effect of statistical fluctuations. The different $\Delta H\rho$ groupings give a spread of intercepts of the same order of magnitude as that produced by the former process. These considerations indicate a probable error of about ± 0.1 Mev.

The conclusions drawn by Oliphant, Kempton and Rutherford[6] from their observation of the charged particles emitted when beryllium is bombarded with deuterons indicate that no gamma-radiation should accompany these particles. Therefore it is logical to associate the gamma-ray and neutron spectra.

In the investigation of the neutron energies

TABLE I. *Comparison of predicted and observed gamma-rays.*

A Line Number	*B* Gamma-Ray Energies Predicted from Neutron Data	*C* Observed Gamma-Ray Energies	*D* Relative Intensity of Gamma-Rays	*E* Observed Half-Width ($H\rho$)	*F* Theoretical Half-Width ($H\rho$)
1	0.55 Mev	0.51 Mev	10.0	1000	790
2	1.30	1.07	10.2	1900	700
3	1.60	1.44	5.8	1400	725
4	2.15	1.96	5.5	1400	800
5	2.90	2.81	5.4	1400	950
6	3.45	3.21	1.7	700	1075

[6] Oliphant, Compton and Rutherford, Proc. Roy. Soc. **A150**, 241 (1935).

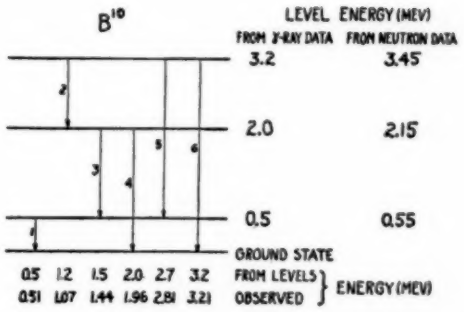

FIG. 2. Energy level diagram for B^{10}. Numbers on the transition arrows correspond to peak numbers in Fig. 1.

Bonner and Brubaker[1] found four groups from whose energies they deduced excited levels of 0.55, 2.15 and 3.45 Mev (± 0.2 Mev) for the B^{10} nucleus. If the gamma-rays originate from transitions between these levels their energies must be the level differences. Crane, Delsasso, Fowler and Lauritsen[2] found gamma-rays of energies 0.8, 1.3, 2.0, 2.5, 2.9, 3.3 and 4.0 Mev, of which the 4.0 Mev line is probably due to proton contamination of the bombarding beam. These energies were obtained by analyzing 206 tracks ejected from the glass wall of an expansion chamber. Inaccuracies introduced by the thick electron source, which flattens the distribution curve, and large relative statistical fluctuations due to the small number of tracks, make impossible a close correlation of these gamma-ray energies with the neutron energy levels.

The energies corresponding to transitions between the levels given by Bonner and Brubaker are entered in Table I, column *B*. Our observed gamma-ray energies (column *C*) agree with these transition energies within the probable errors assigned (± 0.1 and ± 0.2 Mev, respectively), but it will be noted that our values are all lower than those of Bonner and Brubaker, indicating a systematic error entering into one of the determinations.

A set of energy levels which best fits all six gamma-ray lines was determined by trial, and is shown in Fig. 2. The level energies are 0.5, 2.0 and 3.2 Mev and are somewhat lower than Bonner and Brubaker's values. At the bottom of Fig. 2 the observed energies are compared with the energies to be expected from transitions between levels of 0.5, 2.0 and 3.2 Mev and the ground state.

If we assume that the energy levels are associated with B^{10}, the reaction is

$$
\begin{array}{l}
{}_4Be^9 + {}_1H^2 \rightarrow {}_5B^{11} \rightarrow {}_5B^{10*} + {}_0n^1 \\
\qquad\qquad\qquad\qquad\qquad\quad \downarrow \\
\qquad\qquad\qquad\qquad\qquad\quad {}_5B^{10} + \gamma .
\end{array}
$$

The alternative assumption would require the energy levels to be inverted and associated with the composite nucleus, B^{11}. Under such an assumption the highest temporary semistable state would be at 15.6 Mev (as calculated from mass data) and the lowest at 12.3 Mev, since no gamma-rays of energy higher than 3.3 Mev have been detected. In addition all neutron transitions would have to end in the ground state of B^{10}. Moreover, in general, the probability of mechanical decay of the light elements is much greater than that of radiation. All of these considerations indicate that the energy levels are excited states of the B^{10} nucleus. It will be noted that all possible transitions between the four levels occur.

The relative intensities of the gamma-ray lines given in Table I were calculated from the area included under the distribution curve (corrected curves, Fig. 1) between the abscissa corresponding to the half-maximum values of the ordinate. These areas are proportional to the intensities of the gamma-rays but do not represent relative intensities on account of the dependence of electron ejection on the gamma-ray energy. To get relative intensities, the areas must be divided by the appropriate intensity correction factor as given by Richardson and Kurie.[4] It is difficult to estimate the accuracy of these intensities, but it is probably better than thirty percent.

A tentative classification of the energy levels of Fig. 2 can be obtained in the following way. By applying the relation $I \propto P_i(Sw)_f \nu^3$, where I is the intensity of the line, P_i the population of the initial state, $(Sw)_f$ the statistical weight of the final state, and ν the frequency of the line, to two lines originating on the same upper level, but ending on two different lower levels, one obtains $(Sw)_1 = (E_0^3/E_1^3)(I_1/I_0)(Sw)_0$, where E is the energy of the line and the subscripts 0, 1 refer to the ground state and first level, respectively. By using lines 5 and 6 of Table I and considering that the possible values of j for the ground state may be $j_0 = 1$; 3; 1, 2; 2, 3; or 1, 2, 3, and $(Sw)_0 = 3$, 7, 8, 12 and 15; one gets

$$(Sw)_1 = 14,\ 33,\ 38,\ 56,\ \text{and}\ 70. \qquad (1)$$

Repeating the process for lines 3 and 4 gives

$$(Sw)_1 = 8,\ 19,\ 21,\ 32,\ \text{and}\ 40. \qquad (2)$$

Of the values in (1) only

$$(Sw)_1 = 14 \qquad (1')$$

and in (2) $$(S_w)_1 = 8 \qquad (2')$$

are allowed. All others give statistical weights which are too large. Thus one must conclude that $j_0 = 1$ and $j_1 = 1$, 2 and 3. These j values agree with the results of the calculations of Feenberg and Wigner[7] which give the ground state as $^3S_1$ and the next higher level as $^3D_{1,2,3}$ (our 0.5 Mev level).

From the mass defect difference between B^{10} and Be^{10} it seems likely that the 2 Mev level is $^1D_2$. However it may also include $^1S_0$. On account of the large relative intensity of line 2 it seems likely that the 3.2 Mev level is $^3D_{1,2,3}$. This is supported by the large difference between the observed line width and the theoretical line width given in Table I. However in view of the limited resolving power of the method used in this experiment and the accompanying inaccuracy of the intensity estimates it must be emphasized that this interpretation of the level system, though in agreement with the calculations of Feenberg and Wigner, is tentative and needs much additional information before it can be considered certain.

The authors wish to thank Professor Wigner for his helpful comments concerning the tentative level classification.

One of us (P. G. K.) wishes to acknowledge a Grant-in-Aid from the National Research Council and generous aid from the Graduate School Research Board of the University of Illinois.

[7] Feenberg and Wigner, Phys. Rev. **51**, 95 (1937).

The Induced Radioactivity of Titanium and Vanadium

HAROLD WALKE*
Radiation Laboratory, Department of Physics, University of California, Berkeley, California
(Received August 26, 1937)

A study has been made of the radioactivities induced in titanium and vanadium by irradiation with deuterons, slow and fast neutrons and in titanium with 11 Mev alpha-particles. Bombardment of titanium with deuterons renders it extremely radioactive, the radiations emitted being mainly positrons and hard gamma-rays. An analysis of the decay curve shows the presence of six radioactive isotopes. Of these three have been found to be chemically inseparable from vanadium. Evidence is considered which suggests that the isotopes formed are V^{48} half-life 16.0 ± 0.2 days, V^{49} half-life 33 ± 1 minutes and V^{50} half-life 3.7 ± 0.2 hours. A short lived activity of half-life 2.8 minutes is probably due to Ti^{51} as the same isotope is formed when titanium is bombarded with slow neutrons. There is evidence of a weak activity with a half-life of 50 hours which is probably due to Sc^{44} formed in the reaction $Ti^{46}+H^2\rightarrow Sc^{44}+He^4$. Sc^{46} is also formed as evidenced by the presence of an isotope with a half-period of 85 ± 5 days and by the energy distribution of the soft negative electrons which accompany the positrons. The energy distribution of the positrons emitted by V^{48} has been studied using a large hydrogen-filled cloud chamber. The upper limit of the spectrum is at 1.0 (5) Mev, in reasonably good agreement with the value 1.1 (5) Mev deduced from absorption measurements in aluminum. The maximum energy of the positrons from V^{49} as determined by absorption measurements in aluminum is approximately 1.9 Mev. V^{49} and V^{50} have also been formed by bombarding titanium with 11 Mev alpha-particles. In addition two new periods of 68 ± 4 hours and longer than 180 days have been detected. The isotopes responsible for these activities have not been identified. When bombarded with fast neutrons it seems likely that Ca^{45}, Sc^{43} and Sc^{46} are formed from titanium. Sc^{43} is also produced by the transmutation $V^{51}+n^1\rightarrow Sc^{48}+He^4$, its half-life being 41 ± 3 hours. In addition, evidence has been obtained for the reaction $V^{51}+n^1\rightarrow V^{50}+2n^1$. This reaction can be induced by the fast neutrons from the Be^9+H^2 reaction, though it is more probable when $Li+H^2$ neutrons are used V^{52} has been produced in several reactions; its half-life is 3.9 ± 0.1 minutes.

INTRODUCTION

IN a previous communication[1] it was shown that when calcium is bombarded with deuterons reactions of the type $Ca^A+H^2\rightarrow Sc^{A+1}+n^1$ are very probable. The present paper is a report of experiments made on the induced radioactivity of titanium which disclosed that the same type of reaction is very probable with this element. During this study a positron radioactive isotope was discovered which has been identified as V^{48}, which has some rather unusual properties. Included in this paper is a preliminary discussion of these properties.

By a number of nuclear reactions it has been found possible to identify the mass numbers of some previously undetected radioactive isotopes.

The deuterons, neutrons and alpha-particles used in this investigation were produced in the Berkeley cyclotron under conditions similar to those mentioned in other papers.[1] Decay measurements were made using a Lauritsen type quartz fiber electroscope, the absorption of radiations being observed by interposing aluminum and lead sheets between the sample and the electroscope window.

BOMBARDMENT OF TITANIUM WITH DEUTERONS AND SLOW NEUTRONS

Metallic titanium and chemically pure TiO_2 were activated with 5.5 Mev deuterons. The metal was found to contain sodium so that the analysis of the decay curve was made using samples of TiO_2. The powdered metal, however, is readily soluble in dilute nitric acid so that chemical analyses were carried out using the activated metal.

In a preliminary study of the radioactivity induced in titanium by deuterons, a small quantity of the metal was activated for 12 microampere hours. The sample was found to be so intensely radioactive that it was only possible to make measurement on its decay by interposing 16 mm of aluminum between it and the electroscope window. Under these conditions the fiber discharged at the rate of five divisions per second (which is equivalent to 5×10^4 electrons entering the electroscope per second).

* Commonwealth Fund Fellow.
[1] Walke, Phys. Rev. **51**, 439 (1937).

The early decay of the activity was rapid showing the presence of a short lived isotope. On correcting for the ionization due to longer lived bodies it was found that the half-life of this isotope is 2.8 ± 0.1 minutes. By activating titanium with slow neutrons the same radioactive substance was produced as the decay of the activity indicates a half-life of 2.9 ± 0.1 minutes. This isotope emits negative electrons and gamma-radiation. The mass numbers and percentage abundances of the isotopes of titanium and neighboring elements as given by Aston are as below:

Calcium	40(96.76%)	42(0.77%)	43(0.17%)	44(2 30%)	
Scandium	45(100%)				
Titanium	46(8.5%)	47(7.8%)	48(71.3%)	49(5.5%)	50(6.9%)
Vanadium	51(100%).				

Since titanium has stable isotopes for all mass numbers from 46 to 50 inclusive the half-life of 2.9 ± 0.1 minutes observed by activating titanium with slow neutrons must be associated with Ti^{51}. Thus Ti^{51} has been formed in the two reactions:

$$Ti^{50}+n^{1}\rightarrow Ti^{51}+\gamma;\quad Ti^{51}\rightarrow V^{51}+e^{-}$$
$$Ti^{50}+H^{2}\rightarrow Ti^{51}+H^{1}.$$

For convenience the decay curves of this isotope are shown with those of other short lived bodies in Fig. 11 at the end of the paper.

After the Ti^{51} has died away the decay curve indicates the existence of several isotopes. Cloud chamber observations show that the sample emits large numbers of positrons, though too many electrons are seen to be accounted for entirely by Compton recoils from the annihilation radiation. Moreover, the metal shows a very strong activity of half-life 15 hours which emits negative electrons of approximately two million volts energy and hard gamma-radiation. These properties are characteristic of Na^{24} which is probably formed from sodium contamination as it is not observed at all with the chemically pure TiO_2. Thus many of the negative electrons seen in the cloud chamber are due to sodium contamination. On the other hand a certain number of electrons persist for several months and as will be discussed later it is quite likely that these are due to Sc^{46} formed in the reaction

$$Ti^{48}+H^{2}\rightarrow Sc^{46}+He^{4};\quad Sc^{46}\rightarrow Ti^{46}+e^{-}.$$

A detailed analysis of the decay curve of the radioactivity induced in titanium by deuterons indicates the existence of three main periods (in addition to the period due to Ti^{51}) with values 33 ± 1 minutes, 3.7 ± 0.2 hours and 16.0 ± 0.2 days. There is also a weak activity with a half-life of approximately 50 hours, together with a long period of 85 ± 5 days, which is only observed in samples which have been very strongly activated. This last half-life is the same as that of Sc^{46} and cloud chamber evidence to be considered later suggests that this isotope is formed. The 50 hour period might well be due to Sc^{44} [2] though the weak activity of this isotope does not allow of an accurate determination of its half-life.

The strong positron activity suggested, however, that most of the radioactive bodies must be isotopic with vanadium and this was confirmed by chemical analyses using activated titanium metal. (The chemical separation adopted was suggested to the author by Dr. Glen Seaborg of the department of chemistry.)

About 30 mg of active titanium metal in the form of powder was dissolved in $6N.HNO_3$ which was gently heated and to the resulting solution was added 25 mg of Sc_2O_3 and 1 cc of $M/4.NH_4VO_3$. The mixture was evaporated in a small flask until its volume was reduced to 3 cc. 5 cc of $16N.HNO_3$ was added and the solution evaporated until approximately 3 cc were left. Nine cc of $9N.HClO_4$ were then added, evaporation again being proceeded with until only 3–4 cc remained. Ten cc of water were gradually added, the mixture being boiled gently for 10–15 minutes. In this way the titanium was precipitated as oxide; it was filtered out and rejected.

To the filtrate was added $6N.NH_4OH$ until the solution was just neutral. Two cc of $1N.Pb(NO_3)_2$ were added and the vanadium was precipitated as lead vanadate. This was filtered off and washed. To the residual solution was added 1 cc of saturated oxalic acid and the mixture was heated for several minutes. The scandium was thus precipitated as oxalate and was filtered out and thoroughly washed.

Both the vanadium and scandium precipitates were found to be active though the scandium oxalate decayed with a single period of 15 hours. A similar but weaker activity was also found in the vanadium precipitate. These effects were undoubtedly due to the sodium contamination.

[2] Walke, Phys. Rev. **52**, 400 (1937).

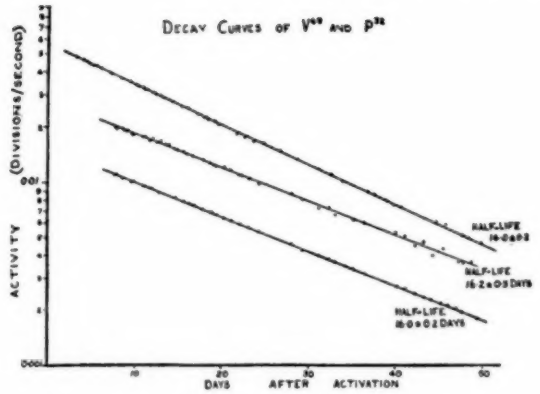

FIG. 1. Decay curves of V^{48} and P^{32}. The half-life 16.0 ±0.2 days is associated with the total activity of a sample of titanium metal after activation with deuterons (shown in this figure = activity $\times 10^{-1}$). The half-life 16.2±0.3 days is associated with the γ-ray decay of this sample. The γ-radiation was filtered through 1.6 cm of aluminum.

No other period was detected in the scandium precipitate, showing that no short lived scandium isotopes are formed in the reactions under consideration. The intensity of the 50-hour period observed in the unseparated samples was sufficiently weak to make it unlikely that this would be observed in the presence of the strong sodium activity. Moreover, to prevent too great an activity due to the 16-day period (which might have obscured shorter periods) the sample was activated for only 7 microampere hours. Thus the amount of Sc^{46} formed would be inappreciable and could not have been detected. Hence although the chemical separation shows that reactions involving alpha-particle emission following deuteron capture are not highly probable the presence of the weak 50 hour period in the unseparated samples of TiO_2 suggests that Sc^{44} may be formed in the reaction:

$$Ti^{46}+H^2 \rightarrow Sc^{44}+He^4; \quad Sc^{44} \rightarrow Ca^{44}+e^+.$$

Associated with the vanadium precipitate were found the three main periods of 33±1 minutes, 3.7±0.2 hours and 16.0±0.2 days. These bodies are then all radioactive isotopes of vanadium, perhaps formed in reactions of the type

$$Ti^A+H^2 \rightarrow V^{A+1}+n^1; \quad V^{A+1} \rightarrow Ti^{A+1}+e^+,$$

in which stable isotopes of titanium capture the proton of the deuteron to form radioactive isotopes of vanadium which decay by positron emission to produce stable titanium isotopes with mass numbers greater by unity than the original titanium isotopes.

By bombarding a sample of TiO_2 free from sodium contamination with 10 microamperes of deuterons for only 10 minutes it was found possible to verify that the emitted particles are mainly positrons by deflecting them in a magnetic field. No negative electrons could be detected.

IDENTIFICATION OF THE RADIOACTIVE VANADIUM ISOTOPES

Of the four possible vanadium isotopes $V^{47, 48, 49}$ and V^{50} which could be formed in the reactions under consideration only one, namely V^{48}, could be produced from scandium by bombardment with alpha-particles. The reaction involved is:

$$Sc^{45}+He^4 \rightarrow V^{48}+n^1; \quad V^{48} \rightarrow Ti^{48}+e^+.$$

In such experiments[3] the formation of a positron radioactive isotope was observed which was chemically separated with vanadium and which decayed with a half-life of 16.2±0.3 days. Thus the isotope with half-life 16.0±0.2 days formed by the activation of titanium with deuterons must be V^{48}. In Fig. 1 is shown a comparison between decay curves of this isotope and that of P^{32}. The remaining two periods can then be associated with V^{47}, V^{49} or V^{50}.

Of these isotopes only two, *viz.* V^{49} and V^{50} could be formed by bombarding titanium with alpha-particles in the reactions

$$Ti^{46, 47}+He^4 \rightarrow V^{49, 50}+H^1.$$

In this connection it is significant that titanium when activated with 11 Mev alpha-particles becomes quite strongly radioactive. The activity induced is complex in character but can be analyzed into well-defined periods. The two shortest half-lives observed have the values 34±1 minutes and 3.8±0.2 hours. These values agree within the limits of experimental error with the two short periods observed with deuterons. Visual observation using a cloud chamber showed that the short period activities formed by the alpha-particle activation of titanium emit mainly if not entirely positrons. A small number of negative electrons were seen but these may have

[3] Walke, "The Induced Radioactivity of Scandium," Phys. Rev. **52**, 669 (1937).

been due to Compton recoil electrons from the annihilation radiation.

This evidence suggests that the periods of 33 ± 1 minutes and 3.7 ± 0.2 hours should be associated with V^{49} and V^{50}. There is thus no definite evidence for V^{47} which if it is formed in the deuteron activation of titanium must have a half-life less than one minute or greater than several months.

In order to distinguish between the two isotopes a search was made for V^{50} formed in the reaction,

$$V^{51}+n^1\rightarrow V^{50}+2n^1.$$

Samples of vanadium metal and vanadic acid were bombarded for many hours with neutrons from beryllium and lithium targets bombarded with deuterons. Only a relatively weak activity was detected but this showed the presence of two radioactive isotopes, one of which decayed with a half-life of 3.8 ± 0.3 hours, this being observed both with vanadium metal and vanadic acid and with the beryllium and the lithium fast neutrons.

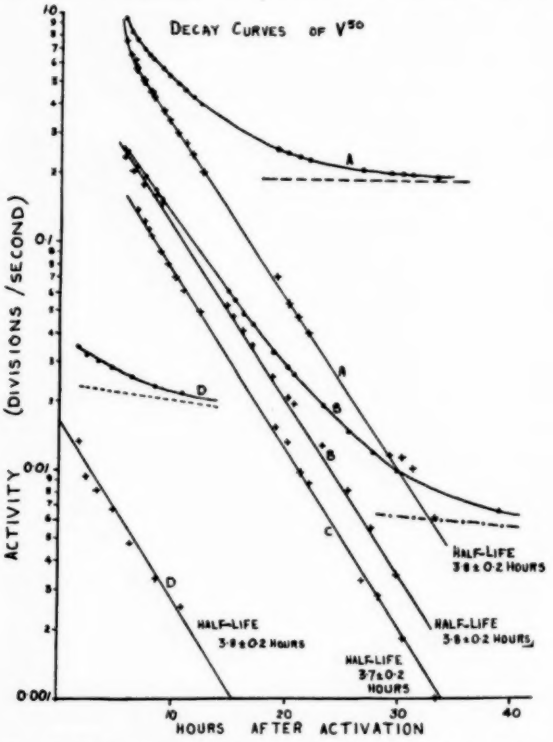

FIG. 2. Decay curves of V^{50}. A. Titanium oxide activated by deuterons. Dots represent total activity; dashes, activity due to longer lived isotopes. The crosses have been corrected for the long period activities. B. Titanium oxide activated by 11 Mev alpha-particles. Dots represent total activity; dots and dashes, activity due to longer periods. The crosses have been corrected for longer lived activities. C. Titanium oxide+deuterons sample II corrected for long lived activities. D. Vanadic acid activated with the fast neutrons from $Li+H^2$ reactions. Total activity shown by dots. Background due to Sc^{48}, dashes. The crosses show the corrected activity.

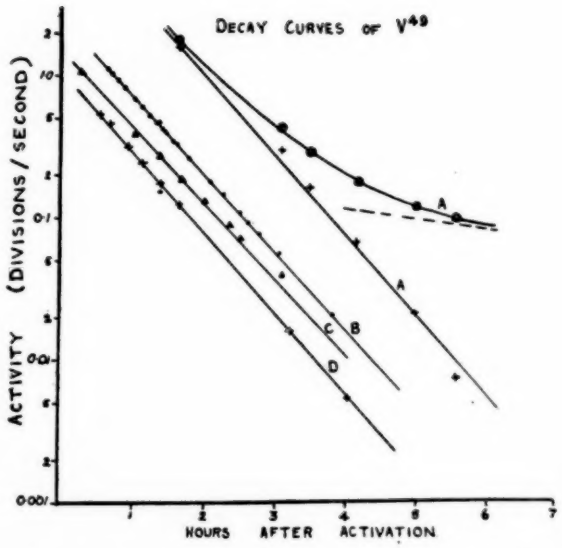

FIG. 3. Decay curves of V^{49}. A. Sample of chemically pure TiO_2 activated with deuterons. Dotted circles, total activity; dashes, activity due to other longer lived isotopes; plus signs, have been corrected for this longer lived activity. B. γ-radiation from titanium metal activated by deuterons after being filtered through 1.6 cm of aluminum. C. $\beta+\gamma\beta$-rays from C.P. titanium oxide activated by 11 Mev alpha-particles. D. γ-radiation from C.P. titanium oxide activated by deuterons. B, C, and D have all been corrected for longer period activities.

The association of this period (which agrees within the limits of experimental error with the periods of 3.7 ± 0.2 hours and 3.8 ± 0.2 hours detected with titanium bombarded with deuterons and alpha-particles) with vanadium bombarded with fast neutrons thus suggests that it is characteristic of V^{50}. Thus, V^{50} may be formed in the three reactions

$$Ti^{49}+H^2\rightarrow V^{50}+n^1;\quad V^{50}\rightarrow Ti^{50}+e^+$$
$$Ti^{47}+He^4\rightarrow V^{50}+H^1$$
$$V^{51}+n^1\rightarrow V^{50}+2n^1,$$

its half-life being 3.7 ± 0.2 hours.

This evidence is summarized graphically in Fig. 2.

The half-life of 33 ± 1 minutes must then be associated with V^{49} produced in the reactions:

$$Ti^{48}+H^2\rightarrow V^{49}+n^1$$
$$Ti^{46}+He^4\rightarrow V^{49}+H^1.$$

Decay curves of the isotope formed by these reactions are shown in Fig. 3.

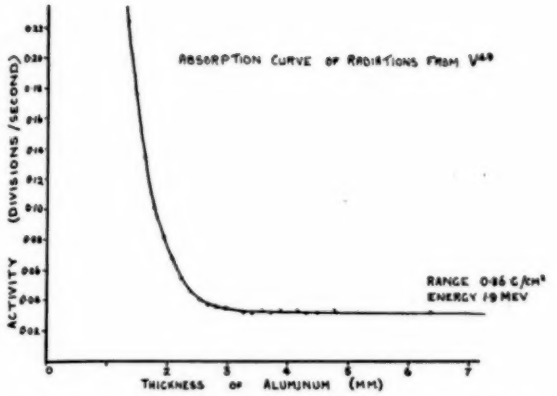

FIG. 4. Absorption curve in aluminum of radiations emitted by V^{49}. Range of positrons 0.86 g/cm². Maximum energy 1.9 Mev.

MAXIMUM ENERGY OF POSITRONS FROM V^{49} AND V^{48}

An estimate of the maximum energy of the positrons emitted by V^{49} has been obtained by making absorption measurements in aluminum. The absorption curve is reproduced in Fig. 4. The range of the positrons is 0.86 g/cm² corresponding by Feather's rule to a maximum energy of approximately 1.9 Mev.

Similar measurements were made on the absorption of the positrons emitted by V^{48}. The range in aluminum as found from the curve of Fig. 5 is 0.51 g/cm² corresponding to an energy of approximately 1.1(5) Mev.

The energy distribution of the positrons emitted by V^{48} has also been studied in the large hydrogen-filled expansion chamber previously discussed.[2] The positron tracks were photographed in a magnetic field of 285 oersteds, measurements on their curvature being made by the reprojection method previously adopted. The curvature of 502 tracks was measured, the resulting momentum distribution being shown in Fig. 6. The upper limit of the spectrum has been estimated by inspection, no attempt having been made to extrapolate beyond the highest energy track measured. The dotted curve shown in Fig. 6 has been fitted to the distribution without reference to any theory of β-decay. The upper limit at 4850 $H\rho = 1.0(5)$ Mev is in reasonably good agreement with the absorption measurements.

In addition to large numbers of positron tracks the cloud chamber pictures showed a small percentage of negative electrons of low energy. Some of these are undoubtedly due to Compton recoil electrons but the number is too great to be accounted for entirely in this manner. Measurements were made on 209 such tracks and it was found that they were distributed very much as in the β-ray spectrum of Sc^{46}. Especially noticeable (Fig. 7) is the well-defined maximum at 1500 $H\rho$ which was shown in a previous paper[3] to be characteristic of Sc^{46}. However, there are several tracks of higher energy than the upper limit of Sc^{46}, there being isolated tracks with energies as high as 7000 $H\rho$. Many of these are probably due to the strong gamma-radiation from V^{48}. However, the sharp maximum at 1500 $H\rho$ and the general form of the distribution when compared with that of Sc^{46} (shown in Fig. 7 as the dotted curve) suggests that most of the low energy electrons are due to this isotope formed in the reaction

$$Ti^{48}+H^2 \rightarrow Sc^{46}+He^4; \quad Sc^{46} \rightarrow Ti^{46}+e^-.$$

These results are supported by the fact that a weak long period of 85±5 days (which agrees with the half-life of Sc^{46} *viz.* 85±2 days) has been found in titanium after activation with deuterons (Fig. 8).

PRODUCTION OF V^{48} FROM CHROMIUM

Experiments have also been carried out to extract radioactive vanadium isotopes from chromium activated with 5.5 Mev deuterons.

In two such experiments negative results were obtained. Chromic oxide was bombarded for about an hour with a beam of 12 microamperes and was chemically separated by Dr. Glen Seaborg into three fractions containing manga-

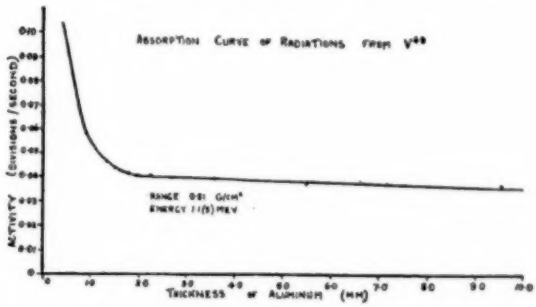

FIG. 5. Absorption curve in aluminum of the radiations emitted by V^{48}. Range of positrons 0.51 g/cm². Maximum energy 1.1(5) Mev.

nese, chromium and vanadium. The manganese was extracted as dioxide and was filtered off. It was found to be quite active as will be reported later by Doctors Livingood and Seaborg. From the residual solution chromium was precipitated as lead chromate by adding lead nitrate in acid solution. After filtering off the precipitate of lead chromate excess of lead was removed from the filtrate by passing into it H_2S. The precipitated lead sulphide was removed and the vanadium brought back to the pentavalent state by warming the solution with bromine. This was finally made just neutral by the addition of NH_4OH and lead vanadate was precipitated by adding lead acetate.

The chromium fraction was found to be inactive though a weak activity was found in the vanadium precipitate. This, however, decayed with the characteristic period of Na^{24}. Similar results were obtained from a second example, there being no appreciable activity in either the chromium or vanadium precipitates. It thus seems likely that the half-lives of Cr^{55} and Cr^{51} are either very short or very long. Moreover, the failure to observe any activity in the vanadium precipitate suggests that the reaction

$$Cr^{52}+H^2 \rightarrow V^{50}+He^4$$

is a rather improbable one.

More recently, however, a piece of copper coated with an electrolytic deposit of metallic

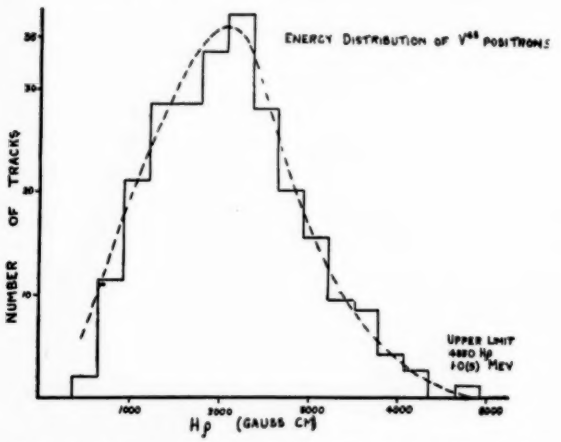

FIG. 6. Momentum distribution of the positrons from V^{48}. Magnetic field 285 oersteds. Number of tracks measured 502. Upper limit by inspection 4850 $H\rho=1.0(5)$ Mev. Curve shown by dashes has been fitted to the distribution by inspection. No attempt has been made to extrapolate beyond the highest energy track measured nor to fit the distribution to any theoretical curve.

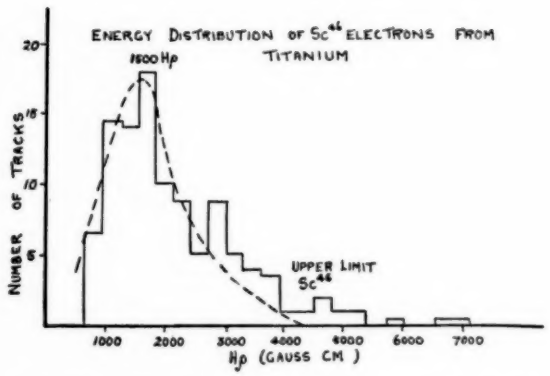

FIG. 7. Momentum distribution of negative electrons emitted by titanium metal after activation with deuterons. The dashed curve is that of Sc^{46} (as obtained by previous measurements on the electrons emitted by chemically separated scandium oxide after activation with deuterons) fitted to the distribution at $1500H\rho$.

chromium was bombarded with deuterons for sixty microampere hours. This sample was rendered strongly radioactive and from it Dr. Seaborg has separated for the author a radioactive isotope of vanadium. This emits only positrons and gamma-radiation and decays to half-value in 16.0 ± 0.3 days. It is thus V^{48} formed in the reaction

$$Cr^{50}+H^2 \rightarrow V^{48}+He^4; \quad V^{48} \rightarrow Ti^{48}+e^+.$$

The chromium fraction was also weakly radioactive, observations of its decay showing that the isotope or isotopes formed are long lived.

YIELDS OF THE RADIOACTIVE ISOTOPES FORMED WHEN TITANIUM IS BOMBARDED WITH DEUTERONS

By correcting for the finite period of bombardment the saturation of yields of the isotopes formed when titanium is bombarded with deuterons have been calculated. By multiplying these values by the relative abundance of the parent isotope we may obtain relative cross sections of the reactions which occur. These results are summarized in Table I:

A striking fact which emerges from these figures is the high probability of the formation of V^{48}, especially if it is produced by the reaction

$$Ti^{47}+H^2 \rightarrow V^{48}+n^1,$$

since this is so much more probable than the formation of V^{49} by a similar reaction. This great

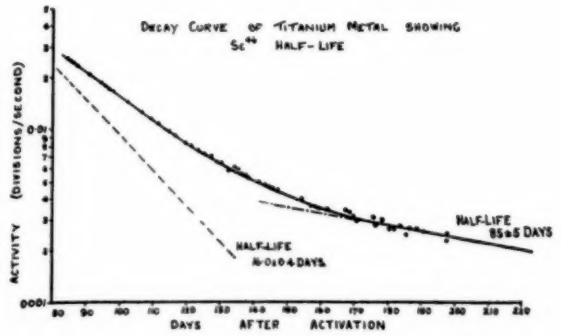

FIG. 8. End portion of decay curve of a sample of titanium metal after activation with deuterons showing the presence of 85±5 day period due to Sc^{46}.

difference might be explicable if V^{48} were also being formed in another reaction, especially if such a reaction involved the very abundant isotope Ti^{48}. A possible reaction according to the nuclear model proposed by Professor Bohr is:

$$Ti^{48}+H^{2}\rightarrow V^{48}+2n^{1}.$$

If this is the case, then the highly excited V^{50} formed by the penetration of the deuteron into the Ti^{48} nucleus evaporates two neutrons at the nuclear temperature resulting rather than ejecting one high energy neutron on which is concentrated most of the energy available in the transformation.

If such processes involving multiple neutron emission do occur, the formation of V^{48} should result in a relatively high neutron yield from titanium bombarded with deuterons. Dr. Luis Alvarez has compared the number of neutrons emitted from a titanium target bombarded with 15 microamperes of deuterons of 5.5 Mev energy with the number emitted by a beryllium target under the same conditions, and finds a ratio of 2 to 5.

PROPERTIES OF V^{48}

The gamma-ray intensity from V^{48} seemed to be much higher relative to the positron intensity than was observed with other positron radioactive isotopes such as Sc^{43} etc. Accordingly rough absorption measurements on the gamma-radiation were made using lead absorbers. Plotted on semi-logarithmic paper a linear absorption curve was obtained of which the slope was considerably less than would be expected if only annihilation radiation were being absorbed. It was thus shown that more penetrating gamma-rays accompanied the annihilation radiation. The fact has been recently proved by Dr. J. Reginald Richardson, who will report his results in more detail later. Dr. Richardson has investigated the distribution of Compton electrons ejected from a thin celluloid absorber by the gamma-rays from a strongly active titanium source in an expansion chamber. The distribution shows the existence of two well marked peaks corresponding to gamma-ray energies of 0.5 and 1.0 Mev, respectively. The measurements suggest that there are approximately twice as many quanta with energy 1.0 Mev as 0.5 Mev, i.e., there are 4 quanta of million-volt gamma-radiation emitted for every positron. This radiation may be due to nuclear γ-ray transitions but a complicated level system would have to be invoked to account for this high ratio of gamma-radiation to positron emission.

On the other hand this fact may be related to the phenomenon of nuclear capture of the K electrons which Dr. Luis Alvarez discovered occurs with V^{48}.[4] Dr. Alvarez studied the absorption in thin sheets of aluminum of the rays emitted by an active titanium sample which was acted on by a magnetic field so that no positrons could reach his thin walled counter. The absorption curve showed the presence of the characteristic K radiation of titanium. This is emitted as the K orbit which is emptied by the capture of the K electron by the radioactive nucleus is filled by an electron from an outer orbit. The 1.0 Mev γ-radiation emitted from V^{48} may in some way be connected with the capture of the K electron.

Since V^{48} emits four quanta of 1.0 Mev gamma-radiation per positron and as it has such a high probability of formation from titanium bombarded with deuterons a sample of the metal bombarded for about 100 microampere hours forms a rather convenient and relatively strong

TABLE I. *Relative cross sections of the reactions which occur when titanium is bombarded with deuterons.*

RADIOACTIVE ISOTOPE	HALF-LIFE	RELATIVE CROSS SECTIONS DEUTERONS PER ACTIVE ATOM × ABUNDANCE
Ti^{51}	2.9±0.1 min.	2.8×10^{7}
V^{50}	3.7±0.2 hours	1.7×10^{8}
V^{49}	33 ±1 min.	2.1×10^{9}
V^{48}	16.0±0.2 days	4×10^{6}
Sc^{44}	52 ±2 hours	1.9×10^{9}
Sc^{46}	85 ±2 days	1.4×10^{10}

[4] Alvarez, Phys. Rev. **52**, 134 (1937).

source of gamma-radiation. The fact that its half-life is as long as 16 days enables it to be used for quite long periods of time.

Activation of Titanium with 11 Mev Alpha-Particles

As has already been mentioned in the discussion of the deuteron induced radioactivities of titanium, bombardment of titanium with 11 Mev alpha-particles gives rise to V^{49} and V^{50}. These isotopes were identified by their half-lives. Visual observations using a cloud chamber showed that the great majority of the particles emitted are positrons.

In addition to these isotopes, however, two other radioactive bodies have been detected with half-lives of 68 ± 4 hours and approximately 200 days, respectively. The value of the long period cannot be determined accurately as its intensity is weak and fluctuations are considerable. However, one can say that its half-life is probably greater than 180 days.

The yields of the various isotopes are given in Table II.

The reactions which might occur when titanium is bombarded with alpha-particles (excluding those in which V^{49} and V^{50} are formed) are as below:

$$Ti^{48,\ 49,\ 50}+He^4\rightarrow V^{51,\ 52,\ 53}+H^1,$$

in which the ejection of a proton follows the capture of the bombarding alpha-particle and

$$Ti^{46\ 47,\ 48,\ 49,\ 50}+He^4\rightarrow Cr^{49,\ 50,\ 51,\ 52,\ 53}+n^1,$$

in which a neutron is ejected by the compound nucleus formed by the capture of the alpha-particle. Of these nuclei V^{51} and $Cr^{50,\ 52}$ and Cr^{53} are stable so that possible radioactive nuclei which might be formed are V^{52} and V^{53} and Cr^{49} and Cr^{51}. The half-life of V^{52} has been found to be 3.9 ± 0.1 minutes but no evidence for such a short period was found when a sample of titanium metal was bombarded for only five minutes. The activity produced decayed with the half-life of 33 minutes, though the presence of the 3.7 hour period in small intensity was suggested by the gradual bending of the curve after one hour's decay. Thus the reaction

$$Ti^{49}+He^4\rightarrow V^{52}+H^1$$

must be a relatively improbable one. The half-lives of 68 ± 4 hours and >180 days are then probably associated with two of the isotopes Cr^{49}, Cr^{51} and V^{53}. The intensity of the two longer periods is such that the sign of emitted particles could not be determined with the cloud chamber.

Table II. *Yield of active atoms when titanium is bombarded with 11 Mev alpha-particles.*

Radioactive Isotope	Half-Life	Yield Alpha-Particles/ Active Atom
V^{49}	33 ±1 min.	5×10^6
V^{50}	3.7 ± 0.2 hours	7.5×10^6
?	68 ± 4 hours	3.5×10^6
?	>180 days	1×10^6

Bombardment of Titanium with Fast Neutrons

A. Neutrons from beryllium bombarded with deuterons

As was mentioned in a previous paper[1] the bombardment of titanium with fast neutrons results in the formation of Ca^{45} which decays to half-value in 2.4 ± 0.2 hours by the emission of negative electrons according to the reaction

$$Ti^{48}+n^1\rightarrow Ca^{45}+He^4;\quad Ca^{45}\rightarrow Sc^{45}+e^-.$$

Following prolonged bombardment, however, two additional periods of 14.5 ± 0.3 hours and 75 ± 5 hours were detected, the latter being relatively weak. The 14.5-hour period is undoubtedly due to Na^{24} formed from the sodium present as impurity in the titanium as observed in the deuteron experiments. The long period, however, may well be much shorter than measured as experiments with the higher energies available using the $Li+H^2$ neutrons have disclosed a further very long period which has the effect of shortening the observed half-life of the order 80 hours to 42 ± 4 hours. Hence, although it is possible that the apparent half-life of 75 ± 5 hours is to be associated with a new radioactive isotope it seems more likely from the results of experiments with the more energetic neutrons that this period is due to a combination of a shorter period and a weak longer period which would have been detected had the period of observation been prolonged. On this assumption we will consider in greater detail the experiments

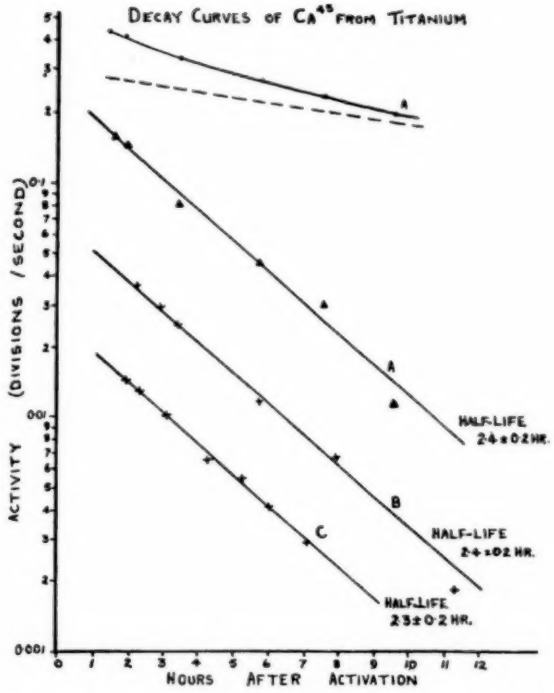

FIG. 9. Decay curves of 2.4 hour period from titanium activated by fast neutrons. A. Titanium metal powder Li+H^2 neutrons. Dots indicate total activity, dashes, background due to other longer periods. The points, solid triangles, have been corrected for these longer periods. B and C are decay curves of titanium metal after activation with fast neutrons from Be+H^2 reaction. The crosses have been corrected for longer period activities.

made by bombarding titanium with the fast neutrons from the Li+H^2 reaction.

B. Neutrons from lithium bombarded with deuterons

The radioactivity induced in titanium after activation with the 14–20 Mev neutrons from lithium bombarded with 5.5 Mev deuterons was found to be relatively strong, the decay curve showing the presence of several radioactive isotopes. Of these the shortest has a half-life of 2.4±0.2 hours due to the formation of Ca^{45}. The decay curves associated with this isotope are shown in Fig. 9. There is also a period of value 14.5±0.3 hours due to the sodium contamination. In addition, however, are present two isotopes, one of which has a half-life of 40±3 hours and the second of which is long lived. Observations made for a period of about five weeks suggest that the half-life of this body is of the order 85±5 days. Both these isotopes emit negative electrons as determined by means of a trochoid analyzer.

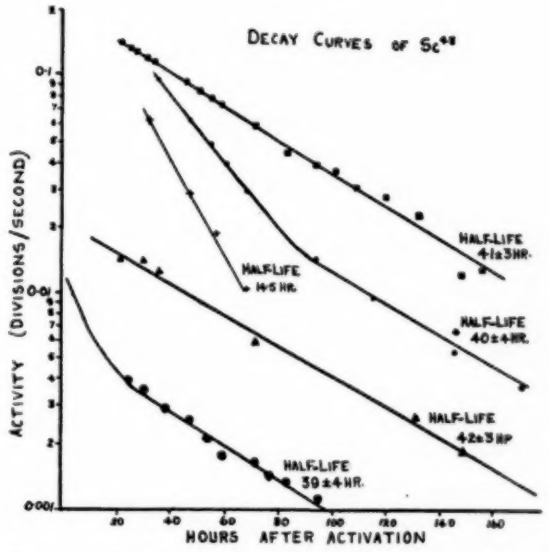

FIG. 10. Decay curves of Sc^{48}. The squares indicate activity of vanadic acid after activation with Li+H^2 neutrons (corrected for trace of very weak longer period). The dotted curve is that of titanium metal powder after activation with Li+H^2 neutrons showing 40 hour period and sodium contamination. The solid triangles represent the decay of scandium precipitate from titanium metal after activation with Li+H^2 neutrons. These last two curves have been corrected for the activity due to the 85-day period. Dots show the decay of vanadium metal after activation with the fast neutrons from a Be+H^2 source.

That they are isotopes of scandium is suggested by a somewhat rough chemical separation which was carried out as below.

The titanium was dissolved in $6N.HNO_3$ which was gently heated. To the resulting solution was added some inactive Sc_2O_3 and $CaCl_2$. The mixture was evaporated until its volume was reduced considerably and was distilled first with $16N.HNO_3$ and then with $9N.HClO_4$. Finally water was added, the solution being warmed gently for 10–15 minutes. By this method the titanium was precipitated as oxide. This precipitate was found to be weakly active though the presence of sodium in the metal makes it seem likely that this weak activity may be due to contamination.

Scandium was then precipitated from the filtrate by the addition of ammonium hydroxide. Most of the activity was retained by the precipitated hydroxide, the decay curve of which shows the presence of two radioactive isotopes, both of which emit negative electrons. The shorter period has the half-life 42±3 hours. The other is very long and measurements made for a month suggest

that it probably has the same value as the long period observed with the unseparated sample of metal, namely 85±5 days.

This period agrees well with that of Sc^{46} *viz.* 85±2 days. It thus seems likely that this isotope has been formed by the reaction

$$Ti^{46}+n^1 \rightarrow Sc^{46}+H^1; \quad Sc^{46} \rightarrow Ti^{46}+e^-.$$

There may of course be still longer activities associated with the samples. However, time does not permit the author to look for such periods. On abundance grounds one would expect that Sc^{48} should be formed by a similar reaction, in which a proton is ejected from Ti^{48} for this isotope is present to an extent of 71 percent. Sc^{48} could also be formed by the ejection of an alpha-particle from vanadium, thus

$$V^{51}+n^1 \rightarrow Sc^{48}+He^4.$$

Accordingly a search was made for this isotope by bombarding vanadium metal and vanadic acid with fast neutrons. The metal was bombarded for many hours with the fast neutrons from a beryllium target bombarded with deuterons and a weak activity was detected. The decay curve showed the presence of two isotopes with half-lives of 3.8±0.3 hours (which is probably due to V^{50} as already discussed) and 39±3 hours which agrees within the limits of experimental error with the period of 42 hours found with titanium (see Fig. 10). A sample of vanadic acid was then irradiated with the fast neutrons from a lithium target bombarded with 15 microamperes of 5.5 Mev deuterons. The activity was considerably enhanced and two periods were again observed together with a trace of a longer period which has not been identified but which may be due to contamination. The two half-lives were found to be 3.8±0.3 hours and 41±3 hours. The particles emitted by the isotope with half-life 41±3 hours were found by means of a trochoid analyzer to be negative electrons.

This evidence thus suggests that Sc^{48} has been formed by the two reactions

$$Ti^{48}+n^1 \rightarrow Sc^{48}+H^1; \quad Sc^{48} \rightarrow Ti^{48}+e^-$$
$$V^{51}+n^1 \rightarrow Sc^{48}+He^4,$$

its half-life being 41±3 hours.

It is interesting in connection with these results to note that Pool, Cork and Thornton[5] have recently completed a survey of the activities induced in many elements by the fast neutrons emitted by a lithium target bombarded with deuterons. In vanadium they have observed a very weak period of 1.8 days (43 hours) which agrees well with the value 41±3 hours observed by the author. They have not, however, detected the 3.8 hour period. The present experiments (see Fig. 2) have shown that the reaction $V^{51}+n^1 \rightarrow V^{50}+2n^1$ is not a very probable one so that the failure of Pool, Cork and Thornton to observe this period might be due to the fact that their samples were not as strong as those used in the present experiments.

With titanium they observed periods of 1.7 hours and 28 hours, neither of which have been detected by the author. The isotopes responsible are stated to emit negative electrons. The evidence which has been presented here would suggest that the 28-hour period may be a combi-

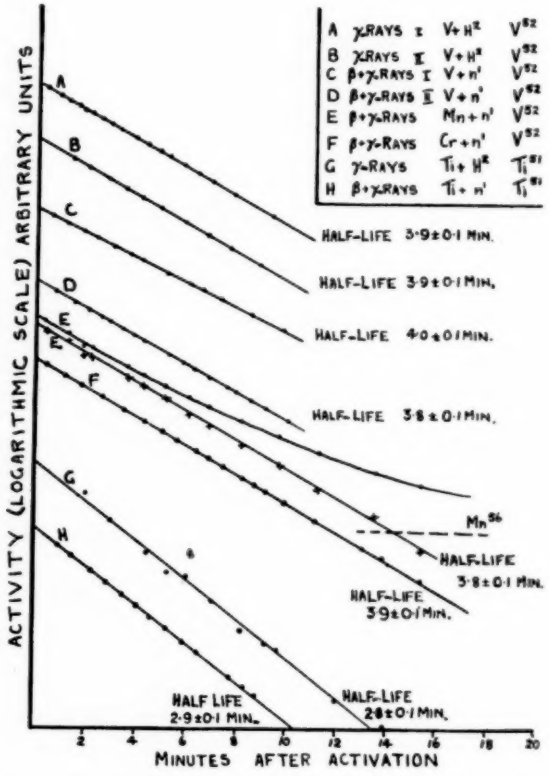

FIG. 11. Decay curves of short period activities of vanadium and titanium.

[5] Pool, Cork and Thornton, Phys. Rev. **52**, 239 (1937).

nation of the 41-hour period and the 14.5-hour period. The 1.7-hour period might well correspond with the 2.4-hour period observed by the author.

The Production of V^{52}

Vanadium when bombarded with deuterons or slow neutrons becomes strongly radioactive, emitting negative electrons and gamma-rays. The same isotope is formed in each case, namely V^{52} (half-life 3.9 ± 0.1 m) according to the reactions,

$$V^{51}+H^2\rightarrow V^{52}+H^1; \quad V^{52}\rightarrow Cr^{52}+e^-$$
$$V^{51}+n^1\rightarrow V^{52}+\gamma.$$

This has been confirmed by producing the same isotope by bombarding chromium and manganese with fast neutrons. In each case the decay curves show the presence of an isotope whose half-life is 3.9 ± 0.1 minutes. V^{52} is accordingly produced in the reactions

$$Cr^{52}+n^1\rightarrow V^{52}+H^1$$
$$Mn^{55}+n^1\rightarrow V^{52}+He^4.$$

Decay curves illustrating these reactions are shown in Fig. 11.

Acknowledgments

The author is greatly indebted to Professor E. O. Lawrence for the privilege of working in the Radiation Laboratory and for his continued interest and encouragement during the progress of this research. The author wishes to thank Dr. E. M. Lyman for frequent use of his trochoid analyzer and Dr. Glen Seaborg of the Department of Chemistry for valuable discussions of chemical separations. He is also grateful to Dr. Hugh C. Paxton for taking the cloud chamber photographs.

The friendship and cooperation of the staff of the Radiation Laboratory are gratefully acknowledged.

The research has been aided by the grants to the laboratory from the Research Corporation, the Chemical Foundation and the Josiah Macy, Jr., Foundation.

OCTOBER 15, 1937 PHYSICAL REVIEW VOLUME 52

Note on the Interaction Between Nuclei and Electromagnetic Radiation

A. J. F. Siegert
Physics Department, Stanford University, Palo Alto, California

(Received July 1, 1937)

The exchange character of nuclear forces makes it impossible to formulate in a consistent way the coupling between the electromagnetic field and a nucleus described by a model which involves only heavy particles. This difficulty does not occur in a theory which introduces light particles as carriers of the charge in the exchange processes. The actual contribution of these light particles to the transition probabilities is proved to be negligible in the limit of wavelengths of the radiation large compared with nuclear dimensions and nonrelativistic motion of the heavy particles. In this limit one is justified in taking as coupling term $-(\mathbf{ED})$, where $\mathbf{D}$ is the dipole moment calculated from the heavy particle model, and $\mathbf{E}$ is the electric field. A marked influence of the exchange processes on the radiation properties of the nucleus exists even in the limit considered.

FOR the treatment of the nucleus as a mechanical system, it is considered as built up solely of protons and neutrons. To get agreement with the observed mass defects of light nuclei, one has to assume the interaction forces between these heavy particles to be of finite range and to be—at least partly—exchange forces. One would like to use this model also for calculating probabilities of emission and absorption of gamma radiation. Here, however, a serious difficulty appears, as Condon and Breit have pointed out.[1] It is not possible to justify any specific form of the interaction between nuclei and radiation from the heavy particle model only. In fact, because of the exchange processes implied by the

[1] E. U. Condon and G. Breit, Phys. Rev. **49**, 904 (1936).

model, the charge of a heavy particle varies with time. If, for instance, there are Majorana forces acting between the heavy particles the Hamilton function of the nucleus contains terms exchanging spin and charge of two particles.[2] This means physically that a heavy particle in a nucleus does not always remain a proton, respectively neutron, but changes its charge and is sometimes a proton, sometimes a neutron. If now the interaction with the electromagnetic field is to be consistent with Maxwell's equations, one has to define the currents so as to satisfy the equation of continuity. There must then be currents flowing at points of space where there are no heavy particles. The motion of the charge is therefore not described completely by the motion of the heavy particles. On the other hand, the validity of the equation of continuity does not determine the form of the interaction, for this equation enables us to define only the curl-free part of the current. In the interaction with a light wave, however, the contribution of the curl-free part of the current vanishes because div $\mathbf{A}=0$. It is therefore not possible to define a current from the heavy particle model alone which can be used to find the interaction of nuclei with radiation. This difficulty does not occur if one tries to explain the mechanism of the exchange by that suggested in Fermi's theory of the β-decay. Although this theory has not succeeded so far in giving a satisfactory explanation of nuclear binding forces we want to use it here to illustrate the situation assuming that the general features will remain in any theory in which the exchange is explained by the creation and reabsorption of light particles. There the electric current and density are given by the ordinary expressions for the electron current and proton current and satisfy the equation of continuity. Having thus a reasonable definition of the current density $\mathbf{i}$ one may use as interaction the common form $-(1/c)\int \mathbf{A}\mathbf{i}d\tau$. From this basis we want to consider the limiting case of nonrelativistic velocities of the heavy particles and wave-lengths of the radiation large compared with nuclear dimensions. This limit is realized rather well in the photoelectric disintegration of the deuteron. In this case Condon and Breit took as interaction $-(\mathbf{ED})$, where $\mathbf{D}$ is the electric dipole moment of the heavy particles relative to the center of gravity, as given by the heavy particle model. This procedure is plausible for the following reason: Though one meets difficulties in defining a current in the heavy particle model, one can reasonably define the charge density and therefore the electric dipole moment. It then seems plausible to take $-(\mathbf{ED})$ as interaction for emission and absorption of radiation of long wave-lengths, by analogy with systems in which there are no exchange forces. To justify this assumption we notice that for long wave-lengths on the basis of Maxwell's theory the interaction is $-\mathbf{E}(\mathbf{D}_h+\mathbf{D}_l)$,[3] where $\mathbf{D}_h$ and $\mathbf{D}_l$ are the dipole moments of the protons and electrons, respectively. The error which one incurs in taking $\mathbf{D}_h$ from the heavy particle model and neglecting $\mathbf{D}_l$ altogether is certainly smaller than $-(\mathbf{ED}_l)$. What one neglects is in fact the possibility of finding, in the deuteron, the neutron split into proton and electron; or in terms of the Fermi theory, one neglects those parts of the wave function which represent states with electrons present. The relative order of the error will therefore be given by the probability of finding an electron in the nucleus. To estimate this roughly one may introduce an "exchange frequency" which will be of the order I/h, where I is the average potential energy. One may further suppose that during an exchange process the electron exists on the average for approximately the time a/c. Here a is the range of nuclear forces, and c is the velocity of light, since the exchange electrons move practically with light velocity. The probability of finding an electron is then $(I/h)(a/c)$.[4] Since I is of the

[2] The description of Majorana forces as an exchange of positional coordinates is equivalent to this on account of the Pauli principle.

[3] For long wave-length $-(1/c)\int \mathbf{A}\mathbf{i}d\tau=-(\mathbf{A}/c)\int \mathbf{i}d\tau$ $=-(\mathbf{A}/c)\int \mathbf{r}\dot{\rho}d\tau$ by partial integration using the equation of continuity. This is equal to $-(1/c)(\mathbf{A}\dot{\mathbf{D}})$ which gives in the resonance case $-(\mathbf{ED})$.

[4] The connection with the Fermi theory is given by the following consideration. Suppose one would be able to calculate the exchange forces between neutron and proton by a perturbation method, taking the Fermi operator as perturbation. One might start with a wave packet for the neutron and proton as wave function in zeroth approximation. In first approximation wave functions would occur which represent states with two protons and one electron and neutrino present. If one has chosen the right function as zeroth approximation, the energy perturbation due to these parts of the wave function will represent the main

order of the average kinetic energy of the heavy particles $mv^2/2$ one has $Ia/hc \sim (mva/h)\cdot(v/c)$. The first factor is of order one. The neglected term therefore contains a factor v/c and its neglect is justified in the nonrelativistic limit.

The meaning of Condon and Breit's approximation is thus that one considers the exchange as a sudden change in the dipole moment, and neglects the retardation of the forces between heavy particles. One has by no means neglected the exchange itself. The influence of the exchange processes in our limit is evident from the following considerations. We take as interaction $-(\mathbf{E}\mathbf{D}_h) = -\mathbf{E}\sum_\mu e\rho_\mu \mathbf{r}_\mu \cdot \rho_\mu$ is the character variable of the μth particle, with the eigenvalues 0 and 1 corresponding to neutron and proton. $\mathbf{r}_\mu$ is the coordinate relative to the center of gravity. Due to the exchange processes the ρ_μ are not constants of motion. If for instance the Hamilton function of the heavy particles contains a Majorana term

$$\tfrac{1}{2}\sum_{\mu\nu} I(r_{\mu\nu})\Omega_{\mu\nu}$$

one has

$$\dot{\rho}_\mu = (i/\hbar)\sum_{\mu\nu} I(r_{\mu\nu})(\rho_\nu - \rho_\mu)\Omega_{\mu\nu}.$$

Here $\Omega_{\mu\nu}$ is an operator which exchanges charge and spin of two particles μ and ν if they are of different charge and is zero otherwise. I is a function of their relative distance $r_{\mu\nu}$. It is this time-dependence of the ρ_μ which makes the sum of oscillator strengths

$$\sum_l f_{0l} = (2m/\hbar^2)\sum_l (E_l - E_0)\,|D_{0l}|^2$$

differ from its value for ordinary forces[5] as soon as exchange forces are involved. The summation gives

$$(\hbar/i)(m/\hbar^2)(D\dot{D} - \dot{D}D)_{00},$$

where

$$\dot{D} = \sum_\mu \rho_\mu \dot{x}_\mu + \dot{\rho}_\mu x_\mu.$$

From this one obtains

$$\sum_l f_{0l} = Z\left(1 - \frac{Z}{A}\right) - \frac{1}{2}\frac{m}{\hbar^2}\left(\sum_{\mu\nu}(x_\mu - x_\nu)^2 F(r_{\mu\nu})\Omega_{\mu\nu}\right)_{00}$$

$$= Z\left(1 - \frac{Z}{A}\right) - \frac{1}{2}\frac{m}{\hbar^2}A(A-1) \times ((x_1 - x_2)^2 F(r_{12})\Omega_{12})_{00},$$

where the second term comes from the part $\sum \dot{\rho}_\mu x_\mu$. If one assumes that the energy of a nucleus does not depend strongly on the shape of the potential hole F, one gets as an estimate of the magnitude of the extra term

$$(m/\hbar^2)\cdot(a^2/4)\cdot E_p,$$

where a is the range of nuclear forces, and E_p is the total potential energy of the nucleus. The extra term can thus become of the same order as the first term. This means that the exchange processes have a marked influence on radiation properties of the nucleus even in the limit considered here in which the details of its mechanism do not essentially enter into consideration.

The author wishes to thank Professor F. Bloch and Dr. A. Nordsieck for many helpful discussions.

part of the potential energy of the deuteron. The probability of finding the system in one of the higher states β is given by

$$P = \sum_\beta |F_{\beta 0}|^2/(E_\beta - E_0)^2,$$

where F is the Fermi operator. For those states which contribute essentially to the binding $E_\beta - E_0 \sim (\hbar c/a)$, since the wave-lengths of the electron and the neutrino must be of the order of the range a of the exchange forces. Then P is of the order

$$\frac{a}{\hbar c}\sum_\beta \frac{|F_{\beta 0}|^2}{E_\beta - E_0} \sim \frac{aI}{\hbar c}.$$

[5] This was noticed by E. Feenberg, Phys. Rev. **49**, 328 (1936).

Normal States of Nuclear Three- and Four-Body Systems

HENRY MARGENAU AND DANA T. WARREN
Sloane Physics Laboratory, Yale University, New Haven, Connecticut
(Received August 5, 1937)

A variational method employing orthogonal (Hermite) functions in linear combination is used for calculating the binding energies of H^3 and He^4, with the following choice of nuclear constants:

$$A=35.60 \text{ Mev}; \quad a=2.25\times10^{-13} \text{ cm}; \quad g=0.20,$$

and an error function potential. Two types of coordinates are used for H^3; (1) normal, (2) individual particle coordinates. Their advantages and disadvantages are discussed. With the use of a certain limited set of functions of normal coordinates the energy has been depressed from -6.21 Mev in zeroth approximation to -7.21 Mev, while a suitable set of functions involving only individual particle coordinates reduced it from -6.16 Mev to -6.84 Mev. The second Schrödinger perturbation is less effective than the latter scheme by 0.22 Mev. Functions of different symmetry, called into play by the Heisenberg operators, are found to contribute 0.07 Mev on the basis of a modified variation method. He^4 has been treated only with the use of individual particle coordinates (Hartree method). A similar group of functions lowers the energy from -24.81 Mev in zeroth approximation to -25.85 Mev, which is better than the effect of Schrödinger's perturbation theory by 0.25 Mev. General estimates of convergence limits are given.

THE theory of nuclear forces appears to have reached a stage in which it allows most of the details in the interaction of nuclear particles to be understood in a reasonably quantitative manner, so that there can be but little doubt as to its essential correctness. The chief obstacle in the way of exact formulations lies in the mathematical difficulties surrounding the quantum-mechanical many-body problem. These obstacles are bound to become more serious as theories become more refined. It is in an attempt at understanding the limitations of the various methods designed to treat the three- and four-body problems, if not at the partial removal of these limitations, that the present calculations were undertaken.

The list of papers which deal with applications of the variational method to the problem at hand, starting with the publications of Wigner[1] and of Feenberg,[2] is already long. In the papers just mentioned an elegant and simple scheme for estimating the energy of the lowest state of many-body systems, known as the "equivalent two-body method," has been designed, a scheme which has proved very useful in the evaluation of probably universal nuclear constants.[3] It is clearly desirable to provide as refined as possible a variational basis for the use of the equivalent two-body method, an objective which has inspired the work to be described. We feel that the results are such as to strengthen confidence in the abbreviated two-body procedure.

The most adequate and extensive variational calculations have been applied to the three-body problem by Present,[4] and by Rarita and Present.[5] Their method, while probably superior to the one here developed in several points—particularly the rapidity of convergence—has the serious disadvantage of being very difficult to apply to more than three particles. It seems important, however, to have a method which permits application without change in principle to any number of particles, and it is perhaps a further point in favor of the present line of attack that it starts with Feenberg's[2] elementary procedure as a first approximation. Rarita and Present[5] reach the conclusion that the values of nuclear parameters which will yield correctly the mass defect of H^3, while satisfying experimental data of neutron-proton scattering and the mass defect of H^2, give too large a binding energy for He^4. This result stimulates reinvestigation by another method. In our work we find, employing the usual values of nuclear parameters, an apparent convergence of the energy of H^3 to -7.21 Mev, 1 Mev above the experimental value. If this value were near the true convergence limit, the present results would support the conclusions of

[1] E. Wigner, Phys. Rev. **43**, 252 (1933).
[2] E. Feenberg, Phys. Rev. **47**, 850 (1935).
[3] E. Feenberg and J. K. Knipp, Phys. Rev. **48**, 906 (1935).
[4] R. D. Present, Phys. Rev. **50**, 635 (1936).
[5] W. Rarita and R. D. Present, Phys. Rev. **51**, 788 (1937).

Rarita and Present and require considerable revision of the present theories. On the other hand we know, from an application of the methods of this paper to H^2, that there occurs a similar semblance of convergence toward an energy value which is not at all near the true energy, if an analogous, limited set of functions is used. Because of this circumstance we suggest that there may be no necessity for seriously questioning the usual values of nuclear parameters.

Schrödinger perturbation theory has been applied to light nuclei by Inglis.[6] Nothing is known with certainty about the convergence of this method for nuclei, and the best way to test it is to make a variational calculation with the same functions as those used in the perturbation scheme. This was done for He^4, and it was found that the two methods do not differ very much in their results, the present method being slightly better. Such a coincidence is not trivial or in general predictable. While it might be expected in cases where the variation functions approximate the correct ones reasonably well, so that the unperturbed eigenvalues are nearly equal to the diagonal elements of the correct operator, it is somewhat of an accident in the nuclear problem; for here the oscillator eigenvalues employed by Inglis are often quite different from the corresponding H_{ii} which enter in the variational calculation, sometimes by 100 percent. The coincidence is therefore not without interest. For H^3 the variation method also gives, with the use of the same functions, a slightly lower energy than the perturbation theory, as will be shown.

I. Outline of Method

The simple variation functions of the Gauss type in relative coordinates, used by Feenberg[2] and by Bethe and Bacher[7] represent the lowest member of a complete set of functions, the Hermite orthogonal functions. It is therefore natural to inquire what the effect of an inclusion of the higher members of this set will be. Since all these functions have the wrong asymptotic behavior one might expect the convergence to the energy limit to be none too rapid, and a special investigation of this point is necessary. This we have carried out by applying the method to the case of the deuteron where the correct limit is known. The results, together with certain findings regarding the use of different types of coordinates and their adequacy for nuclear calculations, will be published in a subsequent paper.

Having once chosen n orthogonal and normal functions in a suitable set of coordinates, and having ascertained the correct form of the Hamiltonian operator H in these coordinates, the problem of calculating the lowest energy reduces to solving the determinantal equation $|H_{ij}-\delta_{ij}E|=0$ for E. This process is simplified if we are interested only in the lowest of the n roots, which, for the nuclear problem, is widely separated from the next higher one. For we may then write for E the difference $H_{00}-\Delta E$ and introduce an estimated value of ΔE in all diagonal elements except the one involving H_{00}, which becomes ΔE. We write this element in the lower right-hand corner of the determinant and reduce the latter numerically by adding the first row with a suitable factor to all other rows so as to put zeros in the first column. Every single application of this process adds a negative increment to ΔE, and after an $(n-1)$-fold application the equation reads $\Delta E-\epsilon=0$. If ϵ is not sufficiently close to the original estimate the reduction is repeated with the new value. In the cases we have chosen the process is quite insensitive and highly stable with respect to the original choice of ΔE, and it is not very time consuming, even with as many as 20 linear variation functions. Most of the work is involved in the calculation of the elements H_{ij}. This, however, was found somewhat laborious and has forced us to use a single fixed form for the interaction between nuclear particles, symmetric in all of them, *viz.*

$$U_{ij}=-Ae^{-r^2_{ij}/a^2}[(1-g)P_{ij}{}^M+gP_{ij}{}^H], \quad (1)$$

where the symbols have the usual significance.[3] The parameters were chosen so as to make the binding energy of H^2 equal to 2.15 Mev, to give very approximately the experimental binding energies of H^3, He^4 with the use of the equivalent two-body method, and to be consistent with

[6] D. R. Inglis, Phys. Rev. **51**, 531 (1937).
[7] H. A. Bethe and R. F. Bacher, Rev. Mod. Phys. **8**, 82 (1936).

scattering data,[8] as follows:

$$A=35.60 \text{ Mev.}, \quad a=2.25\times10^{-13} \text{ cm}, \quad g=0.20.$$

The Coulomb energy, which according to previous calculations affects the total energy but slightly, will be omitted from the variational calculation on He^4 for convenience and added in afterwards. We shall also neglect for the present the effect upon the lowest state of functions unsymmetrical in like particles, which should properly be included because of the term $P_{ij}{}^H$ in (1); their effect is also known to be small.[9] (Cf. Section II, C.) If thus we limit ourselves to functions which are completely symmetrical in like particles, assumption (1) leads to the following form[10] for the Hamiltonian operator, written in central, individual particle coordinates:

$$H=\frac{\hbar^2}{2M}\sum_i \Delta_i{}^2-B\sum_{ij}{}_1 \exp\left[-(\mathbf{r}_i-\mathbf{r}_j)^2/a^2\right]P_{ij} -C\sum_{ij}{}_2 \exp\left[-(\mathbf{r}_i-\mathbf{r}_j)^2/a^2\right]P_{ij} \quad (2)$$

where Σ_1 is extended over pairs of unlike, Σ_2 over pairs of like particles. $B=(1-\frac{1}{2}g)A=32.10$ Mev; $C=(1-2g)A=21.77$ Mev; P_{ij} simply permutes the position coordinates of the ith and jth particles.

As to the choice of variation functions, the general rule is that they should at once be combined so as to possess the same symmetry in the various particles as does (2). This reduces the number of independent functions and hence the labor in reducing the determinant. Furthermore it is usually unnecessary to include functions which do not combine directly with the one corresponding to the lowest energy, for their contribution was found in most cases to be of secondary magnitude. Elimination of a function may sometimes be made by trial and error, using the function alone in combination with the "lowest" one; but this procedure is not always safe because a function, while feeble alone, may gain power in collaboration with others. Finally, as one would gather from the symmetry of (2) with respect to the three Cartesian axes, the best function for the lowest states of H^3 and He^4, neither of which has orbital space degeneracy, is one which is symmetrized in x, y, and z. Hence this procedure is carried out on all trial functions.

All the present work involves simple harmonic oscillator functions; it is related in this respect to the investigations of Houston,[11] and Heisenberg.[12] We shall use the following notation: Single Hermite functions will be denoted by

$$\varphi_n(x)=N_n e^{-x^2/2}H_n(x), \quad (3)$$

where N_n is a normalizing factor and H_n a Hermite polynomial. We define further

$$\varphi_{lmn}(i)=\varphi_l(x_i)\varphi_m(y_i)\varphi_n(z_i) \quad (4)$$

and

$$\Phi_{lmn}=(1/6)^{\frac{1}{2}}(1+\delta_{lm}+\delta_{ln}+\delta_{mn}+2\delta_{lm}\delta_{ln}\delta_{mn})^{-\frac{1}{2}} \times(\varphi_{lmn}+\varphi_{lnm}+\varphi_{mln}+\varphi_{mnl}+\varphi_{nlm}+\varphi_{nml}). \quad (5)$$

Eq. (5) is merely a compact way of writing the result of symmetrizing a function like (4) with the correct normalizing factor.

II. Variation Method Applied to H^3

A. Use of relative coordinates

The Hamiltonian for the H^3 problem reads (the index 1 here refers to the proton)

$$H=-(\hbar^2/2M)(\nabla_1{}^2+\nabla_2{}^2+\nabla_3{}^2) -B\exp\left[-r_{12}{}^2/a^2\right]P_{12} -B\exp\left[-r_{13}{}^2/a^2\right]P_{13} -C\exp\left[-r_{23}{}^2/a^2\right]P_{23}.$$

The transformation to relative and center of mass coordinates,

$$\xi_1=(1/2)^{\frac{1}{2}}(2x_1-x_2-x_3), \quad \xi_2=(1/2)^{\frac{1}{2}}(x_2-x_3), \quad X=(1/3)^{\frac{1}{2}}(x_1+x_2+x_3),$$

with similar relations between η and y, ρ and z, changes the form of H into

$$H=-(\hbar^2/2M)(\nabla^2+3\nabla_1{}^2+\nabla_2{}^2) -B\exp\left[-(\boldsymbol{\varrho}_1-\boldsymbol{\varrho}_2)^2/2a^2\right]P_{12} -B\exp\left[-(\boldsymbol{\varrho}_1+\boldsymbol{\varrho}_2)^2/2a^2\right]P_{13} -C\exp\left[-2\rho_2{}^2/a^2\right]P_{23},$$

[8] G. Breit, E. U. Condon, and R. D. Present, Phys. Rev. **50**, 825 (1936); M. A. Tuve, N. P. Heidenburg, and L. R. Hafstad, Phys. Rev. **50**, 806 (1936).

[9] G. Breit and E. Feenberg, Phys. Rev. **50**, 850 (1936); R. D. Present, Phys. Rev. **50**, 870 (1936).

[10] Cf. for instance Bethe and Bacher, reference 7.

[11] W. V. Houston, Phys. Rev. **47**, 942 (1935).

[12] W. Heisenberg, Zeits. f. Physik **96**, 473 (1935).

where $\rho^2=\xi^2+\eta^2+\zeta^2$. It allows us to separate off the motion of the center of mass, ∇^2, but we pay for this advantage by having to use more complicated P-operators. They become linear substitutions:

$$P_{12}\xi_1=\tfrac{1}{2}(-\xi_1+3\xi_2) \quad P_{12}\xi_2=\tfrac{1}{2}(\xi_1+\xi_2)$$
$$P_{13}\xi_1=-\tfrac{1}{2}(\xi_1+3\xi_2) \quad P_{13}\xi_2=-\tfrac{1}{2}(\xi_1-\xi_2)$$
$$P_{23}\xi_1=\xi_1 \quad P_{23}\xi_2=-\xi_2 \qquad (6)$$

with similar relations for η and ζ. This complication, of course, accompanies the transition from individual particle coordinates to any new set which corresponds to the correct number of degrees of freedom. We note that the function

$$\psi=\varphi_{n_{\xi_1}}(q_1^{\frac{1}{4}}\xi_1)\varphi_{n_{\eta_1}}(q_1^{\frac{1}{4}}\eta_1)\varphi_{n_{\zeta_1}}(q_1^{\frac{1}{4}}\rho_1)\varphi_{n_{\xi_2}}(q_2^{\frac{1}{4}}\xi_2)$$
$$\times\varphi_{n_{\eta_2}}(q_2^{\frac{1}{4}}\eta_2)\varphi_{n_{\zeta_2}}(q_2^{\frac{1}{4}}\rho_2) \qquad (7)$$

satisfies the equation

$$(\hbar^2/2M)\{-(3\nabla_1^2+\nabla_2^2)+(3q_1^2\rho_1^2+q_2^2\rho_2^2)\}\psi=E\psi$$

and has the eigenvalue

$$E(n_{\xi_1}\cdots n_{\zeta_2})=(\hbar^2/M)[(n_{\xi_1}+n_{\eta_1}+n_{\zeta_1}+3/2)3q_1$$
$$+(n_{\xi_2}+n_{\eta_2}+n_{\zeta_2}+3/2)q_2].$$

If, therefore, we use functions of the type (7) the kinetic energy is easily calculated from the relation

$$-(\hbar^2/2M)(3\nabla_1^2+\nabla_2^2)\psi=E(n_{\xi_1}\cdots n_{\zeta_2})\psi$$
$$-(\hbar^2/2M)(3q_1^2\rho_1^2+q_2^2\rho_2^2)\psi. \qquad (8)$$

In setting up variation functions we have at our disposal not only the coefficients with which functions (7) enter into linear combination, but also the parameters q_1 and q_2. These must be fixed before the coefficients can be determined. The plausible thing to do in this connection is to choose q_1 and q_2 so that the "lowest" function minimizes the energy, as was also done by Inglis.[6] We have checked this method with some care for H^3 and found that the final energy varies with q in nearly the same manner as H_{00} over a surprisingly large range.[14]

The zero-order function of the set (7) is, if written explicitly,

$$\psi_0=\exp[-q_1\rho_1^2/2-q_2\rho_2^2/2]$$
$$=\exp[-q_1(r_{12}^2+r_{13}^2+2\mathbf{r}_{12}\cdot\mathbf{r}_{23})/4-q_2r_{23}^2/4].$$

It differs from the one employed by Feenberg[2] and by Bethe and Bacher[7] by having the product term in the exponent. As far as the minimization of H is concerned, however, this term is indifferent; for while the expression for $\int\psi_0H\psi_0d\tau$, in terms of q_1 and q_2 looks different, the substitutions

$$p=4q_2/(9q_1+q_2), \quad \sigma=(9q_1+q_2)a^2/8$$

reduce it to the same form as that given by Bethe and Bacher, Eq. (118). The minimum E_0 is therefore the same except for the slight difference in the parameters. Its value is -6.21 Mev, it occurs for $q_1=0.1263$, $q_2=0.3394$.

Calculations were carried out chiefly with the following functions:

$$\psi_0=\Phi_{000}(1)\Phi_{000}(2), \quad \psi_7=\Phi_{000}(1)\Phi_{400}(2),$$
$$\psi_2=\Phi_{110}(1)\Phi_{110}(2), \quad \psi_8=\Phi_{400}(1)\Phi_{000}(2),$$
$$\psi_2=\Phi_{200}(1)\Phi_{000}(2), \quad \psi_9=\Phi_{200}(1)\Phi_{400}(2),$$
$$\psi_3=\Phi_{000}(1)\Phi_{200}(2), \quad \psi_{10}=\Phi_{400}(1)\Phi_{200}(2), \qquad (9)$$
$$\psi_4=\Phi_{200}(1)\Phi_{200}(2), \quad \psi_{11}=\Phi_{220}(1)\Phi_{220}(2),$$
$$\psi_5=\Phi_{220}(1)\Phi_{000}(2), \quad \psi_{12}=\Phi_{400}(1)\Phi_{400}(2).$$
$$\psi_6=\Phi_{000}(1)\Phi_{220}(2),$$

The effect of the functions having quantum numbers (112)(110); (310)(110); (220)(200); (400)(220) has also been considered and found to be small.

If i and j refer to two functions of this set, and q_1 and q_2 are given the above values, the matrix elements are, in view of (8),[13]

$$H_{ij}=E_i\delta_{ij}-(S_{ij}+T_{ij}+U_{ij}+7.770(q_1\rho_1^2)_{ij}$$
$$+6.958(q_2\rho_2^2)_{ij}) \qquad (10)$$

$(q_1\rho_1^2)_{ij}$ and $(q_2\rho_2^2)_{ij}$ are pure numbers, at once expressible in terms of oscillator matrix elements:

$$(\xi^2)_{n,\,n}=n+\tfrac{1}{2}, \quad (\xi)^2_{n,\,n+2}=\tfrac{1}{2}[(n+1)(n+2)]^{\frac{1}{2}}.$$

[13] Energies are expressed throughout in Mev, and the unit of length is 10^{-13} cm, as in reference 7.

Furthermore,

$$S_{ij}=B\int\psi_i\exp\left[-(\rho_1-\rho_2)^2/2a^2\right]P_{12}\psi_j d\tau,$$

$$T_{ij}=B\int\psi_i\exp\left[-(\rho_1+\rho_2)^2/2a^2\right]P_{13}\psi_j d\tau,$$

$$U_{ij}=C\int\psi_i\exp\left[-2\rho_2^2/a^2\right]P_{23}\psi_j d\tau.$$

S_{ij} splits up into sums of terms, each of which is a product of three integrals of the type

$$S_{kl;\,mn}=N_{klmn}\int\int H_k(q_1^{\frac{1}{2}}\xi_1)H_l(q_2^{\frac{1}{2}}\xi_2)\times\exp\left[(-q_1+1/2a^2)\xi_1^2-(q_2+1/2a^2)\xi_2^2+\xi_1\xi_2/a^2\right]H_m(q_1^{\frac{1}{2}}P_{12}\xi_1)H_n(q_2^{\frac{1}{2}}P_{12}\xi_2)d\xi_1 d\xi_2.$$

The algebraic expressions for the s integrals are lengthy and will not be given. As a consequence of the symmetry of the Hamiltonian the T_{ij} terms are related to the S_{ij} and need not be calculated separately. T differs from S only by an application of P_{23} to the factor $\exp\left[-(\rho_1-\rho_2)^2/2a^2\right]$ in the integrand. But P_{23} may be applied to the whole integrand without changing the value of the integral. P_{23}, however, affects only the variable ρ_2, changing its sign. Hence the passage from S to T changes the sign of the integral if the integrand is odd in ρ_2, leaves it unchanged if it is even. We see, therefore, that

$$T_{ij}=\pm S_{ij},$$

the upper sign holding when ψ_i and ψ_j are both even or both odd in ξ_2. U_{ij} is easier to calculate because P_{23} causes no mixing of the coordinates. It is zero unless ψ_i and ψ_j contain the same function of ρ_1.

The result of the variational calculations is best seen from Table I. The functions are labeled in accordance with (9). The functions indicated below that list have also been considered and found to lower the energy by as much as 0.08 Mev if combined with certain others, but if they are included together with $\psi_0-\psi_{12}$ their effect is inappreciable. It is clear that the chief contribution comes from the quadruply excited states, a result which agrees with the calculations of Inglis, using perturbation theory.

It has seemed too laborious a task to introduce all the octuply excited functions. What, then, may we say about convergence at the present stage? There is certainly a semblance of convergence toward the value -7.21 Mev. Nevertheless experience with the deuteron problem[14] has taught us that a similar group of functions, employed in the same way, leaves about half a megavolt of binding energy unaccounted for, and that, when it is difficult to get beyond a certain energy value, that value may not be the limit. On the other hand the variation functions for H^3 are more concentrated than those for H^2, which implies that the present method will reach the limit somewhat faster. Taking account of these considerations and realizing that the error for H^3 with similar functions of the same degree of concentration is probably somewhat larger than for H^2, we believe the true limit of the present scheme to lie at about -7.7 Mev. The true theoretical binding energy with the interaction parameters here chosen would be slightly below this value since the mixing effect[9] due to Heisenberg forces and relativity corrections[15] have here been neglected. The equivalent two-body method gives approximately the experimental value -8.3 Mev with the present parameters.

B. Use of individual particle coordinates

When applied to more particles, the method outlined so far becomes unwieldy because of the complicated nature of the permutation operators. Recourse is therefore often had to functions of individual particle coordinates in analogy with Hartree's atomic method. It seemed of interest to investigate in connection with the simple example of H^3 the relative merits of the two procedures.

TABLE I. *Variational energies of H^3 for different combinations of functions in normal coordinates.*

FUNCTIONS INCLUDED	$-E$(Mev)
ψ_0	6.214
ψ_0, ψ_1	6.243
$\psi_0-\psi_2$	6.244
$\psi_0-\psi_3, \psi_5$	6.39
$\psi_0, \psi_4-\psi_8$	7.11
$\psi_0-\psi_9$	7.21
$\psi_0-\psi_{12}$	7.21

[14] The results will be published shortly.

[15] D. Blochinzew, Physik. Zeits. Sowjetunion **8**, 270 (1935); H. Margenau, Phys. Rev. **50**, 342 (1936); E. Feenberg, Phys. Rev. **50**, 674 (1936).

Hartree functions describing the state of a nucleus include the motion of the center of mass, and this must be subtracted operationally from the Hamiltonian. The term to be subtracted from the usual H is the kinetic energy of the center of mass which, for N particles all of the same mass M, has the form

$$-(\hbar^2/2NM)(\sum_i \nabla_i)^2$$

Thus we have left as the significant Hamiltonian to be used in the variational problem[6]

$$H=-(\hbar^2/2M)[(1-1/N)\sum_i \nabla_i^2 - 2/N\sum_{i>j}\nabla_i\cdot\nabla_j]+E_{\text{pot.}} \quad (11)$$

For H^3 we have

$$H=-(\hbar^2/3M)[\sum_i \nabla_i^2-\sum_{i>j}\nabla_i\cdot\nabla_j] - B\exp[-r_{12}^2/a^2]P_{12}-B\exp[-r_{13}^2/a^2]P_{13} - C\exp[-r_{23}^2/a^2]P_{23}. \quad (12)$$

We have employed the following 21 normalized variation functions:

$$\begin{array}{lll}
\phi_{000}(1)\phi_{000}(2)\phi_{000}(3)=\psi_0 & \phi_{000}(1)\phi_{200}(2)\phi_{200}(3) & \phi_{200}(1)\phi_{100}(2)\phi_{100}(3) \\
(1/2)^{\frac{1}{2}}\phi_{000}(1)[\phi_{200}(2)\phi_{000}(3)+] & (1/2)^{\frac{1}{2}}\phi_{200}(1)[\phi_{200}(2)\phi_{000}(3)+] & (1/2)^{\frac{1}{2}}\phi_{100}(1)[\phi_{200}(2)\phi_{100}(3)+] \\
\phi_{200}(1)\phi_{000}(2)\phi_{000}(3) & (1/2)^{\frac{1}{2}}\phi_{000}(1)[\phi_{100}(2)\phi_{300}(3)+] & (1/2)^{\frac{1}{2}}\phi_{000}(1)[\phi_{220}(2)\phi_{000}(3)+] \\
\phi_{000}(1)\phi_{100}(2)\phi_{100}(3) & (1/2)^{\frac{1}{2}}\phi_{300}(1)[\phi_{100}(2)\phi_{000}(3)+] & \phi_{220}(1)\phi_{000}(2)\phi_{000}(3) \\
(1/2)^{\frac{1}{2}}\phi_{100}(1)[\phi_{000}(2)\phi_{100}(3)+] & (1/2)^{\frac{1}{2}}\phi_{100}(1)[\phi_{300}(2)\phi_{000}(3)+] & (1/2)^{\frac{1}{2}}\phi_{000}(1)[\phi_{120}(2)\phi_{100}(3)+] \\
(1/2)^{\frac{1}{2}}\phi_{000}(1)[\phi_{400}(2)\phi_{000}(3)+] & \phi_{000}(1)\phi_{110}(2)\phi_{110}(3) & (1/2)^{\frac{1}{2}}\phi_{100}(1)[\phi_{000}(2)\phi_{120}(3)+] \\
\phi_{400}(1)\phi_{000}(2)\phi_{000}(3) & (1/2)^{\frac{1}{2}}\phi_{110}(1)[\phi_{110}(2)\phi_{000}(3)+] & (1/2)^{\frac{1}{2}}\phi_{120}(1)[\phi_{000}(2)\phi_{100}(3)+].
\end{array} \quad (13)$$

A plus sign indicates that a function similar to the foregoing one, but with particles 2 and 3 interchanged, has been added. (13) represents oscillator eigenfunctions for a potential energy

$$(\hbar^2/2M)q^2(r_1^2+r_2^2+r_3^2),$$

that is, the oscillator "stiffness" is taken to be equal for all particles. We are thus at once disposing of possible variation parameters whose retention would, however, give only a very slight improvement. q appears of course in the functions (13). To allow comparison with the work of Inglis[6] we introduce the dimensionless quantity $\sigma\equiv qa^2$.

As before, we fix σ by minimizing H_{00}. The minimum occurs at $\sigma=1.83$ and has the value -6.16 Mev. This compares not unfavorably with the value -6.21 Mev obtained in the previous section for H_{00} with the use of two parameters. Expressing again the energy in Mev and distances in units of 10^{-13} cm, we find in this instance

$$H_{ij}=2/3E_i\delta_{ij}-4.945/(3)[(\sum qr^2)_{ij} - (\sum_{n>m}\nabla_n\cdot\nabla_m)_{ij}/q]-2S_{ij}-U_{ij}.$$

$E_i=(\hbar^2/M)q(9/2+\Sigma n_i)=14.83(9/2+\Sigma n_i)$, where the n_i are the quantum numbers of state i. The matrix elements are written so that the terms in parentheses are pure numbers. The expression $(\sum_{n>m}\nabla_n\cdot\nabla_m/q)_{ij}$ at once decomposes into products of two integrals of the form

$$d_{st}=\int_{-\infty}^{\infty}\varphi_s(x)\frac{d}{dx}\varphi_t(x)dx=\left(\frac{s+1}{2}\right)^{\frac{1}{2}}\delta_{t,\,s+1}.$$

Since the functions chosen are symmetrical in particles 2 and 3, the integrals over the two terms of (12) involving B are equal, and P_{23} may be ignored. This makes the integrations very easy. All S_{ij} and T_{ij} reduce to products of integrals

$$f_{kl,\,mn}=\left(\frac{\sigma+2}{\sigma}\right)^{\frac{1}{2}}\int_{-\infty}^{\infty}H_k(\xi_1)H_l(\xi_2) \times\exp\{-[\xi_1^2+\xi_2^2+(\xi_1-\xi_2)^2/\sigma]\} \times H_m(\xi_1)H_n(\xi_2)d\xi_1 d\xi_2,$$

many of which have already been given by Inglis. These f's are polynomials in the quantity

$$u=1/(\sigma+2).$$

The coefficients of the various powers of u for the integrals needed in this work are tabulated in Table II, where no entry indicates a zero.

After calculation of the H_{ij}, the secular determinant, which now has 21 rows and columns, was reduced as explained before. The effect of simpler combinations among the functions was not studied in as much detail as in the previous section, the results being somewhat parallel to that case. The 20 functions here considered in addition to ψ_0 lower the energy from -6.16 Mev to -6.84 Mev. It is seen that the Hartree method is distinctly poorer than the one employed in II, A.

If the same functions are used with the Schrödinger perturbation method it is found that the second perturbation depresses the energy from -6.16 Mev to -6.62 Mev.

C. Effect of Heisenberg operators

Although previous calculations[9] show that the depressing effect of an antisymmetrical function in the position coordinates of the two neutrons upon the energy of the normal state is small, we have made a careful study of this matter for the case of H^3, using what is essentially a variation method.

We wish to satisfy the equation

$$H\psi = E\psi,$$

in which[14]

$$H = T + U_{12} + U_{13} + U_{23}.$$

T denotes the kinetic energy as it appears explicitly in (11) (we shall use "Hartree functions" in this section), and the U's are defined in Eq. (1). If we let

$$\psi = auS^0 + bvS^1, \tag{15}$$

where S^0 and S^1 are the spin functions used by Breit and Feenberg,[9] u is symmetrical and v antisymmetrical in particles 2 and 3, and a and b are normalizing factors,[16] then the orthogonality of S^0 and S^1 will cause (14) to reduce to two equations:

$$\left.\begin{aligned} H_0 au + Xbv &= Eau \quad \text{(a)} \\ H_1 bv + Xau &= Ebv \quad \text{(b)} \end{aligned}\right\} \tag{16}$$

where H_0 is the Hamiltonian (11) which was previously used,

$$X = (3^{\frac{1}{2}}/2)g(J_{13}P_{13} - J_{12}P_{12}),$$

$$J_{ij} = -A \exp\left[-r_{ij}^2/a^2\right]$$

and

$$H_1 = T - J_{23} + (1 - 3g/2)(J_{13}P_{13} + J_{12}P_{12}). \tag{17}$$

Let us put

$$E_1 = \int vH_1 v d\tau. \tag{18}$$

We have already found an approximation to

$$E_0 = \int uH_0 u d\tau.$$

[16] u and v are assumed normalized.

TABLE II. *Numerical coefficients occurring in f-integrals (individual particle coordinates).*

	1	u	u^2	u^3	u^4		1	u	u^2	u^3	u^4
$f_{00,\,00}$	1					$(2/3)^{\frac{1}{2}}f_{41,\,10}$			-2	$5/2$	
$f_{11,\,00}$		1				$(2/3)^{\frac{1}{2}}f_{41,\,01}$			$1/2$	$-5/2$	
$f_{10,\,10}$	1	-1				$(1/3)^{\frac{1}{2}}f_{42,\,00}$				$-5/4$	
$f_{20,\,00}$		$-(1/2)^{\frac{1}{2}}$				$(1/3)^{\frac{1}{2}}f_{40,\,20}$		-1	2	$-5/4$	
$f_{11,\,11}$	1	-2	3			$f_{22,\,22}$	1	-4	15	-30	$105/4$
$2^{\frac{1}{2}}f_{21,\,10}$		2	-3			$(2/3)^{\frac{1}{2}}f_{32,\,21}$		2	-9	20	$-35/2$
$2^{\frac{1}{2}}f_{21,\,01}$		-1	3			$f_{33,\,11}$			$9/2$	-15	$35/2$
$f_{20,\,20}$	1	-2	$3/2$			$f_{31,\,21}$	1	-4	$27/2$	-25	$35/2$
$f_{22,\,00}$			$3/2$			$(2/3)^{\frac{1}{2}}f_{42,\,20}$			$9/2$	-15	$105/8$
$f_{31,\,00}$			$-(3/2)^{\frac{1}{2}}$			$f_{43,\,10}$				5	$-35/4$
$(2/3)^{\frac{1}{2}}f_{30,\,10}$		-1	1			$f_{41,\,30}$		2	-9	15	$-35/4$
$f_{40,\,00}$			$(3/8)^{\frac{1}{2}}$			$f_{44,\,00}$					$35/8$
$f_{21,\,21}$	1	-3	$15/2$	$-15/2$		$f_{40,\,40}$	1	-4	9	-10	$35/8$
$f_{22,\,11}$		2	-6	$15/2$							
$2^{\frac{1}{2}}f_{22,\,20}$		-1	6	$-15/2$							
$(2/3)^{\frac{1}{2}}f_{31,\,11}$		-1	4	-5							
$(1/3)^{\frac{1}{2}}f_{32,\,10}$			$3/2$	$-5/2$							
$(1/3)^{\frac{1}{2}}f_{32,\,01}$			-1	$5/2$							
$(1/3)^{\frac{1}{2}}f_{31,\,20}$		1	-3	$5/2$							
$f_{33,\,00}$				$5/2$							
$f_{30,\,30}$	1	-3	$9/2$	$-5/2$							

If now we multiply 16 (a) and (b) by u and v, respectively, and integrate, we obtain

$$\left.\begin{aligned} E&=E_0+(b/a)\int uXv\,d\tau \quad \text{(a)}\\ E&=E_1+(a/b)\int vXu\,d\tau \quad \text{(b)}\end{aligned}\right\} \tag{19}$$

The two integrals appearing here are equal and will be denoted by

$$s=\int uXv\,d\tau. \tag{20}$$

b/a may be eliminated from 19 (a) and (b), so that the result will be

$$E=E_0+\tfrac{1}{2}\{E_1-E_0\pm[(E_1-E_0)^2+4s^2]^{\frac{1}{2}}\}. \tag{21}$$

To make this as small as possible the negative sign must be chosen. For small s this equation reduces to

$$E=E_0-s^2/(E_1-E_0),$$

which is essentially the result of Breit and Feenberg in a form in which it shows more clearly the meaning of E_1.

Both E_1 and s depend upon the choice of the antisymmetrical function v. The procedure now is to select a somewhat flexible v, to calculate E_1 and s according to (18) and (20), and to find the lowest value of (21). Two types of function were tried. The first was

$$v=(1/2)^{\frac{1}{2}}\phi_{000}(1)[\phi_{200}(2)\phi_{000}(3)-\phi_{000}(2)\phi_{200}(3)]$$

with a variable stiffness q in the oscillator functions. This gave somewhat poorer results than the second choice

$$v=c(J_{13}-J_{12})\psi_0(\sigma'). \tag{22}$$

$\psi_0(\sigma')$ is the function appearing in the list (13), but with a variable parameter σ' which need not be the same as σ. The normalizing constant turns out to be

$$c=2^{-\frac{1}{2}}A^{-1}\left[\left(\frac{\sigma'}{\sigma'+4}\right)^{\frac{3}{2}}-\left(\frac{\sigma'}{\sigma'+1}\cdot\frac{\sigma'}{\sigma'+3}\right)^{\frac{3}{2}}\right]^{-\frac{1}{2}}$$
$$\equiv 2^{-\frac{1}{2}}A^{-1}F(\sigma')^{-\frac{1}{2}}. \tag{22a}$$

With the use of (22), lengthy calculation gives

$$E_1=\left\{\frac{3}{2}\frac{\hbar^2}{Ma^2}\left[\left(\frac{\sigma'}{\sigma'+4}\right)^{\frac{1}{2}}-\frac{\sigma'^4(\sigma'+4)}{(\sigma'+1)^{5/2}(\sigma'+3)^{\frac{1}{2}}}\right](\sigma'+2)\right.$$
$$+3(1-g)\left(\frac{\sigma'^2}{\sigma'^2+6\sigma'+6}\right)^{\frac{1}{2}}A-(2-\tfrac{3}{2}g)$$
$$\left.\times\left(\frac{\sigma'}{\sigma'+3}\right)^{3}A-(1-\tfrac{3}{2}g)\left(\frac{\sigma'}{\sigma'+6}\right)^{\frac{1}{2}}A\right\}\Big/F(\sigma'),$$

$$s=(\tfrac{3}{2})^{\frac{1}{2}}Ag\left(\frac{\sigma}{\bar\sigma}\cdot\frac{\sigma'}{\bar\sigma}\right)^{9/4}F(\bar\sigma)/F^{\frac{1}{2}}(\sigma'),$$

where $\bar\sigma=\frac{1}{2}(\sigma+\sigma')$ and F is defined by 22a.

E_1 is in the range considered very nearly a linear function of σ', rising from 10.8 Mev at $\sigma'=0$ to 65.6 Mev at $\sigma'=2$. The best value of E_0-E comes at $\sigma'\approx 1.10$, where $E_1\doteq 42$ Mev and $s\doteq 1.85$; it is 0.070 Mev, an amount which is rather insignificant in view of the inadequacies of most variation methods.

According to (19), $(b/a)^2=[(E_0-E)/s]^2$. This, with our values, is 1.4×10^{-3}. It represents the probability that in the normal state of H^3 the neutron spins shall be parallel.

III. Variation Method Applied to He^4

An application of the method described in II A to the alpha-particle entails considerable labor and has not been carried out at present. It has seemed preferable first to employ the Hartree method with the same class of functions as that used in Section II B. We know that, for H^3, this procedure misses 1/3 Mev of what the use of relative coordinates would yield, and the latter is probably in error by +1/2 Mev. The true convergence limit for He^4 is therefore expected to be probably about 1 Mev below the value obtained with the use of the present scheme.[17]

[17] The value of σ for He^4 is 2.6 as against 1.83 for H^3. This means that the wave function is more strongly concentrated about the origin and that the *wrong* asymptotic behavior of the Hermite functions is less serious. Hence the convergence is more rapid for He^4 than for H^3 (and for H^3 than for H^2). On the other hand, the absolute error in He^4, for equal rates of convergence, is greater than for H^3 because of the greater number of $E_{pot}-E_{kin}$ terms in the Hamiltonian.

The Hamiltonian operator (11) has the form

$$H=(\hbar^2/M)(-\tfrac{3}{8}\sum_i\nabla_i^2+\tfrac{1}{4}\sum_{i>j}\nabla_i\cdot\nabla_j)-B\sum_1 \times\exp[-r_{ij}^2/a^2]P_{ij}-C\sum_2\exp[-r_{ij}^2/a^2]P_{ij}.$$

If we choose 1,2 and 3,4 to be the pairs of like particles, H is invariant with respect to the following group of permutations:

$$\begin{aligned} P_0&=E, & P_4&=P_{13}P_{24},\\ P_1&=P_{12}, & P_5&=P_{13}P_{24}P_{12},\\ P_2&=P_{34}, & P_6&=P_{13}P_{24}P_{34},\\ P_3&=P_{12}P_{34}, & P_7&=P_{13}P_{24}P_{12}P_{34}. \end{aligned}$$

We choose functions of the same symmetry. If this is done explicitly with the use of the P symbols in the above table, the calculation of the matrix elements is greatly facilitated. We have used the following functions

$$\begin{aligned}
&\phi_{000}(1)\phi_{000}(2)\phi_{000}(3)\phi_{000}(4) &&=\psi_0\\
&\tfrac{1}{2}(P_0+P_1+P_4+P_7)\phi_{200}\phi_{000}\phi_{000}\phi_{000}\\
&(1/2)^{\frac{1}{2}}(P_0+P_4)\phi_{100}\phi_{100}\phi_{000}\phi_{000}\\
&\tfrac{1}{2}(P_0+P_1+P_2+P_3)\phi_{100}\phi_{000}\phi_{100}\phi_{000}\\
&\tfrac{1}{2}(P_0+P_1+P_4+P_7)\phi_{400}\phi_{000}\phi_{000}\phi_{000}\\
&\tfrac{1}{2}(P_0+P_1+P_4+P_7)\phi_{220}\phi_{000}\phi_{000}\phi_{000}\\
&\tfrac{1}{2}(P_0+P_1+P_4+P_7)\phi_{300}\phi_{100}\phi_{000}\phi_{000}\\
&(1/8)^{\frac{1}{2}}\sum_{i=0}^{7}P_i\phi_{300}\phi_{000}\phi_{100}\phi_{000}\\
&(1/2)^{\frac{1}{2}}(P_0+P_4)\phi_{200}\phi_{200}\phi_{000}\phi_{000}\\
&\tfrac{1}{2}(P_0+P_1+P_2+P_3)\phi_{200}\phi_{000}\phi_{200}\phi_{000}\\
&\tfrac{1}{2}(P_0+P_1+P_4+P_7)\phi_{210}\phi_{100}\phi_{000}\phi_{000}\\
&(1/8)^{\frac{1}{2}}\sum_{i=0}^{7}P_i\phi_{210}\phi_{000}\phi_{100}\phi_{000}\\
&(1/2)^{\frac{1}{2}}(P_0+P_4)\phi_{110}\phi_{110}\phi_{000}\phi_{000}\\
&\tfrac{1}{2}(P_0+P_1+P_2+P_3)\phi_{110}\phi_{000}\phi_{110}\phi_{000}.
\end{aligned}$$

Except in ψ_0, the arguments of the functions have not been indicated explicitly; they are understood to run consecutively. In computing the H_{ij} we make use of the invariance of H with respect to all P_i's, and look up products of the P_i in a suitably constructed group table. This allows identical terms in every H_{ij} to be recognized at once and aids in collecting them.

The potential energy terms corresponding to the previous S_{ij}, T_{ij}, U_{ij} are again separable into products of f integrals which were listed in Table II. H_{00} has its minimum value of -25.63 Mev for $\sigma=2.60$. The Coulomb energy raises this to -24.81 Mev. (This result is very sensitive to the choice of force parameters, and since these were chosen somewhat arbitrarily in this work, we do not wish to emphasize it too strongly.) The functions included in the list above contribute -1.04 Mev. This amount agrees almost exactly with that obtained by Inglis if only the second order perturbation, with a similar set of functions, is employed. The third order raises this value again by 0.25 Mev, so that the variation method, for the case of He, is more effective than perturbation theory by this amount.

We hope to return to the He^4 problem and to treat it in a manner similar to that of Section II A. For the present it seems well to be cautious in estimating the convergence limit. We feel, for reasons already mentioned, that the binding energy may lie as much as 1 Mev below the limit we have obtained. This estimate would place it at 27 Mev, not far from the experimental value, 27.6 Mev.

Cosmic Rays on the Pacific Ocean

A. H. COMPTON
University of Chicago, Chicago, Illinois

AND

R. N. TURNER
Canadian Australasian Steamship Company

(Received August 30, 1937)

Records of cosmic-ray intensity obtained on the R. M. S. Aorangi during 12 voyages between Vancouver, Canada and Sydney, Australia, from March 17, 1936, to January 18, 1937, using a Carnegie model C cosmic-ray meter, are described and discussed. Typical records exhibiting the latitude effect are shown. A summary of the data taken at sea is given in the form of graphs, in which each datum point represents the average of 6 hours readings with a probable statistical error of ±0.13 percent. Any variations due to a possible temperature coefficient of the instrument are negligible. The observed minimum of cosmic-ray intensity near the equator averages 10.3 percent less than the intensity at Vancouver, in satisfactory agreement, considering the difference in experimental conditions, with earlier measurements. The critical latitudes above which changes in intensity are less rapid, are found to be somewhat lower, 38.4°N and 34.2°S, than previously reported, and beyond these latitudes the intensity is found to continue to increase with latitude. At the higher latitudes is observed a variation, which appears to be seasonal, with the maximum in the cold months in both hemispheres. This variation is closely correlated with the atmospheric temperature. It is hence ascribed to changes in some atmospheric barrier of unknown nature, such as perhaps an atmospheric potential gradient, of whose strength the temperature of the atmosphere is an approximate but not exact index. Changes in this atmospheric barrier have been approximately allowed for by determining the external temperature coefficient and correcting the observations accordingly (this external temperature coefficient is comparable with that reported by Hess and his collaborators). The latitude effect curves as thus corrected should show the effect of the earth's magnetic field alone. They are now nearly flat beyond the critical latitudes and show a magnetic latitude effect of about 7.2 percent. This implies that a latitude effect of about 3.1 percent owes its origin to the atmospheric barrier. Seasonal variations in the corrected latitude effect curve are almost eliminated. Geomagnetic analysis of the energy distribution of the rays indicates a prominent component with a sharp energy threshold of about 7.5×10^9 ev, and a component so weak as to be questionable, whose energy threshold is not greater than 2.5×10^9 ev. It is not found possible to explain the 7.5×10^9 ev threshold in terms of atmospheric absorption as has previously been supposed. Two alternative interpretations are suggested. The difference in cosmic-ray intensity between the northern and southern hemispheres under comparable conditions, as calculated from these data in various ways, appears to be no larger than the probable error of about ±0.1 percent. This result is in conflict with the prediction by Compton and Getting of an excess in the north of about 0.5 percent, due to the motion of the earth with the rotation of the galaxy, but is not inconsistent with the small diurnal variation that has been found to follow sidereal time, if it is supposed that the cosmic rays acquire a part of the galactic motion.

THROUGH the courtesy of the Canadian Australasian Steamship Company, we have been able to carry through a year of almost continuous cosmic-ray measurements on their motor ship Aorangi (17,500 tons), as it has plied the Pacific Ocean between Vancouver, British Columbia, and Sydney, New South Wales. This route, shown in the map of Fig. 1, covers the greatest range of geomagnetic latitudes of any of the regular passenger lines. The two main objectives were to obtain a precise comparison of the cosmic rays in the northern and southern hemispheres, and to learn more accurately their intensity at different latitudes at different seasons.

COLLECTING THE DATA

The measurements were made with one of the Carnegie model C cosmic-ray meters. This consists of a 19.3*l* ionization chamber, shielded with lead shot equivalent to 12 cm of solid lead, and has been described in detail elsewhere.[1] The only modifications required were mounting the meter on a strong conical steel base to hold it firmly during the rolling of the ship, and the use of a special Lindemann electrometer. This electrometer had a suspension so stiff as to operate at about twice the usual voltage on the quadrants. The

[1] A. H. Compton, E. O. Wollan and R. D. Bennett, Rev. Sci. Inst. 5, 415 (1934).

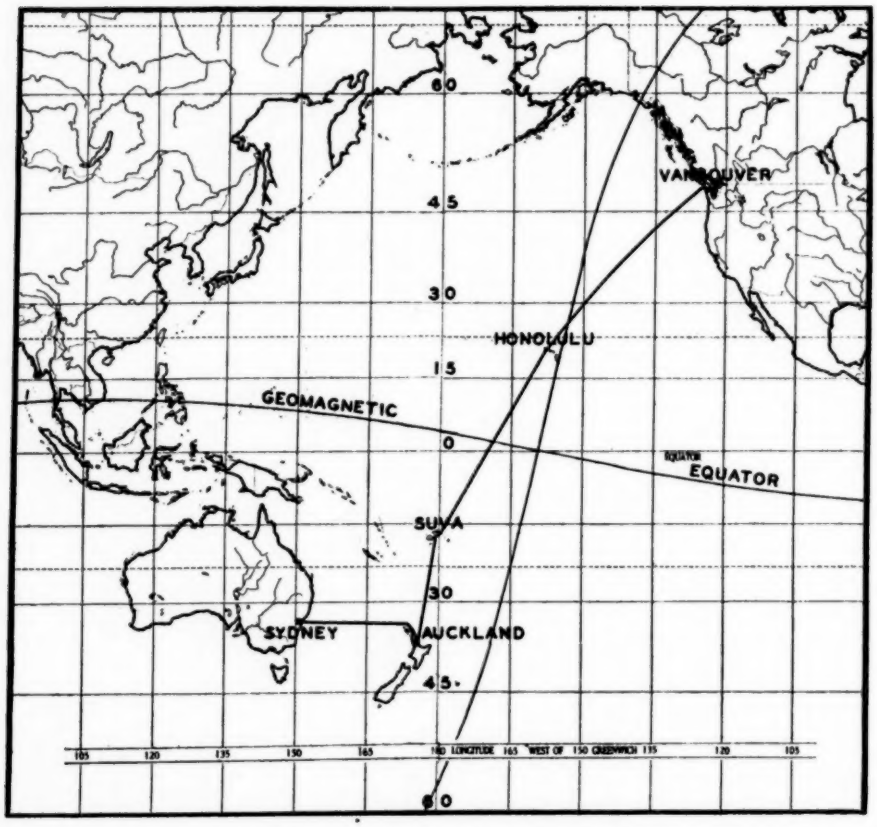

FIG. 1. Route of R. M. S. Aorangi.

effect of this is to increase the relative importance of the electrical forces on the needle as compared with the mechanical forces introduced by the rolling and pitching of the ship. During rough weather the ship's motion blurred the record appreciably, but did not prevent it from remaining accurately legible.

The meter was placed in a small wooden house built for the purpose on the aft deck of the ship (Fig. 2). While no attempt was made to keep the meter at constant temperature, the observatory has a double roof with a ventilated air space between the two layers to avoid excessive heating by the sun, and is supplied with an electric heater used to prevent the temperature from falling below about 12°C.

In Fig. 3 is shown a typical portion of the record, taken between 39° and 8° south geomagnetic latitude. The white line shows the drift of the electrometer needle, which is grounded at the end of each hour. The position of the uranium rod is so adjusted that the cosmic-ray ionization is approximately balanced by the beta-ray ionization in the balance chamber. At higher latitudes it will be seen that the electrometer needle moves upward, indicating an excess of cosmic rays; whereas the downward motion near the equator means a reduced intensity of the cosmic rays. The dark line is the photobarograph trace. Greenwich dates and hours are used.

In Fig. 4 the cosmic-ray minimum near the equator is made more evident by tracing the electrometer record for every eighth hour on a run from Auckland (41°S) to Vancouver (55°N). The high readings near 44°N are attributable to a low barometer. The record taken nearest the local noon hour is indicated in each case by the letter *M*. In the equatorial regions, daily variations can be noticed with their maxima near noon.

Daily readings were made of the ship's mercury barometer in order to standardize the photobarograph readings, and the ship's barograph record was used as an additional check. The daily

log included also the ship's position, the outside and meter-house temperatures, and the weather conditions. For standardizing the data, the daily values of the argon pressure (about 750 lbs. per in.^{2}), the sensitivity voltage (about 1.5 volts) applied once every four hours to the electrometer needle, and the ionization chamber voltage (about 250 volts) were also recorded.

Analysis of the Data

In analyzing the data, the hourly deflections were tabulated and averaged in groups of 6 hours to reduce the labor of calculation. When a burst of ions causing a sudden deflection of more than 1 division was recorded, as, for example, at 17:20 GT on April 28 (cf. Fig. 3), the burst deflection was subtracted to obtain the net deflection for the hour. From the observed sensitivity of the electrometer over this interval, this average deflection was reduced to millivolts per standard atmosphere of argon. The barometer effect was determined by correlating these values with the barograph readings averaged over the same intervals. From the first few months a barometer effect of -10 millivolts per atmosphere of argon per inch of mercury was determined, which value was used throughout. This corresponds to -1.6 percent per cm of mercury, which is close to the mean value found by Doan[2] for a group of similar meters. Following the usual procedure,[1] the absolute ionization at the latitude of Chicago, as reduced to standard barometer and corrected for residual ionization as determined in a deep mine near Chicago, was found to be 249 millivolts per hour per atmosphere of argon. This corresponds to 82 ions per cm^3 per sec. in 50 atmospheres of argon, or 1.22 ions per cm^3 per sec. in standard air. Our final observed intensities, after applying the barometer correction, are expressed in percentages of this normal ionization.

All of the data obtained while the ship was at sea between Auckland and Vancouver during the interval from March 17, 1936 to January 18, 1937 are shown in Fig. 5. To avoid too much overlapping, the curves are grouped into seasons, with a different base-line for each season. Here each point represents the average of 6 hours' record, calculated as described above. Judging from the variations from hour to hour, the probable statistical variation of each hour's reading is 0.3 percent, whence that for a 6-hour reading is 0.13 percent. As we shall see below, the temperature coefficient of the meter is insignificant, and we have been unable to find any source of appreciable systematic error. When there is an abnormally high or low barometer, a possible error in the assumed value of the barometer coefficient may introduce a small error into the reduced data. This cannot, however, account for the observed changes at low latitudes, where the barometer changes are small. Thus, for example, the fluctuations of the order of 0.6 percent in cycles of four 6-hour intervals are to be considered as diurnal variations of significant magnitude.

Annual Mean and Seasonal Differences

Figure 6 shows the mean of all the observations taken between Auckland and Vancouver. Each point represents the arithmetic average of the values observed within the corresponding 2.5°

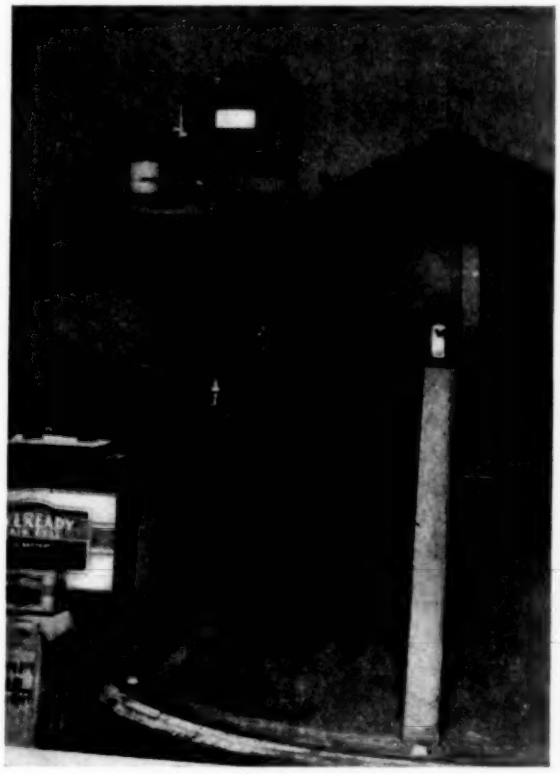

Fig. 2. Cosmic-ray meter in observatory on deck of Aorangi.

[1] R. L. Doan, Phys. Rev. 49, 107 (1936).

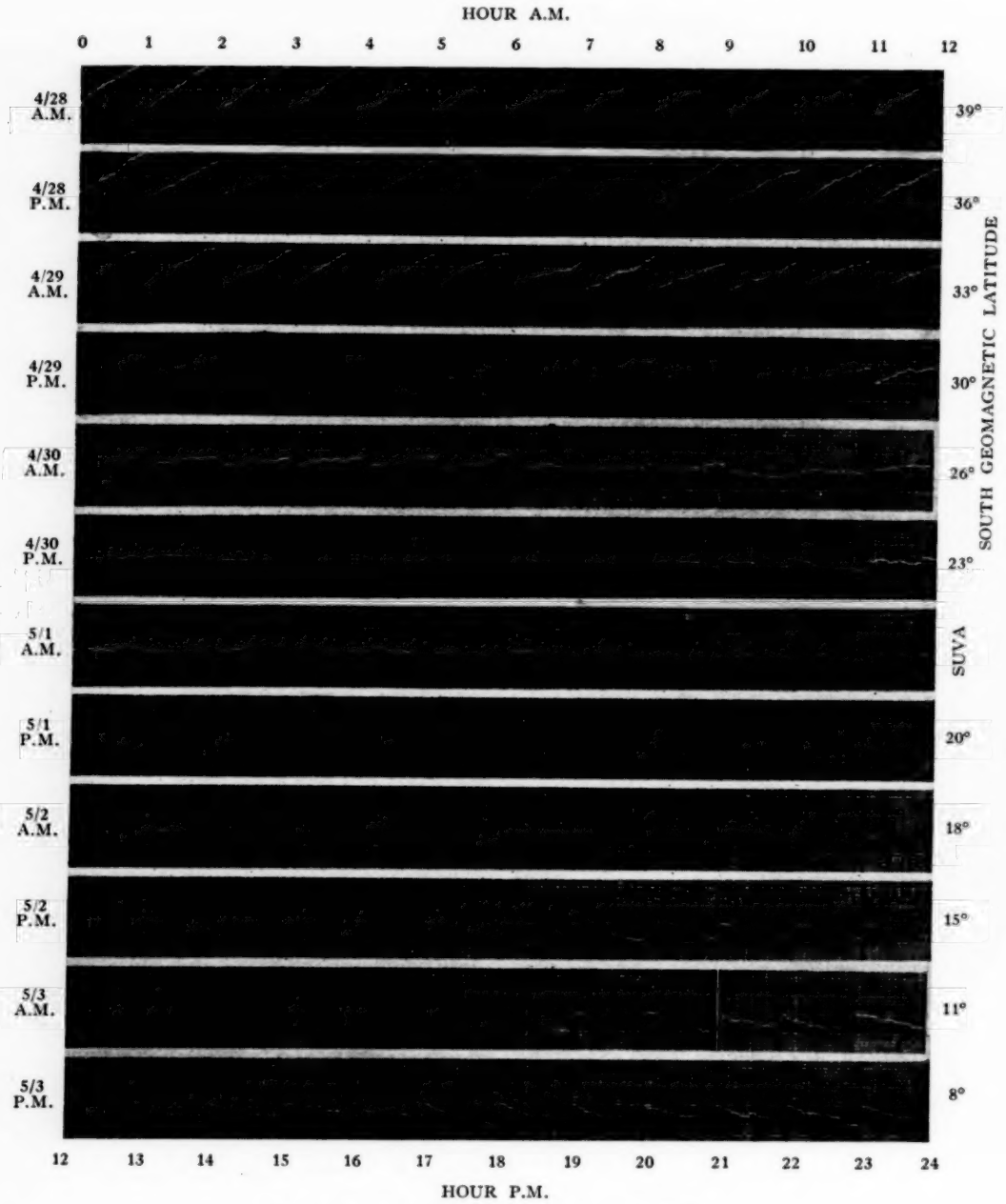

FIG. 3. Typical record showing latitude effect.

interval. The slight fluctuations near 20°N are not ascribable to experimental error, but rather to the fact that the ship was always at Honolulu (21.2°N) at noon, when the cosmic rays are most intense. The total change between Vancouver and the equator is 10.3 percent, which is the average of seasonal means that vary from 8.7 percent in the autumn to 12.4 percent in the winter months.

Previous measurements over the same route include the value of 13 percent given by Compton,[3] as based on measurements with a shield equivalent to 6.5 cm of lead, and the value of 11 percent given by Millikan and Neher,[4] who used a shield equivalent to 12 cm of lead, the same as

[3] A. H. Compton, Rev. Sci. Inst. **7**, 71 (1936), Fig. 1.
[4] R. A. Millikan and H. V. Neher, Phys. Rev. **50**, 15 (1936), Fig. 14.

that for the measurements here reported. Because of the greater consistency of the data and the larger number of trips from which the results are averaged, the variation of cosmic rays with latitude shown in Fig. 6 is of a higher order of reliability than are the isolated exploratory data given in these earlier reports.

A striking difference between the annual mean latitude effect curve here obtained and those previously reported[5] is the absence of any really flat "plateau" for the high latitudes. The well-known "knee" is confirmed, though it is found at a somewhat lower latitude (34.2°S and 38.4°N) than previously observed (e.g., 40–45° by Compton,[6] 41° by Millikan and Neher[4] on the Pacific, and 55° by Hoerlin[7] in Europe. At latitudes higher than the knee, however, the intensity continues to increase with latitude, though at a slower rate. This phenomenon is more clearly apparent in Fig. 7, which compares the latitude effect as observed during the various seasons, and shows marked differences in the high latitude portions of the curves at different times of year. Most noticeable is the fact that in the winter the curve remains steep as far north as Vancouver, whereas in the autumn the change north of 40° is very small.

Closely associated with this difference in shape is the fact, evident from Fig. 7, that in both the northern and southern hemispheres the intensity is greater during the cold months. Since after about a year the latitude effect curve has returned to approximately its original form, it would appear that the change follows an annual cycle. On the basis of the present evidence, these maxima and minima of cosmic-ray intensity seem to occur approximately during the cold and hot months respectively, rather than at the winter and summer solstices. This indicates that the origin of the change is atmospheric rather than astronomical.

Correlation of Ionization with Atmospheric Temperature

The design and previous tests[1] had seemed to preclude the possibility of a temperature coefficient of the meter itself. We have, however, obtained a further test with the meter as it is used, in the following manner: For each of the four seasonal curves the departure of the ionization from the annual mean was noted for each 2.5° interval of latitude. These departures in the ionization were compared (Fig. 8) with the departure in the temperature of the meter from

[5] E.g., references 3 and 4. It is noteworthy that the recent counter measurements of T. H. Johnson and D. N. Read (Phys. Rev. **51**, 557, 1937) between New York and Valparaiso show a sloping plateau and season variations which, though provisionally ascribed to a temperature coefficient of the meter, appear to be of the same kind as those noted here.

[6] A. H. Compton, Phys. Rev. **43**, 387 (1933).

[7] H. Hoerlin, Nature **132**, 61 (1933); Naturwiss. **21**, 822 (1933).

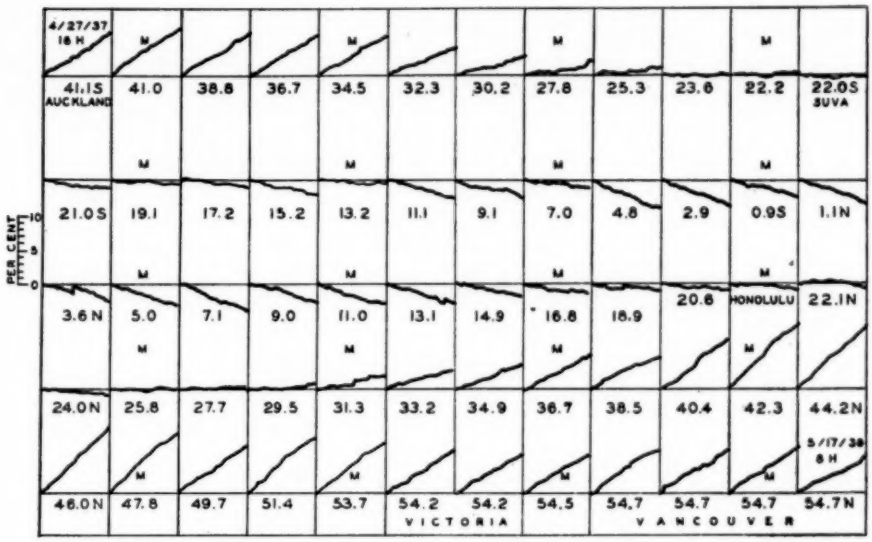

FIG. 4. Record of every eighth hour from Auckland to Vancouver.

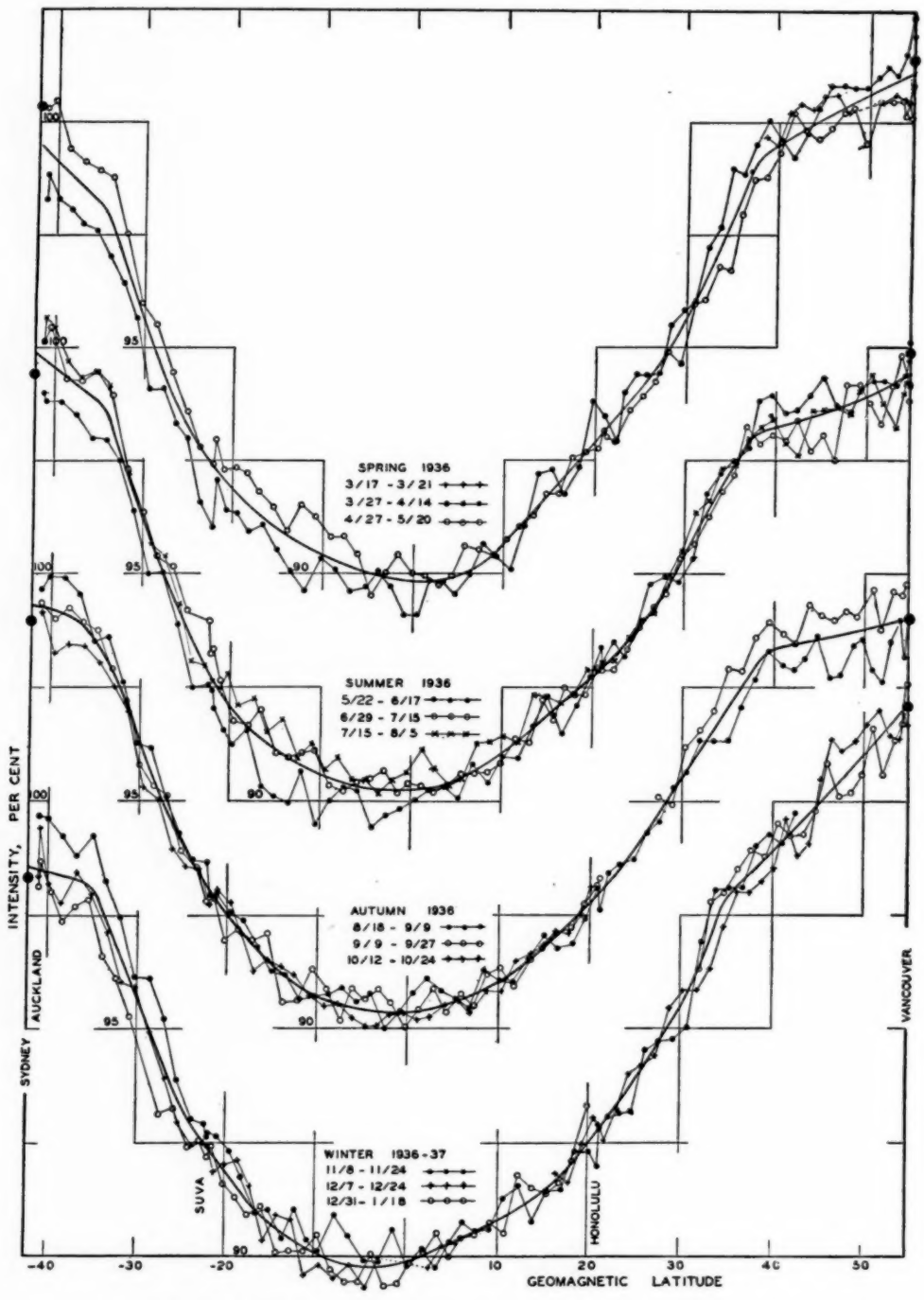

FIG. 5. Individual latitude effect curves for each trip, grouped into seasons.

its annual mean at the same latitude. The temperature of the meter was measured by the argon pressure, which thus served as a gas thermometer. Fig. 9 shows the scatter diagram of the points thus obtained. The erratic character of the pattern is of itself evidence that temperature changes of the meter cannot account for the main part of the fluctuations. The apparent temperature coefficient of the meter, in terms of the argon pressure changes, as calculated from these

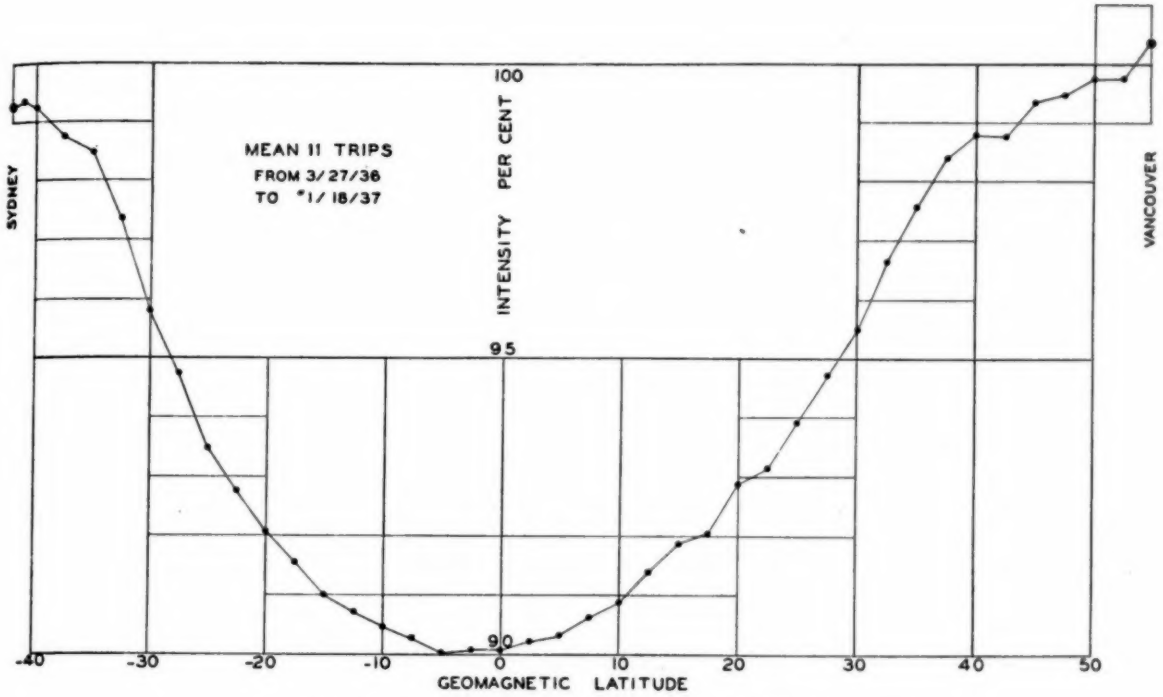

FIG. 6. Year's average of all data between Auckland and Vancouver.

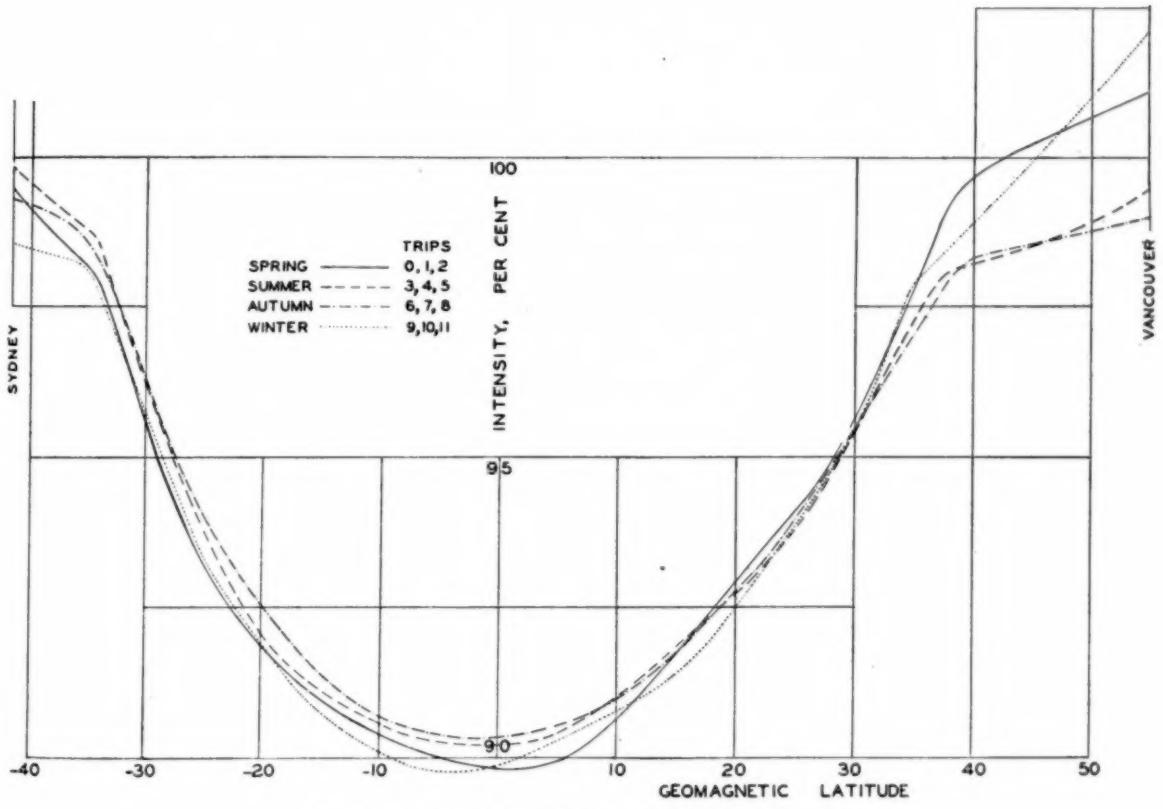

FIG. 7. Latitude effect curves for the various seasons.

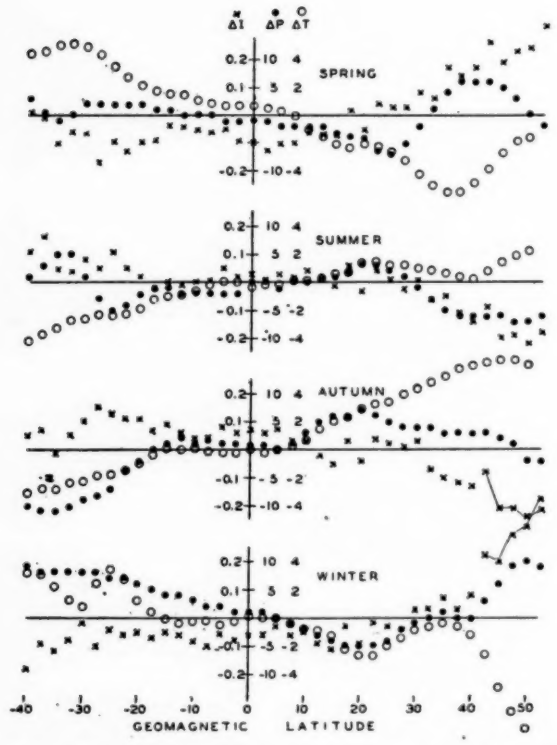

FIG. 8. Seasonal departures from annual mean of ionization (ΔI), argon pressure (ΔP, which measures the meter temperature), and shade temperature of the outside air (ΔT), plotted for the various latitudes.

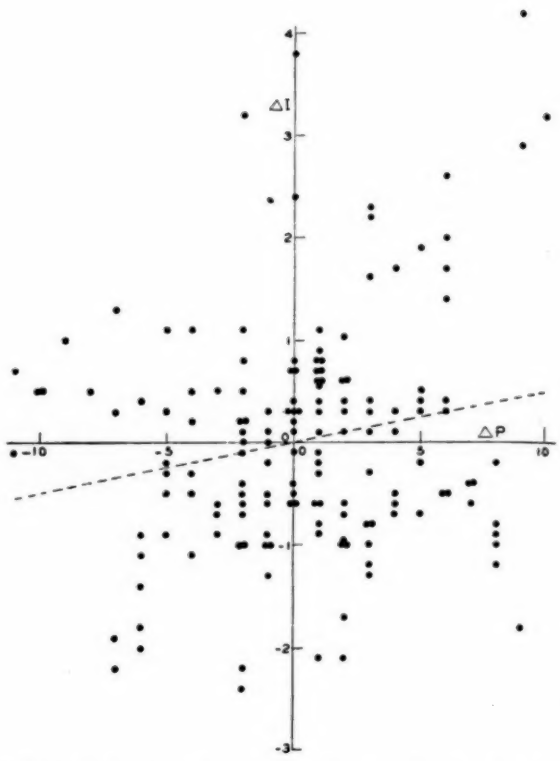

FIG. 9. Scatter diagram of ΔI *vs.* ΔP, showing low correlation and negligible temperature coefficient of the meter.

data, is 0.048 ± 0.014 percent per °C, with a correlation factor of only 0.18 ± 0.05. A slight positive correlation must occur between the argon pressure and the observed ionization because during the cold months when the ionization is high the meter house was so heated that the argon pressure averaged slightly higher than during the warm months. The small observed correlation does not therefore imply any true temperature coefficient of the meter. When a correction of the calculated magnitude is applied in accord with the temperature of the meter, no appreciable change in the slope of the curves is effected, nor is the difference between the winter and the summer curves appreciably reduced. This means that any possible temperature coefficient of the meter is insignificant.

On the other hand, a similar analysis shows a definite correlation of opposite sign between the external shade temperature and the observed ionization. In Fig. 8 are shown the departures from the annual mean values at each latitude of the external temperature for each season of the year. The opposing trend of this temperature and the ionization is evident in every curve. From a scatter diagram of δT *vs.* δI similar to Fig. 9, it is found that the correlation factor is -0.68 ± 0.03 and the external temperature coefficient of the ionization is -0.18 ± 0.011 percent per °C. This is 16 times the probable error, and hence real. In a similar manner, the values of the external atmospheric temperature coefficient have been obtained from the records made in port. These are given in Table I.

It will be noted that at Vancouver and Auckland the observed coefficient is in acceptable agreement with that found at sea. At Sydney, however, the coefficient observed differs from that at sea by much more than the experimental error. This difference seems to reflect the fact that at Sydney the air from over the land is subject to much wider temperature fluctuations than is the sea air which is prevalent at the other ports. This indicates in turn that the effect on the cosmic rays is not due directly to temperature changes in the lower atmosphere in the im-

mediate neighborhood of the meter, but rather to some other changes in atmospheric condition for which the temperature serves as an approximate index. Such atmospheric conditions might for example include the electric potential gradient, or the height of the Heaviside layer.

Atmospheric and Magnetic Latitude Effects

In Fig. 10, in the broken lines, are shown the corrections to be applied to the seasonal curves of Fig. 7 to correct for the changes in this atmospheric barrier, supposing that its strength is represented by an external temperature coefficient of -0.18 percent per °C, and reducing the data to the mean value of 21°C. These broken curves thus represent a latitude effect of atmospheric origin, differing with the seasons, which must be subtracted from the observed latitude effect curves to obtain the effect caused by the earth's magnetic field. The solid curves of Fig. 10, as thus calculated, should accordingly represent the part of the latitude effect which is of magnetic origin. It will be noted that the atmospheric latitude effect is roughly half as great as the magnetic latitude effect (average of 3 percent and 7 percent respectively). Moreover, the resulting magnetic latitude effect curves now show much smaller, almost insignificant, seasonal changes, smaller north-south asymmetry, and the plateaus beyond 35°S and 39°N have become nearly flat.

Correlation of cosmic-ray ionization with temperature and with time of year similar to that here discussed has been noted by others. Thus, Hoffmann,[8] Messerschmidt,[9] Hess and Steinmaurer,[10] and Steinke,[11] among others, have considered the possible effect of temperature changes on the diurnal variations in ionization. Hess, Graziadei and Steinmaurer[12] have found in the data collected on the Hafelekar during 1932–34 evidence similar to that here presented for greater intensity in the cold months than for the warm months of the year, showing a close correlation with the external temperature. The difference which they observe between the months November to April and the months May to October is 1.2 percent as compared with our differences of 2.4 percent at Vancouver and -1.0 percent at Auckland and Sydney. The mean annual external temperature coefficient which they observe is -0.09 percent, not greatly different from that which we find for Sydney. From the more detailed study of these data by Priebsch and Baldauf,[13] however, it appears that the temperature coefficient varies from month to month. This supports the view expressed above that we are not concerned here with an effect due directly to changes in the temperature of the atmosphere, but rather with an effect of some other origin, presumably atmospheric, to which the temperature is only an approximate index.

Some earlier reports dealing with seasonal changes in cosmic rays by Clay,[14] Steinke,[15] and Priebsch and Steinmaurer,[16] indicated several percent change with a maximum in summer. This is opposite in sign to the effect present in our records and those of Hess, Graziadei and Steinmaurer.[12]

Variations at the Equator—Absence of Solar Rays

At the equator the curves of both Figs. 7 and 10 show a small change which appears to follow an annual cycle. Since seasonal differences do not occur at the equator, it seems reasonable to associate the 0.4 percent greater intensity observed during the half-year May to October with the greater distance of the earth from the sun during this interval. It will be recalled that the eccentricity of the earth's orbit is 1.68 percent,

Table I. *Atmospheric temperature coefficient of cosmic-ray ionization (reduced to standard barometer)*

Location	Coefficient Percent	Prob. Error Percent	Correlation Factor
Vancouver	-0.22	± 0.02	-0.85 ± 0.04
Auckland	-0.16	± 0.04	-0.47 ± 0.15
Sydney	-0.10	± 0.02	-0.67 ± 0.10
At sea	-0.18	± 0.01	-0.68 ± 0.03

[8] G. Hoffmann, Zeits. f. Physik **69**, 259 (1931).
[9] W. Messerschmidt, Zeits. f. Physik **78**, 668 (1932).
[10] V. F. Hess and R. Steinmaurer, Berlin Ber. **22**, 672 (1933).
[11] E. G. Steinke, *Handbuch der Physik*, Geiger u. Scheel, **23** II, 521 (1933).
[12] V. F. Hess, H. Th. Graziadei and R. Steinmaurer, Ber. Wien Ak. IIa, **143**, 313 (1934).
[13] J. A. Priebsch and W. Baldauf, Ber. Wien Ak. IIa, **145**, 583 (1936).
[14] J. Clay, Proc. Roy. Acad. Amsterdam **23**, 711 (1930).
[15] E. G. Steinke, Zeits. f. Physik **64**, 48 (1930).
[16] J. A. Priebsch and R. Steinmaurer, Gerl. Beitr. z. Geophys. **37**, 296 (1932).

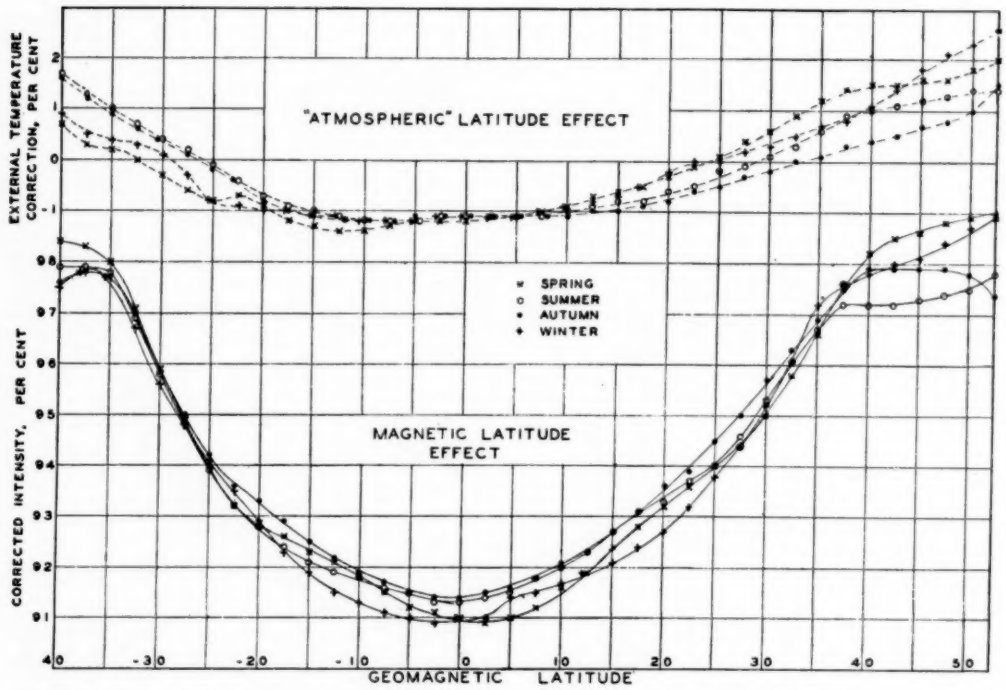

FIG. 10. Magnetic (solid lines) and atmospheric (broken lines) latitude effect for the four seasons. Sum of these two effects gives observed total effect of Fig. 7.

with the perihelion on January first. Assuming the inverse square law to apply, the intensity of the solar component should thus be 6.7 percent greater in January than in July. The observed excess of cosmic rays during the middle of the year is thus opposite in sign to any variation that would be caused by rays emitted from the sun itself, and confirms the conclusion previously drawn from other evidence that any contribution to the cosmic rays by the sun must be relatively small. Vallarta's hypothesis[17] of a shielding effect caused by the sun's magnetic field would, however, lead to an annual change of the observed sign and very possibly of the observed order of magnitude. One would anticipate on this hypothesis a minimum on January first, which is not in perfect phase agreement with our data. The difference is, however, within the probable error of a single year's measurements.

In a recent note,[18] Julian Thompson has called attention to the diurnal variation that is evident in the data of Fig. 5. He finds that the average daily variation of 0.6 percent at the equator is almost identical with that at latitude 50°, and has its maximum near noon, as has been found by others working at the higher latitudes. It is hoped that a further analysis of these diurnal changes may be published in the near future.

COMPARISON OF THE NORTHERN AND SOUTHERN HEMISPHERES

The interpretation of our data with regard to the relative intensity in the northern and southern hemispheres depends upon our treatment of the seasonal variations. When uncorrected for external temperature, though no flat intensity maxima occur, it is nevertheless possible to locate corresponding cosmic-ray latitudes in the two hemispheres by locating the "knees" between the steeply-sloping and the gradually-sloping parts of the curves. Fig. 11 shows the location of these knees, obtained from the individual curves of Fig. 5 by drawing approximately straight lines through the datum points. The average positions of the knees is thus found to be, at geomagnetic latitude 38.4 ± 0.4°N, critical intensity $I_n=98.87\pm0.16$ percent; at 34.2 ± 0.1°S, critical intensity $I_s=98.41\pm0.16$ percent. Thus the intensity of the cosmic rays as directly observed at the

[17] M. S. Vallarta, Nature **139**, 839 (1937).
[18] J. Thompson, Phys. Rev. **52**, 140 (1937).

northern knee is greater than that at the southern knee by

$$I_n - I_s = 0.46 \pm 0.22 \text{ percent.}$$

In a preliminary report based upon a part of these data,[19] this difference was given as 0.6 percent.

This determination, however, leaves out of account the significant factor which causes the increase in cosmic-ray intensity above the critical latitude of the knee. The fact that this increase varies with the seasons shows that it is not determined by either the earth's magnetic field or the absorption in the atmosphere. Its close correlation with the atmospheric temperature indicates that we are, however, concerned with some kind of atmospheric barrier. If we assume that the temperature gives a reliable measure of the strength of this barrier, a correction for the difference in external temperature at the two knees will account for the corresponding difference in this barrier. Thus the average shade temperature at the northern knee was 2.1°C lower than at the southern knee. If the external temperature coefficient is taken as 0.18 deg.$^{-1}$ C, as determined above, a correction of 0.38 percent should be applied, leaving the critical intensity greater in the north by

$$I_n - I_s = 0.08 \pm 0.15 \text{ percent,}$$

which is an insignificant difference. (The probable error is reduced because the differences in the individual corrected values of I_n and I_s are less than in the uncorrected values.)

An alternative method of applying the correction for the atmospheric barrier is to compare the mean values of the corrected seasonal intensities as shown in Fig. 10 on the northern and southern plateaus. For the 7.5° zone south of the southern knee, the average intensity is 97.87 percent, while for an equal range north of the northern knee the intensity is 97.88 percent. This difference is,

$$I_n - I_s = 0.01 \pm 0.11 \text{ percent,}$$

which is likewise insignificant.

Another though less precise procedure is to compare the uncorrected intensities at the same north and south geographic latitudes, in both cases taken well above the critical latitude so that the earth's magnetic field no longer has a determining influence on the intensity. Our data do not extend to sufficiently high latitudes to ensure freedom from all magnetic effects. By way of illustration, however, at geographic latitudes 36° north and south, which correspond to geomagnetic latitudes 38.4°N and 40.2°S, the mean ionizations uncorrected for external temperature are $I_{36n} = 98.87 \pm 0.16$ percent and $I_{36s} = 99.30 \pm 0.18$ percent. The difference is now opposite in sign,

$$I_{36n} - I_{36s} = -0.43 \pm 0.24 \text{ percent,}$$

which considering the magnitude of the probable error is of doubtful significance.

It would thus appear that under comparable conditions, at latitudes of about 40°, the intensities in the northern and southern hemispheres probably do not differ by more than the experimental error, which is of the order of 0.1 or 0.2 percent. This result seems to be in definite conflict with the prediction by Compton and Getting[20] of an excess in the north of about 0.5

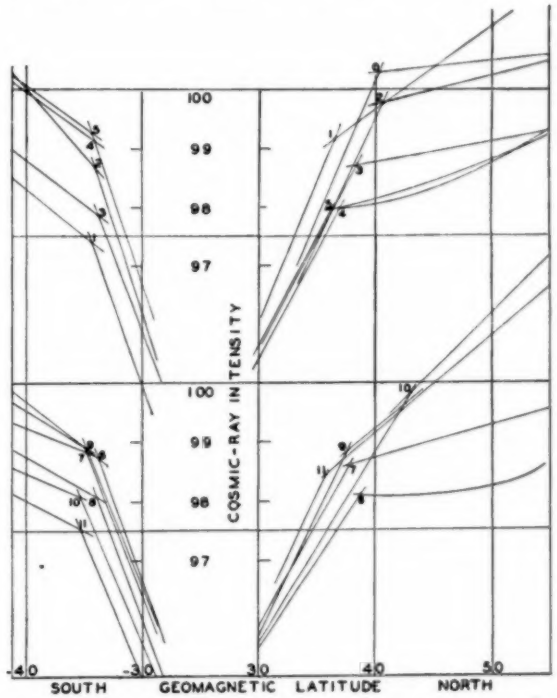

FIG. 11. Location of the critical latitude "knees" of the latitude effect curves of Fig. 5.

[19] A. H. Compton, Phys. Rev. **50**, 1119 (1936).

[20] A. H. Compton and I. A. Getting, Phys. Rev. **47**, 817 (1935).

percent, due to the motion of the earth with the rotation of the galaxy.

Studies by Illing[21] of the data obtained by Hess in Austria, and by Schonland, Delatizky and Gaskell[22] in South Africa have strongly confirmed the existence of a diurnal variation following sidereal time, whose phase accords with that predicted from the galactic rotation theory, but whose magnitude is somewhat smaller than anticipated.[19] If the cosmic rays come directly from outside the Milky Way, the only means of reconciling these measurements with the theory of Compton and Getting would seem to be on the assumption that the sun's motion with the rotation of the galaxy is only a small fraction of the 300 km per second estimated by the astronomers. A more probable solution would seem to be that the cosmic rays are for the most part trapped within the galaxy and to a large extent share its motion. It will be noted that the present experiments would be consistent with an excess in the north at least 30 percent as great as predicted by the theory, and are hence not inconsistent with such a modified interpretation of the sidereal time variation observations. It may be added that if the cosmic rays are for the most part trapped within the galaxies, they should presumably be free from the "red-shift" loss of energy which affects starlight, and the problem of accounting for the stupendous energy of the rays becomes somewhat less difficult.[23]

Energy Distribution of Primary Cosmic Rays

Following the procedure of Zanstra,[24] we may use these latitude data as a basis for an approximate determination of the energy distribution of the primary cosmic rays. If E_0 is the threshold energy of the electrical particles which are able to transverse the magnetic field of the earth at a given magnetic latitude λ, the cosmic-ray ionization I may be plotted as a function of E_0. Thus in Fig. 12 is shown the mean cosmic-ray intensity I for the year, corrected for the atmospheric barrier as in Fig. 10, as a function of λ. E_0 as a function of λ is given by Lemaitre and Vallarta[25] for various angles of incidence. We have used their curve for vertical incidence as a sufficiently close approximation to the average for all angles, and the units used are those appropriate to electron primaries. Thus the solid curve of Fig. 13, giving I as a function of E_0, is obtained. The values of I represented by the datum points on this curve are the arithmetical means of the corrected observed values within the corresponding ranges, and are identical with those of Fig. 12. The energy distribution, in terms of the fraction of the ionization per unit energy range of the primary particles, is then

$$\phi(E) = -dI/dE_0. \tag{1}$$

This function, as obtained graphically from the solid line of Fig. 13, is shown in the broken line of the same figure. It will be seen that within experimental error the distribution consists of two sharply-separated portions, one of 1.35 percent per 10^{10} ev for energies less than 7.5×10^9 ev, and the other of 8.5 percent per 10^{10} ev for energies greater than 7.5×10^9 ev.

Again the question arises whether this analysis should be applied to the uncorrected curve (Fig. 6) or the curve (Fig. 12) that has been corrected for the external atmospheric temperature coefficient. The answer seems clear. The analysis depends solely upon the action on the cosmic rays by the earth's magnetic field, which is independent of both the temperature and the seasons. The variations in intensity which are found to be so closely correlated with the atmospheric temperature should accordingly be eliminated. While application of the temperature correction may not completely take account of the effect of variations in the unknown atmospheric barrier, the high correlation between the intensity changes and the temperature indicates that most of the effect of this barrier should thus be removed.

In a preliminary presentation of these results,[19] a similar analysis was made using, however, the uncorrected data, and Störmer's instead of Lemaitre-Vallarta's relation between λ and E_0. The results differ from those of Fig. 13 chiefly in

[21] W. Illing, Terr. Mag. and Elec. **41**, 185 (1936).
[22] B. F. G. Schonland, B. Delatizky and J. P. Gaskell, Nature **138**, 325 (1936).
[23] Cf. A. H. Compton and P. Y. Chou, Phys. Rev. **51**, 1104 (1937).
[24] H. Zanstra, Naturwiss. **22**, 171 (1934).
[25] G. Lemaitre and M. S. Vallarta, Phys. Rev. **50**, 493 (1936), Fig. 10.

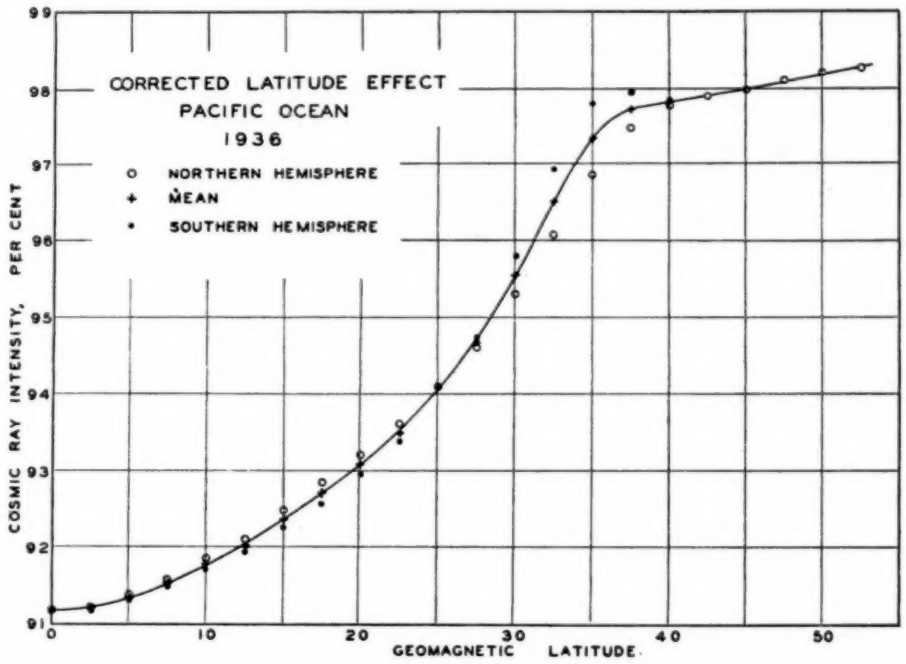

FIG. 12. Magnetic latitude effect averaged for complete year's data for both hemispheres.

assigning a value to the lower energy part of the energy distribution spectrum which is about twice that shown in Fig. 13. This reflects the fact that the uncorrected latitude curve is steeper than the corrected one for latitudes higher than the knee.

Millikan and Neher[4] have emphasized the conclusion that the slope of the latitude effect curve is zero above 40°. Their measurements, however, are inadequate to detect a slope of the small magnitude under consideration here. There can be but little doubt that the consistency of the present data is sufficient to justify a value of $\phi(E)$ greater than zero in the region of E_0 less than 7.5, as shown in Fig. 13. It is, however, not impossible that some error in our correction procedure may have resulted in a false indication of a low energy component.

Assuming the validity of the energy spectrum here obtained, its interpretation in terms of the action of the earth's magnetic field is clear: Two primary components of cosmic rays produce effects at sea level, the more prominent of which has energies only greater than a sharp limit of 7.5×10^9 ev, whereas the weaker component occurs with all energies greater than 2.5×10^9 ev. Strong support for the view that the primary cosmic rays are complex, and that the magnetic latitude effect continues well beyond 40°, comes from the observations of Alvarez,[26] Johnson,[27] Rossi,[28] Clay,[29] and others that in equatorial regions the direction of approach of the primary cosmic rays is predominantly from the west, and that the westward predominance continues in America[27b, c] to at least geomagnetic latitude 50°. According to Lemaitre and Vallarta's theory,[30] this observation means that a magnetic latitude effect, due predominantly to positive particles, must be present up to 50°. This result is in accord with our corrected latitude effect curves. Since, as far as is known, positrons are always paired with negatrons, it seems probable that the excess of positive particles consists of protons. We would thus suggest that the low energy component required to account for the observed

[26] L. Alvarez and A. H. Compton, Phys. Rev. **43**, 835 (1933).
[27] T. H. Johnson, (a) and J. C. Street, Phys. Rev. **43**, 381 (1933); (b) Phys. Rev. **43**, 834 (1933); (c) and E. C. Stephenson, Phys. Rev. **44**, 125 (1933); (d) Phys. Rev. **47**, 318 (1935).
[28] B. Rossi, (a) Ricerca Scient. **4**, 365 (1933); (b) and S. de Benedetti, Ricerca Scient. **5**, 594 (1934).
[29] J. Clay (a) and P. M. Alphen, C. G. 't Hooft, Physica **I**, 829 (1934); (b) and H. Zanstra, Physica **I**, 839 (1934).
[30] G. Lemaitre and M. S. Vallarta, Phys. Rev. **43**, 87 (1933).

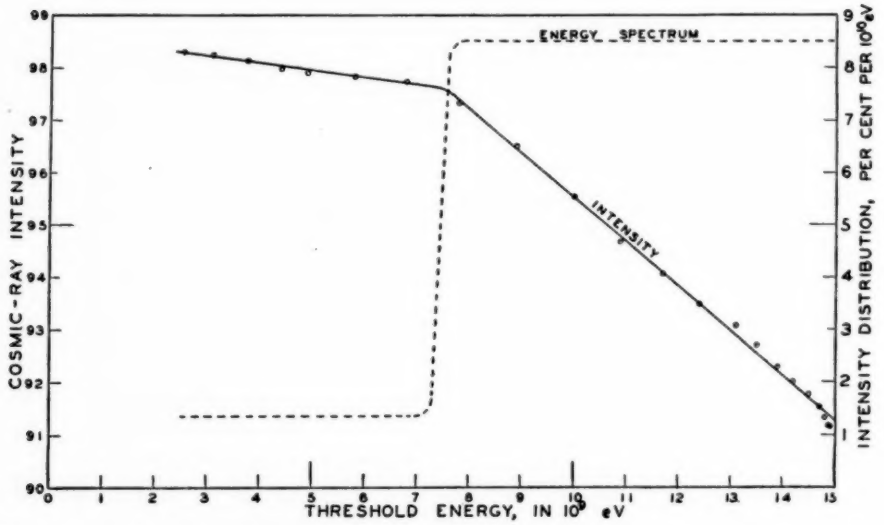

FIG. 13. Solid line, cosmic-ray ionization as function of geomagnetic energy threshold. Broken line, energy distribution of primary cosmic rays, according to geomagnetic analysis.

magnetic latitude effect persisting to the highest latitudes here studied may be due to protons.

It would be very desirable to continue similar observations to still higher latitudes, where any true magnetic effect should certainly disappear, because of the energy threshold imposed by the absorption of the atmosphere. As yet practical difficulties have prevented our carrying through such a program. Perhaps the best data now available at such high latitudes are those recently obtained by Clay, 't Hooft and Clay,[31] who carried a shielded and an unshielded meter from Amsterdam (54° geomagnetic) to North Cape (67°) and return. They found no difference within an experimental error of ±0.6 percent. Since their measurements were made only in the summer, there is no basis for distinguishing between a magnetic and an atmospheric latitude effect. Their results suggest, however, that north of 54° the magnetic latitude effect may be zero, which it should be if the tentative identification of the small effect here found between 38° and 54° as due to protons is valid.

It is not possible from these experiments to place an upper limit on the fraction of the cosmic rays that is electrically charged. Between 52.5° and the equator the difference shown by the corrected curve of Fig. 12 is only 7.2 percent. Yet from the approximately linear relation between I and E_0 shown in Fig. 13, it is evident that this fraction does not represent all of the electrically-charged primaries, but is limited rather by the finite strength of the earth's field. The trend of the I *vs.* E_0 curve suggests no limit to the magnitude of the latitude effect if a sufficiently large value of the threshold energy is assigned. The data thus give no suggestion of primaries of a nonelectrical type.

ORIGIN OF SHARP KNEE IN LATITUDE EFFECT CURVES

A formidable difficulty is presented by the sharpness of the 36° knee of the latitude effect curve. Clay,[32] Compton,[6] Millikan,[4, 33] and others have confidently ascribed this knee to the fact that penetration of the atmosphere sets a threshold value upon the energy of the particles capable of reaching the meter, and that where this atmospheric threshold is greater than the geomagnetic threshold, no further increase in ionization with increasing latitude is to be expected.[34] This theory assumes that the primary particles shall have a sharply defined range in air. Recent theoretical and experimental studies

[31] J. Clay, C. G. 't Hooft and P. H. Clay, Physica **2**, 1033 (1935).

[32] G. Clay, Proc. Roy. Akad. Amsterdam **35**, 1282 (1932).

[33] I. S. Bowen, R. A. Millikan and H. V. Neher, Phys. Rev. **46**, 641 (1934).

[34] A detailed exposition of this theory is given by A. H. Compton, Proc. Phys. Soc. London **47**, 762 (1935).

have, however, shown rather definitely that, both for particles known to be electrons and for the cosmic rays which show the latitude effect, the absorption is not primarily of the range type but is more nearly exponential in character.[35] The only sharply defined range for high energy electrical particles that is anticipated according to current theories is that due to the gradual loss of energy spent in electron collisions. For electrons of energy greater than 10^8 ev, this is on the average of much less importance than the energy loss by photon (i.e., x-ray) production. There is, however, always a chance, though a small one, that a higher energy electron may come to the end of the range determined by electron collisions before it has suffered a photon producing collision. In this case, its range should be that due to the electron collisions alone. The energy thus spent by an electron passing vertically through the atmosphere would be about 2.4×10^9 ev. The energy loss by a proton through electron collisions would be of nearly the same amount; though here also is the possibility of nuclear collisions whose frequency and importance is unknown. The result is, however, that we now have no reason to anticipate any threshold of energy as determined by atmospheric absorption other than that of about 2.4×10^9 ev, due to electron collisions. This statement applies to any singly-charged electrical primary whose rest mass is not greater than that of a proton.

In the present experiments, the 12 cm lead shield is adequate to eliminate the "shower producing" primaries and to leave only the penetrating component of the cosmic rays. This component would at present appear to consist of particles more massive than electrons, but with a single electronic charge. Such auxiliary evidence as that from the ratio of the ionization produced to the number of incident penetrating particles supports the theoretical calculation of the loss of 2.4×10^9 ev by these rays on traversing the atmosphere.

The critical geomagnetic latitude corresponding to an energy threshold of 2.4×10^9 ev is, according to Lemaitre and Vallarta's theory, 50°. The experiments of Hoerlin[7] and of Clay,[29, 31, 36] and his collaborators indicate that in Europe the geomagnetic latitude of the prominent knee is much higher than we find in the Pacific Ocean. In fact a value of 54° for the critical latitude would be consistent with their data.[37] On the other hand, Millikan and Neher[4] find the critical latitude on the west coast of Europe to be 41° geomagnetic, just as they found on the Pacific Ocean. It is not unlikely that the differences between these observers are partly of the seasonal type, like those between the winter and summer curves of Fig. 7. It is noteworthy that all of the European cosmic-ray observations north of 54° were made in the warm months, when we find the curve to be flat for the higher latitudes. This may account for the apparently sharp knee which occurs at about the latitude of Amsterdam and Hamburg. Thus a reliable comparison of the European and the Pacific Ocean data is not now possible. Nevertheless, what comparisons are possible suggest a considerably higher critical latitude in Europe than in Western America.

In the part of the Pacific Ocean where the present measurements were made there are no marked magnetic anomalies, and the longitude is nearly midway between that of the maximum and that of the minimum horizontal magnetic fields at the equator. We should thus expect the energies calculated from the geomagnetic latitudes to be relatively reliable over this route. The difference between the observed critical latitudes of 38.4°N and 34.2°S and the calculated critical latitude of 50° accordingly appears to be too great to admit the validity of the explanation of the knees as due to sharply-defined ranges of the cosmic-ray particles in the atmosphere.

The immediate significance of this 36° knee,

[35] An account of this work, including latitude effect experiments at different altitudes by A. H. Compton, measurements of the stopping of cosmic-ray electrons by C. D. Anderson, and theoretical studies of the energy dissipation by electrical particles by Bethe and Heitler, Oppenheimer, and Swann, is given in reference 19, pp. 1128–29. Cf. also, I. S. Bowen, R. A. Millikan and H. V. Neher, Phys. Rev. **52**, 80 (1937).

[36] J. Clay, E. M. Bruins, and J. T. Wiersma, Physica **3**, 746 (1936).

[37] Cf. reference 34, Fig. 12. Between latitudes 41° and 54° geomagnetic, Hoerlin, reference 7, finds an increase of 3.8 percent, Clay, references 29 and 31, of 4.2 percent in the East Atlantic and, reference 36, of 2.4 percent in the middle Atlantic.

as indicated by the discussion of Fig. 13, is that the cosmic-ray ionization is due to electrical primaries approaching the earth with a threshold energy of about 7.5×10^9 ev. If atmospheric absorption is inadequate to account for this sharply defined threshold, what may be its origin? Vallarta's recent suggestion[17] of a limit imposed by the magnetic field of the sun may supply the answer. Or is there perhaps some sharply defined atmospheric barrier, analogous to a potential barrier, whose seasonal fluctuations may cause the seasonal fluctuations of the cosmic-ray ionization? To these questions, our observations have not supplied the answer.

ACKNOWLEDGMENTS

We wish to thank the Canadian Australasian Steamship Company for permitting us to build the cosmic-ray observatory on the R. M. S. Aorangi, and to use it for the year, the Union Carbide and Carbon Corporation for supplying the batteries required for operating the meter, and the Carnegie Institution of Washington for the use of the cosmic-ray meter. Mrs. Ardis Monk and Mr. Piara Gill have carried through most of the laborious calculations. Professor P. W. Burbidge of Auckland University College and Mr. F. L. Code of Vancouver have given valued help in the adjustments of the meter.

OCTOBER 15, 1937 PHYSICAL REVIEW VOLUME 52

The Emission Spectrum of Diatomic Arsenic. II

G. D. KINZER AND G. M. ALMY
Department of Physics, University of Illinois, Urbana, Illinois
(Received August 13, 1937)

The emission spectrum of diatomic arsenic, previously studied in the interval 2100A to 3700A, has been extended to 7000A. The two prominent systems have been greatly extended so that the ground state of the molecule has been followed to $v=70$, in energy to nearly 0.8 of the heat of dissociation, $D(X)$. $D(X)$ is 3.9 volts by extrapolation and the same value is obtained from analysis of predissociation occurring in the two most prominent systems. Two new systems have been found, one having the same lower state as those previously reported and the other forming a double array. The latter has been tentatively assumed to be due to As_2^+.

INTRODUCTION

A VIBRATIONAL analysis of the emission spectrum of As_2 found between 2100A and 3700A has been given by Almy and Kinzer in a previous report.[1] The spectrum, complex in appearance, consists of three overlapping systems having a common lower state. By careful control of the source consisting of a quartz discharge tube filled with arsenic vapor and heated in an oven or by a flame, it has been possible to extend the spectrum to 7000A (see Fig. 1). A more complete analysis of the reported systems has been made and two additional systems found. A brief abstract of the new results has been included in a recent paper comparing the spectra of elements of the fifth periodic group.[2]

[1] G. M. Almy and G. D. Kinzer, Phys. Rev. **47**, 721 (1935).
[2] G. M. Almy, J. Phys. Chem. **41**, 47 (1937). The designation of states in the present paper corresponds to that in reference 1.

VIBRATIONAL ANALYSIS

The three systems originally reported[1] as lying between 2100A and 3700A have been extended to about 5600A. These are designated as $A\rightarrow X$, $B\rightarrow X$, and $C\rightarrow X$. Another system $D\rightarrow X$ was also found between 3700A and 4500A. The wave numbers of the new band edges with an estimate of the intensities and sharpness of edges of bands in these four systems are given in Table I. The v', v'' arrays for the $A\rightarrow X$, $B\rightarrow X$, and $D\rightarrow X$ systems are shown in Fig. 2 and Fig. 3. System $C\rightarrow X$ consists of a single $(v'=0)$ progression. Averaged values of $\Delta G''(v+\frac{1}{2})$ are the same in these four systems, showing that they have a common lower state, X. In a study of the absorption spectrum of As_2, Gibson and MacFarlane[3] found the $A\rightarrow X$ system well developed in v' progressions, showing that the X state is

[3] G. E. Gibson and A. MacFarlane, Phys. Rev. **46**, 1059 (1934).

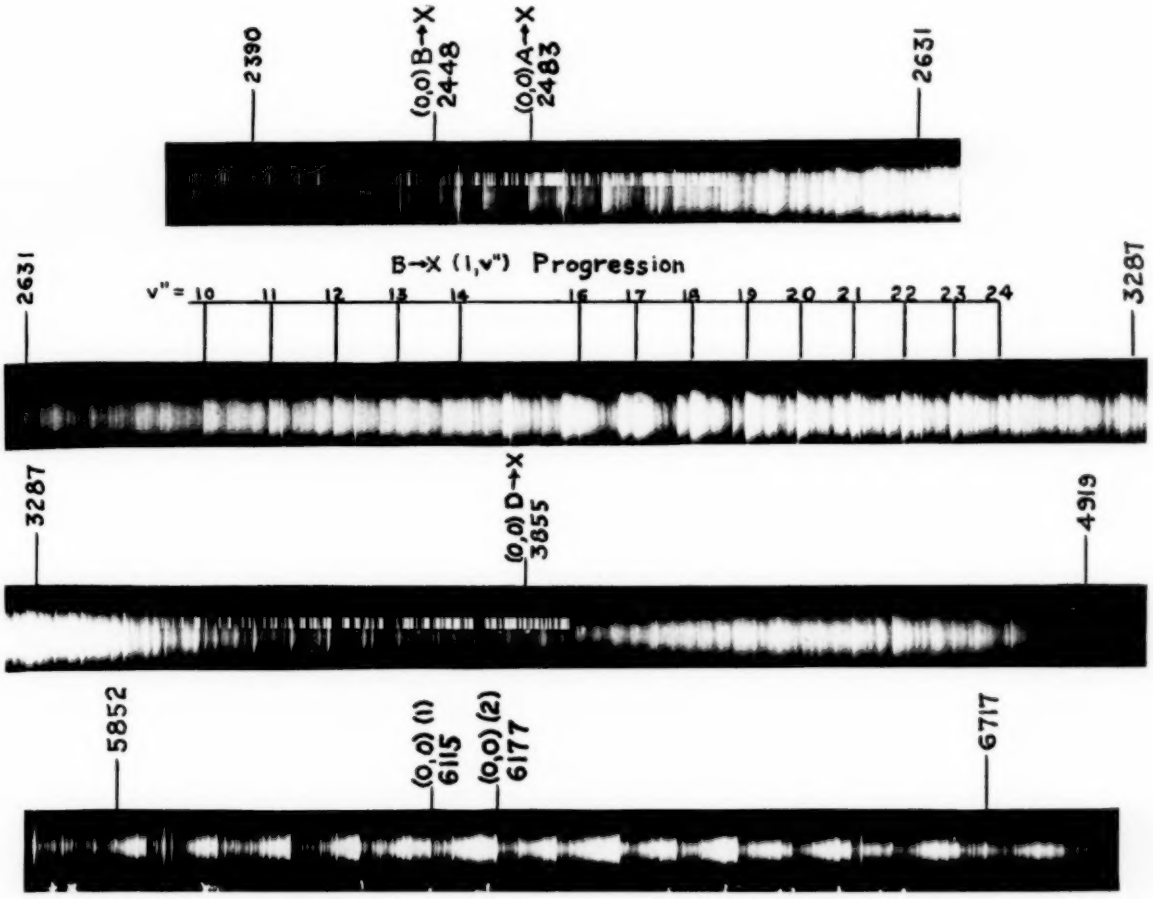

FIG. 1. Spectrum of discharge in arsenic vapor. The position and wave-length of the (0,0) band of each of four well-developed systems is shown, though actually observed only in the red system (bottom strip) due presumably to As_2^+. A part of a strong progression in the $B\rightarrow X$ system is indicated. The $A\rightarrow X$ and $B\rightarrow X$ systems extend with faint bands to 5600A though the reproduction shows them only to about 4900A.

the normal state of the molecule. Values of $\Delta G_X(v)$[4] are plotted in Fig. 4 against $G_X(v)-G_X(0)$, obtained by adding the averaged vibrational intervals. Attempts to obtain an equation for $G_X(v)$ over the entire range of v failed. Plotting $dG_X(v)/d\Delta G_X(v)$ against $\Delta G_X(v)$, as shown in Fig. 5, by the method of Birge,[5] indicated that there may be a sudden small change in the law of force between the two atoms of As_2 at $\Delta G_X(v)$ $=335$ cm^{-1} or $v=40$. Two equations for $G_X(v)$, one to $v=40$ and the other from $v=41$ to $v=70$, have been calculated by least squares and are:

$v=0$ to $v=40$,

$$G_X(v)=429.44(v+\tfrac{1}{2})-1.120(v+\tfrac{1}{2})^2 +0.005091(v+\tfrac{1}{2})^3-0.00002563(v+\tfrac{1}{2})^4, \quad (1)$$

and, $v=41$ to $v=70$,

$$G_X(v)=-275.28+442.8437(v+\tfrac{1}{2}) -1.39913(v+\tfrac{1}{2})^2+0.00255646(v+\tfrac{1}{2})^3 -0.000025945(v+\tfrac{1}{2})^4. \quad (2)$$

That these equations accurately represent $G_X(v)$ is shown in Table II by the close agreement between values of $G_X(v)$ obtained by summing averaged vibrational intervals and values of $G_X(v)$ calculated from the equations. Following the method outlined in the first report,[1] these equations are used to calculate the wave numbers of the band heads in the $A\rightarrow X$, $B\rightarrow X$, $C\rightarrow X$, and $D\rightarrow X$ systems, giving a check on the assignment of the observed heads. (See obs.-calc. column in Table I.) The apparent perturbations in vibrational levels of the A and B states ob-

[4] $\Delta G(v)=\frac{1}{2}[G(v+1)-G(v-1)]=\omega_e-2(v+\frac{1}{2})x_e\omega_e$.
[5] R. T. Birge, Trans. Faraday Soc. **25**, 707 (1929).

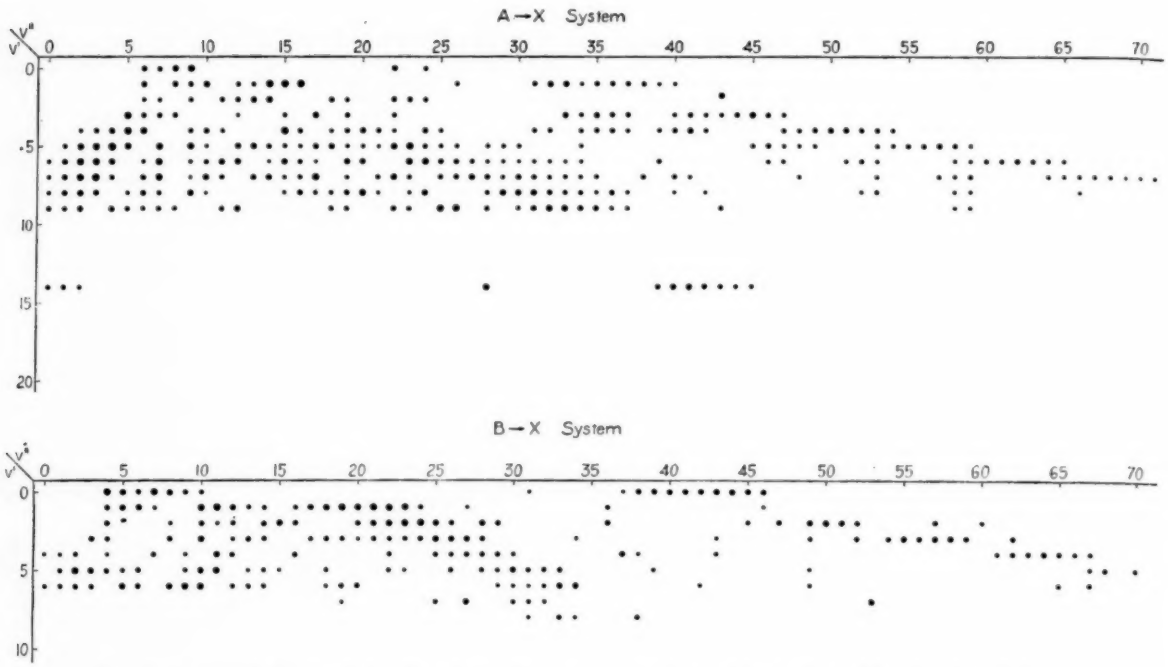

FIG. 2. Observed bands of $A \rightarrow X$ and $B \rightarrow X$ systems with intensities indicated by the size of dots.

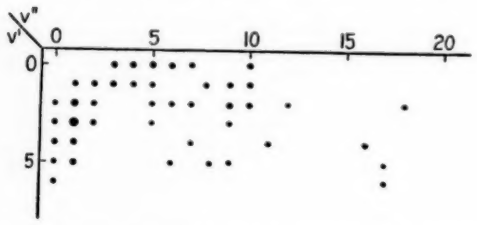

FIG. 3. Observed bands of $D \rightarrow X$ system with intensities indicated by size of dots.

served both in absorption[3] and in emission[1] prevents the calculation of any significant equations for $G_A(v)$ and $G_B(v)$. The few v' levels in the $D \rightarrow X$ system converge regularly, and by least squares calculation:

$$G_D(v) = 337.0(v+\tfrac{1}{2}) - 0.83(v+\tfrac{1}{2})^2. \qquad (3)$$

The bands in the $A \rightarrow X$, $B \rightarrow X$, $C \rightarrow X$, and

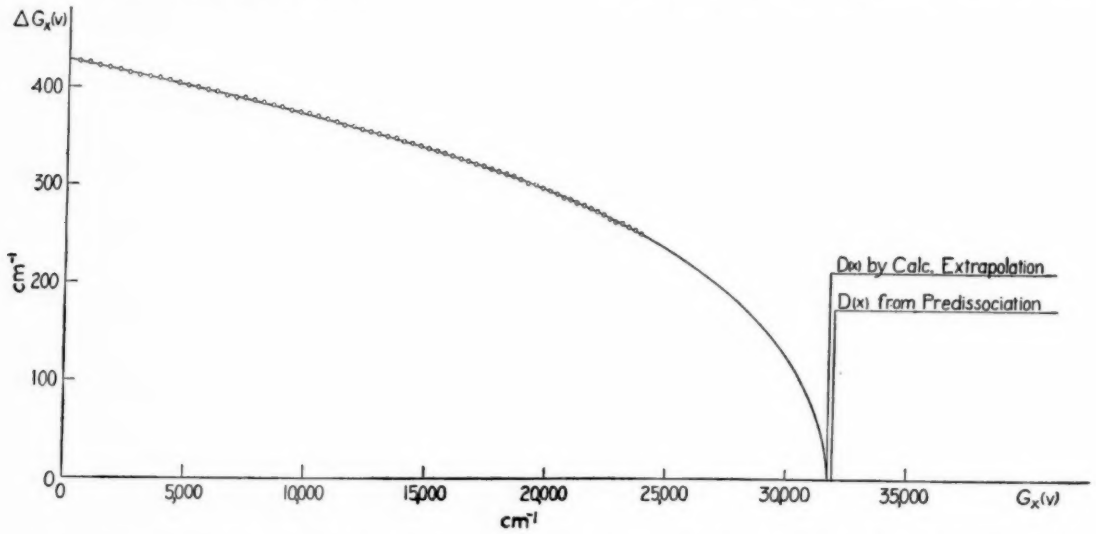

FIG. 4. Plot of $\Delta G_X(v)$ *vs.* $G_X(v)$ for the normal state of As_2. Vertical lines indicate values of $D(X)$ as calculated by two methods.

TABLE I. *Observed band heads not previously reported. Assignment to system A, B, C, and D and to vibrational quantum numbers. Comparison with calculated wave numbers. Under intensities: s = sharp, d = diffuse, dd = very diffuse.*

System and v'v''	Int.	Wave Number (obs.)	Wave Number (obs.-ca'c.)	System and v'v''	Int.	Wave Number (obs.)	Wave Number (obs.-calc.)
A 3,17	3*d*	34034.3	−1.3	*A* 1,36	2*d*	26573.2	+1.3
A 5,20	0*s*	33454.2	−0.9	*B* 0,37	0*s*	26539.2	+1.5
A 3,19	1*d*	33257.7	−0.9	*A* 7,41	0*s*	26439.8	+1.0
B 3,22	1*d*	32770.1	+3.4	*B* 6,42	0*d*	26422.1	+0.5
A 8,24	2*s*	32688.8	+0.1	*A* 8,42	0*d*	26350.4	+1.2
B 7,25	1*d*	32609.0	+1.6	*A* 4,39	0*d*	26323.8	−0.7
A 0,20	3*d*	32142.3	+0.8	*A* 9,43	2*d*	26281.0	−1.2
A 3,22	1*s*	32113.4	+3.2	*D* 5,0	1*dd*	26255.3	0.0
A 7,25	2*d*	32072.9	−2.4	*A* 1,37	2*d*	26232.2	−1.2
B 4,25	2*dd*	31912.1	+2.4	*B* 0,38	3*s*	26199.0	+0.6
A 2,22	2*s*	31897.1	+2.5	*A* 4,40	2*dd*	25987.3	0.0
B 7,27	3*s*	31869.6	+0.8	*D* 4,0	2*dd*	25928.5	0.0
A 6,25	3*d*	31829.6	+0.9	*A* 1,38	2*d*	25891.2	−2.4
B 5,26	2*s*	31784.9	+0.5	*B* 0,39	3*s*	25862.0	−0.8
A 2,23	2*dd*	31515.0	−2.1	*D* 5,1	3*s*	25828.9	0.0
A 9,28	2*d*	31465.7	−1.5	*A* 3,40	1*d*	25685.9	+0.6
A 0,22	3*d*	31380.4	+0.9	*A* 4,41	3*s*	25656.7	−0.1
B 2,25	4*s*	31354.7	−2.4	*B* 4,43	1*s*	25619.1	−0.1
A 2,24	1*dd*	31142.6	+0.7	*D* 3,0	1*d*	25597.6	+1.4
B 6,29	0*dd*	30919.9	+0.8	*A* 1,39	0*s*	25553.8	−2.3
A 4,26			+2.6	*B* 0,40	3*s*	25525.8	−0.4
A 0,24	1*s*	30627.5	+0.7	*D* 4,1	2*s*	25501.7	0.0
A 2,26	0*s*	30400.7	+2.3	*A* 3,41	2*d*	25349.4	+1.4
B 1,27	0*s*	30331.7	+1.0	*A* 4,42	1*d*	25323.0	+0.7
A 1,26	1*d*	30146.7	+1.0	*D* 2,0	0*d*	25263.8	0.0
A 8,31	5*s*	30129.6	+0.6	*A* 1,40	0*d*	25214.6	+1.1
B 6,33	3*s*	29492.1	+1.4	*B* 0,41	3*s*	25189.9	+2.3
B 5,33	2*dd*	29259.7	−0.8	*D* 3,1	2*s*	25167.8	+3.8
B 6,34	3*s*	29140.0	−0.1	*A* 3,42	1*d*	25022.7	0.0
A 4,31	1*s*	29100.0	+2.9	*B* 0,42	3*s*	24864.2	0.0
C 0,33			+1.1	*D* 3,2	1*s*	24745.5	+0.2
C 0,34	0*d*	28752.3	−0.2	*B* 3,43	0*s*	24700.3	+0.1
A 4,32	1*s*	28746.4	−1.1	*A* 3,43	1*s*	24692.6	−0.1
B 0,31	0*s*	28637.4	+1.8	*A* 5,45	1*d*	24620.8	−0.3
A 7,35	1*d*	28478.9	−0.1	*A* 6,46	1*d*	24570.0	+0.5
B 3,34	0*d*	28392.2	+2.0	*B* 0,43	4*d*	24534.3	+0.2
A 8,36	3*d*	28373.9	+0.1	*D* 1,1	1*d*	24504.2	−0.9
A 1,31	1*s*	28330.1	−1.0	*A* 2,43	3*s*	24471.6	−1.0
A 5,34	0*s*	28318.1	+2.5	*B* 2,45	1*d*	24415.9	−2.1
B 8,38	2*s*	28186.5	+4.0	*D* 2,2			+0.2
A 3,33	3*dd*	28086.5	+2.0	*A* 3,44	2*d*	24367.2	+0.2
A 4,34	1*s*	28040.5	+0.5	*A* 5,46	2*d*	24309.1	+0.9
A 8,37	1*dd*	28030.0	+0.6	*A* 6,47	1*s*	24249.6	+2.3
A 1,32	3*d*	27972.6	+1.1	*B* 0,44	4*s*	24209.3	+0.9
A 3,34	1*s*	27735.8	+1.9	*A* 7,48	0*d*	24183.7	+0.7
A 4,35	2*s*	27692.7	−0.6	*B* 6,49			+0.6
B 4,37	3*s*	27621.4	+4.2	*D* 1,2	1*s*	24080.7	+0.9
A 2,34	0*dd*	27521.1	+1.0	*A* 3,45	4*d*	24044.2	−1.2
A 7,38	2*d*	27448.1	+0.1	*A* 5,47	0*s*	23991.0	+0.4
B 2,36	2*s*	27415.5	+3.5	*D* 2,3			−0.2
A 3,35	3*s*	27387.5	+1.3	*B* 5,49	0*d*	23952.0	0.0
A 4,36	2*d*	27344.6	+1.5	*B* 0,45	3*s*	23884.2	−2.6
B 4,38	0*s*	27288.4	−1.4	*B* 1,46	0*d*	23812.0	+0.2
A 1,34	3*s*	27269.6	−0.2	*B* 2,47	2*s*	23777.8	−2.5
B 5,39	1*dd*	27191.9	−1.7	*A* 3,46	2*s*	23723.8	−1.5
B 1,36	1*dd*	27126.4	+1.1	*A* 4,47	1*s*	23710.7	−0.3
A 3,36	2*d*	27042.3	−0.3	*A* 5,48	0*s*	23676.7	+0.8
A 8,40	0*d*	27015.1	+0.1	*D* 1,3	2*s*	23658.0	+0.9
A 4,37	0*s*	27001.0	+1.6	*B* 0,46	3*s*	23566.0	−0.6
A 1,35	2*s*	26921.1	−0.6	*D* 3,5	1*d*	23485.1	+0.4
A 14,45	4*s*	26908.1	+0.6	*B* 2,48	2*d*	23465.0	−0.6
A 6,39	2*s*	26856.2	−2.8	*B* 3,49	1*d*	23438.9	+1.4
A 7,40	2*s*	26777.4	−2.4	*A* 3,47	1*d*	23408.3	+0.6
A 3,37	2*s*	36698.5	+0.8	*A* 4,48	1*s*	23395.7	−0.6
C 0,40			−0.2	*A* 5,49	0*d*	23361.3	−2.6
D 6,0	0*s*	26580.9	0.0	*D* 0,3	1*s*	23321.6	−0.8

TABLE I (*Continued*).

System and v'v''	Int.	Wave Number (obs.)	Wave Number (obs.-calc.)	System and v'v''	Int.	Wave Number (obs.)	Wave Number (obs.-calc.)
D 1,4	1*s*	23234.7	−1.9	*D* 1,9	1*s*	21171.2	+3.8
A 8,52	1*d*	23193.9	+0.5	*A* 8,59	1*d*	21150.4	+0.5
B 7,53	4*s*	23183.8	−0.6	*D* 2,10	1*d*	21096.7	+2.3
B 2,49	3*d*	23152.8	−0.8	*B* 3,57	3*s*	21044.0	−0.4
D 2,5			+0.3	*A* 5,57	3*d*	20971.3	+0.5
A 4,49	2*s*	23084.2	−0.1	*A* 6,58	1*s*	20946.7	+0.7
D 4,6	1*dd*	23056.0	0.0	*A* 7,59	2*s*	20908.1	−0.6
A 6,51	1*s*	23009.1	−0.7	*B* 3,58	3*s*	20762.1	+3.8
D 4,7	0*d*	22986.8	−0.2	*A* 5,58	2*s*	20684.4	−0.3
D 0,4	2*s*	22902.6	+0.6	*A* 6,59	1*s*	20662.8	−0.1
A 8,53	2*d*	22892.7	−0.1	*B* 6,61			0.0
D 5,8			+0.7	*D* 3,12	0*d*	20619.6	0.0
B 2,50	4*d*	22844.6	+0.1	*B* 3,59	2*s*	20473.3	−1.9
D 1,5	2*d*	22817.8	−0.3	*D* 0,10	1*s*	20429.5	+3.9
D 6,9			−0.6	*A* 5,59	0*s*	20402.7	+1.1
A 4,50	3*d*	22765.3	+0.1	*A* 6,60	2*s*	20283.2	+0.4
D 2,6	1*s*	22738.1	−0.5	*D* 2,12	0*d*	20287.4	+0.5
A 6,52	2*d*	22706.5	+0.1	*D* 3,13	0*d*	20219.2	0.0
B 6,54	1*s*	22666.1	+0.1	*B* 4,61	1*d*	20186.4	−1.3
A 7,53	1*d*	22650.2	−1.4	*A* 6,61	2*d*	20106.0	−0.4
B 2,51	3*s*	22537.7	−0.5	*B* 2,60	1*d*	19911.6	+0.4
B 3,52	2*d*	22516.6	−2.1	*B* 4,62			−2.1
D 0,5	2*s*	22854.3	+0.6	*A* 6,62	3*s*	19831.6	0.0
A 4,51	3*s*	22468.8	−0.1	*B* 4,63	2*s*	19641.3	−1.2
A 6,53	1*d*	22406.3	+0.5	*B* 3,62			−2.6
D 2,7	1*s*	22326.8	+0.5	*B* 6,65	1*s*	19590.2	+4.6
B 2,52	2*s*	22235.5	+0.7	*A* 6,63	2*d*	19561.1	+0.7
A 4,52	2*s*	22165.3	−0.2	*A* 7,64	0*d*	19538.6	+0.3
D 4,9			−0.7	*B* 4,64	3*s*	19372.6	−2.0
A 5,53	1*s*	22144.6	+0.1	*D* 4,16	0*d*	19362.0	+2.0
D 0,6	1*s*	22068.2	+0.7	*B* 6,66	1*d*	19325.1	+1.2
B 3,54	2*s*	21919.4	−0.9	*D* 5,17	0*d*	19299.4	−2.4
A 4,53	2*s*	21864.5	−0.4	*A* 6,64	1*d*	19293.6	+1.1
A 5,54	1*s*	21846.9	+0.2	*A* 7,65	0*d*	19273.8	+0.4
A 9,58	0*d*	21690.9	+2.0	*A* 8,66	0*d*	19253.4	+0.5
D 0,7	0*s*	21653.0	−0.7	*B* 4,65	2*s*	19109.1	−0.6
B 3,55	3*d*	21625.6	+0.1	*B* 6,67	1*d*	19064.4	−1.0
D 1,8	0*d*	21576.9	+0.2	*A* 6,65	1*s*	19027.5	−0.1
A 4,54	1*d*	21567.2	+0.1	*A* 7,66	1*d*	19011.0	−0.7
A 5,55	2*s*	21551.9	0.0	*B* 4,66	1*d*	18850.4	−2.4
D 2,9	0*d*	21499.0	−2.5	*B* 5,67	1*d*	18833.9	+0.3
A 7,57	1*s*	21498.2	+0.3	*A* 7,67	1*s*	18752.5	−0.7
A 8,58	1*d*	21433.1	+0.1	*B* 4,67	1*d*	18588.4	−1.1
A 9,59	0*d*	21405.8	0.0	*B* 5,68	2*d*	18576.9	−1.2
D 4,11	0*d*	21354.6	+0.7	*A* 7,68	1*s*	18297.6	−0.1
B 3,56	2*d*	21334.8	+1.4	*A* 7,69	0*s*	18245.3	−0.2
A 5,56	2*d*	21260.6	+1.0	*B* 5,70	1*s*	18077.3	+0.4
A 7,58	1*s*	21191.2	−0.6	*A* 7,70	0*s*	17994.9	−1.6
				D 2,18	0*d*	17920.4	+0.2

$D \rightarrow X$ systems (2100A to 5600A) are degraded to the red, but the bands from 5600A to 7000A are degraded to the violet and have sharp edges on the red side. These bands form two arrays, Table III, in which corresponding bands, i.e., bands with identical values of v', v'', are matched in intensity and separated by a nearly constant interval of 162 cm^{-1}. The bands can be represented by the equation:

$$\nu = \begin{matrix}(16359)\\(16197)\end{matrix} + \{336.8(v'+\tfrac{1}{2}) - 1.04(v'+\tfrac{1}{2})^2\} - \{314.8(v''+\tfrac{1}{2}) - 1.25(v''+\tfrac{1}{2})^2\}. \quad (4)$$

It appears improbable that these bands arise from transitions to or between any of the states *A*, *B*, *C*, *D*, or *X*, and the existence of the 162 cm^{-1} interval suggests that the system may be due to a molecule of even multiplicities, probably

TABLE II. *Term values of normal state. In column 3 $G_X(0)$ is subtracted from $G_X(v)$ as calculated from Eq. (1), or Eq. (2).*

v	$G_X(v)$ (ave. obs.)	$G_X(v)$ (calc.)	obs. − calc.
0	0.0	0.0	—
1	428.1	427.4	+0.7
2	853.5	852.7	+0.8
3	1276.8	1275.4	+1.4
4	1696.6	1695.9	+0.7
5	2115.0	2114.1	+0.9
6	2531.0	2530.3	+0.7
7	2944.3	2944.1	+0.2
8	3355.2	3355.8	−0.6
9	3766.4	3765.1	+1.3
10	4171.8	4172.2	−0.4
11	4577.2	4577.2	0.0
12	4979.3	4979.7	−0.4
13	5379.4	5380.1	−0.7
14	5777.5	5778.2	−0.7
15	6173.5	6174.1	−0.6
16	6567.6	6567.7	−0.1
17	6956.7	6956.0	+0.7
18	7346.3	7348.2	−1.9
19	7733.9	7734.8	−0.9
20	8119.0	8119.4	−0.4
21	8501.5	8501.6	−0.1
22	8882.2	8881.4	+0.8
23	9259.5	9258.9	+0.6
24	9634.0	9634.1	−0.1
25	10007.2	10007.1	+0.1
26	10378.1	10377.6	+0.8
27	10746.4	10745.6	+0.8
28	11112.3	11111.5	+0.8
29	11474.2	11474.7	−0.5
30	11835.1	11835.4	−0.3
31	12193.9	12193.8	+0.1
32	12549.8	12549.6	+0.2
33	12903.2	12903.1	+0.1
34	13254.1	13253.9	+0.2
35	13602.7	13602.8	−0.1
36	13948.8	13948.8	0.0
37	14292.3	14292.3	0.0
38	14633.3	14633.4	−0.1
39	14971.7	14971.8	−0.1
40	15307.6	15307.3	+0.3
41	15641.1	15640.8	+0.3
42	15972.1	15971.2	+0.9
43	16299.8	16298.9	+0.9
44	16625.2	16624.6	+0.6
45	16947.4	16946.2	+1.2
46	17267.8	17266.3	+1.5
47	17584.6	17583.9	+0.7
48	17898.6	17898.6	0.0
49	18210.5	18210.6	−0.1
50	18520.1	18519.7	+0.4
51	18826.8	18826.0	+0.8
52	19130.3	19129.4	+0.9
53	19430.9	19430.0	+0.9
54	19728.6	19727.8	+0.8
55	20022.8	20022.6	+0.2
56	20313.9	20314.7	−0.8
57	20603.5	20603.7	−0.2
58	20890.5	20889.8	+0.7
59	21174.0	21172.9	+1.1
60	21453.6	21453.0	+0.6
61	21729.8	21730.2	−0.4
62	22003.4	22004.2	−0.8
63	22274.8	22275.4	−0.6
64	22542.9	22543.3	−0.4
65	22807.6	22808.2	−0.6
66	23069.8	23069.9	−0.1
67	23329.2	23328.4	+0.8
68	23585.2	23583.9	+1.2
69	23836.8	23836.1	+0.7
70	24085.2	24085.1	+0.1

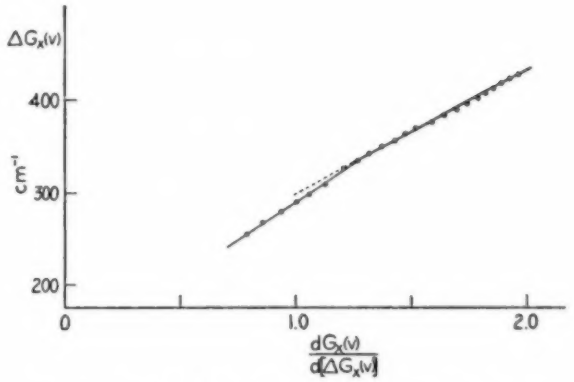

FIG. 5. $dG_X(v)/d[\Delta G_X(v)]$, obtained graphically from Fig. 3, plotted against $\Delta G_X(v)$. The point of intersection of the straight lines shows approximately the position of a change in the law of force between the two atoms in As_2.

As_2^+,[6] since As_2 should have only odd multiplicities.

It is unlikely that these bands are due to an impurity. When the arsenic used was excited in an arc, the only impurities detected were Fe, Sb, and Bi, and in the discharge the atomic lines of these elements were absent. In the spectrographs of the discharge the only molecular spectra which appeared were those described in this paper. No known spectra of molecules containing oxygen, nitrogen, hydrogen or carbon appeared.

The intensity distribution in the $A \rightarrow X$ and $B \rightarrow X$ systems was described in the first report.[1] The extension of these systems to higher v'' quantum numbers brings out an additional locus of maximum intensity in each system. The suggestion[1] that the intensity distribution in both systems would be improved if the $v'=2$ progression of the $A \rightarrow X$ system were interchanged with the $v'=0$ progression of the $B \rightarrow X$ system is supported by the intensity distribution in the extensions of both systems. If this were done the vibrational intervals in the B state would be more regular but those in the A state less regular. In fact, in such an arrangement the break in ΔG_A (vibrational interval) at $v=2$ is so large that the $v'=0$, 1, 2 progressions seem to form a separate system. The assignments in Fig. 2 have, however, been left as in the previous account. With the present data one cannot with certainty classify the bands of small v' of either system. It is clear, however, that there are at least two systems and

[6] N_2^+ bands appear in electrical discharge through nitrogen.

TABLE III. *Superimposed arrays of the bands degraded to the violet showing correspondence in intensity distribution and constant interval of separation, 162 cm^{-1}. Numbers in parentheses give estimated intensities.*

v' \ v''	0	1	2	3	4
0	16348.2(2*s*) 163.2 16185.0(2*s*)	312.6 16035.6(2*s*) 160.3 309.7 15875.3(2*s*)	306.7 15728.9(2*s*) 161.8 308.2 15567.1(2*s*)	306.5 15422.4(2*s*) 160.7 305.4 15261.7(2*s*)	
	334.3 335.9	335.6 334.8		334.5 333.6	
1	16682.5(3*s*) 161.6 16520.9(3*s*)	311.3 16371.2(1*s*) 161.1 310.8 16210.1(0*s*)		15756.0(1*s*) 159.8 15596.2(1*s*)	305.6 15450.4(1*s*) 160.7 306.5 15289.7(1*s*)
	331.4 330.2	331.4 330.3			
2	17013.9(3*s*) 162.8 16851.1(2*s*)	311.3 16702.6(0*s*) 162.2 310.7 16540.4(0*s*)	307.9 16394.1(1*s*) 161.0 307.2 16233.1(1*s*)		
	330.0 329.1	330.1 329.0			
3	17343.9(1*s*) 163.5 17180.2(1*s*)	311.3 17032.7(2*s*) 163.3 310.8 16869.4(2*s*)			
	326.8	328.8			
4	17670.7(0*s*)	17198.2(1*s*)			
5			17376.7(0*s*) 161.5 17215.2(0*s*)		
			322.7		
6			17699.4(0*s*)		

that they both exhibit perturbations. The uncertainty with regard to states A and B does not, of course, affect the conclusions drawn with regard to the ground state.

PREDISSOCIATION, HEATS OF DISSOCIATION

The drop in intensity and possibly complete breaking off of rotational structure of the bands with $v'=8$, 9 of the $A\rightarrow X$ system has been ascribed to predissociation at a total energy of about 42,700 cm^{-1} ($\nu_A(9,0)=42{,}579$ cm^{-1}, $\nu_A(10,0)=42{,}837$ cm^{-1}). The state to which radiationless transitions occur has been assumed to be C since $\nu_C(0,0)=42{,}006$, and with only one v' progression in the $C\rightarrow X$ system the potential energy curve of C must be quite shallow. To satisfy these conditions there must be a pair of atomic states having an energy of around 42,700 cm^{-1} (with respect to $G_X(0)$) into which C dissociates and A predissociates. It is probable that state B predissociates into the same atomic pair since the $B\rightarrow X$ system extends only to $v'=8$ with $\nu_B(8,0)=42{,}824$ cm^{-1}, at which point the vibrational interval is still 210 cm^{-1}.

The heat of dissociation in the normal state (X) can be determined in two ways, (1) by extrapolation of the vibrational levels using Eqs. (2) and (2) by analysis of predissociation. The extrapolation using Eq. (2) was carried out by finding the value of v for which $G_X(v)$ is a maximum, i.e., finding the v for which the vibrational intervals vanished. This gives $G_X(v)$(convergence) $=D(X)=31{,}726$ cm^{-1}. Since $G_X(v)$ was observed to be 24,300 cm^{-1}, nearly 0.8 of the energy of dissociation, this extrapolation of $D(X)$ should be fairly reliable.

When using the data of predissociation to calculate $D(X)$ one must assume a particular pair

of atomic states at an energy of 42,700 cm^{-1} with respect to $G_X(0)$. Atomic states of As arising from the $4p^3$ configuration are the normal ^4S, ^2D at 10,785 cm^{-1} (center of gravity), and ^2P at 18,493 cm^{-1}. Atomic states from other configurations are too high to come into considerations. With $G_X(v)$ followed to 24,300 cm^{-1} (see Fig. 4) and predissociation occurring at 42,700 cm^{-1}, the energy of the atomic pair at 42,700 cm^{-1} cannot be more than $42,700-24,300=18,400$ cm^{-1} above $^4S+^4S$. (As in N_2 and P_2, the ground state of the molecule, undoubtedly $^1\Sigma_g^+$, is assumed to arise from the $^4S+^4S$ atomic pair.) This restriction excludes all pairs of atomic states except $^4S+^2D$ and $^4S+^4S$. The latter pair requires that $D(X)$ be 42,700 cm^{-1}, much higher than the extrapolated value. The former pair gives $D(X)=42,700-10,787=31,915$ cm^{-1}, in good agreement with the calculated extrapolated value, 31,726 cm^{-1}, and is taken to be the correct pair. The mean of the two determinations of $D(X)$, by extrapolation and from predissociation, is 3.93 volts.

Figure 6 gives a term scheme showing the relative positions of atomic and molecular levels. By extrapolation, $D(A)$ is roughly 19,000 cm^{-1} and on this basis A is shown dissociating into $^2D+^2P$ atoms with $D(A)=20,500$ cm^{-1}. State B converges more rapidly than A and is shown dissociating into $^2D+^2D$ atoms giving $D(B)=10,600$ cm^{-1}. Closer agreement with the extrapolated energy of dissociation (uncertain because of perturbations) is obtained however if B is assumed to dissociate into $^4S+^2P$. The D state converges very slowly, and $D(D)$ by linear extrapolation is around 30,000 cm^{-1}, probably much too high. In Fig. 6 D is drawn as dissociating into $^4S+^2D$ atoms giving $D(D)=17,800$ cm^{-1}. With the assumption that state C causes the predissociation in A and dissociates into $^4S+^2D$ atoms at 42,700 cm^{-1}, $D(C)=700$ cm^{-1}. Almy,[2] in making a comparison between As_2 and other molecules of the same group, has made a tentative classification of the molecular states of As_2.

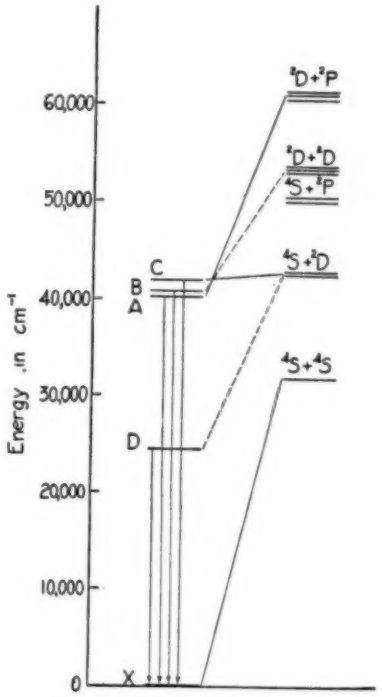

FIG. 6. Term scheme of As_2. Dissociation products indicated by dotted lines are uncertain.

Magnetic Rotation Spectra of Diatomic Molecules†

THOMAS CARROLL*
Sloane Physics Laboratory, Yale University, New Haven, Connecticut
(Received July 6, 1937)

The general theory of the Faraday effect associated with a single molecular absorption line is presented. The effect of the perturbation of the transition probabilities by the field in producing asymmetrical rotation is discussed, and calculated for alkali band systems and for I_2. The observations on asymmetrical rotation in I_2 agree with the predictions. The longitudinal Zeeman patterns and the changes in these patterns produced by the field are related to the vector model by use of the criterion that transitions which involve little change in the direction of J, the rotational axis, are the most probable ones. It is shown that all known facts about the $^1\Sigma \leftarrow {}^1\Sigma$ magnetic rotation systems of Na_2 and K_2 can be explained by assuming the upper state to be perturbed by an unknown $^3\Pi_0$ state. The constants have been calculated for this predicted perturbing state in Na_2.

THE magnetic rotation spectrum of a gas is the spectrum of the light transmitted through crossed polarizing prisms when the magnetized gas is placed between the prisms so that the light travels along the magnetizing field. The observation by Righi in 1898 that I_2, Br_2 and NO_2 produced such spectra provided the first evidence that a magnetic field could affect band lines.[1] Wood, from 1906 to 1909 cataloged extensively lines of the magnetic rotation spectrum of Na_2 in the region of the red and blue-green band systems, and as well measured the sign of the rotation outside six iodine absorption lines covered by the broadened mercury green line.[2] After the advent of the modern theory of band spectra, Loomis[3–5] observed that magnetic rotation lines appeared just outside the heads of the absorption bands of $^1\Pi \leftarrow {}^1\Sigma$ band systems of the alkali molecules. He and his students used the magnetic rotation spectra of such band systems with conspicuous success to obtain extended vibrational analyses and thus to estimate accurately the heats of dissociation. After the rotational analysis of the Na_2 red bands made it clear that these bands are of the $^1\Sigma \leftarrow {}^1\Sigma$ type, the problem arose of explaining the strong magnetic rotation spectrum of Na_2 in the red. $^1\Sigma \leftarrow {}^1\Sigma$ lines should show no Zeeman effect, nor Faraday effect, since $^1\Sigma$ states are insensitive to a magnetic field. Fredrickson and Stannard[6] succeeded in assigning quantum numbers to the magnetic rotation lines of the Na_2 red system in a very plausible way, which suggested strongly that perturbation of a few of the levels of the upper $^1\Sigma$ state was responsible for the appearance of the magnetic rotation spectrum. It is the purpose of this paper to corroborate this hypothesis as to the nature of this long puzzling magnetic rotation spectrum of the $^1\Sigma \leftarrow {}^1\Sigma$ system of Na_2. In particular, it will be shown that the sign of the rotation as well as its asymmetry is in agreement with modern theory. The magnetic rotation spectrum of the analogous infrared system of K_2 has been investigated, and its general characteristics fit nicely with the same explanation used for Na_2. In the theoretical discussion particular attention is given to the difference between the Faraday effect connected with a molecular spectral line, and that connected with an atomic line. Emphasis is placed on the quantum mechanical refinement of Faraday effect theory.

1. EXPERIMENTAL DETAILS

For the magnetic field a solenoid was used, as had been done by Loomis and Fredrickson. The

† Part of a dissertation presented to the Faculty of the Graduate School of Yale University in candidacy for the degree of Doctor of Philosophy.

* Now at College of New Rochelle.

[1] A. Righi, Comptes rendus **127**, 216 (1898); **128**, 45 (1898).

[2] R. W. Wood and F. E. Hackett, Astrophys. J. **30**, 399 (1909).

[3] F. W. Loomis and R. E. Nussbaum, Phys. Rev. **40**, 380 (1932).

[4] F. W. Loomis and M. J. Arvin, Phys. Rev. **46**, 286 (1934).

[5] P. Kusch, Phys. Rev. **49**, 218 (1936).

[6] W. R. Fredrickson and Carl R. Stannard, Phys. Rev. **44**, 632 (1933).

solenoid has two layers of flat copper ribbon ($0.5'' \times 0.056''$) wound on edge, with the plane of the ribbon perpendicular to the axis of the solenoid. There is a space of $\frac{1}{4}''$ between the layers for cooling water, and a water jacket surrounds the two layers. Thin dipped enamel provides sufficient insulation between turns. The completed solenoid is $2\frac{1}{2}$ feet long, with a useful working space 2 inches in diameter. Laminar type windings of flat copper ribbon use the winding space most efficiently, and at the same time allow for effective cooling. Heat developed in the coil never has to pass through more than one layer of insulation before it reaches the cooling water, which makes contact with both edges of every turn. The completed solenoid weighs about 75 pounds.

The maximum current obtainable, 125 amperes, was run through the two layers in series. The resistance under these conditions is about 0.3 ohm, and $\int Hdl$ along the axis of the solenoid is $1.2(10)^5$ gauss cm. The field at the center of the solenoid is therefore about 2000 gauss.

The continuous light source, condensing lens, polarizing prism, absorption tube inside the solenoid, analyzing prism and focusing lens were mounted in the order named directly in line with the slit of the grating spectrograph. A 100 cp Pointolite lamp was used for continuous source, because this highly concentrated source could be collimated rather well into a parallel beam before passage down the long absorption tube. Steel absorption tubes 4 feet long and 1 inch in diameter were used for the alkali metals. It was found that the steel did not appreciably shield the inside of the tube from the magnetic field of the solenoid. Electrical heating was provided for the two and one-half feet of the absorption tube actually inside the solenoid. The ends of the tube were cooled and the windows waxed on. A few lumps of the metal were placed at the middle, and distillation to the cool ends was hindered by the presence of about 5 mm of nitrogen or helium.

The proper vapor density for obtaining the magnetic rotation spectra was always determined in advance by finding the temperature of the absorption tube which gave strong, but well defined, discrete absorption lines. In general, for frequencies well outside the Zeeman pattern of a line, the magnitude of the rotation due to the line is proportional to the number of molecules per unit volume, the path length, and the field strength. In a molecular band system, however, too high a vapor density develops so many overlapping bands that absorption becomes practically complete and no magnetically rotated light can be observed. The temperatures used for Li_2, Na_2, and K_2 were approximately 850°, 460°, and 350°C, respectively. All spectrograms were made with a 21-foot grating in a stigmatic mounting, which gave a dispersion of 4.9A per mm in the first order around 8000A. The exposure times necessary for photographing magnetic rotation spectra ranged from one hour for the rotation in the Na_2 red bands, to 36 hours for the infrared K_2 system, using Eastman *Q* plates.

Some information about the sign of the rotation in the red Na_2 system and the infrared K_2 spectrum was obtained by the familiar quartz wedge scheme. A pair of 25° wedges was used, placed directly in front of the slit. For these spectrograms the crossed analyzing prism was placed between the slit and the mirror of the stigmatic mounting.

2. General Theory of the Faraday Effect Associated with a Single Spectral Line

Light propagated along the field through a magnetized medium experiences longitudinal magnetic double refraction. There are two and only two types of electromagnetic waves which progress along the field without change of form, but with different velocities. If the medium is isotropic except for the field, these two types are circularly polarized waves which rotate in the sense of a right- (+) or left-handed (−) screw advancing along the field direction. Light of any polarization entering such a medium can be considered decomposed uniquely into the sum of two circular waves with opposite polarizations. The character of the polarization at any point in the medium is most easily obtained by considering the difference in phase of the two circular polarizations occasioned by the difference of their velocities of propagation to the point. This difference of indices of refraction of the two circular polarizations is determined by the longitudinal Zeeman pattern of the absorption lines. Those components absorbing right- or

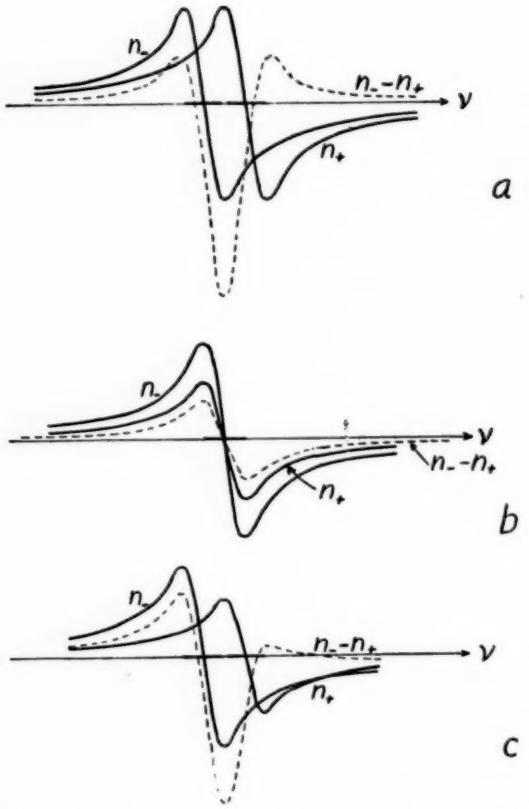

FIG. 1. Dispersion curves and Faraday rotations for light propagated along the magnetic field through a gas with a single sbsorption line. The half-widths of the components in absorption are indicated by the thickened portions of the frequency axis. (a) Lorentz doublet on classical theory. (b) Hypothetical line for which the intensities of the components are perturbed by the field, but for which there is no change in their frequencies. (c) Lorentz doublet with components both shifted in frequency and perturbed in intensity by the field.

left-handed polarizations affect the indices of refraction for right- or left-handed polarizations respectively, and to the same relative degree that they affect the absorption. Let plane polarized light, equivalent to two equal waves of opposite circular polarizations, be incident normally on a slab of magnetized medium. The longitudinal double refraction of the magnetized substance causes these disturbances to be propagated with unequal velocities. If the absorption coefficient for both waves is the same, their resultant at a distance l inside the medium will again be plane polarized, but with its plane of polarization turned through an angle θ given by

$$\theta=(\pi l/\lambda_{\text{vac}})(n_- - n_+), \qquad (1)$$

where $n\pm$ = index of refraction of right- (+) or left- (−) handed polarized light.

If the absorption coefficients for the two circular waves are unequal, the originally plane polarized light will become elliptically polarized at any point in the medium. The angle θ represents in this case the angle through which the major axis of the ellipse has been turned. The dotted line in Fig. 1a has a height proportional to $(n_- - n_+)$. This line shows the variation of θ connected with one absorption line showing a normal Lorentz doublet in longitudinal observation, with both components of the doublet of equal intensity. The rotation is symmetrical about the no-field position of the absorption line, approximately (exactly, if ν^2 is plotted along the horizontal axis instead of ν). Fig. 1b illustrates the case of a hypothetical line whose two magnetic components are not split apart by the magnetic field, but only changed in intensity. In this case, θ varies antisymmetrically about the absorption line. Fig. 1c illustrates the case where the field both splits apart the magnetic components of the line and changes the intensities at the same time. In this case the magnitude of θ is largest outside the low or high frequency side of the line according as the high or low frequency circular component is weakened by the field.

The rotation connected with absorption lines with more complex Zeeman patterns can be determined when the splittings and intensities of the components in the field are known. With no field, the sum of the intensities of the components affecting right circular light is exactly equal to the sum of the components affecting left circular light. This sum rule is just the mathematical statement of the fact that an unmagnetized gas does not alter the state of polarization of a light wave, provided that the direction of propagation of the light wave does not destroy the isotropy of the gas, producing optical activity. When a magnetic field is applied there are two distinct ways in which the sum of the intensities of the right- and left-handed components may become unequal. (1) If the ground state is magnetic, the different magnetic components of the ground level will have altered Boltzmann factors, which produce a difference in their populations. This will cause a difference in intensities of right- and left-handed components of the line roughly pro-

portional to $(\Delta\nu)_n/kT((\Delta\nu)_n=$normal Zeeman splitting). This is the so-called "paramagnetic rotation," important mainly at low temperatures. This type of rotation is asymmetric about an absorption line. Since no known band magnetic rotation spectrum is due to paramagnetic molecules, we shall discuss only the asymmetrical rotation arising from the second cause. (2) The perturbation of the transition probabilities by the magnetic field may cause the sum of the intensities of the right-handed to be different from the sum of the intensities of the left-handed components of a line, the difference being proportional to the field strength. (Throughout the paper we calculate only the Zeeman splittings and intensity changes which are linear in H. In all cases we assume that the Zeeman splitting of the absorption line and the change in intensity of the Zeeman components are due to the magnetic sensitivity of the upper level of the absorption line.)

The Zeeman splitting of the upper state energy levels, proportional to H, is caused by the diagonal matrix elements of the perturbing potential $-\mu_z H$, while the difference in intensities is produced by nondiagonal matrix elements of μ_z. ($\mu_z=$electronic magnetic moment along z, the field direction.) In atoms μ_z is a diagonal matrix, in the J, M representation; hence the Zeeman pattern of an atomic absorption line is symmetrical about the no-field line both as to position and intensities, and the resulting variation of θ is symmetrical about the line as in Fig. 1a. (This statement is not true if there is a tendency toward the Paschen-Back effect, but no Faraday rotations have ever been observed near atomic lines at field strengths high enough for the Paschen-Back effect to become important.) Physically, this means only that the motion of the atom in the upper state is one of pure precession, in which the J vector remains constant in magnitude but precesses with uniform speed about the field direction, making a constant angle with it.

In molecules, on the other hand, μ_z is not a diagonal matrix in the quantum number J. While the total angular momentum of the molecule along z is fixed, $\mathbf{J}$ itself varies both in magnitude and direction. In other words the axis of rotation of the molecule wobbles as it precesses about the field. The magnetic field exerts a torque on the molecule which tends to line up with the field the magnetic moment μ_J, which is directed oppositely to J in all regular states. The resulting nutational motion of the $\mathbf{J}$ vector is a compromise between this tendency and the gyroscopic action which tends to produce pure precession. The nutational or "lining up" action of the field on the molecule produces changes in the energy levels proportional to H^2, and the higher even powers of H only, and such higher order effects we are neglecting. Nevertheless, the transition probabilities of any transition of the molecule to or from such a "nutating" state will be changed by an amount proportional to H (and higher odd powers of H). The ψ functions for a molecule in such a nutating state, correct to the first order of H, will be

$$\psi(n, J, M)=\psi^0(n, J, M)$$
$$+\frac{(-H\mu_z(n, J, M; n', J+1, M))}{E_J-E_{J+1}}\psi^0(n', J+1, M)$$
$$+\frac{(-H\mu_z(n, J, M; n', J-1, M))}{E_J-E_{J-1}}\psi^0(n', J-1, M). \quad (2)$$

The total angular momentum of the molecule is no longer constant either in magnitude or direction, since the correct ψ function is a linear combination of ψ functions belonging to several J values. One may describe the fact that J is no longer rigorously a good quantum number by saying that the field causes radiationless transitions in which $\Delta J=\pm 1$, with appreciable probability. The nutating ψ function of Eq. (2) will have new nondiagonal matrix components of the electric moment, so that the transition probabilities to or from the nutating state (2) will be affected by the field linearly in H.

3. Rigid Molecules

We shall show in this section how both the sign and the asymmetry of the rotation due to a single magnetically sensitive absorption line of a rigid molecule can be predicted qualitatively and calculated. The Verdet constant (rotation per unit path length per unit field strength) con-

nected with a single magnetically sensitive absorption line is composed of two parts,

$$V \equiv V_A + V_B.$$

V_A varies symmetrically with frequency about the absorption line (outside the Zeeman pattern, the frequency dependence is $(V_A \propto \nu^2/(\nu_{jk}^2 - \nu^2)^2)$. This is the rotation which one gets on a classical theory where only the Zeeman splitting of the lines is considered, and not the change in intensity which may be produced by the field (Fig. 1a). V_B varies antisymmetrically about the absorption line. (Well outside the half-width of the line this variation with frequency is $V_B \propto \nu^2/(\nu^2 - \nu_{jk}^2)$.) This part of the rotation comes from calculating the difference produced by the field between the sum of the intensities of the components which scatter right-handed light and the sum of intensities of the components which scatter left-handed light. This term is calculable only by quantum mechanics, and is the essential quantum mechanical refinement in Faraday effect theory.

Making the rigid molecule assumption that the motion of the electrons about the internuclear axis is unaffected by the rotation of the molecule as a whole, only matrix elements of μ_z in (1) need be considered which are diagonal in the electronic quantum numbers n. Ω, the component of the electronic angular momentum along the internuclear axis, can be considered rigorously a good quantum number.

Explicit calculations for V_A due to a single line of a $^1\Pi \leftarrow {}^1\Sigma$ system (Li_2, Na_2, K_2 visible absorption bands) have been given by Serber.[7] The explicit formulae for the V_B terms produced by the individual lines of the $^1\Pi \leftarrow {}^1\Sigma$ systems are given in Appendix I. These V_B terms produced by the perturbation of the transition probabilities by the field are proportional essentially to the ratio of the Larmor frequency to the frequency of rotation of the molecule about **J**, which is given by the difference in energy between two adjacent rotational levels, $2BJ = h^2/4\pi^2 I$. The greater the moment of inertia I of the molecule, or the higher the magnetic field, the more nearly will the precessional frequency of J become comparable to the frequency of rotation of the molecule about J, and the more important the nutation terms become.

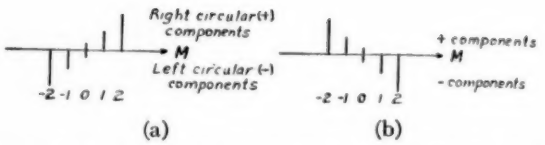

(a) (b)

FIG. 2. (a) Longitudinal Zeeman pattern for an R branch line with $J=2$ in its upper state. The vertical lengths of the components are proportional to the intensities. (b) Longitudinal Zeeman pattern for a P branch line with $J=2$ in its upper state.

The sign of the rotation outside a line depends on the relative strengths and positions of the components of the longitudinal Zeeman pattern. Serber has shown that outside an R line of a $^1\Pi \leftarrow {}^1\Sigma$ transition, the rotation should be positive, while outside a P line, the rotation should be negative, considering only the V_A terms. Fig. 2a is the longitudinal Zeeman pattern for an R branch line with $J=2$ in its upper state. The vertical lengths of the components are proportional to the intensities. The upper half gives the pattern for right circular (+) light, the lower half for left circular (−) light. Assuming that the upper (magnetic) state is regular, that is, that the positive M levels lie highest in energy, and neglecting the perturbation of the intensities by the field, the diagram represents the longitudinal Zeeman pattern with ν increasing toward the right. Using the diagrams of Fig. 1, the rotation outside the line will be positive. Fig. 2b gives the corresponding pattern for a P branch line with $J=2$ in its upper state. In this case the rotation outside the line will be negative. The physical reason for the difference in the two patterns can be ascertained qualitatively from the following vector diagrams. (Fig. 3a, 3b.) When a molecule absorbs a + quantum $(M' = M'' + 1)$, the **J** vector is turned more nearly parallel to the field (z direction). When the line is an R branch line $(J' = J'' + 1)$, the amount of the turning is greater when M' is negative than when it is positive. Hence one should expect the components with negative M' to be weaker than those with positive M'. The molecule more frequently absorbs quanta in transitions which require little change in the orientation of the **J** vector, the axis of rotation. Stated wave mechanically, the ψ functions for states whose axes of rotation have nearly the same orientation in space overlap

[7] R. Serber, Phys. Rev. **41**, 489 (1932).

better to produce nonvanishing elements of the electric moment. Fig. 3 illustrates this. The relative probability or improbability of the various transitions indicated by arrows is judged by the amount of change in the orientation of the **I** vector which they entail. All the transitions are absorptive, in which the arrows point to the final, higher energy state. (Thus the dotted arrows apply to absorption transitions in which the ground state is magnetic.) The essential point which such diagrams illustrate is that when J and M change in the same algebraic sense during a transition, little change in the orientation of the molecule is entailed when M is positive and the transition is probable. When, however, M is negative, Fig. 3b, the change of M and J in opposite senses (algebraically) entails the least change in direction of **J**, and hence is the more probable case. Similar diagrams for Q branch transitions illustrate why the components with $M=0$ are strongest.

From Appendix 1 it can be seen that for an R branch line $V_B=k^2\nu^2/(\nu^2-\nu_{jk}^2)$, where k^2 is a positive number independent of ν. For a P branch line $V_B=-k^2\nu^2/(\nu^2-\nu_{jk}^2)$. This results from the fact that the presence of the field augments the + components of an R branch line, and diminishes the − components. The field has just

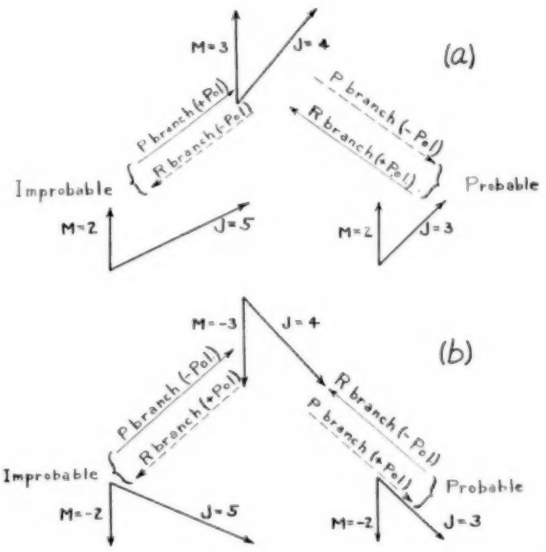

FIG. 3. Diagrams illustrating the change of orientation of the rotational axis (J vector) of a molecule when it absorbs circular quanta. The most probable transitions are those which can be accomplished with least change in the orientation of J. (a) Positive M; (b) negative M.

the reverse effect on the components of a P branch line. This change in the intensities is greatest for the components with $M=0$. The torque on the molecule exerted by the field is $\boldsymbol{\mu}_j\times\mathbf{H}$, where μ_j is the average electronic magnetic moment along **J**. The nutation effect is largest therefore when **J** is perpendicular to **H**. ($M=0$.)

In Fig. 4 the upper diagram symbolizes the nutating upper state level with $M=0$. The two lightly drawn vectors represent the orientation of the rotational axis of the molecule as it nutates in the field. The projection of these vectors on the field direction is not zero, but the angular momenta connected with their precession just balances their projections along z, so that the total angular momentum about z is zero during all phases of the nutatory motion. (M remains a good quantum number, even with nutation; μ_z is a matrix diagonal in M.) The two light vectors when rotated about z generate cones which are the libration limits for the rotational axis in its nutatory motion. The top diagram of Fig. 4 assumes a regular state, that is that μ_j is opposite to **J** (μ_j = the average electronic moment along **J** on which the field exerts its torque). In this case, just as with classical tops, the angular momentum about the rotational axis increases to $J=4$ as μ_j is pulled toward alignment with the field, and decreases to $J=2$ when the nutation swings μ_j toward the antiparallel position.

Again in Fig. 4 all the transitions indicated by the arrows are to be considered absorptive transitions, that is, the arrows always point toward the state of highest energy. Probability of transition is improved by the field if the nutation makes the transition possible with less change in the direction of **J** than was necessary without the field. For the two transitions illustrated at the right of the diagram, the intensity is increased by the field, because the field itself tends part of the time to turn the rotational axis toward the direction of the J vector of the ground level. For the transitions indicated by the arrows at the left of Fig. 4, during the time when the field tends to make the rotational axes of the two states more aligned, the J values differ by 2, and radiation can only produce a unit change in the magnitude of J in any dipole transition. Hence nutation diminishes this transition probability.

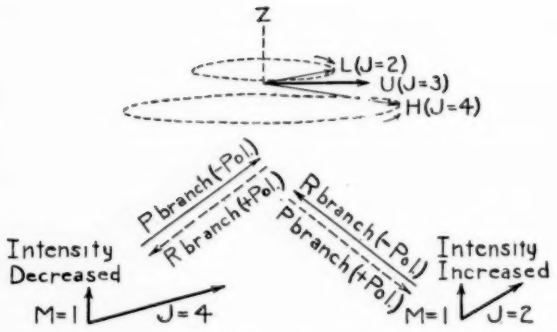

FIG. 4. Diagrams illustrating the effect of nutation on the transition probabilities.

It may seem at first sight curious that such quasi-classical vector diagrams give qualitatively the same effects on V_B and V_A as are calculated quantitatively with matrix elements. To be sure, when J and M for a state are known, we cannot say anything about the azimuth of J with the field, and we have only a probability distribution for the angle θ which J makes with the field. However, the vector of length $[J(J+1)]^{\frac{1}{2}}$ and projection M on H does have the most probable value of θ, or the direction of the maximum of the probability distribution in θ. The criterion that the orientation of J shall not change much in probable transitions is just another way of stating that the state functions of two levels connected by a probable transition must overlap well.

No detailed observation of the nature of the rotation due to a single band line of a $^1\Pi \leftarrow ^1\Sigma$ system has been made. Considered together, the V_A and V_B terms predict, for R branch lines, strong positive rotation for frequencies just greater than that of the line, and weaker positive rotation for frequencies just less than that of the line. This makes another reason why only strong lines just to the violet of R band heads appear in Loomis' work.

The alteration of the transition probabilities in the presence of the field can be interpreted in terms of an energy level diagram (Fig. 5). Without the field, the anomalous dispersion curve for light of + polarization associated with the absorption line $U \leftarrow G$ is associated with scattering processes in which the molecule absorbs a quantum to enter the state U and then re-emits it spontaneously in returning to G. Suppose that the state U has a magnetic moment and that the rotational frequency is comparable to the Larmor frequency. Then the molecule will nutate in a magnetic field and the state U will share properties with the adjacent rotational states H and L, because there exist nondiagonal elements of the magnetic moment between these states and the state U. If now the transition $L \leftarrow G$ takes place, there is a finite chance that the magnetic field will cause a "radiationless transition" to the state U, from whence the molecule may emit a coherent quantum in returning to the state G. Thus the field affects the anomalous dispersion curve of + light in the vicinity of the line $U \leftarrow G$. Whether the change in intensity of the anomalous dispersion curve about the line $U \leftarrow G$ is an increase or decrease can be determined from the diagram of Fig. 4, as has already been explained.

4. Asymmetrical Rotation Near Iodine Lines

That magnetized I_2 vapor between crossed Nicols caused light to be transmitted through them in the region of the visible band system was discovered by Righi.[1] High dispersion and resolving power study of the spectrum was carried out later by Wood and Ribaud.[8, 9]

Modern theory ascribes the visible bands to an intersystem transition $^3\Pi_{0u}{}^+ \leftarrow ^1\Sigma_g{}^+$, to the case a approximation, or $0_u{}^+ \leftarrow ^1\Sigma_g{}^+$ if the large spin-orbit interaction is taken into account. At first sight this description of the electronic nature of the states involved in the visible bands seems to preclude the existence of the magnetic rotation spectrum, for the molecule does not have a magnetic moment along J, to the rigid molecule approximation. To be sure the upper $^3\Pi_0$ state has a magnetic moment of one Bohr magneton along the internuclear axis as a result of the magnetic anomaly of the spin. Because $\Omega=0$ the magnetic moment remains perpendicular to J as the molecule rotates, and contributes nothing to the magnetic moment along J.

Serber has shown that the molecule in the upper state will acquire a magnetic moment along J when rotational distortion is taken into account.[7] This is due to nonuniform precession about the internuclear axis of the component of

[8] R. W. Wood and G. Ribaud, Phil. Mag. **27**, 1009 (1914).
[9] R. W. Wood and G. Ribaud, J. de phys. **4**, 378 (1914).

spin angular momentum perpendicular to this axis. Stated another way, the magnetic moment along J is produced by rotational distortion of the $^3\Pi$ spin multiplet. As we should expect, the faster the rotation, the larger the magnetic moment produced by rotational distortion. This explains why the magnetic rotation lines in I_2 appear to correspond to absorption lines of high J, and to be weak or absent near band heads or band origins. This hypothesis of spin uncoupling explains nicely the unusual sign of the rotation outside P and R lines. The wide $^3\Pi$ spin multiplet which contains the upper state for the visible bands is inverted, that is, states of largest Ω lie lowest in energy. This inversion of the spin multiplet causes magnetic energy sublevels with negative M to have the highest energy. Fig. 2 represents the polarization pattern for I_2 lines when frequency is assumed to increase toward the left in the direction of negative M. Formula (1) and the anomalous dispersion curves of Fig. 1 show that outside R branch lines the rotation should be negative, while outside P branch lines it should be positive.

Wood and Ribaud examined at high dispersion and resolving power the nature of the rotation outside six I_2 absorption lines covered by the broadened mercury green line.[8, 9] Loomis[10] found that five of these lines which show positive rotation were P lines, and the one which showed negative rotation on each side was an R line. Serber's hypothesis of spin uncoupling in an inverted $^3\Pi$ state explains this.

Wood and Ribaud published a qualitative sketch showing the nature of the rotation outside the six lines they observed.[8] They noted that the rotation seemed much stronger on one side of a line than on the other, in many cases as observed visually. Their qualitative sketch shows that outside the strongest P line observed (line 4 in Wood's numbering scheme), the positive rotation is strongest on the low frequency side of the line, while outside the strong R line observed, the negative rotation is strongest on the violet side of the line (line 3 on the published sketch).

Inasmuch as these are the only band lines outside which the detailed character of the rotation has ever been observed, it seemed of interest to see whether these asymmetries observed by Wood could be verified by extending Serber's calculation to take account of the perturbation of the intensities. The results of the calculation are given in Appendix 2. The calculations are not so readily visualized as those for rigid molecules, since we are now concerned with the effect of the simultaneous distortion of the electronic structure of the molecule in its upper state both by rotation of the molecule and by the field. The magnetic moment along J worked up by the rotation of the molecule is exceedingly small (of the order of 0.003 Bohr magneton when $J=100$).

In estimating the magnetic moment worked up by rotational distortion, Serber considered the nondiagonal rotational distortion matrix elements between $^3\Pi_0$ and $^3\Pi_1$ states. If the nondiagonal matrix elements of the magnetic moment between the same two states are considered, a V_B term also results for each line. The explicit formulae are in Appendix 2. The important thing about the formulae is the similarity in sign for the V_B terms for P and R branch lines. ($V_B=k\nu^2/(\nu_{jk}^2-\nu^2)$ for both branches, where k is a positive constant.) These V_B terms, when considered together with the V_A part of the rotation give just the type of asymmetry discernible near two lines in Wood's published sketch, which has been described above. Quantitative comparison of the V_B terms with the V_A terms calculated by Serber is impossible, for reasons given in the appendix, but qualitatively the V_B term does seem to explain the observed asymmetry, which was not expected by Wood in 1915, because all atomic lines give symmetrical rotations. Wood supposed the asymmetry to be

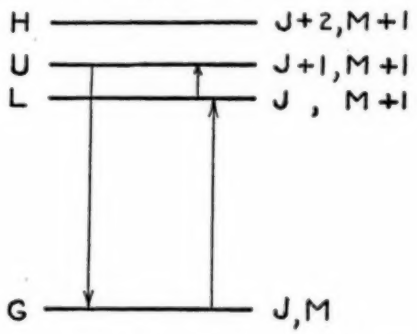

FIG. 5. Energy level diagram, illustrating the mechanism of the alteration of the intensities of the Zeeman components by the field.

[10] F. W. Loomis, Phys. Rev. **29**, 123 (1927).

due to the influence of neighboring lines, but the very discreteness of the I_2 magnetic rotation spectrum makes this not very plausible.

5. Magnetic Rotation of the Sodium Red Bands

Strong magnetic rotation spectra are produced in the absorption band systems of Na_2 and K_2, which are due to transitions from the ground $^1\Sigma$ state to the first excited $^1\Sigma$ state of each molecule. The analogous absorption system of Li_2 gives no magnetic rotation spectrum. The Na_2 bands in question extend from the D lines to around 8800A; the K_2 bands have been observed from the K_2 resonance lines at 7600A to 10,500A. Ever since the analysis of these absorption bands in the light of modern quantum theory showed that the electronic states involved are $^1\Sigma$ states, the existence of a magnetic rotation spectrum produced by these bands has been a puzzle. To the rigid molecule approximation, molecules in $^1\Sigma$ states do not have on the average a magnetic moment in any direction. Hence there should be no Zeeman splitting of such states in a magnetic field, or no Zeeman or Faraday effects for band lines involving transitions to or from them. There are three difficulties with ascribing the effect to rotational distortion. First, all high J lines should be affected and cursory inspection of the spectra shows that this is not so. Secondly, Van Vleck's theory of rotational distortion shows that the magnetic moment along J produced by rotational distortion of the upper $^1\Sigma$ state is proportional to the ratio of the rotational frequency about J to the frequency of precession of the perpendicular component of electronic angular momentum about the internuclear axis. This is equal to the ratio of the energy difference between adjacent rotational levels of the $^1\Sigma$ state to the energy difference between the $^1\Sigma$ and the $^1\Pi$ state above it. This ratio is small in all these molecules, even for high J values, in agreement with the fact that the Λ doubling in the $^1\Pi$ states is exceedingly small. The third difficulty is the absence of the spectrum in Li_2. In connection with this work, a further search for magnetic rotation was made in the Li_2 red bands, but none was observed.

The absence of the spectrum in Li_2 makes it seem plausible that spin orbit interaction may be the cause of the unexpected magnetic rotation in Na_2 and K_2, for spin orbit interaction increases roughly as the cube of the nuclear charge. The separation of the Li, Na and K atomic resonance lines, which are proportional to the spin orbit interaction energies of the valence electrons are respectively 0.3, 17.2, and 57.5 cm^{-1}.

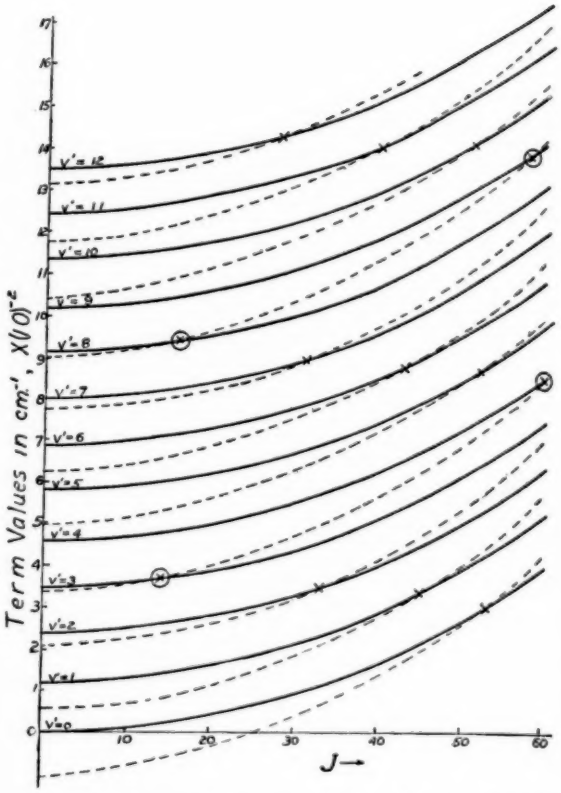

Fig. 6. Solid curves: energy levels of the upper state of the Na_2 red bands. ($^1\Sigma_u^+$). Broken curves: predicted energy levels of a $^3\Pi_{0u}^+$ state.

Fredrickson[6] succeeded in finding an assignment of quantum numbers for the lines of the red Na_2 magnetic rotation spectrum.[7] He discovered that most of the magnetic rotation lines involved a certain few of the upper state levels. He suggested on this basis the hypothesis that the spectrum was due to the perturbation of the upper $^1\Sigma$ state by some unknown magnetically sensitive state. The solid parabolic curves in Fig. 6 give the energies of the rotational states of the $^1\Sigma$ state as a function of J. (Since the B_v term in the rotation energy expression varies only slightly with v, the parabolas are almost parallel.) The energy levels found by Fredrickson to give magnetic rotation lines are marked by crosses.

Each of these levels will acquire a magnetic moment if it is perturbed by a level of a $^3\Pi$ state which does possess a magnetic moment. A perturbation between two levels may be described as a repulsion of the levels accompanied by a sharing of their properties. The magnetic moment which the perturbed $^1\Sigma$ level gets in this way will cause a Zeeman splitting for the level in a magnetic field, and hence magnetic rotation for transitions to this level. It is a fundamental rule in perturbation theory that the perturbation between two levels is appreciable only if the levels have the same J value and nearly the same energy. Therefore it should be possible to represent the levels of the $^3\Pi$ perturbing state on the diagram of Fig. 6 by a set of approximately parallel and equidistant parabolas which intersect the solid line parabolas very near the points indicated by crosses. It has been found that the set of perturbing state levels represented by the dashed curves in Fig. 6 do have their intersection point with the solid line parabolas very nearly at the crosses. The scale of the figure is too small to show the deviations. The positions of the dotted curves were arrived at in the following manner. (Unprimed letters refer to the constants of the $^3\Pi$ state.) It was observed that the large energy difference between perturbed rotational level $J'=14$, $v'=3$, and the next higher perturbed level $J'=60$, $v'=4$ can best be explained by the assumption that they are both perturbed by rotational levels belonging to a single vibrational level of the perturbing $^3\Pi$ state. In other words, a single dashed line parabola in Fig. 6 must pass through the points marked by circled crosses in levels $v'=3$ and $v'=4$. This requirement fixes the B value of the $^3\Pi$ state. Likewise the J values and term values of the perturbed levels in vibrational states $v'=8$ and $v'=9$ indicated by circled crosses, were used to fix the B value of another set of rotational levels of the $^3\Pi$ state. In both cases the B value turned out to be 0.140 cm^{-1}. The slight dependence of B on v was therefore neglected. Thus, from the known positions of the four circled crosses, we can determine the B constant for the $^3\Pi$ state and as well the positions of two of its vibrational levels, which will be determined by the points on the energy axis intersected by the two dotted parabolas through the circled crosses. We assume that these dotted parabolas refer to the levels $v=3$ and $v=7$ of the $^3\Pi$ state, and assume $x_e\omega_e$, which affects the calculations only slightly, to be 0.42 cm^{-1}, which is certainly of the right order of magnitude. Then we may calculate ω_e, knowing the energy difference between the $v=3$ and $v=7$ vibrational levels of the $^3\Pi$ state. It turns out to be 145 cm^{-1}.

With these approximate values of B and ω_e we may predict the positions of the rotational levels belonging to other vibrational levels of the $^3\Pi$ state to be those indicated by the other dotted parabolic curves in the figure. These dotted parabolas should intersect the solid parabolas at or near the circled crosses, in order that the required perturbations should occur at these places. Calculations show that they do, as is indicated on Fig. 6, where the scale is too small to make the deviations observable. Of course the v numbering of the vibrational levels of the perturbing state is arbitrary, and may have to be raised, with slight attendant change of ω_e. The constants of the $^3\Pi$ perturbing state so arrived at ($B=0.140$ cm^{-1}, $\omega_e=145$ cm^{-1}) agree with expectations, for they are intermediate between those of the ground state and those of the upper $^1\Sigma$ state of the red bands, as Mulliken has predicted for Li_2, and as is observed for H_2.[11]

6. Sign of the Rotations in the Sodium Red Bands

That the nature of the perturbing state must be $^3\Pi_{0u}{}^+$ can be deduced from the energy curves which Mulliken shows at the top of page 16 of reference 11, giving all the electronic states which can be formed out of one normal ^2S atom and one ^2P excited atom. The more complete label of the upper state of the red bands is $^1\Sigma_u{}^+$. Application of the perturbation theory rules that only levels with the same J and the same g or u and $+$ or $-$ symmetry can interact, excludes all but the $^1\Pi_u$ and $^3\Pi_u$ states from consideration as possible perturbers. The $^1\Pi$ state (upper state of the blue green bands) is known to lie too far above the $^1\Sigma$ state to cause any perturbations.

Singlet and triplet states may interact only by virtue of spin orbit interaction. Van Vleck has shown that the spin orbit interaction is diagonal in Ω. That is, only states with the same Ω may

[11] R. S. Mulliken, Rev. Mod. Phys. **4**, 16 (1932).

interact via spin orbit interaction. This consideration leaves us no other choice but to ascribe the perturbation to the $^3\Pi_{0u}{}^+$ component of the $^3\Pi_u$ state. (Thus we were justified in neglecting the sextuplicity of the $^3\Pi$ state in our previous calculation of its probable constants.)

To the rigid molecule approximation the $^3\Pi_0$ state does not have a magnetic moment along J for the $^1\Sigma$ state to borrow in the perturbation. The $^3\Pi_0$ state may fairly easily acquire magnetic moment along J due to rotational distortion. The separation of the $^3\Pi_0$ and $^3\Pi_1$ levels may be calculated from the separation of the sodium D lines and Mulliken's table on page 35 of reference 11 to be just 5.7 cm^{-1}. Therefore, the $^3\Pi_0$ state will acquire a sizable magnetic moment due to rotational distortion, which increases with J. This increase with J of the magnetic moment in the $^3\Pi_0$ perturbing state may explain the variation of the intensities of Fredrickson's doublets, which can be noted on the top strip of Plate 1A of reference 7. Clearly the higher the J' value of a doublet, the more intense it is, taking due cognizance of the falling plate sensitivity toward the right. We should expect this, ceteris paribus, if the perturbing $^3\Pi_0$ levels of high J possessed the larger magnetic moments.

The $^3\Pi$ multiplet in Na_2 is a regular, not an inverted, spin multiplet. From this fact it follows that a rotationally distorted $^3\Pi_0$ level in a magnetic field will have its highest energy for positive M values. We suppose that this rotationally distorted $^3\Pi_0$ level engages in a spin orbit perturbation with a close lying $^1\Sigma$ level in the presence of a magnetic field. The spin orbit perturbation can be considered simply a repulsion between like M levels which is greater the closer the levels are together. Clearly this repulsion of like M levels will push apart the degenerate sublevels of the $^1\Sigma$ state in such a way that positive M values have the highest energy. Reference to Eq. (1) and the polarization patterns of Fig. 1 will show that the rotation should be positive outside R branch perturbed lines, and negative outside P branch lines.

These signs as predicted were just the reverse from those listed by Fredrickson, which were taken from the early work of Wood and Hackett.[2] Inspection of a quartz wedge spectrogram of the region below 7000A, where all of Wood and Hackett's observations on the sign of the rotation were made, showed that the signs in this paper should be just reversed. There can be no doubt about the signs on this plate because the positive rotation outside the D lines was visible on the plate along with the molecular lines. The signs in Wood and Hackett's paper are correct if it be assumed that by the term "positive rotation" they mean rotation produced outside lines due to positive electron oscillators, which on 1908 theory should be in the negative sense about the field.

Observationally then, the rotation outside R branch perturbed lines is positive, and that outside P branch perturbed lines is negative. This is precisely the behavior required by the theory of the perturbed lines presented above. The negative rotation outside these P branch lines was in 1908 taken as a possible indication that they were produced by positive electron oscillators. It is amusing to note that rather refined perturbation theory considerations are needed to show that these negatively rotated lines are after all just P branch lines due to conventional negative electrons.

It was noted long ago by Wood that magnetic rotation in these sodium bands seems always to occur on one side or the other of the absorption lines, and very rarely is equally strong on both sides. This behavior is just what we might expect on the hypothesis that they are due to perturbations, if we take into account changes in the transition probabilities of the various Zeeman components of the perturbed line, attendant on the perturbation process. Those magnetic sublevels of the $^1\Sigma$ level which are perturbed most by a nearby $^3\Pi$ level will have weakened transition probabilities with the ground state. This follows from the fact that a perturbation between two levels involves a sharing of properties between them. The normalization condition for the mixed wave function of a perturbed level shows that the more $^3\Pi$-like the perturbed level becomes, the less $^1\Sigma$ likeness it can exhibit. Transitions from the singlet ground state to a perturbed level occur only to the extent that the wave function of the perturbed level is $^1\Sigma$ like. Thus transitions to positive or negative M values of the $^1\Sigma$ perturbed level are likely to be inhibited most by the perturbation, depending on whether the $^3\Pi$ perturbing level is below or above the $^1\Sigma$ level it

perturbs. Referring to the polarization patterns of Fig. 2, we can see that the sum of the intensities of the + and − circularly polarized components may not be equal any longer for the perturbed line in the presence of the field. This leads as before to asymmetrical rotation about the perturbed line. In fact if the difference in intensity of the + and − circular components is very marked, the rotation may conceivably be of opposite sign on the two sides of the line.

7. Magnetic Rotation Spectrum of the Infrared Potassium Band System

The magnetic rotation spectrum of this band system was photographed in the region from 8100A to 10,000A. The lines in general are sharper than the iron comparison lines. The exposure times varied from 12 to 36 hours. An attempt to assign quantum numbers to the lines was unsuccessful, apparently because it was not possible to reduce the temperature of the vapor sufficiently to show only the $v''=0$ progression. This maneuver enabled Fredrickson to solve the Na_2 spectrum. The lower ω_e value for the ground state of K_2 makes it relatively harder to do this. In the heavier molecule, the rotational levels lie closer together, and at the same time the spin orbit interaction responsible for the perturbation is larger. Fredrickson likewise observed toward the red end of the Na_2 spectrum that the lines occurred in groups whose center of gravity could be arranged into doublets. This means that in Fig. 6 we should have marked a cluster of crosses at adjacent rotational levels of the lowest three vibrational states, because a number of adjacent rotational levels of these vibrational states show magnetic rotation lines as evidence of their being perturbed. In K_2 it appears that there are large groups of perturbed levels in each vibrational level, which give rise to so many magnetic rotation lines that the assignment of quantum numbers is well-nigh impossible.

Toward the red end of the spectrum the magnetic rotation lines form clearly defined groups of around 40 lines each, the centers of gravity of these groups being about 84 cm^{-1} apart. This spacing is almost certainly indicative of ground state progressions.

Out of all of the magnetic rotation lines measured, some certain empirical regularity was found at the extreme red end of the spectrum. Most of the lines in several of the groups near 9600A could be arranged into constant spaced series, with spacings of from 2 cm^{-1} to 5 cm^{-1}. Each series contained from fifteen to twenty-five lines, and each group had about 5 or 6 series in it. These series almost certainly represent small segments of P and R branches whose upper state levels have received magnetic moment by being perturbed. We do not think that the upper levels of these short series could acquire their magnetic moments by rotational distortion, for rotational distortion affects all high J levels and should be observable for more than 25 levels if it produces big enough magnetic moments to cause magnetic rotation for any lines at all. Using a plausible predicted B constant for the upper state rotational levels, one finds that the most closely spaced series correspond to J values around 65, while the widest spaced series corresponds to J values around 150. The series appear to have constant spacing, of course, because the parabolas of the Fortrat diagram cannot be distinguished from straight lines at such high J values over such a short piece of a branch, containing only 25 lines.

Quartz wedge spectrograms supply the strongest evidence that the K_2 infrared magnetic rotation spectrum is produced by perturbations, just as is the analogous Na_2 magnetic rotation spectrum. The similarity between the wedge spectrograms of K_2 and those published by Wood for the similar sodium system[8] is very striking. The similarity extends even to the one-sidedness of the magnetic rotation at most absorption lines, as was first noted by Wood for sodium. Close examination of the wedge spectrograms reveals that the needles of light jut down into the central dark band on one side or the other of an absorption line. The point to be emphasized is the unusual character of such wedge spectra. The $^1\Pi \leftarrow {}^1\Sigma$ absorption systems of the alkalis give a magnetic rotatory effect because they have a perfectly normal rigid molecule Zeeman effect in the upper $^1\Pi$ state. The Zeeman and Faraday effects for the lines of a band are inversely proportional to J. All one obtains on a magnetic rotation spectrum of the bands is a single strong line outside the R head of each band. The single strong magnetic rotation line just outside the

head of each band is due to the contributions to the rotation at this frequency from the numerous low J lines piled up at the head of the band. We took wedge spectrograms of these bands in order to try to verify that the rotation outside the heads (formed in the R branch) was positive. It was found that the rotations were too small to be detected by the quartz wedge method. Precisely the same magnetic field, path length, and optimum vapor conditions were used for these bands as were used to produce the strong indications of rotation (and dichroism) near certain of the infrared lines. No needles of light outside the heads of bands could be observed to penetrate into the central dark fringe. The conclusion seems inescapable that the type of wedge spectrograms which is found only in the Na_2 and K_2 $^1\Sigma\leftarrow{}^1\Sigma$ absorption systems shows pathologically large rotations for band spectra. On the perturbation hypothesis, this unusually large effect is explained as has been outlined above, not only by the large magnetic moment which the perturbed level may possess, but also by the difference between the intensities of the right- and left-handed circularly polarized components of the perturbed level under the action of the magnetic field.

Conclusions

This study of diatomic magnetic rotation spectra was undertaken as a preliminary step with a view toward applying magnetic rotation spectra as a tool in the analysis of complicated polyatomic spectra, as had been suggested by Wood and Diecke,[12] and Loomis and Kusch.[13] These hopes appear not so very promising now. For one thing perturbations occur more frequently in polyatomic molecules than in diatomic ones. As in the Na_2 and K_2 systems just discussed, the magnetic rotation spectrum would just show the perturbations, the more complicated features of the spectrum, rather than its simplicities. The only case where any simplification might reasonably be expected would be the case of rigid linear molecules, which could give magnetic rotation lines at the heads of bands, similar to Loomis' spectra of alkali $^1\Pi\leftarrow{}^1\Sigma$ systems. If the magnetic rotation lines of a spectrum do not correspond to absorption heads, it is probable that the analysis of the magnetic rotation lines will be more difficult than the analysis of the absorption spectrum. The magnetic rotation spectrum seems most adapted as a sensitive means of detecting the presence of small magnetic moments in molecular levels, smaller than could be detected by other means (cf. the smallness of the magnetic moments responsible for the I_2 magnetic rotation spectrum. Section 4). The improvement in our understanding of the finer details of the Faraday effect in molecules which has been achieved by introducing quantum mechanical refinements, suggests the possibility that similar refinement of the transverse or Cotton-Mouton effect will lead to a better understanding of the details of that phenomenon, in particular its temperature dependence. Also it would seem interesting both to calculate theoretically and to look experimentally for the onset of saturation terms in the Faraday effect, particularly for heavy molecules with large moments of inertia where the first-order effect of nutation is appreciable, and the terms in the higher odd powers of H should become appreciable.

In conclusion I wish to thank Professor W. W. Watson, who suggested this problem, for his valuable discussions and encouragement throughout the course of the work. I wish also to express my appreciation for the opportunity of having studied the theory of these problems under Professors L. Page and H. Margenau.

[12] R. W. Wood and G. H. Diecke, Nature **128**, 535 (1931).
[13] P. Kusch and F. W. Loomis, Phys. Rev. **49**, 879 (A) (1936).
[14] R. deL. Kronig, Zeits. f. Physik **45**, 458 (1927).

Appendix 1

Substituting in Serber's formula (10) matrix elements given for instance by Kronig in reference 14 one obtains

$$V_B(R\text{ branch})=\frac{4\pi|e|\nu^2P^2}{3hmc^2}\,\frac{B^0e^{-Wi/kT}}{\nu^0(1,\,J+1;\,1J)(\nu^2-\nu(1,\,J+1;\,0J))}\,\frac{J(J+2)}{J+1},$$

$$V_B(P\text{ branch})=\frac{4\pi|e|\nu^2P^2}{3hmc^2}\,\frac{B^0e^{-Wi/kT}}{\nu^0(1,\,J;\,1J-1)(\nu^2-\nu(1,\,J-1;\,0J)^2)}\,\frac{-(J-1)(J+1)}{J},$$

$$V_B(Q\text{ branch})=\frac{4\pi|e|\nu^2P^2}{3hmc^2}\,\frac{B^0e^{-Wi/kT}}{2B'_{v'}(\nu^2-\nu(1J,\,0J)^2)}\,\frac{-(2J+1)}{J^2(J+1)^2}.$$

We have used the rotational energy formula $h\nu(J)=Bv'J(J+1)$ in order to simplify expression for the Q branch. The notation is the same as Serber's. J is the rotational quantum number of the ground level. If one makes the assumption that ν is well outside the triplet of lines emanating from a given ground level J, all the V_B and V_A terms for these lines add together to give a rotation proportional only to the number of molecules per unit volume with that J value, and otherwise independent of J. This checks with Serber's application of Niessen's rule to rigid molecules.[7]

Appendix 2

Calculation of the asymmetrical notation outside iodine lines

Substituting matrix elements obtained from reference 14 into the third term of formula 8 of Serber's paper, one obtains

$$V_B(R\text{ branch})=\frac{\pi|e|Nv,\,J}{3hmc^2}\left[\frac{\nu^2}{\nu(^3\Pi_0,\,v',\,J+1;\,^1\Sigma,\,v,\,J)^2-\nu^2}\right]\left[\frac{J+1}{2J+1}\right]\left[\frac{\{Px'(^1\Sigma,\,^3\Pi_1)Sy'(^3\Pi_1,\,^3\Pi_0)Pz'(^3\Pi_0,\,^1\Sigma)\}}{\nu(^3\Pi_0,\,^3\Pi_1)}\right],$$

$$V_B(P\text{ branch})=\frac{\pi|e|Nv,\,J}{3hmc^2}\left[\frac{\nu^2}{\nu^2(^3\Pi_0,\,v',\,J-1;\,^1\Sigma,\,v,\,J)-\nu^2}\right]\left[\frac{J}{2J+1}\right]\left[\frac{\{Px'(^1\Sigma,\,^3\Pi_1)Sy'(^3\Pi_1,\,^3\Pi_0)Pz'(^3\Pi_0,\,^1\Sigma)\}}{\nu(^3\Pi_0,\,^3\Pi_1)}\right],$$

where $Nv,\,J$ = number of molecules per unit volume with vibrational quantum number v and rotational quantum number J of the ground electronic state ($^1\Sigma$),

$\nu(n,\,n')=(En-En')/h$, where En is the energy of the state with quantum numbers symbolized by the index n,

$x',\,y',\,z'$ = coordinates referred to axes fixed in the molecule, with z' axis running through the nuclei,

$Pz'(n,\,n')$, $Px'(n,\,n')$ = matrix elements of the components of the electric moment of the molecule, with no magnetic field,

$Sy'(n,\,n')$ = matrix element of the component of spin angular momentum perpendicular to the internuclear axis with no magnetic field.

The above V_B terms, together with V_A calculated by Serber, estimate the effect on the rotation of rotational distortion and the magnetic field. First-order perturbation of the intensities of transition by rotational distortion are considered negligible, because the terms would have the square of the large precessional frequency $\nu(^3\Pi_0,\,^3\Pi_1)$ in their denominators ($\sim$3800 cm^{-1}).

The formulae for V are not supposed to be quantitatively accurate. For one thing, in the calculations the diagonality with respect to v' was assumed of the various elements of the electric and magnetic moments between the $^3\Pi_0$ and $^3\Pi_1$ states. This is not at all legitimate, because the spin orbit interaction in I_2 is so large that the energy curves for these two components of the $^3\Pi$ spin multiplet are very different, and hence possess different sets of vibrational eigenfunctions. (Cf. the energy curves drawn in reference 15.)

As to the factors in the preceding expressions, the first brackets show the dependency on frequency. The second brackets give the variation with J. The numerator of the third factor, in curly brackets, is positive. Likewise the denominator is positive, because the $^3\Pi$ state is inverted. It is the curly bracket expression in the final factor which makes quantitative comparison of the relative magnitudes of V_B and V_A impossible. This factor makes V_B depend on a geometric mean of the intensities of the intersystem bands, $^3\Pi_1\leftarrow{}^1\Sigma$, and $^3\Pi_0\leftarrow{}^1\Sigma$. These transitions are observed only because of the strong spin orbit interaction, which renders the spin not rigorously a good quantum number. Van Vleck, in reference 15, tells why the intensities of two such intersystem transitions may be radically different. V_A, on the other hand, depends only on the intensities of the $^3\Pi_0\leftarrow{}^1\Sigma$ bands.

The important thing about the above formulae is the sign of the V_B term, which is the same for P and R branches. Taken in conjunction with V_A as calculated by Serber, these formulae produce the asymmetry of rotation outside P and R lines which was found by Wood and Ribaud and has already been discussed in Section 4.

---

[15] J. H. Van Vleck, Phys. Rev. **40**, 544 (1932).

The Electric Quadrupole Moment of In^{115}

R. F. Bacher and D. H. Tomboulian
Cornell University, Ithaca, New York
(Received August 16, 1937)

Measurements of the lines λ7852 ($5s6p\ ^1P \rightarrow 5s6s\ ^1S$) are λ8241 ($5s6p\ ^1P \rightarrow 5s5d\ ^1D$) of In II show deviations from interval rule. These deviations are satisfactorily accounted for by the presence of a nuclear electric quadrupole moment which from the first of the lines is found to be $Q = 0.82 \times 10^{-24}$ cm². No trace of lines due to In^{113} was found.

MEASUREMENTS on the hyperfine structure of the lines of indium II by Paschen and Campbell[1] have shown that the nuclear spin is $4\frac{1}{2}$ from the use of the interval rule. Several terms of the $5sns$ and $5s6p$ configurations lead uniquely to this value for the nuclear spin. Further work by Paschen[2] has showed that the interval rule is followed more closely by the low ^3S terms than by the ^3P and ^3D terms. The higher ^3S terms show marked deviations from the interval rule. These deviations and those in the ^3P and ^3D terms are due mainly to the presence of nearby levels so that perturbations occur between terms of the same total angular momentum F. Paschen has discussed these deviations for higher series members in some detail. In order to ascertain whether there were also deviations from interval rule which were not due to perturbations of this sort but which might arise if the nucleus possessed an electric quadrupole moment, lines involving the $5s6p\ ^1P$ and $5s5d\ ^1D$ terms were investigated.[3] The $5s6p\ ^1P$ term is sufficiently removed from the ^3P term of the same configuration so that perturbation of the type mentioned is negligible. This is also true for the $5s5d\ ^1D$ term but, due to a different type of perturbation from the $5p^2\ ^1D$, it is not useful for determining the quadrupole moment. This latter perturbation does not affect the interval rule however, and the observed deviations may be attributed to electric quadrupole moment.[3]

The indium spectrum was excited in a hollow-cathode discharge tube operated under a variety of conditions. The cathode was run hot and the current in the lamp frequently exceeded one ampere. This did not seem to broaden the lines appreciably. The radiation was studied with a Fabry-Pérot etalon with fixed separators used in conjunction with a Zeiss three prism spectrograph. The interferometer and the spectrograph were kept in a constant temperature room and the interferometer remained in adjustment for days at a time though the exposures were never longer than two hours. For accurate measurements, it was found advisable to use small grain, high contrast plates, though when weaker components were sought the faster plates were used. Most attention was confined to the lines λ7852 $5s6p\ ^1P \rightarrow 5s6s\ ^1S$ and λ8241 $5s6p\ ^1P \rightarrow 5s5d\ ^1D$. For the first of these lines a rather large number of photographs were taken and the separations reduced in order to get an idea of the deviations which might be expected in measurements on a simple well resolved line. For this purpose 3, 5 and 8 mm separators were used. The separators completely change the relative spacings of the components as can be seen in Fig. 1. For this line about ten orders of the interference pattern were measured on each plate.

Table I shows the results obtained for different plate separations for the three component line λ7852. The separations show *maximum* deviations from the mean of 2×10^{-4} cm^{-1} and 3×10^{-4} cm^{-1} for the larger and smaller intervals respectively. There does not seem to be any dependence of the measured interval on the interferometer separator which was used. Such a dependence might have been expected had certain systematic errors which were due to the relative spacing of the observed components, been present in the measurements. It seems that the measurements of a completely resolved and well separated pattern are really very accurate. The measure-

[1] Paschen and Campbell, Naturwiss. **22**, 136 (1934).
[2] Paschen, Sitzungsbericten der Preussischen Akademie der Wissenschaften 456 (1934); 431 (1935).
[3] Bacher and Tomboulian, Phys. Rev. **50**, 1096 (1936).

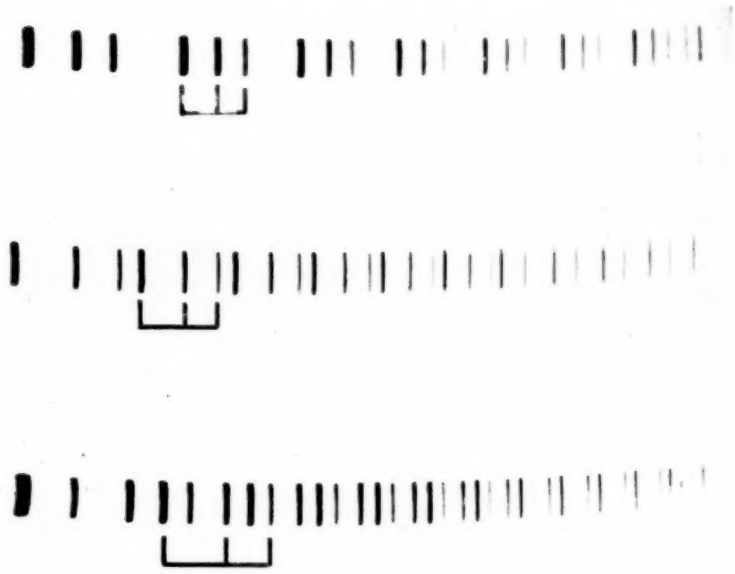

FIG. 1. Interferometer patterns of λ7852 ($5s6p\ ^1P \rightarrow 5s6s\ ^1S$) taken with 8 (bottom), 5 (middle) and 3 mm separators.

ments of λ7852 give the hyperfine separations of the ^1P term directly as seen from Fig. 2. The separations of the ^1P state show definite deviations from the interval rule. Using the same over-all separation, the central level would necessarily be so placed that the two hfs. separations would be 357.7 and 437.1×10^{-3} cm^{-1} (Fig. 2) if the interval rule holds. The values differ from the observed separations by 5.2×10^{-3} cm^{-1} which is respectively 17 and 26 times the *maximum* deviation found in these measurements.

The interval rule follows directly from the simple form of interaction between the nuclear magnetic moment and the electrons. A deviation from the interval rule does not mean that this form of the interaction is insufficient or incorrect. Such deviations are frequently found where two states of different angular momentum J approach each other. If the distance of such states approaches the hyperfine separations, then large deviations are expected. The deviations are appreciable for separations of the states of different J of 100 cm^{-1} or more. In the present case of $5s6p\ ^1P$ the nearest states are those of the $5s6p\ ^3P$. All of these should perturb the ^1P slightly but the effect of the $^3P_0$ would be greatest since it would affect only the central hyperfine level of $^1P_1$. This perturbing effect would be less than 10^{-4} cm^{-1} and is therefore neglected here. No other perturbations are expected and it appears that the deviations from the interval rule are due to the inadequacy of the interaction term. They can be accounted for by assumption of an electric quadrupole moment for the nucleus as found in other cases.

That this explanation is plausible will be seen from the measurements on the nine component line λ8241 ($5s6p\ ^1P_1 \rightarrow 5s5d\ ^1D_2$). This line is considerably more complex and the measurements of the intervals less accurate. Fig. 3 shows the level scheme and pattern of the line and

TABLE I. *Separations of the $5s6p\ ^1P_1$ state of In II. The separations of the $^1P_1$ state were measured from λ7852 ($5s6p\ ^1P \rightarrow 5s6s\ ^1S$).*

SEPARATOR MM	INTERVAL 11/2–9/2 10^{-3} CM^{-1}	DEV. FROM MEAN 10^{-3} CM^{-1}	INTERVAL 9/2–7/2 10^{-3} CM^{-1}	DEV. FROM MEAN 10^{-3} CM^{-1}
3.1226	432.0	+0.1	363.2	+0.3
3.1223	431.9	0.0	362.8	−0.1
"	432.0	+0.1	362.8	−0.1
"	431.7	−0.2	362.9	0.0
5.0136	432.1	+0.2	362.7	−0.2
"	431.7	−0.2	362.6	−0.3
"	431.7	−0.2	363.0	+0.1
8.0083	431.9	0.0	362.8	−0.1
"	432.1	+0.2	363.2	+0.3
"	432.0	+0.1	362.9	0.0
Mean	*431.9*		*362.9*	

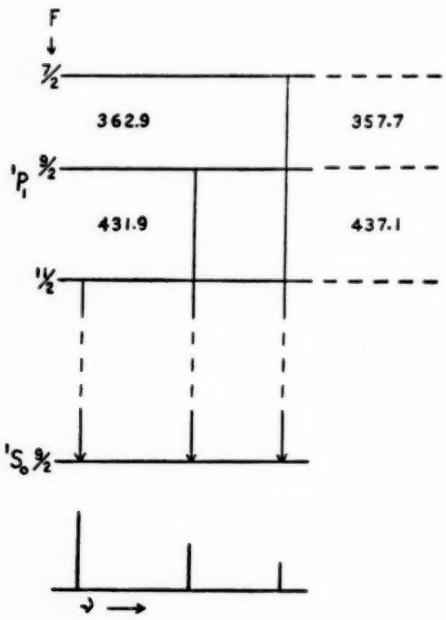

FIG. 2. Level scheme and line structure observed for λ7852.

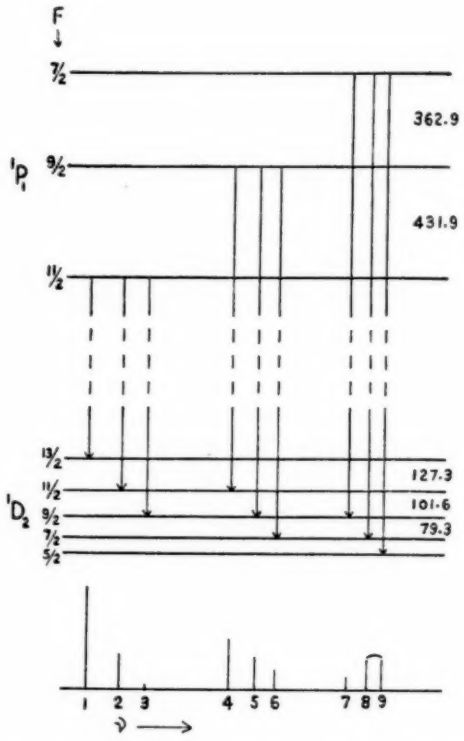

FIG. 3. Level scheme and line structure observed for λ8241.

Table II gives the measured separations of the $^1D_2$ level. Component 3 was too weak for accurate measurements and components 8 and 9 were resolved only in one or two cases and their measured separations thus unreliable. Fig. 4 shows the separations of the $^1D_2$ level observed, and also by using the over-all separation to determine the interval factor and assuming the interval rule to be correct. The center of gravity found from the two unresolved lines was used. These deviations are not due to perturbations for there are no perturbing levels nearer than 3700 cm^{-1}. The $5s5d\ ^1D$ is, however, perturbed by the $5p^2\ ^1D$ but the interval rule is not affected thereby. The deviations must be due to a different form for the interaction energy presumably from the presence of an electric quadrupole moment. Such a moment gives rise to a characteristic change in the hyperfine separations. The separation of any two hyperfine levels F and F' can be written[4]

$$\Delta(F-F')=\tfrac{1}{2}A(K-K') + \tfrac{3}{8}B\{K(K+1)-K'(K'+1)\}, \quad (1)$$

where $K=F(F+1)-I(I+1)-J(J+1)$

and A and B are constants, the first associated with the separation due to the nuclear magnetic moment and the second arising from the contribution of the electric quadrupole moment. The observed values of the two largest separations of $5s5d\ ^1D_2$ have been used to determine $A=18.47$ and $B=0.0615\times10^{-3}$ cm^{-1} and the remaining separations and over-all separation determined from them. In Fig. 4 the levels on the right show the separations so determined. The agreement indicates that the assumption of an electric quadrupole moment is justified. The determination of the moment itself from the above value of B cannot be carried out with any

TABLE II. *The separations of the $5s5d\ ^1D_2$ state of In II as measured from the line λ8241 ($5s6p\ ^1P\rightarrow5s5d\ ^1D$).*

Separator mm	Interval 13/2–11/2 10^{-3} cm^{-1}	Dev. from mean 10^{-3} cm^{-1}	Interval 11/2–9/2 10^{-3} cm^{-1}	Dev. from mean 10^{-3} cm^{-1}	Interval 9/2–7/2 10^{-3} cm^{-1}	Dev. from mean 10^{-3} cm^{-1}
3.0015	127.1	−0.2	101.0	−0.6	79.2	−0.1
"	128.1	+0.8	101.5	−0.1	83.0	+3.7
3.1223	126.9	−0.4	103.5	+1.9	—	—
3.1226	127.7	+0.4	102.2	+0.6	76.0	−3.3
"	126.6	−0.7	100.0	−1.6	79.2	−0.1
Mean	*127.3*		*101.6*		*79.3*	

[4] See H. B. G. Casimir "On the Interaction between Atomic Nuclei and Electrons." Prize Essay published by "Tyler's Tweede Genootschap."

degree of accuracy for this level due to the perturbation by $5p^2\,{}^1D$ which makes the character of the level uncertain.

The value of the nuclear electric quadrupole moment can be found from a consideration of the $5s5p\,{}^1P_1$ level. From the observed separations using (1), $A=-79.37\times10^{-3}$ cm^{-1} and $B=0.141\times10^{-3}$ cm^{-1}. In the case of only three levels there is no check on the value of B. The value of the quadrupole moment[4] in terms of B is found to be

$$Q=\frac{-BJ(2J-1)I(2I-1)}{7.9\langle((3\cos^2\theta-1)/r^3)_{JJ}\rangle_{Av}}, \qquad (2)$$

where $\langle((3\cos^2\theta-1)/r^3)_{JJ}\rangle_{Av}$ depends upon the electron configuration, the coupling and upon relativistic corrections and B is given in units 10^{-3} cm^{-1}. For $sp\,{}^1P_1$,

$$\left\langle\left(\frac{3\cos^2\theta-1}{r^3}\right)_{JJ}\right\rangle_{Av}=-\left\{c_1{}^2\frac{(2l-1)(l+2)2l}{(l+1)(2l+1)(2l+3)}\left\langle\frac{1}{r^3}\right\rangle_{Av}^{\prime,\prime}-\frac{12c_1c_2[l/(l+1)]^{\frac{1}{2}}}{(2l+1)(2l+3)}\left\langle\frac{1}{r^3}\right\rangle_{Av}^{\prime,\prime\prime}\right\}.$$

The factors c_1 and c_2 depend on the coupling

$$c_1=\cos(\theta-\theta_0);\quad c_2=-\sin(\theta_0-\theta),$$

where $$\theta_0=\arctan[l/(l+1)]^{\frac{1}{2}}$$

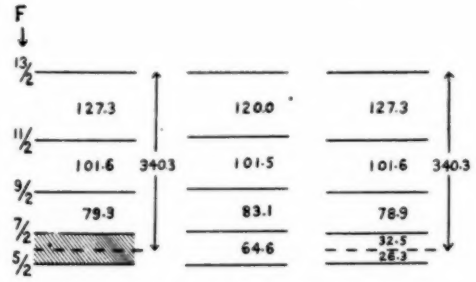

FIG. 4. Measured intervals of $5s5d\,{}^1D_2$ are shown on the left. The center sketch shows the separations obtained assuming the interval rule and with the separation constant determined from the over-all separation. On the right are the calculated levels found by using the two larger level separations for the determination of A and B.

and $\sin^2\theta=\Delta/d$, Δ being the deviation of the $^3P_1$ term from its position if the interval rule held exactly and d the $^3P_1-{}^1P_1$ separation. $\langle1/r^3\rangle_{Av}{}^{\prime,\prime}$ and $\langle1/r^3\rangle_{Av}{}^{\prime,\prime\prime}$ are equal to certain relativistic correction terms[4] times $\langle1/r^3\rangle_{Av}$.

For indium $5s6p$, $c_1=0.915$ and $c_2=-0.404$

$$\langle((3\cos^2\theta-1)/r^3)_{JJ}\rangle_{Av}=-0.425\langle1/r^3\rangle_{Av}.$$

The value of $\langle1/r^3\rangle_{Av}$ can be obtained in terms of the doublet separation, or here, in order to include the screening of the $5s$ electron, from the $5s6p\,{}^3P$ separation. $\langle1/r^3\rangle_{Av}$ can be found to be

$$\langle1/r^3\rangle_{Av}=\delta/\{HZ_i(l+\tfrac{1}{2})R\alpha^2\}.$$

Here δ is the separation, H a relativistic correction factor[4] 1.06, Z_i is taken as $(Z-4)$ and $\langle1/r^3\rangle_{Av}=1.84$ which gives

$$Q=0.82\times10^{-24}\text{ cm}^2.$$

This value of Q is essentially the same as the value $R^2=1.0\times10^{-24}$ cm^2 reported previously,[3] since $Q=2IR^2/(2I+3)$.

$Q=0.82\times10^{-24}$ cm^2 is also in agreement with the value $Q=0.8\pm0.2$ recently reported by Schüler and Schmidt[5] from a study of the $5p\,{}^2P_{3/2}$ term of In I.

A considerable search was made to find evidence of In^{113} expected[6] to be present to the extent of about 4.5 percent. Though long exposures of several lines were made which clearly showed components whose intensity represented only 2 percent of the total intensity of the line, no trace of components attributable to In^{113} was found. This indicates that the components of In^{113} are probably concealed under those of In^{115} which means that the angular momenta and magnetic moments are probably the same for the two isotopes; $I=9/2$, $\mu=5.7$ nuclear magnetons. Such a value for the nuclear spin of In^{113} is quite adequate[7] to explain the stability of this isotope and Cd^{113}, since the change from one to the other would be highly forbidden with $\Delta I=4$.

[5] Schüler and Schmidt, Zeits. f. Physik **104**, 468 (1937).
[6] Aston, Proc. Roy. Soc. **149**, 396 (1935); Sampson and Bleakney, Phys. Rev. **50**, 456 (1936).
[7] Bethe and Bacher, Rev. Mod. Phys. **8**, 200 (1936).

Dissociation Processes Produced in $SbCl_3$, $AsCl_3$ and PCl_3 by Electron Impact

P. KUSCH,* A. HUSTRULID AND JOHN T. TATE
Department of Physics, University of Minnesota, Minneapolis, Minnesota

(Received August 16, 1937)

The products of dissociation of $SbCl_3$, $AsCl_3$ and PCl_3 by electron impact have been investigated. Ions of the types XCl_3^+, XCl_2^+, XCl^+, X^+, XCl_2^{++}, XCl^{++}, X^{++} and Cl^+ have been observed. The efficiencies of production of these ions for various electron energies have been investigated. The appearance potentials have been determined and a partial analysis of the results has been made.

THE work to be described in this paper is the outgrowth of a search which was made for weak isotopes of the elements antimony, arsenic and phosphorus. The trichlorides of these elements were introduced into a mass spectrograph and the peaks due to the ions of these elements, produced from the trichlorides by dissociation due to electron impact, investigated. Because dissociation of the trichlorides into chlorine and the ion of the corresponding element does not occur to any large extent, no effective search for previously undiscovered isotopes was possible. Because of the fact that chlorine itself has two isotopes, no useful information could be obtained from an investigation of the peaks due to the various chlorides. It is possible to say that no isotopes of antimony exist between mass numbers 119 and 125, except those previously known at 121 and 123, to within one part in a thousand. The relative abundance of the isotopes 121 and 123 was found to be $Sb^{121} : Sb^{123} = 57.1 \pm 0.1$ percent : 42.9 ± 0.1 percent. Aston[1] has found the value 56 : 44 for the same ratio.

During the course of this investigation a great deal of information was obtained about dissociation processes occurring in $SbCl_3$, $AsCl_3$ and PCl_3 under electron impact and this will be discussed.

The mass spectrograph used in this investigation was similar to that described by Tate, Smith and Vaughan.[2] It was possible to obtain fairly good resolution of the mercury isotopes. Measurements at the maximum attainable field gave a background between the peaks due to the mercury isotopes equal to about one-tenth the peak height. The peaks measured in the present investigation overlapped so little that the peaks due to $SbCl_3^+$ at 234, 232, 230, 228 and 226 had almost exactly the relative intensities predicted from the known isotopic constitution of antimony and chlorine.

The antimony and arsenic trichlorides were placed in bulbs attached to the mass spectrograph and the pressure in the ionizing chamber was adjusted by adjusting the temperature of the bulbs. The phosphorus trichloride was introduced to the system through a capillary leak described by Smythe.[3]

It was not feasible to bake out the apparatus between the various runs. No appreciable impurities were present when the first runs were made on $SbCl_3$, and it was possible to determine both the intensity and the appearance potential of the Cl^+ produced from this molecule. When the runs on $AsCl_3$ were made, $SbCl_3$ and its products of dissociation were present as impurities, and in the runs on PCl_3, $SbCl_3$, $AsCl_3$ and their products of dissociation were present as impurities. In neither of the last two cases could significant data on Cl^+ be obtained.

No differential pumping system was used to keep products of thermal dissociation at the filament from diffusing back into the ionizing region. It is possible, therefore, that some of the ions observed are, in part, due to such products of thermal dissociation.

The observed ions, their relative intensities at an electron energy of about 120 volts, and their appearance potentials are listed in Table I. The probable error in the determination of the appearance potentials of the intense singly

* Now at Columbia University.
[1] Aston, *Mass Spectra and Isotopes* (Longmans, 1933).
[2] Tate, Smith and Vaughan, Phys. Rev. **48**, 525 (1935).
[3] Smythe, Rev. Sci. Inst. **7**, 435 (1936).

ionized products is about a half volt. For the other ions the error is greater and may be as much as three times as great. Ions of the type XCl_3^{++} were unobservable as were the ions As^{++} and P^{++}. No Cl_2^+ was found.

Efficiency of ionization curves were obtained for the first four ions for each element listed in Table I. The curves for $SbCl_3^+$ and PCl_3^+ show no maximum for electron energies up to 135 volts, and the efficiency of ionization reaches an essentially constant value at 60 volts electron energy. The curve for $AsCl_3^+$, however, shows a sharp maximum at 30 volts and then decreases to a value which is constant from 60 to 135 volts. The ratio of the efficiency at its maximum value to its constant value is about 1.6. Similarly the curves for $SbCl_2^+$ and PCl_2^+ show no maxima, and the efficiency reaches a nearly constant value at about 100 volts. The efficiency of production of $AsCl_2^+$ shows a sharp maximum at 28 volts and then decreases to a value which is constant between 45 and 135 volts. The ratio of the efficiency at its maximum value to its constant value is about 1.2. $SbCl^+$ and $AsCl^+$ have a maximum efficiency of production at 30 volts. For PCl^+ the maximum lies at about 33 volts. The efficiency decreases slowly up to the limit of measurement at 135 volts for all three of these ions. The ions Sb^+, As^+, and P^+ all show maximum efficiencies of production at about 42 volts, after which the efficiencies drop slowly up to the limit of measurement.

The most striking feature of the results is the high intensity of ions of the type XCl_2^+. Ordinarily the probability of dissociation plus ionization is much smaller than the probability of ionization alone. While it is possible that dissociation at the filament may in part account for the high intensities of these ions, it is believed that this factor is of small importance. The fact that the relative intensities of the ions XCl_2^+ and XCl_3^+ are independent of the pressure in the ionizing region points to the conclusion that XCl_2^+ is formed directly from the XCl_3 by an electron impact. Further evidence on this point is the fact that the production of the ions X^+ and Cl^+, with their observed appearance potentials can readily be explained on the assumption that they arise from a single electron impact on XCl_3. If thermal dissociation at the filament occurred to any large degree, the ions Cl_2^+ should be observable. No such ions were detected.

TABLE I. *Ions formed in $SbCl_3$, $AsCl_3$ and PCl_3 by electron impact. i = Relative intensity at an electron energy of 120 volt. A = Appearance potential (volts).*

	Sb		As		P	
Ions	i	A	i	A	i	A
XCl_2^+	100	11.4	100	12.3	100	12.2
XCl_2^+	171	12.3	166	13.0	182	12.5
XCl^+	30	16.4	26.4	17.0	38	17.5
X^+	40	17.0, 19.8	17.2	21.6	36	22.1
XCl_2^{++}	5.2	32.1	3.8	33.1	2.4	
XCl^{++}	4.5	34.8	0.6		0.4	
X^{++}	0.4	38.0				
Cl^+	16.7	20.7, 24.0				

The relative configurations and position of the hypersurfaces which represent the energy of the molecule as a function of the nuclear coordinates in the normal state and in some state of the ionized molecule determines, in part, the relative probability of formation of the different species of ion. Apparently the relative configuration is such that when the energy of XCl_3 is raised to a point on the hypersurface corresponding to an electronic state of the ionized molecule, it is more probable that the molecule falls into the trough in the surface leading to dissociation into the system $XCl_2^+ + Cl$ than into the depression corresponding to XCl_3^+. The more usual case in which dissociation plus ionization is less probable than ionization alone, means that the depression in the hypersurface of the normal state corresponding to the normal molecule occurs for about the same values of the nuclear coordinates of the nuclei as does the depression in the hypersurface of an ionized state corresponding to the ionized molecule. Transitions may, of course, occur between the normal state and several of the excited states of the ionized molecule. Different conditions may obtain for these different transitions, and certain of the ions may be produced by one electronic transition and others by another transition. The observed probability of formation of an ion then depends on the relative probability of the possible electronic transitions, as well as on the configuration of the energy hypersurfaces representing these electronic states.

The low observed appearance potentials of the

ions XCl_2^+ are rather surprising. It must be argued either that the binding energy of Cl to XCl_2 is much smaller than the binding energy of the remaining chlorine atoms, or else that the ionization potential of XCl_2 is much smaller than that of XCl_3.

Sufficient thermochemical and spectroscopic data are not available to permit a complete analysis of the results to be made. From thermochemical data given by Bichowsky and Rossini,[4] and from the spectroscopic value of the energy of dissociation of chlorine given by Sponer,[5] the energies of dissociation of the processes

$$XCl_3 \rightarrow X + 3Cl \qquad (1)$$

are calculated to be 8.8 volt for Sb, 7.7 volt for As and 8.1 volt for P. The energies of dissociation of the processes

$$XCl_3 \rightarrow X + Cl_2 + Cl \qquad (2)$$

are less than the above by the dissociation energy of chlorine, 2.5 volt. From these results and from the known ionization potentials, $I(Sb) = 8.35$ volt, $I(As) = 10.5$ volt, $I(P) = 10.9$ volt, the following values are obtained for the minimum energy required for the formation of the ions X^+ by the processes (1) and (2):

	(1)	(2)
Sb	17.2 volt	14.7 volt
As	18.2	15.7
P	19.0	16.5

The observed values of the appearance potentials will be greater than these minimum energies by some small amount which includes the minimum kinetic and excitational energies with which the products can dissociate. This quantity will be called the excess energy. If the excess energy is to remain fairly small, the process (1) satisfactorily accounts for the higher appearance potential of Sb^+ and for the appearance potentials of As^+ and P^+. The excess energies are $W(Sb^+) = 2.6$ volt, $W(As^+) = 3.4$ volt and $W(P^+) = 3.1$ volt. Process (2) has been observed for Sb^+ only, and accounts for the lower of the two appearance potentials. In this case the excess energy is 2.3 volt.

The second ionization potential of Sb is 18 volt. The minimum energy required to produce Sb^{++} by the process

$$SbCl_3 \rightarrow Sb^{++} + 3Cl \qquad (3)$$

is 35.2 volt, and by the process

$$SbCl_3 \rightarrow Sb^{++} + Cl_2 + Cl \qquad (4)$$

is 32.7 volt. In view of the measured appearance potential of Sb^{++} of 38 volt, process (3) seems more likely. The excess energy is 2.8 volt.

Cl^+ may, of course, be produced in a number of ways. From the values given above for the energy of dissociation of $SbCl_3$, and from the known ionization potential of chlorine, 13 volt, the minimum energy required for the formation of Cl^+ by the process

$$SbCl_3 \rightarrow Sb + 2Cl + Cl^+ \qquad (5)$$

is calculated to be 21.8 volt, and by the process

$$SbCl_3 \rightarrow Sb + Cl_2 + Cl^+ \qquad (6)$$

19.3 volt. The two observed appearance potentials are 24.0 and 20.7 volt. If these correspond to the processes (5) and (6), the excess energy in process (5) is 2.2 volt and in process (6), 1.4 volt. Since any other type of dissociation process is certain to require less energy than these processes, the excess energy will be greater for any other process. Since usual experience indicates that the excess energies are small, it seems likely that the above processes account for the occurrence of Cl^+.

[4] Bichowsky and Rossini, *Thermochemistry of Chemical Substances* (Reinhold, 1936).
[5] Sponer, *Molekulspektren* (J. Springer, 1935).

The Dissociation of HCN, C_2H_2, C_2N_2 and C_2H_4 by Electron Impact

P. KUSCH,* A. HUSTRULID AND JOHN T. TATE
Department of Physics, University of Minnesota, Minneapolis, Minnesota
(Received August 16, 1937)

The dissociation of HCN and C_2H_4 by electron impact has been investigated. An analysis of the results for these two molecules together with an analysis of previously published results on the dissociation processes occurring in C_2H_2 and C_2N_2 is presented. It is possible to assign reasonable processes of formation to all the observed ions from a knowledge of their appearance potentials, the known ionization potentials of certain atoms and atomic aggregates and the energies of dissociation of the parent molecule into various configurations. By a comparison of the results obtained for these four molecules, upper limits are assigned to the ionization potentials of various fragments obtained as dissociation products of hydrocarbons.

INTRODUCTION

THIS paper is the report of a series of experiments on the dissociation of organic molecules by electron impact. The dissociation of benzene and related molecules has recently been investigated in this laboratory. It is apparent from the results obtained that an understanding of the processes occurring in complex molecules is difficult to obtain without some further study of relatively simple organic compounds. Smith[1] has recently observed the dissociation processes occurring in methane and has made an analysis of them. The present work concerns an analysis of new data obtained on dissociation processes in hydrogen cyanide (HCN) and in ethylene (C_2H_4). An analysis of previous data by Tate, Smith and Vaughan[2] on cyanogen (C_2N_2) and on acetylene (C_2H_2) will also be presented.

A comparison of the results obtained on the dissociation processes of several related molecules will yield more information about the properties of the ions produced and about the nature of the processes than a consideration of results on any single molecule alone can yield. For example, an ion may conceivably be produced from a molecule by several different processes. If sufficient data are available to determine the energy of dissociation of these processes, and if the energy required to produce the ion from the parent molecule is known, alternative upper limits for the ionization potential may be computed for each of the processes. Comparison with alternative upper limits for the ionization potential computed for the same ion produced from another molecule, may permit the determination of a unique upper limit of the ionization potential, as well as a determination of the process responsible for its formation. Similar combinations of data may permit the determination of the energies of dissociation of the various processes which may occur.

The mass spectrograph is capable of providing considerable information about dissociation processes occurring in gaseous molecules. It is possible to determine the nature of the ions produced under various conditions by an approximate determination of the M/e of the observed ion. Such information gives valuable clues as to the arrangement of atoms within a molecule. The relative probability of formation of the ions may be observed for various pressures and electron energies. The variation of ion intensity with pressure will indicate whether an ion is produced from the parent molecule by a single electron collision or whether collisions with other ions or molecules are responsible for its formation. Smyth and Mueller[3] have observed, for example, that the peak due to H_3O^+, observed in the dissociation of water, varies in intensity approximately as the square of the pressure in the ionizing chamber, whereas the peak due to H_2O^+ varies in intensity approximately linearly with the pressure. This indicates that H_2O^+ is formed as a primary product, but H_3O^+ by some process of recombination.

* Now at Columbia University.
[1] Smith, Phys. Rev. **51**, 263 (1937).
[2] Tate, Smith and Vaughan, Phys. Rev. **48**, 523 (1935).
[3] Smyth and Mueller, Phys. Rev. **43**, 116 (1933).

The minimum energy required to produce the ion may also be determined. This energy, usually designated by the term appearance potential, is the sum of a dissociation energy, an ionization potential and the minimum excitational and kinetic energy, hereafter called the excess energy, with which the products can dissociate. If the appearance potential and two of the other quantities involved in this relationship are known, the remaining quantity may, of course, be determined. Even if either the ionization potential or the dissociation energy and the excess energy are unknown, upper limits may be set on the remaining quantity. The usual experience is that the excess energy is small, and that the upper limit set on an ionization potential or a dissociation energy in this way is quite close to its true value. Any large amount of kinetic energy imparted to an ion in the dissociation process would be manifested by a displacement of the peak from its ideal position. In the present series of experiments the kinetic energy was in all cases less than a half-volt. No statement can, in general, be made about the excitational energy with which the fragments dissociate. Since the excess energy is not known for any of the cases which will be discussed in this paper, a criterion of the goodness of the assignment of any process to an observed ion will be the requirement that the excess energy be small.

Apparatus

The same mass spectrograph was used for the present series of observations as was used in the recent study of dissociation processes occurring in benzene. It is similar to that used by Tate, Smith and Vaughan[2] in their work on cyanogen and acetylene. The resolving power was sufficiently great to resolve all the peaks observed for ethylene and for hydrogen cyanide.

Ordinary anaesthetic ethylene, purified by distillation at liquid-air temperatures was used. The hydrogen cyanide was distilled from liquid anhydrous HCN prepared by Kahlbaum. Both of these gases were admitted to the mass spectrograph through capillary leaks patterned after one described by Smythe.[4]

Argon was used to calibrate the mass scale and to determine the corrections to be applied to the apparent accelerating potential on the electrons. This correction was at all times small and remained practically constant throughout the course of the investigation.

Results and Analyses

To simplify the presentation of the analyses the following nomenclature will be used:

$A(X^+)$ ≡ Appearance potential of the ion X^+.
$I(X)$ ≡ Ionization potential of X.
$D(X)$ ≡ Energy of dissociation of X to atoms in the gaseous state.
$Q(X)$ ≡ Energy evolved in the formation of X from its elements in the states in which they exist at room temperature and atmospheric pressure.
$W(X^+)$ ≡ Excess energy required to produce the ion X^+ from the parent molecule.
$L(C)$ ≡ Heat of sublimation of carbon.

1. Hydrogen cyanide

All the ions observed as dissociation products of HCN together with their relative intensities at an electron energy of 75 volts and their appearance potentials are listed in Table I. Observations were made on the variation of peak heights as a function of pressure. Since the relative peak heights remained essentially constant it is safe to say that the ions are the result of direct dissociation of HCN by a single electron impact.

CO was an important impurity in the mass spectrograph and occurred from an undetermined

[4] Smythe, Rev. Sci. Inst. 7, 435 (1936).

Table I. *Ions observed in hydrogen cyanide. Column (1) observed ions; (2) relative intensity; (3) appearance potential (volts); (4) probable process. HCN→; (5) calculated minimum energy (volts); (6) excess energy or deduced ionization potential (volts).*

(1)	(2)	(3)	(4)	(5)	(6)
HCN^+	100	13.7±0.1	HCN^+	I(HCN)	I(HCN) = 13.7
CN^+	14.8	20.1±0.2	CN^++H	3.7+I(CN)	I(CN) ≤ 16.4
NH^+	0.12	24.9±0.5	NH^++C	5.7+I(NH)	I(NH) ≤ 19.2
N^+	1.1	25.6±0.5	N^++H+C	24.4	$W(N^+)$ = 1.2
CH^+	1.2	21.8±0.5	CH^++N	6.4+I(CH)	I(CH) ≤ 15.4
C^+	3.0	23.8±0.5	C^++N+H	21.1	$W(C^+)$ = 2.7
HCN^{++}	1.2	40.0±1.0	HCN^{++}	I(HCN)+I(HCN^+)	I(HCN^+) = 26.3

source. About 20 percent of the peak observed for C^+ and indicated in Table I is due to the presence of this CO. Vaughan[5] has measured the appearance potential of C^+ produced from CO as 22.5 ± 0.2 volt. This value is so close to that observed in the present case, that it is not certain that the present value is due to C^+ produced from HCN. The intensity of the peak N^+ of $M/e=14$ is in error to a small extent due to the presence of CO^{++} of identical M/e. Because of the high appearance potential of CO^{++}, no error is introduced in the value $A(N^+)$. Considerable molecular hydrogen was observed, but since its appearance potential was the same as the ionization potential of H_2, it was concluded that the H_2 existed as an impurity and not as a product of dissociation of HCN. The very small amount of atomic hydrogen present could be satisfactorily accounted for as the result of dissociation of H_2.

Table II shows the energies of the possible states of combination in which a carbon, a hydrogen and a nitrogen atom may exist.

Bichowsky and Rossini[6] give $Q(\mathrm{HCN})=-30.7$ kcal·mole$^{-1}=-1.33$ volt. Sponer[7] gives $D(H_2)=4.46$ volt and $D(N_2)=7.35$ volt. Considerable doubt exists as to the value of the quantity $L(C)$. Goldfinger and Jeunehomme[8] conclude that the balance of evidence is in favor of the value $L(C)=5.36\pm0.02$ volt, and this value will be used throughout. Smith[1] has used this value in his work on the dissociation of methane and finds that it is compatible with his observed energies.

For the determination of $D(\mathrm{HCN})$ the following cycle may be written:

$$\begin{aligned} H_2+N_2+2C_{dia}&=2HCN+2Q(\mathrm{HCN}),\\ 2C_{dia}+2L(C)&=2C_{gas},\\ H_2+D(H_2)&=2H,\\ N_2+D(N_2)&=2N,\\ 2H+2N+2C_{gas}&=2HCN+2D(\mathrm{HCN}). \end{aligned}$$

This shows that

$$2D(\mathrm{HCN})=D(H_2)+D(N_2)+2L(C)+2Q(\mathrm{HCN}),$$

which yields

$$D(\mathrm{HCN})=9.93 \text{ volt}.$$

[5] Vaughan, Phys. Rev. **38**, 1687 (1931).
[6] Bichowsky and Rossini, *Thermochemistry of Chemical Substances* (Reinhold, 1936).
[7] Sponer, *Molekulspektren* (J. Springer, (1935)).
[8] Goldfinger and Jeunehomme, Proc. Faraday Soc. **32**, 1591 (1936).

TABLE II. *Energies of possible states of combination in which a carbon, hydrogen and nitrogen atom may exist.*

STATE	CONFIGURATION	ENERGY (VOLTS)
a	H+C+N	9.9
b	CH+N	6.4
c	NH+C	5.7
d	CN+H	3.7
e	HCN	0

This value determines the energy of the state *a* in Table II.

Some doubt exists as to the value of $D(\mathrm{CH})$. Sponer[7] gives a value of 3.5 volt, estimated from spectroscopic data. This value differs from the value 4.323 volt given by Pauling and Sherman[9] for the energy of the C−H bond. Dietz[10] has calculated the energy of the C−H bond to be 3.97 volt. The energy of the C−H bond, as calculated from the known energies of formation of organic molecules, may, of course, be expected to be higher than the spectroscopically determined $D(\mathrm{CH})$. If we use the value given by Sponer, the energy of the state *b* is 3.5 volt below that of *a*.

The energy of the state *c* is 4.2 volt below that of *a*, calculated from Sponer's value, $D(\mathrm{NH})=4.2$ volt. Finally the state *d* is 6.2 volt below *a*, calculated from a value given by Herzberg,[11] $D(\mathrm{CN})=6.159$ volt.

All available evidence of a chemical and spectroscopic nature points to the conclusion that hydrogen cyanide exists in the configuration

$$H-C\equiv N.$$

However, a small proportion of hydrogen cyanide, variously estimated at from 0.5 to 4 percent, exists in the isomeric configuration HNC. Williams[12] has come to this conclusion from a comparison of the infrared absorption of organic cyanides and their isomeric configurations with that of hydrogen cyanide. Reichel and Strasser[13] have come to the same conclusion from a similar comparison in the ultraviolet. Dadieu[14] has found lines in the Raman spectrum of hydrogen cyanide

[9] Pauling and Sherman, J. Chem. Phys. **1**, 606 (1933).
[10] Dietz, J. Chem. Phys. **3**, 58 (1935).
[11] Herzberg, Nature **137**, 620 (1936).
[12] Williams, J. Chem. Phys. **4**, 84 (1936).
[13] Reichel and Strasser, Ber. der Deutschen Chem. Gesellschaft **64B**, 1997 (1931).
[14] Dadieu, Ber. der Deutschen Chem. Ges. **64B**, 358 (1931).

whch could only be associated with the isomeric form HNC.

The state c in Table II has, therefore, a real significance, and since HCN and HNC probably have very nearly equal heats of dissociation, the energy assigned to state c is correct to within the limits of error of the energies involved in its computation.

HCN^+. The observed ionization potential of HCN is 13.7 ± 0.1 volt. Sponer[7] quotes the value 14.8 volt from old sources. Price[15] has observed a series of absorption bands of HCN in the region 1450A to below 1000A. Some of these bands seem to form a Rydberg series converging to an ionization potential of about 14.8 volt.

CN^+. Since CN^+ can occur only by the transition $e\rightarrow d$, we can write at once:

$$A(CN^+)=D(HCN)-D(CN)+I(CN)+W(CN^+),$$

$$I(CN)=16.4 \text{ volt}-W(CN^+),$$

or

$$I(CN)\leq 16.4 \text{ volt},$$

depending on the excess energy required to produce CN^+.

NH^+. This ion can also occur in only one way, and as above we can find:

$$I(NH)\leq 19.2 \text{ volt}.$$

This value might be compared to a similar value calculated from the dissociation of NH_3. Bartlett[16] has observed the appearance potentials of the ions NH_3^+, NH_2^+ and NH^+ to be 11.2, 12.0 and 11.2 volt, respectively. He believes the ions NH_2^+ and NH^+ to be the result of some secondary process. Even if no dissociation energy were required to produce NH^+ from ammonia, his low appearance potential cannot be reconciled with the high upper limit of its ionization potential found in the present case. It seems likely that his value is due to overlapping of neighboring peaks.

The fact that the peak NH^+ occurs at all lends strong support to other evidence that hydrogen cyanide exists in the isomeric configuration HNC. No valid estimate of the abundance of HNC in HCN can be made from the present work. From the low intensity of the NH^+ peak it can be seen that the concentration of HNC is small.

N^+. From the energies shown in Table II and from the ionization potential $I(N)=14.5$ volt, the minimum energy required for the formation of N^+ by the transition $e\rightarrow a$ is found to be 24.4 volt, and by the transition $e\rightarrow b$, 20.9 volt. The excess energy required for the formation of N^+ from HCN is the difference between the observed appearance potential, $A(N^+)=25.6$ volt, and the minimum required energy. The excess energy required in the transition $e\rightarrow a$ is 1.2 volt and in the transition $e\rightarrow b$ 4.7 volt. While the second of these transitions cannot be definitely excluded, it seems probable that N^+ is produced by the first, and that the process responsible for its formation is

$$HCN\rightarrow N^+ + H + C.$$

CH^+. No good value is available for the ionization potential of CH. Since CH^+ can arise only from the process,

$$HCN\rightarrow CH^+ + N,$$

the upper limit $I(CH)\leq 15.4$ volt may be calculated from the appearance potential and the energies in Table II. Smith[1] has calculated two alternative values of the ionization potential of CH, depending on the two possible alternatives for the formation of CH^+ from CH_4. If

$$CH_4\rightarrow CH^+ + 3H,\ I(CH)\leq 11.7 \text{ volt},$$

and if

$$CH_4\rightarrow CH^+ + H_2 + H,\ I(CH)\leq 11.7+D(H_2)=16.2 \text{ volt}.$$

If the first of these processes is correct the minimum excess energy required for the formation of CH^+ from HCN is 3.7 volt. If the second

TABLE III. *Ions observed in acetylene. Column (1) observed ions; (2) appearance potential (volts); (3) probable process. $C_2H_2\rightarrow$; (4) calculated minimum energy (volts); (5) excess energy or deduced ionization potential (volts).*

(1)	(2)	(3)	(4)	(5)
$C_2H_2^+$	11.2 ± 0.1	$C_2H_2^+$	$I(C_2H_2)$	$I(C_2H_2)=11.2$
C_2H^+	17.8 ± 0.2	$C_2H^+ + H$	$4.0+I(C_2H)$	$I(C_2H)\leq 14.3$
C_2^+	23.8 ± 0.3	$C_2^+ + 2H$	$7.3+I(C_2)$	$I(C_2)\leq 16.5$
CH^+	22.2 ± 0.5	$CH^+ + CH$	$5.8+I(CH)$	$W(CH^+)\geq 1.0$
C^+	24.5 ± 1.0	$C^+ + C + 2H$	24.0	$W(C^+)=0.5$
H^+	21.7 ± 1.0	$H^+ + H + C_2$	20.8	$W(H^+)=0.9$
	25.6 ± 1.0	$H^+ + CH + C$	22.8	$W(H^+)=2.8$

[15] Price, Phys. Rev. **46**, 529 (1934).
[16] Bartlett, Phys. Rev. **33**, 169 (1929).

is correct the minimum excess energy for the formation of CH^+ from CH_4 is 0.8 volt. The second of these two processes, therefore, seems the more probable one.

C^+. The minimum energy required for the formation of C^+ from HCN by the transition $e \rightarrow a$ is 21.1 volt and by the transition $e \rightarrow c$ is 16.9 volt, where $I(C) = 11.2$ volt. The observed appearance potential, $A(C^+) = 23.8$ volt, almost certainly excludes the second of these possibilities. $A(C^+)$ may be in error due to the presence of C^+ from CO, so that the calculated excess energy, $W(C^+) = 2.7$ volt may be in error. The process responsible for the formation of the C^+ is certainly

$$HCN \rightarrow C^+ + H + N.$$

HCN^{++}. The second ionization potential of HCN is found to be 26.3 volt.

A summary of the principal results obtained is included in Table I.

The assignment of processes to the ions observed in HCN is in accord with an observation which Smith[1] has made in the case of CH_4, that the possible processes which require the largest calculated minimum energies are those which actually occur.

2. Acetylene

The data to be used in the present analysis have been obtained by Tate, Smith and Vaughan[2] and are listed in Table III. Table IV shows the possible states of combination of two hydrogen and two carbon atoms and the energies associated with these states. The energies were computed in the same way and from the same sources of data as in the case of HCN. For the additional quantity $D(C_2)$, Sponer's value of 5.5 volt was used. Since all chemical and spectroscopic evidence points to the fact that C_2H_2 is a linear symmetrical molecule of the form

$$H-C \equiv C-H,$$

ions of the type CH_2^+ would not be expected to occur. The nonoccurrence of such ions lends further support to this picture. The state CH_2+C has not therefore been included in Table IV, nor has its energy been calculated.

TABLE IV. *Energies of possible states of combination in which two hydrogen and two carbon atoms may exist.*

STATE	CONFIGURATION	ENERGY (VOLTS
a	2C+2H	12.8
b	CH+C+H	9.3
c	$2C+H_2$	8.4
d	C_2+2H	7.3
e	CH+CH	5.8
f	C_2+H_2	2.8
g	C_2H+H	3.5
h	C_2H_2	0

$C_2H_2^+$. The observed ionization potential of C_2H_2 is 11.2 ± 0.1 volt. Price[17] has obtained the value 11.35 volt by determining the convergence limit of a Rydberg series of bands in the ultraviolet. Mulliken[18] estimates the vertical ionization potential of acetylene at 11.9 volt, which is probably several tenths of a volt higher than the adiabatic ionization potential measured in electron impact experiments and in spectroscopic determinations.

C_2H^+. No very satisfactory value can be obtained for the energy of the state *g*. However, the energy required to remove two hydrogen atoms from C_2H_2 is 7.3 volt. Since the energy required to remove the first of these hydrogen atoms can be expected to be less than that required to remove the second one, a reasonable assumption is that the state *g* is 3.5 volt above *h*. The energy required to remove the second hydrogen atom is then 3.8 volt, 0.3 volt more than that required to remove the first one.

In any case,

$$A(C_2H^+) = D(C_2H_2) - D(C_2H) + I(C_2H) + W(C_2H^+),$$

so that

$$I(C_2H) - D(C_2H) \leq 5.0 \text{ volt}.$$

This value will subsequently be used in the analysis of the data on ethylene. If the state *g* is 3.5 volt above *h*,

$$I(C_2H) \leq 14.3 \text{ volt}.$$

C_2^+. C_2^+ may be produced from acetylene either by the transition $h \rightarrow d$ or by the transition $h \rightarrow f$. For the transition $h \rightarrow d$:

$$A(C_2^+) = D(C_2H_2) - D(C_2) + I(C_2) + W(C_2^+)$$

or

$$I(C_2) \leq 16.5 \text{ volt},$$

and for the transition $h \rightarrow f$:

$$I(C_2) \leq 16.5 + D(H_2) = 21.0 \text{ volt}.$$

[17] Price, Phys. Rev. **47**, 444 (1935).
[18] Mulliken, J. Chem. Phys. **3**, 517 (1935).

There is no way of determining the correct $I(C_2)$ and the process responsible for the formation of C_2^+ from the data on acetylene alone. However in the work on cyanogen which will be discussed later it will be shown that

$$I(C_2) \leq 9.1 \text{ volt},$$

or $$I(C_2) \leq 9.1 + D(N_2) = 16.5 \text{ volt}.$$

The results for these two molecules can be brought into reasonable accord only if $I(C_2) \leq 16.5$ volt. The process responsible for the formation of C_2^+ from C_2H_2 is

$$C_2H_2 \rightarrow C_2^+ + 2H$$

Bleakney, Condon and Smith[19] have found $I(C_2) = 14.7$ volt by the same argument. Their calculations are based on a different value of $L(C)$, than that used here. Their conclusion as to the process which occurs is identical to that obtained here.

CH^+. Either the transition $h \rightarrow b$ or the transition $h \rightarrow e$ may give rise to CH^+. From the first

$$I(CH) \leq 12.9 \text{ volt},$$

and from the second,

$$I(CH) \leq 12.9 + D(CH) = 16.4 \text{ volt}.$$

In the discussion on HCN it has been shown that

$$I(CH) \leq 15.4 \text{ volt}.$$

If CH^+ is produced from C_2H_2 by the transition $h \rightarrow b$, the minimum excess energy required for the formation of CH^+ from HCN is 2.5 volt. If the transition $h \rightarrow e$ is the correct one, the minimum excess energy required for the formation of CH^+ from C_2H_2 is 1.0 volt. Since both of these values are quite reasonable no choice of process can be made. However, if the transition $h \rightarrow b$ is the correct one, then the transition for the production of CH^+ from CH_4 with which the value, $I(CH) \leq 11.7$ volt, is associated must be the correct one. This, as was shown, earlier, gives a rather high value for the excess energy required to produce CH^+ from HCN. It, therefore, seems safe to say that the process:

$$C_2H_2 \rightarrow CH^+ + CH$$

accounts for the formation of CH^+ from C_2H_2.

[19] Bleakney, Condon and Smith, J. Phys. Chem. **41**, 197 (1937).

C^+. The minimum energies required for the formation of C^+ from C_2H_2 by the possible transitions are:

$$\begin{aligned} h \rightarrow a \quad & 12.8 + 11.2 = 24.0 \text{ volt}, \\ h \rightarrow b \quad & 9.3 + 11.2 = 20.5 \text{ volt}, \\ h \rightarrow c \quad & 8.4 + 11.2 = 19.6 \text{ volt}. \end{aligned}$$

The observed appearance potential of 24.5 volt correlates most nearly with the first of these. In this case $W(C^+) = 0.5$ volt. The other transitions cannot be excluded, but give rise to rather high excess energies.

H^+. The minimum energies required for the formation of H^+ by the following transitions are:

$$\begin{aligned} h \rightarrow a \quad & 12.8 + 13.5 = 26.3 \text{ volt}, \\ h \rightarrow b \quad & 9.3 + 13.5 = 22.8 \text{ volt}, \\ h \rightarrow d \quad & 7.3 + 13.5 = 20.8 \text{ volt}, \\ h \rightarrow g \quad & 4.0 + 13.5 = 17.5 \text{ volt}. \end{aligned}$$

The two observed appearance potentials are 21.7 ± 1.0 and 25.6 ± 1.0 volt. The higher of these two values agrees with the calculated minimum energy for the transition $h \rightarrow a$ within experimental error. Very little excess energy is available in that case. If the higher value applies to the transition $h \rightarrow b$, the excess energy is 2.8 volt. The second transition seems more probable. If the lower of the two appearance potentials applies to the transition $h \rightarrow d$ the excess energy is 0.9 volt. If it applies to the transition $h \rightarrow g$ the excess energy is 4.2 volt, which seems rather high. The most probable processes for the formation of H^+ from C_2H_2 are:

$$\begin{aligned} C_2H_2 \rightarrow H^+ + CH + C \cdot W(H^+) = 2.8 \text{ volt}, \\ C_2H_2 \rightarrow H^+ + H + C_2 \cdot W(H^+) = 0.9 \text{ volt}. \end{aligned}$$

A summary of the principal results obtained on acetylene is included in Table III.

3. Cyanogen

The data used in the present analysis are taken from a paper by Tate, Smith and Vaughan[2] and from a report by Dorsch and Kallman.[20] The data are tabulated in Table V. The authors have not given the probable error in the determination of the appearance potentials, nor have they given the relative abundances of the various ions. Tate, Smith and Vaughan observed C^+ and N^+ but the origin of these peaks was uncertain due to

[20] Dorsch and Kallman, Zeits. f. Physik **60**, 376 (1930).

TABLE V. *Ions observed in cyanogen. Column (1) observed ions; (2) appearance potential (volts), (a) Tate, Smith and Vaughan, (b) Dorsch and Kallman; (3) probable process. $C_2N_2\rightarrow$; (4) calculated minimum energy (volts); (5) excess energy or deduced ionization potential (volts).*

	(2)				
(1)	(a)	(b)	(3)	(4)	(5)
$C_2N_2^+$	14.1	13.5	$C_2N_2^+$	$I(C_2N_2)$	$I(C_2N_2)=14.1$
C_2N^+	19.8		C_2N^++N	$6.2+I(C_2N)$	$I(C_2N)\leq 13.6$
CN^+	21.3	18	CN^++CN	$2.7+I(CN)$	$W(CN^+)\geq 2.2$
C_2^+	18.6	17	$C_2^++N_2$	$2.1+I(C_2)$	$I(C_2)\leq 16.5$
C^+		22.5	C^++CN+N	20.0	$W(C^+)=2.5$

the fact that their sample of cyanogen contained CO and N_2.

Table VI shows the possible states of combination of two nitrogen and two carbon atoms and the energies associated with these states. The energies were calculated as before. No data from which to calculate the energy of the state *e* are available. In this case it is assumed that the binding energy of N to C_2N is equal to the dissociation energy of CN. This estimate cannot be in error to any large degree, for if we assume that the total energy of dissociation is equal to the sum of the energy of the C−C bond as given by Dietz[10] and two of the assumed energies of the CN bond, we obtain $D(C_2N_2)=15.5$ volt. This value lies close to the value calculated from thermochemical data.

Since the ion CN_2 has not been observed, the energy of the state CN_2+C has not been calculated.

$C_2N_2^+$. The ionization potential of C_2N_2 is 14.1 volt. No other values with which to compare this result seem to be available.

C_2N^+. This ion must arise from the transition $h\rightarrow e$. We may then write

$$A(C_2N^+)=D(C_2N_2)-D(C_2N)+I(C_2N)+W(C_2N^+).$$

This reduces to

$$I(C_2N)\leq 13.6 \text{ volt}.$$

CN^+. The ion CN^+ may arise from the transition $h\rightarrow c$ or from the transition $h\rightarrow f$. The upper limit for $I(CN)$ in the first case is 12.5 volt, and in the second case, 18.6 volt. Now from the work on HCN an upper limit for $I(CN)$ has been shown to be 16.4 volt. If the transition $h\rightarrow c$ is the correct one, the minimum excess energy required for the formation of CN^+ from HCN is 3.9 volt. If the transition $h\rightarrow f$ is the correct one, the minimum excess energy required for the formation of CN^+ from C_2N_2 is 2.2 volt. Because of the smaller excess energy the transition $h\rightarrow f$ seems more probable. In the molecule C_2N_2, the binding energy between the carbon atoms is much smaller than that between a carbon and a nitrogen atom. Now the transition $h\rightarrow f$ requires only that the C−C bond be broken, while the transition $h\rightarrow c$ requires that a C≡N bond be broken as well. This argument lends weight to the above conclusion that the transition $h\rightarrow f$ offers a better explanation of the occurrence of CN^+ as a dissociation product of C_2N_2, than does the transition $h\rightarrow c$. The most probable process for the formation of CN^+ from C_2N_2 is then

$$C_2N_2\rightarrow CN^++CN. \quad W(CN^+)\geq 2.2 \text{ volt}.$$

TABLE VI. *Energies of possible states of combination in which two nitrogen and two carbon atoms may exist.*

STATE	CONFIGURATION	ENERGY (VOLTS)
a	2C+2N	15.0
b	C_2+2N	9.5
c	CN+C+N	8.8
d	2C+N_2	7.6
e	C_2N+N	6.2
f	CN+CN	2.7
g	C_2+N_2	2.1
h	C_2N_2	0

C_2^+. C_2^+ may arise by either of the transitions $h\rightarrow b$ or $h\rightarrow g$. An upper limit for $I(C_2)$ is 9.1 volt if the transition $h\rightarrow b$ occurs, and 16.5 volt if the transition $h\rightarrow g$ occurs. By comparison with the work on acetylene it is seen that the upper limit for $I(C_2)$ is 16.5 volt. The process responsible for the formation of C_2 from C_2N_2 is then

$$C_2N_2\rightarrow C_2^++N_2.$$

C^+. The minimum energies required to produce C^+ by all the possible transitions are as follows:

$h\rightarrow a$, 26.2 volt,
$h\rightarrow c$, 20.0 volt,
$h\rightarrow d$, 18.8 volt.

The observed appearance potential, $A(C^+)=22.5$ volt, does not permit the transition $h\rightarrow a$ to occur. The excess energies for the transitions $h\rightarrow c$ and $h\rightarrow d$ are 2.5 and 3.7 volt, respectively. No data are available to permit a choice to be

made between these two cases. Because of the smaller excess energy, and because of the known structure of the molecule, the transition $h \rightarrow c$ seems a little more likely than the transition $h \rightarrow d$.

Table V includes a summary of the principal results obtained for cyanogen.

4. Ethylene

All the ions observed as dissociation products of ethylene together with their relative intensities at an electron energy of 75 volts and their appearance potentials are listed in Table VII. A mass spectrum of those ions containing two carbons is shown in Fig. 1 and of those containing one carbon in Fig. 2. The peaks in Fig. 2 show considerable tailing to high mass numbers which indicates that a continuous distribution of kinetic energy is imparted to the ions during formation. The peak CH_2^+ has a satellite separated from the main peak by about 2.2 volt. The satellite may be fairly well resolved from the main peak at low values of the magnetic field. That this satellite originates from dissociation processes rather than from the geometry of the apparatus is attested by the fact that other peaks in the immediate vicinity possess no such satellites, and that the appearance potential of the satellite is much higher than that of the main peak. In this case the appearance potential of the satellite was found to be about 40 volt. The H^+ peak possesses a similar satellite, separated from the main peak by about 2.8 volt. Similar peaks have been observed in our recent work on benzene.

A satellite peak is believed to be due to ion of the same kind as the main peak, but produced by another process in which considerable kinetic energy is imparted to the ion.

The relative positions of all the peaks with M/e values between 28 and 12 were carefully compared. None of the peaks show any displacement from their ideal relative positions, within experimental error. The kinetic energy associated with any of these peaks is certainly less than 0.3 volt. This partially justifies a later assumption that the excess energy is small.

A search was made for negative ions, but none were observed.

Eisenhut and Conrad[21] have observed the ions produced in an arc at fairly high pressures. They have observed the same ions as have been observed in the present case. In addition they have

[21] Eisenhut and Conrad, Zeits. f. Elektrochem. **36**, 654 (1930).

TABLE VII. *Ions observed in ethylene. Column (1) observed ions; (2) relative intensity (volts); (3) appearance potential (volts); (4) probable process.* $C_2H_4 \rightarrow$; *(5) calculated minimum energy (volts); (6) excess energy or deduced ionization potential (volts).*

(1)	(2)	(3)	(4)	(5)	(6)
$C_2H_4^+$	100	10.80±0.05	$C_2H_4^+$	$I(C_2H_4)$	$I(C_2H_4)=10.80$
$C_2H_3^+$	57.2	14.1 ±0.1	$C_2H_3^+ + H$	$3.1+I(C_2H_3)$	$I(C_2H_3)\leq 11.0$
$C_2H_2^+$	51.3	13.4 ±0.2	$C_2H_2^+ + H_2$	13.1	$W(C_2H_2^+)=0.3$
C_2H^+	8.8	19.2 ±1.0	$C_2H^+ + H + H_2$	$5.4+I(C_2H)$	$I(C_2H)\leq 13.8$
C_2^+	2.7	26.4 ±1.0	$C_2^+ + 2H + H_2$	$9.2+I(C_2)$	$W(C_2^+)\geq 0.7$
CH_4^+	0.06				
CH_3^+	0.6				
CH_2^+	5.2	19.2 ±0.3	$CH_2^+ + CH + H$	$8.7+I(CH_2)$	$I(CH_2)\leq 10.5$
			$CH_2^+ + C + H_2$	$7.7+I(CH_2)$	$I(CH_2)\leq 11.5$
			$CH_2^+ + CH_2$	$5.2+I(CH_2)$	$W(CH_2^+)\geq 2.0$
CH^+	2.5	22.9 ±0.5	$CH^+ + CH + H_2$	$7.7+I(CH)$	$I(CH)\leq 15.2$
			$CH^+ + CH_2 + H$	$8.7+I(CH)$	$I(CH)\leq 14.2$
C^+	1.7	24.6 ±0.5	$C^+ + C + 2H_2$	21.4	$W(C^+)=3.2$
			$C^+ + CH + H + H_2$	22.4	$W(C^+)=2.2$
			$C^+ + CH_2 + 2H$	23.4	$W(C^+)=1.2$
H_2^+	0.13	22.4 ±1.5	$H_2^+ + 2CH$	23.1	$W(H_2^+)\sim 0$
			$H_2^+ + C + CH_2$	23.1	$W(H_2^+)\sim 0$
			$H_2^+ + H_2 + C_2$	20.1	$W(H_2^+)=2.3$
			$H_2^+ + H + C_2H$	20.8	$W(H_2^+)=1.6$
H^+	0.51	26.2 ±1.5			
		28.2 ±1.5			
CH_2^++K.E.		~40	$CH_2^+ + CH_2^+$	33.6	K.E.=2.2
H^++K.E.		~40			K.E.=2.8
$C_2H_4^{++}$	0.3				
$C_2H_3^{++}$	0.3	36.0 ±1.0			
C_2H^{++}	0.006				

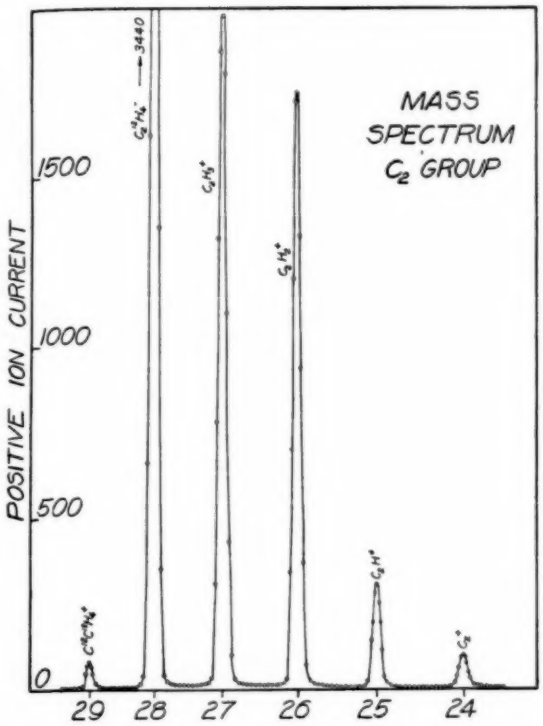

FIG. 1. Mass spectrum of ions containing two carbons.

found larger ions, presumably built up by some secondary process.

It is not certain whether the observed peaks, CH_3^+ and CH_4^+ are genuine products of dissociation of ethylene or whether they are due to small amounts of hydrocarbon impurities in the ethylene.

A small peak was observed due to $C_2^{13}H_4^{++}$. From the height of this peak and from the known abundance ratio of the carbon isotopes, C_{12} and C_{13}, it was possible to determine what part of the peak at $M/e=14$ was due to $C_2H_4^{++}$ and what part was due to CH_2^+. A small part of the peak designated as CH^+ may be due to $C_2H_2^{++}$, and a part of the peak designated as C^+ may be due to C_2^{++}. Corrections were made, whenever possible, for the presence of the C_{13} isotope of carbon.

Table VIII shows the energies of the possible states of combination in which two carbon and four hydrogen atoms may exist. The states are arranged in such a way that the lighter fragments occur in the upper part of the table. The energy of the state *a* is determined in the usual manner from the thermochemical and spectroscopic data. The energies of the states *b*, *c*, *d*, *e*, *f*, *g*, *o*, *p*, and *q* can be determined from that of state *a* by use of the quantities $D(C_2)$, $D(CH)$ and $D(H_2)$. To determine the energies of the states *h*, *i*, *j*, *k*, *l*, *m* and *n* the same values $D(CH_2)=7.0$ volts, $D(CH_3)=10.6$ volts, and $D(CH_4)=15.1$ volts were used as were used by Smith in his work on methane. The states *t* and *u* were determined by use of the previously given

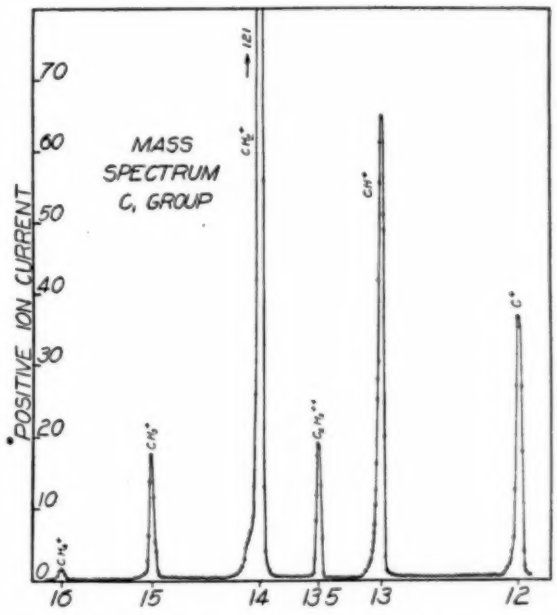

FIG. 2. Mass spectrum of ions containing one carbon.

TABLE VIII. *Energies of possible states of combination in which two carbon and four hydrogen atoms may exist.*

STATE	CONFIGURATION	ENERGY (VOLTS)
a	2C+4H	19.2
b	2C+2H+H_2	14.7
c	2C+2H_2	10.2
d	CH+C+3H	15.7
e	CH+CH+2H	12.2
f	CH+C+H+H_2	11.2
g	CH+CH+H_2	7.7
h	CH_2+C+2H	12.2
i	CH_2+CH+H	8.7
j	CH_2+C+H_2	7.7
k	CH_2+CH_2	5.2
l	CH_3+C+H	8.6
m	CH_3+CH	5.1
n	CH_4+C	4.1
o	C_2+4H	13.7
p	C_2+2H+H_2	9.2
q	C_2+2H_2	4.7
r	C_2H+3H	9.9
s	C_2H+H+H_2	5.4
t	C_2H_2+2H	6.4
u	C_2H_2+H_2	1.9
v	C_2H_3+H	3.1
w	C_2H_4	0

value for $D(C_2H_2)$. No information seems to be available on the values $D(C_2H)$ and $D(C_2H_3)$. However, the energy required to remove two hydrogen atoms from C_2H_4 is 6.4 volts, and that required to remove four hydrogen atoms is 13.7 volts. Evidently the energy required for the removal of the first hydrogen atoms is not as great as that required for the removal of subsequent atoms. If the energy required to remove the successive hydrogen atoms is estimated at 3.1, 3.3, 3.5 and 3.8 volts the energies required to remove two and four hydrogen atoms have the correct values and a reasonable value is obtained for the energies required to remove one and three hydrogens. These values are then adopted in calculating the energies of the states *r*, *s* and *v*.

$C_2H_4^+$. The ionization potential of C_2H_4 has been measured as 10.80 ± 0.05 volt. Price[17] has calculated the ionization potential from the convergence of a Rydberg series of electronic bands in the ultraviolet at 10.41 volt. Mulliken[18] has estimated the vertical ionization potential, which may be from 0.3 to 0.6 volt above the observed adiabatic ionization potential, at 11.0 volt.

$C_2H_3^+$. This ion can arise only by the transition $w\rightarrow v$. An upper limit for its ionization potential can be obtained from the relationship

$$A(C_2H_3^+)=D(C_2H_4)-D(C_2H_3)+I(C_2H_3)+W(C_2H_3^+),$$

which yields

$$I(C_2H_3)\leq 11.0 \text{ volt},$$

depending on the excess energy. This value is subject to error due to uncertainty in the energy of the dissociation process

$$C_2H_4\rightarrow C_2H_3+H.$$

$C_2H_2^+$. This ion can arise either by the transition $w\rightarrow t$ or by the transition $w\rightarrow u$. By use of Vaughan's[2] value $I(C_2H_2)=11.2$ volt, the minimum energy required to produce $C_2H_2^+$ by the first of these processes is calculated to be 17.6 volt, and by the second 13.1 volt. In view of the observed appearance potential $A(C_2H_2^+)=13.4$ volt the second process,

$$C_2H_4\rightarrow C_2H_2^+ + H_2,$$

accounts for the appearance of the $C_2H_2^+$ ion, since the first requires more energy than is available. The excess energy is 0.3 volt. The process

$$C_2H_4\rightarrow C_2H_2^+ + 2H$$

may possibly occur, but in the region above 17.6 volt the curve relating ion intensity to electron energy, from which the appearance potential is determined, rises so rapidly that the onset of a new process would be undetectable.

C_2H^+. This ion can arise either from the transition $w\rightarrow r$ or from the transition $w\rightarrow s$. In the first case

$$A(C_2H^+)=D(C_2H_4)-D(C_2H)+I(C_2H)+W(C_2H^+),$$

which yields

$$I(C_2H)-D(C_2H)\leq 0.$$

In the second case

$$A(C_2H^+)=D(C_2H_4)-D(C_2H)-D(H_2)+I(C_2H)+W(C_2H^+),$$

which yields

$$I(C_2H)-D(C_2H)\leq 4.5 \text{ volt}.$$

In the work on acetylene it was found that

$$I(C_2H)-D(C_2H)\leq 5.0 \text{ volt}.$$

The process responsible for the formation of C_2H^+ from C_2H_4 is then

$$C_2H_4\rightarrow C_2H^+ + H + H_2.$$

An upper limit for the ionization potential is

$$I(C_2H)\leq 13.8 \text{ volt}.$$

C_2^+. Any one of the transitions $w\rightarrow o$, $w\rightarrow p$ or $w\rightarrow q$ may account for the presence of C_2^+. In the previous discussion it has been shown that

$$I(C_2)\leq 16.5 \text{ volt}.$$

If it is assumed, for the moment that the ionization potential is equal to the above value, the minimum energies required for the formation of C_2^+ from C_2H_4 are, for the various possible transitions:

$w\rightarrow o$, 30.2 volt,
$w\rightarrow p$, 25.7 volt,
$w\rightarrow q$, 21.2 volt.

Since the observed appearance potential of C_2^+ is

26.4 ± 1.0 volt, the transition $w\rightarrow o$ is not energetically possible unless the true ionization potential of molecular carbon is at least 3.8 volt below the upper limit. This is improbable. Similarly the production of C_2^+ by the transition $w\rightarrow q$ requires a minimum excess energy of 5.2 volt. It seems probable that the transition $w\rightarrow p$ is responsible for the formation of C_2^+. The excess energy is then at least 0.7 volt, and the process

$$C_2H_4\rightarrow C_2^+ + 2H + H_2.$$

CH_2^+. Smith[1] has observed two appearance potentials for CH_2^+ produced in CH_4. Since CH_2^+ can be produced from CH_4 in only two ways, the lower appearance potential can be assigned to the process requiring the least dissociation energy. From this process,

$$CH_4\rightarrow CH_2^+ + H_2,$$

he concludes that $I(CH_2)\leq 12.0$ volt. For the other process,

$$CH_4\rightarrow CH_2^+ + 2H,$$

he then concludes that $W(CH_2^+)\geq 2.8$ volt. CH_2^+ may be produced from C_2H_4 by any of the transitions $w\rightarrow h, i, j$ or k. If we assume for the moment that $I(CH_2)=12.0$ volt, the minimum energies of formation of this ion by these transitions are 24.2, 20.7, 19.7 and 17.2 volt, respectively. These values are of course high by the discrepancy between the assumed and true ionization potential. This discrepancy is probably small. The transition $w\rightarrow h$ can definitely be excluded for the formation of CH_2^+, since this transition would require unreasonably large excess energies in Smith's cases. For the transition $w\rightarrow i$ the minimum excess energies for the formation of CH_2^+ from CH_4 by the two processes would be 1.5 and 4.3 volt. For the transition $w\rightarrow j$ they are 0.5 and 3.3 volt. For the transition $w\rightarrow k$ the minimum excess energy required for the formation of CH_2^+ from C_2H_4 is 2.0 volt. Since none of these processes seem more likely than any of the others, no choice can be made among them.

CH^+. This ion may occur by any of the transitions $w\rightarrow d$, e, f, g, i or m. From the value $A(CH^+)=22.9\pm0.5$ volt, the values $I(CH)\leq 7.2$, 10.7, 11.7, 15.2, 14.2 and 17.8 volt may be calculated for these transitions. From the work on HCN it was shown that $I(CH)\leq 15.4$ volt. The first three values calculated from the appearance of CH^+ as a dissociation product of C_2H_4 may be excluded since they would require large minimum excess energies for the formation of CH^+ from HCN. The transition $w\rightarrow m$ may probably be excluded on the basis that the known structure of the ethylene molecule would not permit dissociation in such a way. No choice is possible between the transitions $w\rightarrow g$ and $w\rightarrow i$.

C^+, H_2^+, H^+. As is evident from Table VIII, these three ions may be produced in a large number of ways. Of the nine possible transitions by which C^+ could be produced, all but three may be excluded, either because the minimum energy required to produce C^+ by these processes is greater than the observed appearance potential or else because the excess energy is 4.8 volt or greater. The three remaining processes are shown in Table VII. Similarly H_2^+ may occur as the result of nine different processes, all but four of which may be excluded on energy considerations. These four processes are shown in Table VII. H^+ may occur by fourteen different processes but after eliminating those that are unlikely or energetically impossible, six possible processes may be reasonably associated with each of the two observed appearance potentials. No conclusion is possible except that when H^+ does result from an electron impact, it occurs only when the C_2H_4 molecule is broken into a large number of fragments.

The possibility that a large number of processes actually occur in these cases cannot, of course, be overlooked. If the total observed peak is the result of several processes, the present experimental method would be unable to detect any but the process of least energy and any subsequent process requiring considerably more energy.

$CH_2^+ + K.E.$ A satellite was observed for the CH_2^+ peak which possessed a kinetic energy of about 2.2 volt and whose appearance potential was in the neighborhood of 40 volt. The process

$$C_2H_4\rightarrow CH_2^+ + CH_2^+$$

requires a minimum energy of

$$D(C_2H_4) - 2D(CH_2) + 2I(CH_2).$$

If $I(CH_2)=12.0$ volt, the minimum energy is

29.2 volt. To this must be added twice the kinetic energy of one of the fragments. This gives 33.6 volt as the minimum energy required to produce two CH_2^+ ions with kinetic energy from C_2H_4. The estimated value of the appearance potential is close enough to this value to make the above process a reasonable one for the formation of the observed satellite.

$H^+ + K.E.$ The satellite observed for the H^+ peak must also arise from some process involving the production of two charged particles, because of its high appearance potential. No exact explanation of its origin is possible.

A summary of the principal results obtained for the ions produced in ethylene is included in Table VII.

OCTOBER 15, 1937 PHYSICAL REVIEW VOLUME 52

Normal Energy Distribution of Photoelectrons from Thin Potassium Films as a Function of Temperature*

C. L. HENSHAW†
Sloane Physics Laboratory, Yale University, New Haven, Connecticut

(Received July 29, 1937)

With a retarding potential between plane parallel electrodes the normal energy distribution of photoelectrons from thin films of potassium on silver and platinum was studied as a function of temperature. The films were both greater and less than monatomic in thickness and were produced by the molecular ray method. Contact potential was determined by the Kelvin method to within less than 0.02 volt. The resulting current-voltage curves are found under optimum geometrical conditions to be parabolic in shape up to the point of zero field within experimental error. This is shown by plotting (current)$^{\frac{1}{2}}$ *vs.* voltage and testing with a straight line, and also by agreement with the theoretical Fowler curve. These results are compared with various theories. Mitchell's prediction for normal energy distribution has a large deficiency in slow electrons. Hill's calculations in which he uses an image barrier instead of the square barrier of Mitchell show that there should be very little deviation of the energy distribution from DuBridge's simple theory. The agreement of the results with DuBridge's distribution suggests that the image barrier is a much more reasonable approximation although the method is insensitive to small changes in the form of the barrier. The effects of temperature are: (1) temperature dependence of the rates of diffusion of potassium through and sublimation from the base metal, (2) irreversible changes with temperature in the state of the potassium surfaces as shown by changes in contact potential and saturation current, (3) *reversible* changes with temperature in the shape of the Fowler plots, (4) a change of photoelectric current with temperature only 10 to 30 percent of that predicted by DuBridge's theory. (4) is obtained from (3) by determining empirically the optimum temperature at which data should be plotted to give best fits and shifts for the Fowler curve. They range from 90°K to 175°K instead of the actual temperatures of 83°K to 296°K. The temperature effect seems less with thinner films. No theory for thin films predicts this last effect.

INTRODUCTION

IN recent years many studies have been made of the variation of the photoelectric yield as a function of frequency and temperature from very carefully prepared solid surfaces in the attempt to verify Fowler's[1] theory but only a few studies have been made of the energy distribution. DuBridge[2] has developed a theory for the energy distribution, both total and normal,[3] as a function of temperature. Of this there have been two confirmations in the high energy range where the theory is most reliable. Roehr[4] investigated the total energy distribution and DuBridge and Hergenrother[5] the normal. Studies at a single temperature of the total energy distribution for distilled Na[6] indicate that the predicted curves

* Part of a dissertation presented to the Faculty of the Graduate School of Yale University in candidacy for the degree of Doctor of Philosophy.

† Now located at Colgate University, Hamilton, N. Y.

[1] R. H. Fowler, Phys. Rev. **38**, 45 (1931).

[2] L. A. DuBridge, Phys. Rev. **43**, 727 (1933).

[3] By "normal" energy distribution will be understood the distribution associated with the velocity components normal to the emitting surface.

[4] W. W. Roehr, Phys. Rev. **44**, 866 (1933).

[5] L. A. DuBridge and R. C. Hergenrother, Phys. Rev. **44**, 861 (1933).

[6] A. G. Hill and L. A. DuBridge, Phys. Rev. **49**, 877 (1936).

are followed for a wide range of frequencies and over most of the energies. Using a magnetic analyzer, Liben[7] has confirmed at higher energies the predicted theories for surfaces of Ca and CaO.

With thin films less work has been done. Brady[8] found that the total energy distribution for films of K on Ag, 0.8 to 30 atoms thick, did not change with film thickness and agreed over the expected energy range with DuBridge's theory, although no temperature change was studied. Because of suggestions[9, 10] that the photoelectrons come from a region near the surface of a metal, the behavior of thin films is important in obtaining a more exact description of the phenomenon. Accordingly it became the purpose of this investigation to study the variation with temperature of the normal energy distribution of the yield from thin films.

Theory

Photoelectric energy distribution is most readily determined by the retarding potential method. If the retarding field is radial (spherical condenser) the derivative of the current-voltage curve gives the total energy distribution. If the retarding field is uniform (plane condenser) the normal distribution results. The two distributions on the basis of DuBridge's theory and the corresponding current-voltage curves are contrasted in Fig. 1 for absolute zero and some higher temperature. Actual current-voltage curves, when differentiated to give the energy distributions, seem to yield curves more like the dotted lines in Fig. 1a. This discrepancy at low energies indicates that the assumptions of DuBridge's theory are too simple in that region. The barrier is probably not a single step and the transition probabilities of quantum-electron interactions are quite likely to vary with electron energy. Mitchell[11, 12] and Myers[13] have endeavored to take some of these other factors into consideration.

There is a possibility that some of the discrepancy between experiment and theory is due to apparatus defects. Ives, Olpin, and Johnsrud[14] have shown that photoelectric emission as a function of angle follows Lambert's cosine law fairly closely. Since the fastest electrons must be emitted at small angles to the normal many of the slow ones will come off at large angles. These may be lost by traveling into a region of slightly distorted electric or magnetic field which would not appreciably disturb electrons of higher energy. Although the normal distribution suffers from this criticism equally with the total, by either magnetic or electric methods, it has one distinct advantage. The quantum-electron interaction is considered by conservation of momentum to take place near the metal surface and only perpendicular to it. If the transition probability depends upon electron velocity it

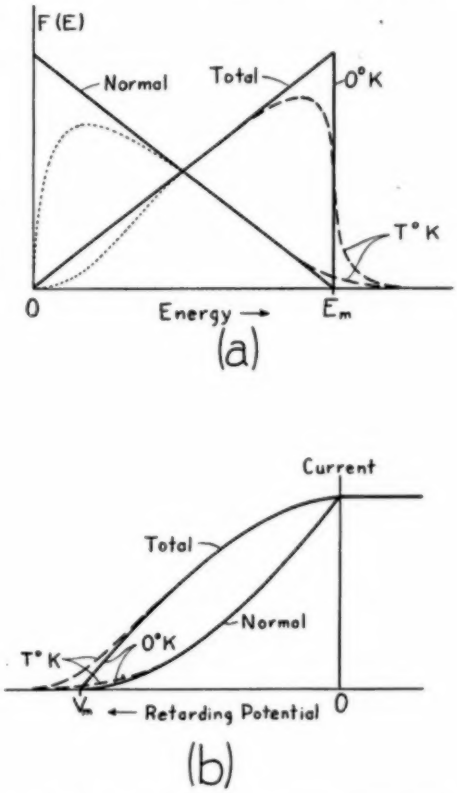

FIG. 1. (a) Total and "normal" energy distributions and (b) current-voltage curves according to DuBridge's theory contrasted at 0°K and a moderately high temperature. The dotted lines in (a) indicate how most experimental results differ from the theory.

[7] Israel Liben, Phys. Rev. **51**, 642 (1937).
[8] J. J. Brady, Phys. Rev. **46**, 768 (1934).
[9] I. Tamm and S. Schubin, Zeits. f. Physik **68**, 97 (1931).
[10] Erik Rudberg, Phys. Rev. **48**, 811 (1935).
[11] (a) K. Mitchell, Proc. Roy. Soc. **A146**, 442 (1934); (b) **A153**, 513 (1936).
[12] K. Mitchell, Proc. Camb. Phil. Soc. **31**, 416 (1935).
[13] R. D. Myers, Phys. Rev. **49**, 938 (1936).
[14] H. E. Ives, A. R. Olpin, and A. L. Johnsrud, Phys. Rev. **32**, 57 (1928).

must depend upon the *normal component* of velocity, and that is what the normal distribution measures, the *peak* of which occurs at very low energies. (cf. Fig. 1a.)

DuBridge's theory predicts a photoelectric current as a function of retarding potential and temperature for the case of plane electrodes according to

$$I=\alpha A T^2\phi(x), \tag{1}$$

where α is a proportionality constant involving light intensity and probability of absorbing a quantum, $A=(4\pi mek^2)/h^3$ (the same A which appears in Richardson's thermionic equation), $x=e(V_m-V)/kT$, $V_m=h(\nu-\nu_0)$, and $\phi(x)$ is an exponential series in x.[15] This equation is amenable to the same method of experimental verification which Fowler[1] developed by taking the logarithm of (1):

$$\log\,(I/T^2)=B+F(x), \tag{2}$$

where B is $\log(\alpha A)$, a constant independent of ν, V, and T, and $F(x)$ is a universal function of x frequently referred to as the Fowler function. If data are plotted in the form of $\log\,(I/T^2)$ *vs.* $-Ve/kT$ the vertical shift required to superpose the data on the curve of $F(x)$ will yield B, and the horizontal shift a value of V_me/kT from which the threshold at absolute zero can be calculated.

The retarding potential, V (which is considered essentially positive), involves the contact potential, V_c, between cathode and anode by

$$V=V_c-V_a, \tag{3}$$

where V_a is the actual applied potential across the tube. Since V_c is subject to change and is known to a smaller precision than V_a both current-voltage curves and Fowler graphs are plotted *vs.* V_a instead of $-V$. Hence the horizontal shift, V_{a0}, on the Fowler graph gives

$$V_{a0}=(V-V_m+V_a)/kT=(V_c-V_m)/kT. \tag{4}$$

Since contact potential is also related to the work functions of the emitting surface and the grid according to

$$V_c=\chi_g-\chi_s, \tag{5}$$

the horizontal shift (4) becomes

$$V_{a0}=(\chi_g-h\nu)/kT, \tag{6}$$

which is entirely independent of characteristics of the emitting surface.

Equation (1) at absolute zero reduces to

$$I=A(V_m-V)^2e^2/k^2=A(V_a-V_{a0})^2e^2/k^2, \tag{7}$$

which is the parabolic current-voltage curve of Fig. 1b. The extent to which α is constant with electron energy can be measured by the extent

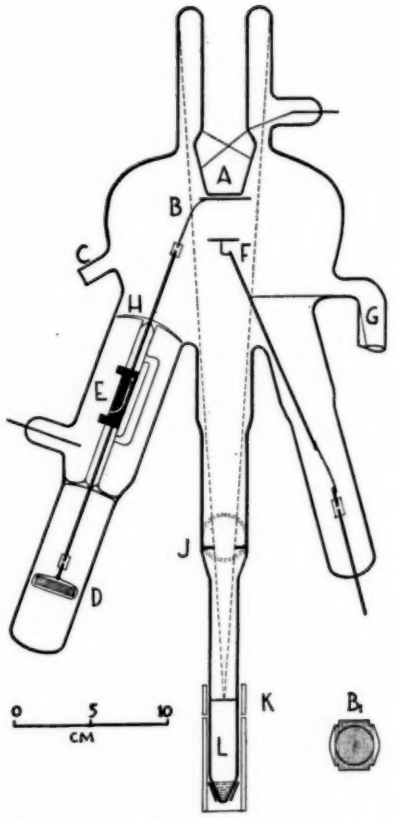

FIG. 2. Cross section of final experimental tube. *A*, reentrant tube the flat end of which held the base metal on which was condensed the potassium film. *B*, the anode consisting of a plane double grid shown in detail at B_1. *C*, small inspection window. *D*, iron armature for manipulating the grid into different positions controlled by the pin and slot guide, *E*. *F*, flat spiral tungsten filament coated with platinum. *G*, side tube containing iron plunger for retracting *F*. *H*, shield to preserve high insulation around anode lead. *J*, magnetically operated gate for controlling potassium deposition on *A* from the pinhole, *K*, and the oven, *L*.

[15] Equation (1) is a more recent derivation by DuBridge (Actualités Sc. et Ind., 268 (1935)) which differs from Eq. (12) in reference 2 by a factor representing the velocity of an electron normal to the surface. It indicates a different interpretation of the number of "available" electrons namely, the number striking the surface per unit area per second whose energies are in the interval $d\epsilon_n$, instead of the number whose normal energies lie in the interval $d\epsilon_n$, which Fowler (reference 1) used originally.

to which current-voltage curves (except for temperature tails) are parabolic, or the extent to which $I^{\frac{1}{2}}$ *vs.* V_a plots are straight lines.

Experimental

Figure 2 shows a cross section of the final experimental tube. The photoelectric cathode consisted of a potassium film condensed upon a base metal (Ag or Pt) which was deposited by evaporation on the circular face of the reentrant tube, *A*. A small spot of light focused on the center of the cathode ejected electrons in the uniform field between the cathode and the plane grid, *B*, which acted as the anode.

Obtaining a uniform field

It is essential in any retarding potential method to have undistorted electric fields, especially for the normal distribution where there are so many electrons with small normal velocities but large tangential velocities. Some distortion may be caused by the edge effect of the parallel plate condenser, but the greatest disturbance when working with alkali metal films is the local contact potential field at the edge of the condensed film. Several designs of phototube were tried before a satisfactory electrode arrangement was obtained. To test for edge effects the grid, *B*, could be placed by magnetic control in several different positions opposite the cathode. It could also be rotated 180° and removed from the potassium beam. The reentrant tube, *A*, was built with a conical end so that some potassium would condense upon the sides and remove the contact potential distorting field as far as possible from the region of the uniform field. The grounded walls of the bulb helped further to minimize the distorting effect.

The end of *A* was ground flat and polished before it was sealed into the tube. The details of the grid are shown at B_1. It consisted of two layers, one on each side, of 0.005″ Mo wire, spaced 0.025″ and spot welded to a Mo ring. A double grid can be shown to have as small variations in its potential distribution as a single grid of the same wires and half the spacing. This form permits it to transmit more light. Careful investigation was made of the variation in the uniform field caused by the grid wires and it was found in no case to be at all serious. The earth's magnetic field was neutralized with a pair of Helmholtz coils.

Deposition of base metal and sensitive surface

Either Ag or Pt was used as base metal. Three Ag sources were distributed around the tube so that they would coat the entire inside walls with an opaque layer. This Ag deposit served two purposes, first to provide an electrostatic shield, and second to prevent any bare glass walls from "seeing" the emitting surface, thus reducing the chance of gas contamination. Each Ag source was a tungsten spiral supporting a globule of 99.9+ percent Ag, both predegassed in an auxiliary vacuum.

Pt was condensed as a base metal on the cathode face on some occasions. The filament, *F*, was a flat spiral of 8″ of tungsten wire upon which pure Pt had been melted and then degassed in an auxiliary vacuum. The filament could be retracted from the potassium beam by magnetic control in the side tube, *G*. A wire wrapped around *A*, or cat whiskers cemented to the walls with Aquadag, made contact to these metal films.

Potassium films of calculable thickness can be deposited by an atom gun method developed by Brady.[16] The only change from his design is in the second aperture, *J*. It can be shown[17] that room temperature is low enough to condense potassium so no refrigerant was applied to this point. Instead a magnetically operated gate served to time the film deposits more accurately. The region of the gate was coated with a film of Aquadag[18] to prevent stray potassium from striking the grid and changing its work function during the course of measurements. Temperatures of the potassium in the oven, *L*, and of the pinhole, *K*, were recorded by thermocouples made of matched Chromel-Alumel wires.

The potassium was purified by repeated vacuum distillation. A sealed off capsule was first prepared on an auxiliary vacuum system and then at the proper time, broken magnetically

[16] J. J. Brady, Phys. Rev. **41**, 613 (1932).
[17] R. G. J. Fraser, *Molecular Rays* (Macmillan, 1931), p. 21.
[18] Aquadag seems to have a strong affinity for alkali metals.

inside the main system. Before it was driven into the chamber, L, it had been distilled twelve or more times.

Production of vacuum

Every available means was adopted for obtaining as high a vacuum as possible. Each metal part in the tube with the exception of the tungsten seals was pre-heat-treated in an auxiliary vacuum before assembling. The apparatus was then given a preliminary baking after which all the filaments were flashed. The final baking lasting three days took place at 450°C during which time the charcoal tube was heated at 550°C to 570°C. The charcoal in this tube was confined to a nickel gauze cylinder somewhat smaller in diameter than the inside of the tube. This produced an auxiliary pump of maximum effective area when immersed in liquid air. When photoelectric observations were being made the pressure was 1×10^{-8} mm of Hg as measured by an ionization gauge.

Control and measurement of film temperature

The temperature of the emitting surface was controlled by introducing various refrigerants in the tube, A. The temperatures of liquid air, dry ice, and room (or 0°C) provided a wide enough fractional change for the study of an alkali film. No data were taken for higher temperatures because the vapor pressure of potassium would cause changes in the film and also scatter potassium around the tube. Close track of the cathode temperature could be kept by means of a calibrated Chromel-Alumel thermocouple attached to the atmosphere side of the cathode face.

Optical system

The light source was a high intensity capillary quartz mercury arc developed especially for the purpose. Since potassium films are sensitive to most of the Hg lines in the visible, glass lenses and windows could be used. (The optical window is out of the plane of the diagram in Fig. 2; C is only a small inspection window.) Part of the light from the arc fell on a Photronic cell which was used to observe the relative intensity of the arc, although most of the time it ran very steadily. The different Hg lines were selected by the proper Corning filter combinations to give sharp cut-off. The light beam, with an angle of incidence of about 60°, made a circular spot on the cathode approximately 2 mm in diameter.

Electrical connections

The photoelectric current collected by the grid was measured by a Dolezalek type quadrant electrometer of 20 cm capacity which performed most satisfactorily at 1500 div./volt. Four high resistances could be shunted across the electrometer to permit the more rapid steady deflection method to be used. Their last measured values were 1.17×10^{8}, 1.28×10^{9}, 8.15×10^{9}, and 6.6×10^{10} ohms, respectively. Their relative values were checked more carefully since the absolute magnitude of the current is unimportant. The rate of drift method could also be used for the smallest currents but on most occasions it was not valuable enough to be worth the time.

Retarding potentials were applied by making the cathode positive to ground with a high resistance potentiometer.

One of the purposes of making the grid, B, movable was to be able to measure contact potentials by the Kelvin method. A 50 percent change in capacity as the grid was moved from 2 mm to 1 mm from the cathode permitted contact potential determinations to a precision of between ±0.02 and ±0.01 volt.

Procedure

The procedure was briefly as follows: After baking, an initial coating of Ag was applied to the interior walls. Then the potassium capsule was broken and the potassium distilled in stages into the oven, L (Fig. 2). Final improvement of the vacuum, by surrounding the charcoal tube with liquid air and depositing a fresh layer of Ag, immediately preceded the production of the potassium film. Photoelectric observations on one film consisted of a series of current-voltage curves going from accelerating potentials of over 25 volts to the largest retarding potentials that would give a detectable current, for three or more of the lines of the Hg arc, and at each of three cathode temperatures. Occasional curves were repeated to detect any change in character of the surface, and frequent measurements of contact potential were also recorded. To study a

new film additional base metal (Ag or Pt) was evaporated over the old one.

The rate of deposition of potassium is known to be proportional to $p/T^{\frac{1}{2}}$ where p is the vapor pressure and T the absolute temperature. Whenever the oven temperature was not strictly constant the integral of $p/T^{\frac{1}{2}} \times$ time was obtained graphically. The accuracy of film thickness, which is probably no better than 10 percent, is limited by vapor pressure data. These calculations were based on data published by Edmondson and Edgerton.[19]

From electrometer deflections, high resistances, and arc intensity (in arbitrary units) values of photoelectric current per unit light intensity were calculated. The actual applied potential across the tube had to be corrected for the drop across the electrometer resistances.

Results

Current-voltage curves

In order to test for distortion of the uniform field, data were taken on several occasions with the grid, B, of Fig. 2 in two positions, 2 mm and 8 mm from the cathode. The general result was no apparent change in the curves except at the high current end where a slower approach to saturation occurred with the grid at the greater distance. An illustration of this is shown by the dotted line of Fig. 5. Since the area of the anode over which electrons are collected increases as retarding potential decreases this change in the approach to saturation is interpreted as representing a few slow electrons which are lost when the condenser electrodes have wider separation. Consequently most of the data were taken with the grid at the closer distance to minimize this effect. This arrangement had the additional advantage of reducing any possible distortion of the uniform field by contact potential fields at the edge of the potassium film. The slight decrease in electron current with accelerating fields noticeable in nearly all current-voltage curves is interpreted as representing a few electrons which pass through the grid wires without being collected.

[19] W. Edmondson and A. Edgerton, Proc. Roy. Soc. **113**, 539 (1926).

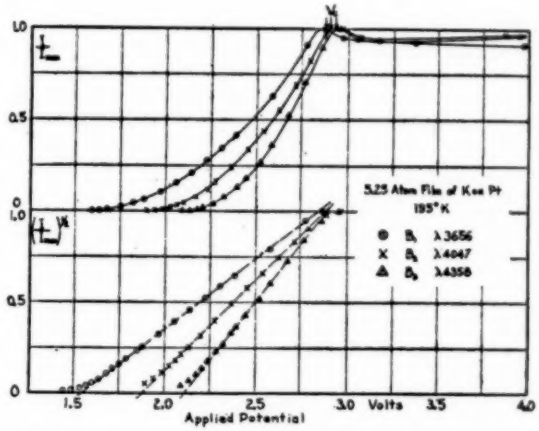

FIG. 3. Sample current-voltage curves for a 5.25 atom thick film of potassium on platinum at 195°K for three light frequencies. To show how nearly parabolic they are (current)$^{\frac{1}{2}}$-voltage curves are plotted below. V_c indicates value of contact potential measured by Kelvin method.

In Fig. 3 are shown representative current-voltage curves for a several-atom-thick film of potassium on Pt. To compare curves for different light frequencies the data are plotted as $I/I_{\max}$ *vs.* applied potential, V_a. Contact potential, V_c, measured by the Kelvin method, is indicated for each curve by a short arrow near the maximum. These curves are seen to be parabolic in shape (except for the temperature tails) and if differentiated graphically should give nearly straight line energy distributions. The frequency and precision of the experimental points do not permit an accurate differentiation to be made. Instead, in order to see how closely parabolic the current-voltage curves are, $(I/I_{\max})^{\frac{1}{2}}$ is plotted *vs.* V_a directly below and the points tested by a straight line. The intersection of this line with the abscissa should give V_{a0} in agreement with the horizontal shift from the Fowler plot. However, the temperature tail slightly influences the drawing of that line, for values of V_{a0} and χ_s obtained in this way although mutually consistent average about 0.01 volt less than those obtained from the Fowler shifts. The closeness with which the $(I/I_{\max})^{\frac{1}{2}}$ points fall on the straight line as they approach the maximum indicates that the current-voltage curves do not differ widely from the theory.

In Fig. 4 are given similar curves for a surface which is not completely covered. They have the same general characteristics as curves for a thicker surface except in the approach to satura-

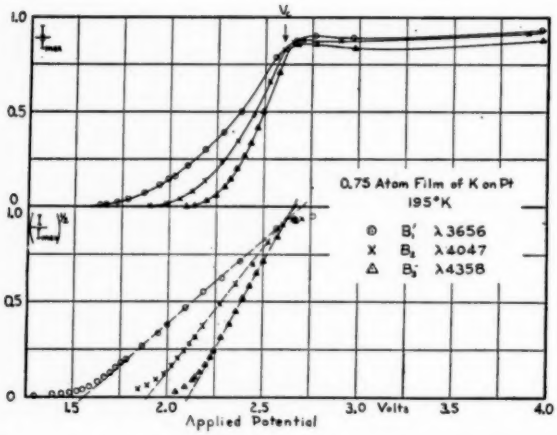

FIG. 4. Sample current-voltage and (current)$^{\frac{1}{2}}$-voltage curves similar to Fig. 3 but for a 0.75 atom thick film of potassium on platinum.

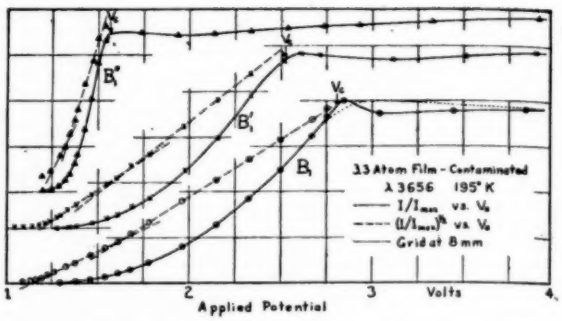

FIG. 5. Effect of progressive contamination on current-voltage and (current)$^{\frac{1}{2}}$-voltage curves for a composite surface. Curve B_1 was taken immediately after deposition; B_1' two hours later; and B_1'' 5½ hours later.

tion. The current-voltage curves rise parabolically to a pseudo-saturation at zero field and then continue to increase slightly until an accelerating potential of about six volts is applied, after which they decrease slightly again. This is consistent with the notion of an incompletely covered surface. The exposed areas of base metal are electronegative to the regions emitting electrons and this prevents some of the slow electrons from escaping until an accelerating field from the anode reduces the effect of the local fields. Becker's[20] patch theory follows this same line of reasoning.

Effect of gas contamination

Because time changes in the work functions of the potassium films occurred occasionally it is necessary to know whether they can be laid to gas contamination. For this purpose several surfaces were studied under a pressure of from 3 to 8×10^{-8} mm of Hg. In Fig. 5 are current-voltage and (current)$^{\frac{1}{2}}$-voltage curves for a composite surface. It was formed by depositing 0.8 atom layers (on Ag at liquid-air temperature) when the pressure was about 6×10^{-8} mm, allowing it to contaminate, and then adding 2.5 atom layers. Curve B_1 was taken immediately after the final deposition, B_1' two hours later, and B_1'' 5½ hours later. The saturation currents of B_1' and B_1'' were 64 percent and 0.9 percent of B_1, respectively. The gradual changes, in the shape of the curves at saturation, in contact potential, and in saturation current, all indicate contamination of the surface by some electronegative substance such as oxygen. Furthermore it becomes impossible to fit a single straight line to the (current)$^{\frac{1}{2}}$-voltage curves, although an approximation can be made with two lines of different slopes.

The Fowler plots of this surface deviate from the theoretical curve at the tail in a manner common to all surfaces, to be discussed below. As contamination progresses the Fowler curves become shorter but there is no great change in their shape. On the Fowler plots it is possible to find two reasonable fits corresponding to the two lines for (current)$^{\frac{1}{2}}$-voltage curves and this suggests that there is emission from two surfaces of different work functions. Jamison and Cashman[21] find such a situation for spectral distribution curves of Ba surfaces, but that interpretation is untenable for retarding potential curves. It was shown in Eq. (6) that the horizontal shift determines only the work function of the anode.

One explanation for the double fitting of a contaminated surface can be made in terms of a distortion of the *directional* distribution rather than the velocity distribution. Some systematic microscopic irregularity of the potassium film might be produced by the contamination which would change the angular distribution of emission from that represented by Lambert's law.

[20] J. A. Becker, Rev. Mod. Phys. **7**, 95 (1932).

[21] N. C. Jamison and R. J. Cashman, Phys. Rev. **50**, 624 (1936).

Effects of temperature

The effects of temperature upon these potassium films can be divided into four categories: (1) temperature dependence of the rates of diffusion of potassium through and sublimation from the base metal, (2) irreversible changes with temperature in the state of the potassium surfaces as shown by changes in contact potential and saturation current, (3) *reversible* changes with temperature in the shape of the Fowler plots, (4) a change of photoelectric current with temperature at the low current ends of the curves only 10 to 30 percent of that predicted by DuBridge's theory.

(1) In phototubes used previous to the one shown in Fig. 2 opportunity was available for studying many characteristics of potassium films as a function of temperature which can be reported only briefly. It was found impossible to "cover up" an old film by depositing more base metal at room temperature although it could be done easily at 85°K or 195°K. If a film is covered with Ag at low temperature and then warmed up it may resensitize itself exponentially in time showing that potassium will diffuse through Ag at room temperature. There was indication of slight diffusion through Pt, less than through Ag. To insure a clean base metal for a new film the most satisfactory method was to cover and warm the surface twice or more. Tests were made to detect any migration of potassium over an Ag surface but none whatever was found beyond 1 mm (the limit of detection).

The sensitivity of the work function of the grid to slight potassium contamination made it an

TABLE I. *Values of work function and threshold wave-lengths as a function of temperature.*

	5.25 ATOM FILM		0.75 ATOM FILM	
T	χ_0	λ_0	χ_0	λ_0
85°K	2.30 volts	5360A	2.37 volts	5210A
195°	2.03	6080	2.33	5290
273°	1.61	7660		
296°			2.33	5290

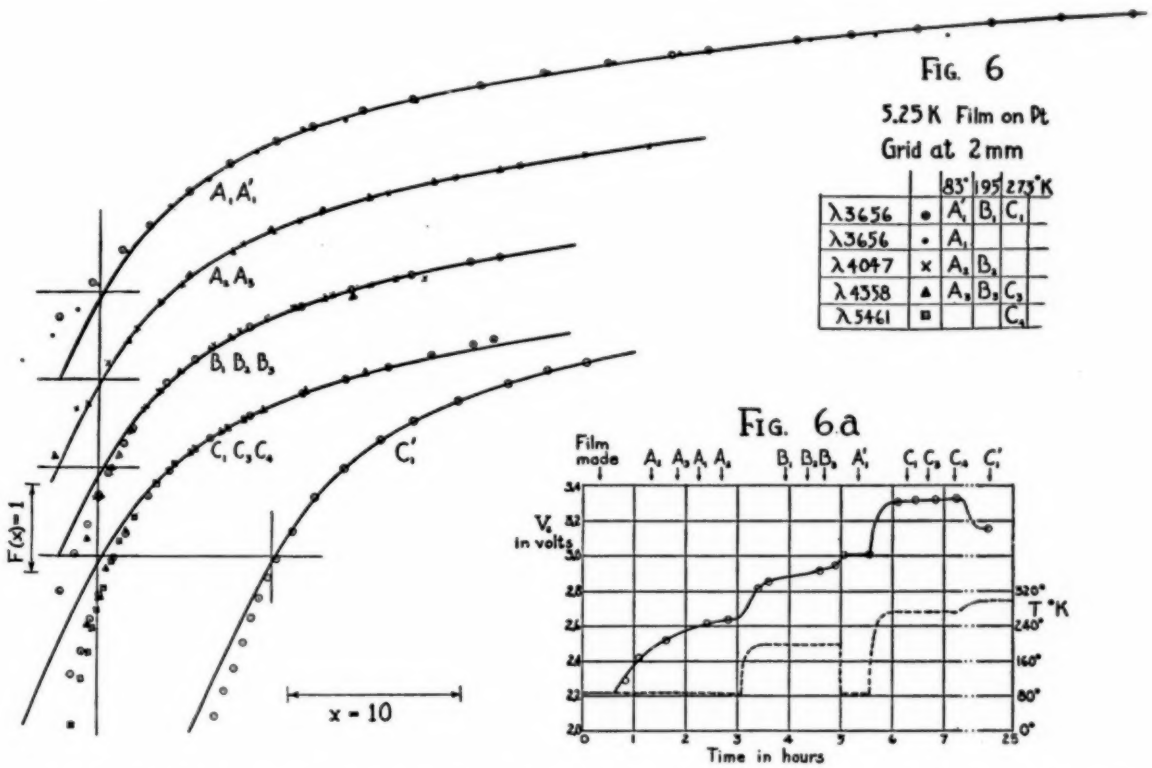

FIG. 6

5.25 K Film on Pt
Grid at 2 mm

		83°K	195°K	273°K
λ3656	•	A'	B,	C,
λ3656	•	A,		
λ4047	×	A,	B,	
λ4358	▲	A,	B,	C,
λ5461	■			C,

FIG. 6a

FIG. 6. Fowler plots for the 5.25 atom potassium film extending from smallest currents to the maximum. Curves for different frequencies and the same temperature are superimposed at positions which give the best appearing fit. (6a) is a record of curve sequence, contact potential, and cathode temperature, as a function of time.

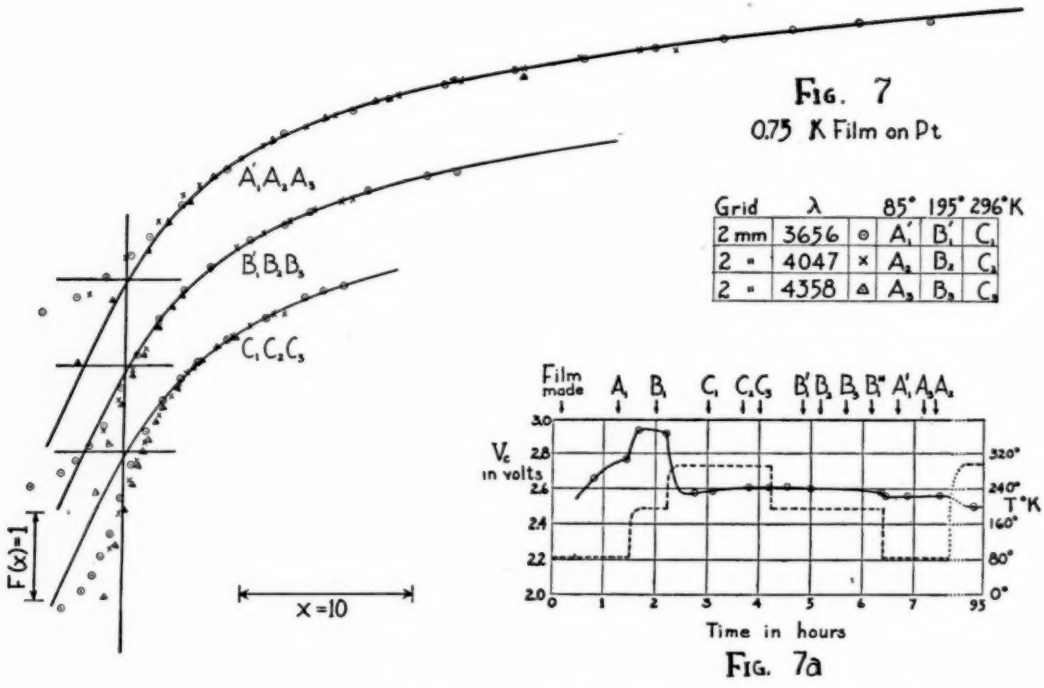

FIG. 7. Fowler plots for the 0.75 atom potassium film arranged similar to those in Fig. 6.

effective detector of sublimation from the film. No suggestion of sublimation of potassium at room temperature was ever found from films two or three atoms thick. Films of five and six atoms begin to sublime above 0°C, and those about twice as thick begin at −40°C or below.

(2) Most of the films studied were made at liquid-air or solid-CO_2 temperatures. When these were warmed for the first time a change in the contact potential and saturation current frequently occurred, but after being brought to room temperature they remained quite constant.[22] A detailed record of contact potential and temperature as a function of time is shown for two surfaces in Figs. 6a and 7a. The extreme strains which must exist in a film after a change of temperature may easily account for changes in work function and saturation current.

The large change in contact potential for the surface whose record is given in Fig. 6a makes one suspect the presence of gas contamination. The changes cannot easily be laid to poor vacuum conditions for the pressure was less than 1×10^{-8} mm Hg and no characteristics of pressure contamination were noticeable. The work function of the surface once it was annealed remained quite constant; the contact potential drop of 0.17 volt in a 17 hour interval was exactly equal to the decrease in work function of the grid caused by potassium striking it as the cathode warmed from 273°K to 296°K. It is possible that the Pt base contained a small amount of impurity which reacted with the potassium during annealing and produced a slightly composite surface.

TABLE II. *Values of χ_0 determined from the best apparent horizontal shifts of the curves in Figs. 6 and 7.*

5.25 ATOM FILM		0.75 ATOM FILM	
Curve	χ_0	Curve	χ_0
A_1'	4.931 volts	A_1'	4.929 volts
A_2'	4.933	A_2	4.946
A_3	4.941	A_3	4.948
B_1	4.957	B_1'	4.948
B_2	4.969	B_2	4.960
B_3	4.973	B_3	4.972
C_1	4.955	C_1	4.959
C_2	4.979	C_2	4.959*
C_4	4.974	C_3	4.959*

* Fit so poor that C_1 value was arbitrarily adopted.

[22] Mayer (Ann. d. Physik 29, 129 (1937)) finds such changes in *K* films on Pt which he attributes to rearrangement of the atoms in the film.

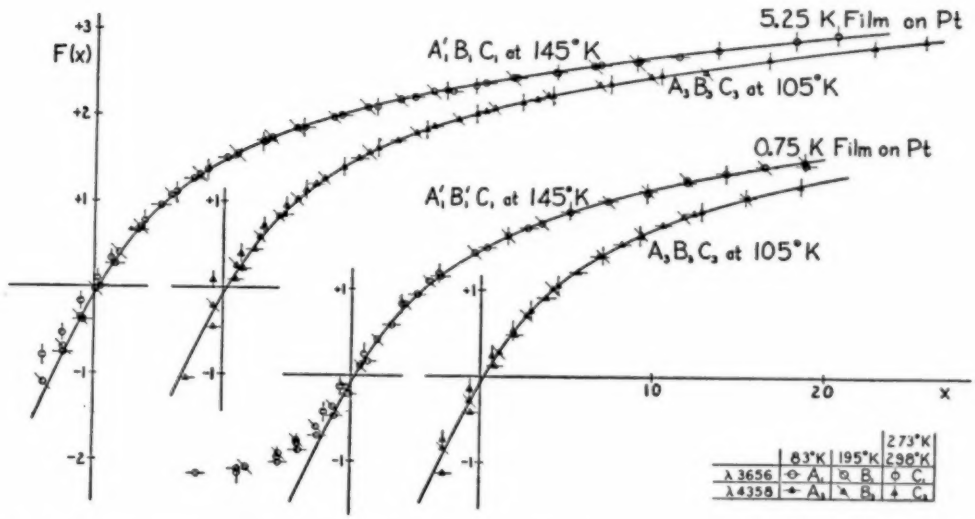

FIG. 8. Data from curves of Figs. 6 and 7 taken at different temperatures replotted at the same temperature to show how the fitting is improved and how small the temperature effect is. The values of 145°K and 105°K permitted the *same* horizontal shift to be used in each case.

For the film described in Fig. 7a the Pt had been still more thoroughly degassed.

Taking the work function of the grid, χ_g, to be 4.933 volts (arrived at below), values of χ_s calculated from contact potential by Eq. (5) are listed in Table I for different temperatures of the surface. The effect of annealing a surface (bringing it first to room temperature) is to reduce greatly subsequent changes.

During the 18 hour interval between curves C_1 and C_1' (Fig. 6a) the saturation current remained the same within accuracy of measurement. In general any changes in saturation current can be laid to changes in work function of the surface, a decreasing work function producing larger saturation currents because of the greater number of electrons available for emission.

(3, 4) The temperature variation of photoelectric emission can be best treated quantitatively by Fowler's method.[1] When it is applied to data for the two surfaces for which sample current-voltage curves are given in Figs. 3 and 4 the curves which result are shown in Figs. 6 and 7. The points cover from the smallest currents measured to the maxima (or pseudo-maxima for the thin film).

The significant features of all the curves is that there is excellent fitting to the theoretical curve (within the reliability of logarithmic plots) from the maximum down to the region of greatest curvature. From there on there are deviations, to the left for liquid-air temperature (A) curves, and to the right for solid-CO_2 (B) curves and room temperature (C) curves. These deviations do not represent irreversible changes in the state of the film, but are *reproducible* and independent of the work function of the surface. (See curves A_1 and A_1' of Fig. 6.) They prevent perfect fitting of the theoretical curve and hence interfere with computations from the horizontal shift. The curves in Figs. 6 and 7 were adjusted to give the best looking fit to the Fowler curve. The resulting values for the work function of the grid, χ_g, are given in Table II.

TABLE III. *Arbitrary temperatures which give the best fi and horizontal shift on a Fowler plot. (Not reliable to better than 5 percent.)*

5.25 ATOM FILM		0.75 ATOM FILM	
Curve	Temperature	Curve	Temperature
A_1'	140°K	A_1'	125°K
A_2'	120°	A_2	125°
A_3	90°	A_3	95°
B_1	150°	B_1'	140°
B_2	135°	B_2	135°
B_3	125°	B_3	110°
C_1	175°	C_1	160°
C_3	150°	C_2	145°
C_4	115°	C_3	120°

The trends in Table II, the directions of the deviations of the curves, and the fact that they are reproducible suggested that possibly the theory was over-correcting for the temperature effect. The Fowler method essentially plots log current as a function of VT^{-1} which compresses horizontally the points for a higher temperature in order to make the longer tails conform to the same universal curve as for a lower temperature. Curves of Figs. 6 or 7 which deviate to the left should fit better if plotted at a higher temperature, and those deviating to the right just the opposite. This procedure when applied to these curves met with astonishing success. By trying a number of different temperatures there was found some value between 90°K and 175°K which would completely eliminate the former deviation. Not only was an excellent fit produced but all the curves yielded the same value of χ_0 (within ± 0.003 volts, the accuracy of fitting). In Table III are listed the optimum temperatures. There apparently is some change of the photoelectric current with temperature but only 10 to 30 percent of what the theory predicts, depending upon which frequency of light is used. It seems to be greatest for the thicker film when the light is near the threshold.

To show how the fit of these curves can be improved by using a different temperature the 3656A and 4358A curves for both surfaces are replotted in Fig. 8 at temperatures of 145°K and 105°K, respectively, all with the same horizontal shift corresponding to $\chi_0 = 4.933$ volts. The slight difference at the tail in the curves of one set gives a measure of the magnitude of the actual temperature change for these thin films.

One prominent difference between the Fowler curves for a completely covered and an incompletely covered surface is exhibited when the 3650 Hg lines are used. The thinner film has an excess number of high speed electrons at all temperatures as shown by the tails in Figs. 7 and 8. Since the phenomenon occurs only when the retarding potential is of the order of one volt, the explanation which requires the fewest a priori assumptions is one involving local fields at the surface. Although no direct evidence is available, it seems reasonable that the combination of the retarding field of the anode plus the retarding fields of the uncovered areas of base metal will combine to deflect a few of the electrons in a direction more nearly perpendicular to the surface than their normal paths. This would cause a slight excess current to the anode detectable when the ordinary current is very small.

Discussion

Approach to saturation

As far as can be judged by the closeness with which (current)$^{\frac{1}{2}}$-voltage points fall upon a straight line (Figs. 3 and 4) or the data's agreement with the logarithmic Fowler curve (Figs. 5–8), the normal energy distribution of photoelectrons is very nearly a straight line such as the solid line of Fig. 1a. Although other workers have found fewer slow electrons than are represented by this distribution the discrepancy may be due at least partially, as pointed out above, to the extreme difficulty of getting sufficiently precise experimental conditions.

Mitchell's[11b] quantum-mechanical calculations of the normal energy distribution show a pronounced decrease in slow electrons, even more than the dotted line of Fig. 1a, but it is well known that the square barrier which he assumed has a high reflection coefficient in the region close to the top. Myers,[13] in comparing the image with the square barrier for calculating the spectral distribution of potassium, found that although the transition probabilities are smaller for an image barrier its larger transmission coefficient predominates giving a larger number of electrons when they have low energies. Quite recently A. G. Hill[23] has carried out a calculation of the yield for sodium using Mitchell's method and the image barrier. He finds that, similar to a square barrier, the transition probabilities differ in absolute value for different frequencies of light, but up to 1.35 volts from the threshold they are essentially constant in electron energy within computational error. The calculations of both Myers and Hill indicate that as far as altering energy distribution the variation of the reflection coefficient of the barrier is much more important than the transition probability.

Since the reflection coefficient for an image barrier falls fairly rapidly from a maximum of

[23] Private communication.

7 percent the net result for energy distribution curves according to Hill is effectively that predicted by DuBridge's simple theory. The similarity in properties between sodium and potassium makes it possible to compare the results of this investigation with Hill's calculations, although he assumes a solid surface and not a thin film. It is thus seen that within experimental error (which may be 5 to 10 percent for slow electrons) there is good indication that the assumption of an image potential or one similar to it at the surface of a metal is far more reasonable than a single potential step. The field emission from potassium[24] seems to confirm this also although thermionic measurements from thoriated surfaces have not followed the Schottky relation well at low accelerating fields. It would be quite possible to make sufficient alterations in the barrier to satisfy field emission measurements for thin films without changing the reflection coefficient by an amount detectable with the present accuracy of retarding potential measurements.

Lack of temperature effect

The most reasonable interpretation of the results given in Table III and Fig. 8 is that there is less change with temperature of the photoelectric emission from thin films of an alkali metal upon a base metal than predicted by the Fermi factor of DuBridge's[2] or Mitchell's[12] theories. Several workers[25] have observed a substantial temperature variation of the emission from alkali metals in bulk, but their results have not been analyzed by the Fowler method. The only studies of thin films by the Fowler method have been by Brady[7] and Smith and DuBridge.[26] The former, using potassium, makes no mention of what temperature was used, and the latter have published only a preliminary report on thoriated tungsten at a single temperature of 900°K.

Presumably with thicker potassium films the temperature effect should increase to what it is for the bulk metal. Unfortunately no data for thicker surfaces are available which were obtained under conditions of comparable quality. The indications from Table III are that the temperature changes are greater for the 5.25 atom film than for the 0.75 atom film. This small temperature effect seems to hold for composite and contaminated surfaces as well as clean surfaces and no particular difference has been observed with Ag as a base metal in place of Pt.

The fact that both these films were deposited upon Pt at liquid-air temperature suggests a possible correlation between temperature of deposition and the average temperature which gives the best fits and shifts (105°K–145°K). Results with other films deposited at solid-CO_2 temperature give no encouragement for such a correlation and indicate the same behavior as described in detail above.

The theoretical approach to an exact description of the energy states of electrons in a thin film of one metal upon another is particularly difficult and has not yet been attempted. Until some advance has been made along that line speculation as to the significance of an effect of this kind is of no great value but it is quite conceivable that the interparticle interactions in a thin film are sufficiently extreme to affect strongly the states of the electrons which contribute to the photoelectric emission at the surface.

The writer is grateful to Dr. A. G. Hill for the privilege of seeing the results of his calculations in advance of publication. He also wishes to express his appreciation for the skillful and patient glassblowing by Mr. F. P. Noble, and to indicate his indebtedness to Professor A. T. Waterman who supervised this investigation and supplied many helpful and encouraging suggestions.

[24] E. O. Lawrence and L. B. Linford, Phys. Rev. **36**, 482 (1930).
[25] H. E. Ives and A. L. Johnsrud, J. Opt. Soc. Am. **11**, 565 (1925); J. C. McLennan, L. A. Matheson, and C. D. Niven, Trans. Roy. Soc. Can. **22**, 279 (1928).
[26] R. E. Smith and L. A. DuBridge, Phys. Rev. **46**, 339 (1934).

The Empty Lattice Test of the Cellular Method in Solids*

W. SHOCKLEY†
Massachusetts Institute of Technology, Cambridge, Massachusetts
(Received August 7, 1937)

The cellular method of constructing wave functions for electrons in crystals developed principally by Wigner and Seitz and Slater is tested by applying it to an artificial crystal in which the potential is constant. Knowledge of the exact solutions for this case, plane waves, shows that the cellular method is quite accurate in the first Brillouin zone but may be in error by a factor of two in the second. Hence calculations of occupied levels in Li and Na are probably quite good; for Cu, Ca, diamond, LiF, and NaCl the errors will be larger. Calculations of excited states are likely to be very much in error. The accuracy of the cellular method is shown to improve very slowly with increasing number of continuity conditions.

I. INTRODUCTION

THE cellular method of constructing lattice functions, developed principally by Wigner and Seitz[1] and Slater[2] has now been applied to a large number of cases. However, no critical evaluation of the rigor of the method has as yet been presented. A new exact method has been developed by Slater,[3] but since this has not been applied to any problem, a comparison with the results of the cellular method is not possible.

In order to obtain lattice functions by the cellular method the lattice is partitioned into Wigner-Seitz cells within which the potential is taken to have spherical symmetry. The lattice function in one cell is then expanded in spherical harmonics times solutions of the radial part of the wave equation. The wave function in other cells is obtained by translation and multiplication by $\exp(2\pi i\mathbf{k}\cdot\mathbf{R})$ where $\mathbf{R}$ is the translation vector and $\mathbf{k}$ is a vector analogous to the momentum for a plane wave divided by h. By the cellular method one obtains a functional relationship between $\mathbf{k}$ and the energy $E(\mathbf{k})$ of the lattice function.

There is only one obvious exactly soluble case to which the cellular method can be applied. This is the trivial case of the "empty lattice"—the spherically symmetrical potential becoming a constant. The radial functions needed in the cellular method are known and the exact solutions are those for the free electron. Hence it is possible to compare cellular solutions with exact solutions and thus gain an estimate of the accuracy of the method.

II. EMPTY LATTICE TEST FOR THE FACE-CENTERED LATTICE

The Schrödinger equation for one electron when expressed in atomic units is

$$\nabla^2\psi+(E-V)\psi=0. \tag{1}$$

For the empty lattice it becomes

$$\nabla^2\psi+E\psi=0 \tag{2}$$

and has solutions

$$\psi=\exp 2\pi i\mathbf{k}\cdot\mathbf{r} \tag{3}$$

with energies

$$E=4\pi^2k^2. \tag{4}$$

Now suppose that an artificial face-centered lattice is inserted in space with lattice vectors $0\pm\frac{1}{2}\pm\frac{1}{2}$, etc. The cell appropriate to this lattice is rhombic duodecahedron bounded by planes bisecting the above set of vectors. The wave equation inside the cell may be separated in spherical coordinates and has solutions of the form

$$\psi_l=S_{ml}(\theta,\varphi)f_c(r), \tag{5}$$

where S_{ml} is a tesseral harmonic of degree l and $f_l(r)$ satisfies the equation

$$\frac{1}{r^2}\frac{d}{dr}r^2\frac{d}{dr}f(r)+\left[E-\frac{l(l+1)}{r^2}\right]f(r)=0. \tag{6}$$

* Reported at the Atlantic City meeting of the American Physical Society, Phys. Rev. **51**, 379A (1937).
† Now with the Bell Telephone Laboratories.
[1] E. Wigner and F. Seitz, Phys. Rev. **43**, 804 (1933) and **46**, 509 (1934).
[2] J. C. Slater, Phys. Rev. **45**, 794 (1934).
[3] J. C. Slater, Phys. Rev. **51**, 846 (1937).

Since the solutions of this equation are the well-known functions[4]

$$j_l(E^{\frac{1}{2}}r)=\left(\frac{\pi}{2E^{\frac{1}{2}}r}\right)^{\frac{1}{2}}J_{l+\frac{1}{2}}(E^{\frac{1}{2}}r), \tag{7}$$

where $J_n(r)$ represents a Bessel function, the procedure of setting up cellular lattice functions may be carried out. The expressions arising from this procedure involve the ratios $s'/s=\sigma$, $p'/p=\pi$, $d'/d=\delta$, $f'/f=\varphi$[5] where s, p, d, and f are the radial wave functions for $l=0$, 1, 2, and 3 and s', p', d' and f' are their derivatives in respect to increasing r. These quantities are evaluated at the midpoints of the intercellular boundaries, $r=r_0=2^{\frac{1}{2}}/4$. Hence the ratios take the form

$$\sigma=s'/s=E^{\frac{1}{2}}j_0'(E^{\frac{1}{2}}r_0)/j_0(E^{\frac{1}{2}}r_0). \tag{8}$$

The cellular method supposes that the lattice wave functions are expressed in the form $\exp(2\pi i\mathbf{k}\cdot\mathbf{x})\varphi(\mathbf{x})$ where $\varphi(\mathbf{x})$ is a periodic function of position in the lattice; the energy $E(\mathbf{k})$ of the wave functions is calculated as a function of $\mathbf{k}$. It is most convenient to suppose that $\mathbf{k}$ is in the first Brillouin zone of k space. The energy and wave function are then multivalued functions of $\mathbf{k}$. The corresponding exact plane wave solutions will be

$$\psi_{K,\,k}(x)=\exp(2\pi i\mathbf{k}\cdot\mathbf{r})\exp(2\pi i\mathbf{K}\cdot\mathbf{r}), \tag{9}$$

$$E_K(\mathbf{k})=4\pi^2(\mathbf{K}+\mathbf{k})^2, \tag{10}$$

TABLE I. *Classification for the six lowest branches of the $E_K(k)$ curves.*

Γ_1	
$E_{000}(u)=4\pi^2 3u^2$	$\psi=\psi_{000}$
$E_{-1-1-1}(u)=4\pi^2 3(u-1)^2$	$\psi=\psi_{-1-1-1}$
$E_{111}(u)=4\pi^2 3(u+1)^2$	$\psi=\psi_{111}$
$E_{1-1-1}(u)=4\pi^2[2(u-1)^2+(u+1)^2]$	$\psi=\psi_{1-1-1}+\psi_{-11-1}+\psi_{-1-11}$
$E_{-111}(u)=4\pi^2[2(u+1)^2+(u-1)^2]$	$\psi=\psi_{-111}+\psi_{1-11}+\psi_{11-1}$
$E_{-200}(u)=4\pi^2[2u^2+(u-2)^2]$	$\psi=\psi_{-200}+\psi_{0-20}+\psi_{00-2}$
Γ_2	
has no representations for energies as low as those considered here.	
Γ_3	
$E_{1-1-1}(u)=4\pi^2[2(u-1)^2+(u+1)^2]$	$\psi=\psi_{1-1-1}+\omega_1\psi_{-11-1}+\omega_2\psi_{-1-11}$ and $\psi=\psi_{1-1-1}+\omega_2\psi_{-11-1}+\omega_1\psi_{-1-11}$
$E_{-111}(u)=4\pi^2[2(u+1)^2+(u-1)^2]$	$\psi=\psi_{-111}+\omega_1\psi_{1-11}+\omega_2\psi_{11-1}$ and $\psi=\psi_{-111}+\omega_2\psi_{1-11}+\omega_1\psi_{11-1}$
$E_{-200}(u)=4\pi^2[2u_2+(u-2)^2]$	$\psi=\psi_{-200}+\omega_1\psi_{0-20}+\omega_2\psi_{00-2}$ and $\psi=\psi_{-200}+\omega_2\psi_{0-20}+\omega_1\psi_{002}$

[4] Excellent tables of these functions are given in *Vibration and Sound* by P. M. Morse, to whom the writer is indebted for their use in advance of their publication.

[5] The notation used in this paper, especially in regard to the face-centered solutions, is that of W. Shockley, Phys. Rev. **51**, 130 (1937). π means 3.14··· when it multiplies $\mathbf{k}$ or its components.

where $\mathbf{K}$ is a vector of the reciprocal lattice and is a sum of vectors of the form $\pm1\pm1\pm1$.

The test described in this work is carried out by calculating $E(\mathbf{k})$ from the solutions worked out by Krutter[6] and comparing them with the exact $E_K(\mathbf{k})$. This comparison is complicated by the fact that both sets of functions are multivalued. For principal crystallographic directions, however, segregation into noncombining types is made possible by symmetry considerations. When $\mathbf{k}$ lies in the 111 direction, whose symmetry is C_{3v}, it is possible to group the wave functions into three different types:[7] Γ_1, functions which are unaltered by the symmetry operations of the three fold rotation and reflection axis in the 111 direction; Γ_2, functions which are unaltered by rotation but change sign on reflection; Γ_3, functions occurring in pairs which transform as do $e^{+i\varphi}$ and $e^{-i\varphi}$ where φ is the angle measured around 111 as an axis. The classification for the six lowest branches of the $E_K(\mathbf{k})$ curves is given in Table I. For brevity only one component of $\mathbf{k}=u,\ u,\ u$ is given; $\psi_{K,\,k}(\mathbf{r})=\psi_K$, and $\omega_1=e^{2\pi i/3}$, $\omega_2=\omega_1^2$.

The classification of the results of the cellular method is given in Table II. The notation is that of reference 5. The energy was computed as a function of u from these relationships. The work is slightly simplified by the fact that all the expressions are homogeneous of zero degree in the quantities σ, π, etc., hence no error is made by omitting the factor $E^{\frac{1}{2}}$ which occurs in Eq. (8).

The results of the work are shown in Fig. 1. For energies below 30 units on this scale, we see

TABLE II. *Classification of the results of the cellular method.*

	Γ_1
111_a	$\tan^2\pi u+2\sigma\,\delta/\pi(\sigma+\delta)=0$
	Γ_2
111_f	u arbitrary for $\varphi=\infty$. (No solutions in the energy range considered.)
	Γ_3
111_b and 111_c	$\tan^2\pi u+4\delta/(\pi+3\varphi)=0$
111_d and 111_e	u arbitrary for $\delta=0$

[6] H. M. Krutter, Phys. Rev. **48**, 664 (1935).

[7] Group theoretical classifications into symmetry types for many crystallographic directions have been given by Bouckaert, Smoluchowski, and Wigner, Phys. Rev. **50**, 63 (1936). The character scheme for this case is given in their Table III.

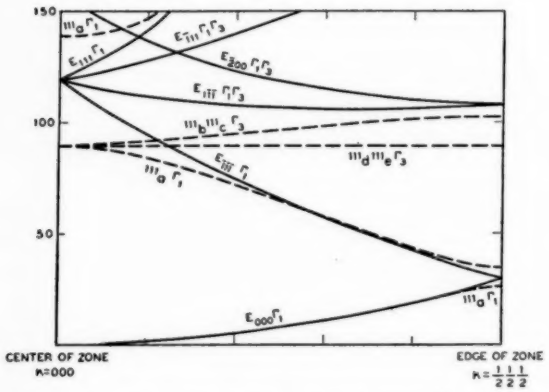

FIG. 1. Comparison of cellular and exact solutions for the face-centered lattice, 111 direction. Cellular solutions, dashed lines; exact solutions, solid lines. Solutions of the same symmetry type should be compared.

that both the cellular method and the exact solution give only one energy value and that the two agree extremely well. The agreement is still fairly satisfactory up to about 80 units. If the method were exact we should find that the Γ_1 curves for the cellular method would coincide with the Γ_1 curves of the exact solution and a similar situation would hold true for the Γ_2 curves. It is readily seen, however, that the results of the cellular method become notably faulty above about 90 units.

For other directions in the face-centered lattice similar results are obtained, the agreement for the lowest curve being nearly but not quite as good.

III. Empty Lattice Test for the Body-Centered Lattice

A similar process can be carried out for a body-centered lattice. For this lattice the translations are composed of vectors of the form $\pm\frac{1}{2}\pm\frac{1}{2}\pm\frac{1}{2}$ with corresponding reciprocal vectors $0\pm1\pm1$. The cell is a truncated octahedron and the midpoints of the faces between nearest neighbors are at $\pm\frac{1}{4}\pm\frac{1}{4}\pm\frac{1}{4}$. From these we find $r_0=3\sqrt{3}/4$, in terms of which σ, π, etc., are found by equation 8. Taking the 100 direction for test purposes, we classify our wave functions according to the symmetry C_{4v} of this direction. There are five classifications:[8] Γ_1, single functions unaltered by the symmetry operations; Γ_2, single functions which change sign when rotated 90° or when reflected in the 011 or $01\bar{1}$ planes; Γ_3, single functions which change sign when rotated 90° or reflected in the 010 or 001 planes; Γ_4, single functions which change sign when reflected in either 010, 001, 011, or $01\bar{1}$ planes; Γ_4, pairs of functions which transform as do $e^{i\varphi}$ and $e^{-i\varphi}$. With this classification and with $k=u00$ the energy curves of Fig. 2 and Table III were constructed. All energies less than 150 units are included.

Not all of the symmetry types are represented in the cellular solutions[2] (Table IV). We see that Γ_2, which gives several energy contours below 150 units, is not represented in the cellular method. Due to the complexity of the curves the symmetry types are compared on separate diagrams.

The curves for the 111 direction of the face-centered lattice and the 100 direction of the body-centered lattice are quite typical. For other directions the agreement is similar on the whole. Being worse in some respects, better in others.

IV. Reason for the Discrepancies

The reason for the good agreement in the first zone and poor agreement in the higher zones is easily understood by considering the expansion of a plane wave in spherical harmonics. This expansion involves zonal harmonics of all orders; however, if we are interested in the expansion within only a fraction of a wave-length about a certain point only the first few terms are large. This is the situation met with in the first zone for which the radius of the cell corresponds to less than $\frac{1}{4}$ wave-length, and the first three or four harmonics give a good expansion. However, the number of terms needed increases rapidly when the region of expansion is doubled—center of the second zone—and not enough harmonics are present in the cellular formulation. Hence the agreement becomes bad.

V. Application of the Results

It is natural to apply these results to calculations previously made with the cellular method with a view to estimating the error arising there. In order to do this it is necessary to compare lattices of the same size. From considerations of

[8] Reference 7, Table II.

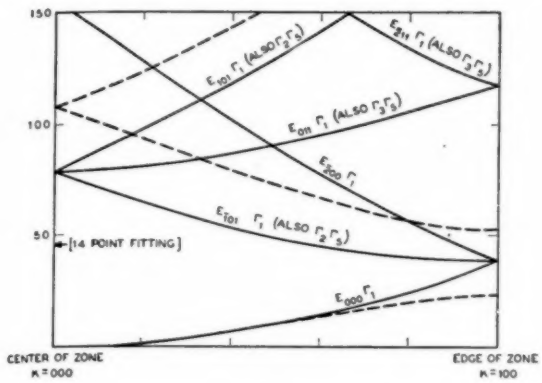

(a)

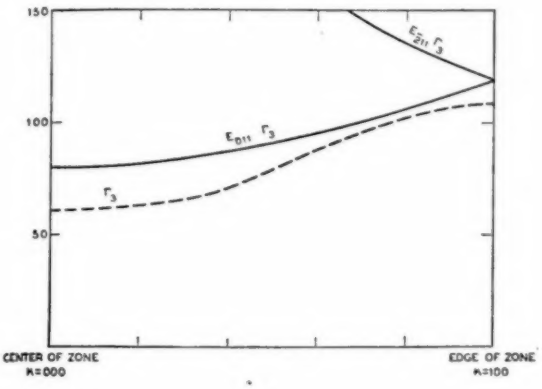

(b)

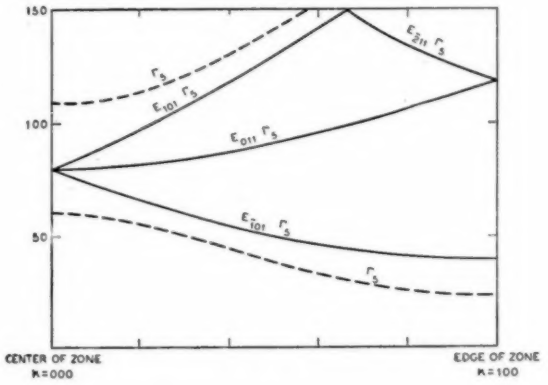

(c)

FIG. 2. Comparison of cellular and exact solutions for the body-centered lattice 100 direction. (a), Γ_1 type cellular solution, dashed line. All exact solutions, solid lines, with energies less than 150 units are shown. An energy curve will originate at point marked "14 point fitting" if continuity conditions are introduced on cubic faces. (b), Γ_3 type. Cellular solutions, dashed line, exact, solid line. (c), Γ_5 type. Cellular solution, dashed line; exact, solid line.

Eqs. (8) and (10) it is readily apparent that with a lattice constant of "a" rather than unity, the shape of the curves in figures will be unaltered but the energy scale will be modified by a factor $1/a^2$. It is, however, more convenient to reduce the results for the actual lattice to those of the unit lattice by multiplying by a^2.

A diagram indicating the error of the cellular approximation was constructed as follows: For various different computed values of the energy, the corresponding correct energies were found; of these the two lying farthest above and below the computed energy and the two lying nearest the computed energy were chosen. These values were taken as liberal and conservative estimates of the error in the method, errors greater than those of the liberal curve or less than those of the conservative curve being regarded as unlikely.

The results of the above analysis are shown in Fig. 3. The energy distribution for some of the crystals for which calculations have been made are also shown reduced to the same scale. Energy values normally occupied are shaded, and in two cases energy gaps between filled and empty bands are shown. It is seen that calculations for the alkali metals,[9] for which the first zone is only partly filled should have quite small

TABLE III. *Representations for the body-centered lattice with the wave functions classified according to the symmetry C_{4v} of the 100 direction. Energies less than 150 units are included.*

	Γ_1
$E_{000}(u)=4\pi^2u^2$	$\psi=\psi_{000}$
$E_{-200}(u)=4\pi^2(u-2)^2$	$\psi=\psi_{200}$
$E_{-101}(u)=4\pi^2[(u-1)^2+1]$	$\psi=\psi_{-101}+\psi_{-110}+\psi_{-10-1}+\psi_{-1-10}$
$E_{101}(u)=4\pi^2[(u+1)^2+1]$	$\psi=\psi_{101}+\psi_{110}+\psi_{10-1}+\psi_{1-10}$
$E_{011}(u)=4\pi^2(u^2+2)$	$\psi=\psi_{011}+\psi_{01-1}+\psi_{0-1-1}+\psi_{0-11}$
$E_{-211}(u)=4\pi^2[(u-2)^2+2]$	$\psi=\psi_{-211}+\psi_{-21-1}+\psi_{-2-1-1}+\psi_{-2-11}$
	Γ_2
$E_{-101}(u)=4\pi^2[(u-1)^2+1]$	$\psi=\psi_{-101}+\psi_{-10-1}-\psi_{-110}-\psi_{-1-10}$
$E_{101}(u)=4\pi^2[(u+1)^2+1]$	$\psi=\psi_{101}+\psi_{10-1}-\psi_{110}-\psi_{1-10}$
	Γ_3
$E_{011}(u)=4\pi^2(u^2+2)$	$\psi=\psi_{011}+\psi_{0-1-1}-\psi_{01-1}-\psi_{0-11}$
$E_{-211}(u)=4\pi^2[(u-2)^2+2]$	$\psi=\psi_{-211}+\psi_{-2-1-1}-\psi_{-21-1}-\psi_{-2-11}$
	Γ_4
has no representations for energies as low as those considered here.	
	Γ_5
$E_{-101}(u)=4\pi^2[(u-1)^2+1]$	$\psi=\psi_{-101}+i\psi_{-110}-\psi_{-10-1}-i\psi_{-1-10}$ and $\psi=\psi_{-101}-i\psi_{-110}-\psi_{-10-1}+i\psi_{-1-10}$
$E_{101}(u)=4\pi^2[(u+1)^2+1]$	$\psi=\psi_{101}+i\psi_{110}-\psi_{10-1}-i\psi_{1-10}$ and $\psi=\psi_{101}-i\psi_{110}-\psi_{10-1}+i\psi_{1-10}$
$E_{011}(u)=4\pi^2(u^2+2)$	$\psi=\psi_{011}+i\psi_{01-1}-\psi_{0-1-1}-i\psi_{0-11}$ and $\psi=\psi_{011}-i\psi_{01-1}-\psi_{0-1-1}+i\psi_{0-11}$
$E_{211}(u)=4\pi^2[(u-2)^2+2]$	$\psi=\psi_{211}+i\psi_{21-1}-\psi_{2-1-1}-i\psi_{2-11}$ and $\psi=\psi_{211}-i\psi_{21-1}-\psi_{2-1-1}+i\psi_{2-11}$

[9] Na: Reference 1 and 2. Li: F. Seitz, Phys. Rev. **47**, 400 (1935); J. Millman **47**, 286 (1935).

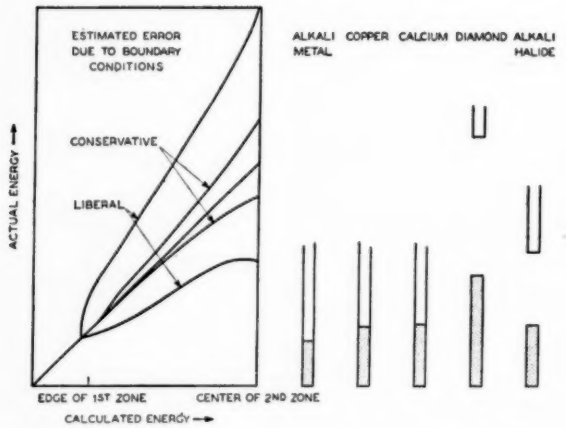

FIG. 3. Estimated error of the cellular method. For an energy calculated by the cellular method, the actual energy probably lies between the limits set by the liberal curves and outside those of the conservative curves. Computed energies for some solids reduced to the same scale are shown. Shaded regions represent occupied levels. Approximate band separations are shown for insulators.

errors due to the defects of the cellular method. For copper[6] and calcium[10] somewhat larger values are expected. For diamond[11] and the alkali halides[12] it is debatable whether the comparison should be made on a basis of lattice constant or spacing between neighboring atoms. From considerations of the number of expansion functions used per unit volume it appears more reasonable to use the lattice constant and the energy values are compared accordingly. We see that the band separations for both diamond and the alkali-halides are so large that we can feel certain of their independence from the particular approximations made. We see, however, that calculations of excited states, such as are needed in the theories of photoconductivity, optical absorption, and fluorescence, cannot well be accurate.

TABLE IV. *Symmetry types for the cellular solutions.*

Wave functions	Equation
Γ_1	
s, $(x/r)p$	$\tan^2 \pi u/2+\sigma/\pi=0$
Γ_3	
$(yz/r^2)d$, $(xyz/r^2)f$	$\tan^2 \pi u/2+\delta/\varphi=0$
Γ_5	
$(xy/r^2)d$, $(xz/r^2)d$, $(y/r)p$, $(z/r)p$	$\tan^2 \pi u/2+\delta/\pi=0$

[10] M. F. Manning and H. M. Krutter, Phys. Rev. **51**, 761 (1937).
[11] G. E. Kimball, J. Chem. Phys. **3**, 560 (1935); F. Hund, Physik. Zeits. **36**, 888 (1935).
[12] LiF: D. H. Ewing and F. Seitz, Phys. Rev. **50**, 760 (1936); NaCl: W. Shockley, Phys. Rev. **50**, 754 (1936).

It is interesting to compare the energy curves computed by Slater for Na with those of the empty lattice test. It is found that the two nearly coincide. From this we can deduce that exact solutions for Na will be very much like plane waves and that the energy discontinuities will be much smaller than those calculated. Slater has proposed a physical explanation for this phenomenon.[13] He points out that the wave function in a lattice may be regarded as a solution of a scattering problem, each ion in the lattice acting as a scatterer. The less the scattering power of the ion, the nearer the wave function will be to a plane wave. Now the Na+ion has the same electron configuration as neon, and it is well known that the rare gas atoms have abnormally small scattering cross sections for low velocity electrons—Ramsauer effect. Thus Slater concludes that the remarkably close approximation to plane waves of the Na wave functions can be regarded as the consequence of a Ramsauer effect in the crystal field.

In some cases, other information may indicate that the results of the cellular method are more accurate than indicated by Fig. 3. In Cu, for example, five d bands whose width is appreciably less than the entire occupied width are calculated. Since this is to be expected on the basis of the atomic energy levels, we can have more confidence in the structure of the d bands than if they came as unheralded results of the cellular method.

The energy scale of Fig. 3 should, of course, be compared in general with band widths rather than spacings between bands. Thus the energy scale of the x-ray levels would be enormous in the figure, however, the breadth of the levels would be extremely small. For this case then, where the Bloch method can be used with very satisfactory accuracy, we should expect the cellular method to give good results.

VI. CONCERNING IMPROVEMENTS IN THE CELLULAR METHOD

The cellular method of joining was originally proposed as a simplification of the problem of

[13] Comments by J. C. Slater at the Symposium on the Structure of Metallic Phases at Cornell University, July 1, 2, 3, 1937.

constructing continuous lattice functions. Rather than requiring the function and its derivatives to be continuous over the entire intercellular boundaries, continuity of value and normal derivative at the midpoint only were demanded. In the body-centered lattice, in fact, only the eight octahedral faces of the cell were considered, no conditions being placed upon the six cubic faces. It is thus natural to seek improvements by imposing further continuity requirements.

Work on the body-centered lattice including the six cubic faces in the joining scheme has been undertaken by Manning and Chodorow.[14] The six new conditions require the introduction of six additional surface harmonics. Elementary considerations indicate strongly that these should be the two d functions, $(x^2-y^2)/r^2$, $(y^2-z^2)/r^2$, the three f functions $(x^3-\frac{3}{5}xr^2)/r^3$, $(y^3-\frac{3}{5}yr^2)/r^2$, $(z^3-\frac{3}{5}zr^2)/r^3$ and the one cubically symmetrical g function. No detailed tests with these new functions have been carried out, however, the following considerations show that no great improvement will result from their use. For $\mathbf{k}=0$, we see that a triple solution is still obtained from old d functions which vanish on the cubic faces. The new d functions vanish on the octahedral faces and satisfy the boundary condition $\delta=0$ on the cubic faces. The function $2x^2-y^2-z^2$ gives the point marked "14 point fitting" on the Fig. 2a. The other y^2-z^2 gives a zero width band of type Γ_2, a missing type for the previous work. If calculations for other values of $\mathbf{k}$ were carried out these points would become energy curves; and the old curves, but not the end points for $\mathbf{k}=0$, would be changed. It is readily seen that the resultant curves could not approximate the exact solutions with much improved accuracy.

For the face-centered lattice it is more natural to seek improvement by requiring continuity conditions in tangential derivatives at the midpoints of the faces. This gives four conditions for each pair of midpoints:

Value

$$Tu_g-u_u=0. \tag{11}$$

Normal derivative

$$(\partial/\partial r)u_g+T(\partial/\partial r)u_u=0. \tag{12}$$

[14] M. F. Manning and M. Chodorow, Phys. Rev. **50**, 399A (1936).

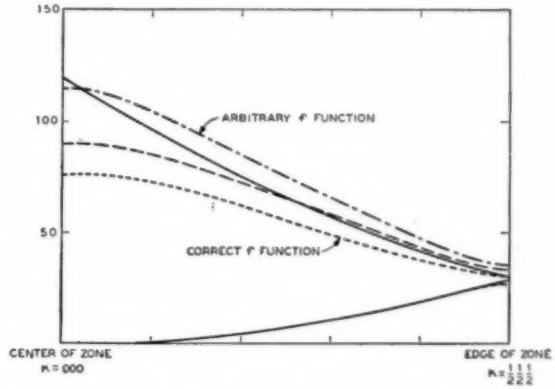

FIG. 4. Result of requiring continuity of tangential derivatives at midpoints of intercellular faces for the 111 direction of the face-centered lattice. Solid line, exact solution; dashed line, old cellular solution; dotted line, new cellular solution using zonal f function; dashed and dotted line, new cellular solution using arbitrary f function.

Tangential derivative

$$(\partial/\partial\theta)u_g+T(\partial/\partial\theta)u_u=0. \tag{13}$$

Tangential derivative

$$(\partial/\partial\varphi)u_g+T(\partial/\partial\varphi)u_u=0. \tag{14}$$

θ and φ are polar coordinates whose axes may be chosen according to convenience and $T=\tan 2\pi\mathbf{k}\cdot\mathbf{r}$ where $\mathbf{r}$ is the radius vector to the midpoint of the face. The functions and derivatives are evaluated at the midpoint.

For the 111 direction, it is convenient to let $\theta=0$ for 111 and $\varphi=0$ for 100. Due to the symmetry of 111, it is sufficient to satisfy the boundary conditions for any given symmetry type only upon 011 and $01\bar{1}$ that is $\cos\theta=(\frac{2}{3})^{\frac{1}{2}}$, $\varphi=\pi$ and $\theta=\pi/2$, $\varphi=\pi/2$. For Γ_1 which is the simplest symmetry type u_u, $\partial u_g/\partial\theta$, $\partial u_g/\partial\varphi$ and T vanish on $01\bar{1}$, so that all but the normal derivative conditions are fulfilled trivially. On 011 the derivatives in respect to φ vanish but those in respect to θ do not. Thus only one new condition arises. In order to satisfy it we must introduce one additional function of type Γ_1. There are two such f-functions: $(\cos^3\theta-3\cos\theta/5)f$ and $\sin^3\theta\cos 3\varphi f$. It is most natural to choose the first function since it is the one which occurs in the expansion of a plane wave in the 111 direction. It is readily verified that both functions have the same value for $(\partial\psi/\partial r)/\psi=\varphi$ at the joining point and values of $-21\times 2^{\frac{1}{2}}$ and $+3\times 2^{\frac{1}{2}}$ respectively for $\varphi'\equiv(\partial\psi/\partial\theta)/\psi$.

The determinantal equation for the continuity condition may be set up in the usual way and reduced to[15]

$$\tan^2 \pi u = -\frac{2\delta(1+1/2^{\frac{1}{2}}\varphi')+(\varphi-\pi)2\times 2^{\frac{1}{2}}/\varphi'}{(\pi+\varphi/2^{\frac{1}{2}}\varphi')(1+\delta/\sigma)}. \quad (15)$$

This is to be compared with the equation

$$\tan^2 \pi u = -2\delta/\pi(\delta/\sigma+1), \quad (16)$$

which is obtained in the absence of tangential boundary conditions. Due to smallness $1/\varphi'$, π/φ' and φ/φ' for energies in the first zone, the new expression is equivalent to the old. In the second zone, however, the results, shown in Fig. 4, using the first f function ($\varphi' = -21\times 2^{\frac{1}{2}}$) are actually worse than the old. From a suitable linear combination of the two f functions any desired value of φ' can be obtained. The arbitrarily chosen value 10.8 gives the curve which fits the correct parabola fairly well.

VII. Conclusions

The results of the cellular method of finding wave functions are probably quite good for the occupied states of the metals so far calculated. For excited states, however, very large errors are to be expected. This cannot be overcome by such simple expedients as adding a few more joining conditions to those already in effect. It appears that the number of new conditions necessary to take care of higher energies would make the labor of calculation prohibitively difficult. However, a new method of attack has been proposed by Slater and it is to be hoped that it will circumvent these difficulties.

Finally it should be remarked that this work has been concerned with only one aspect of the electronic theory of solids. Although accurate solutions of the wave equation in the crystal would be very valuable they suppose that each electron sees a static potential field in which the influence of the other electrons is represented by an average. Actually relative positions of the electrons, correlation effects, must be considered in order to explain many properties, for example the binding energy of the alkali metals[16] and the phenomenon of excitation in insulators.[17]

The writer would like to express his gratitude to Professor Slater, under whose direction work on this problem was commenced, and whose continued interest has been instrumental in its completion.

[15] The reader is referred to references 2, 5 and 6 for the general method of setting up the determinantal equations of the cellular method.

[16] E. Wigner, Phys. Rev. **46**, 1002 (1934).

[17] J. C. Slater and W. Shockley, Phys. Rev. **50**, 705 (1936).

OCTOBER 15, 1937 PHYSICAL REVIEW VOLUME 52

Theory of the Use of More Than Two Successive X-Ray Crystal Reflections to Obtain Increased Resolving Power

Jesse W. M. DuMond
California Institute of Technology, Pasadena, California

(Received April 23, 1937)

If an x-ray beam is selectively reflected from more than two crystal surfaces in succession it is shown in this paper by a simple method of graphical analysis that it should be possible to obtain resolving power considerably superior to the best obtainable with present two crystal x-ray spectrometers. This extension and generalization of the two crystal spectrometer principle in one of its forms (the three crystal spectrometer) should permit the study of the asymmetric diffraction patterns predicted by the theory of Prins but heretofore considered to be completely beyond experimental investigation. In another form (the four crystal spectrometer) a distinct improvement in spectral resolving power is anticipated. The new method of graphical analysis invented for the purpose of discussing these more complicated cases of polycrystalline x-ray reflection is conspicuously useful and clear as a help to understanding the two crystal spectrometer also. An experimental test of these new methods is now in progress.

Introduction

IT is generally believed that the high resolving power of the two crystal x-ray spectrometer permits of no substantial improvement by any extension of its principle of operation. The author here proposes to show by a simple analysis of the action of repeated successive x-ray crystal reflections occurring at or near the Bragg selective angle that this is not the case.

Let us distinguish two classes of x-ray problems and correspondingly two kinds of resolving power which latter we shall call *angular resolving power* on the one hand and *spectral resolving power* on the other hand. In the first class come studies of the diffraction patterns of crystals. Darwin,[1] Ewald,[2] Prins[3] and von Laue[4] have contributed to the theory of such diffraction patterns while on the experimental side the widths of "rocking" curves in the "parallel position" have been studied by Ehrenberg and Mark,[5] Bergen Davis and H. Purks,[6] Allison and Williams,[7] and many others.[8] Von Laue has shown[9] that the two crystal spectrometer in the parallel position is incapable of revealing any asymmetry in the single crystal diffraction pattern if such asymmetry exists as the theory of Prins predicts. One of the purposes of the present paper is to show that by an extension to the use of three successive crystal reflections the asymmetric diffraction patterns of Prins can be experimentally studied. In the second class of problems come refined studies of spectral line shapes and spectral distributions in general such for example as the shape of the foot of the continuous x-ray spectrum. Here spectral resolving power is the essential consideration. In the first class of problems we aim to study how the reflecting power of a crystal for an ideal monochromatic parallel beam varies with slight deviations of grazing angle near the Bragg angle. In the second class of problems we aim to study how the intensity associated with a given wave-length in a beam of x-rays varies with the wave-length.

With a single crystal spectrometer the finite natural breadths of x-ray lines prevents the study of most crystal diffraction patterns almost entirely while the finite size of the crystal diffraction pattern would even with extremely fine slits place a serious limitation on the accurate study of spectral line shapes. To some extent the invention of the two crystal spectrometer removes these limitations and permits a partial separation of the dependence of reflected intensity on the two variables θ and λ. We propose to show here how a generalized extension of the two successive crystal reflections can be made to yield an even more complete separation.

Graphic Method of Analysis

The author has found that purely analytic expositions of the physical optics of the two crystal spectrometer are so involved and difficult that an extension of the problem to the case of more than two successive reflections has led him to invent the following simplified graphic method of thinking. Unquestionably the exact solution of any given configuration of crystal reflections can still best be obtained by writing down the integrals involved but before this point is reached the graphic method here described has great heuristic value as a help in the *choice* of configuration to be analyzed and as an aid to intuitive prediction of the interesting or uninteresting character of the result. The author believes also that the exposition of the physical optics in the simpler case of the two crystal spectrometer is greatly simplified by the use of this graphic method. The reader is urged to familiarize himself with its use as a tool in his thinking without which the present paper will be unintelligible.

Figure 1 represents a plot of the Bragg equation

$$n\lambda = 2d \sin \theta \qquad (1)$$

the ordinates and abscissae being λ and θ, respectively. The individual curves correspond to the different orders n of reflection. Now the

[1] C. G. Darwin, Phil. Mag. **27**, 325, 675 (1914).
[2] P. P. Ewald, Ann. d. Physik **54**, 519, 577 (1917); Zeits. f. Physik **2**, 232 (1920); **30**, 1 (1929); Physik. Zeits. **26**, 29 (1925).
[3] J. A. Prins, Zeits. f. Physik **63**, 477 (1930).
[4] M. von Laue, *Ergebnisse der Exakten Naturwiss.* (Julius Springer, Berlin, 1931), Bd. X, pp. 137–158.
[5] Ehrenberg and Mark, Zeits. f. Physik **42**, 807, 823 (1927).
[6] Bergen Davis and H. Purks, Proc. Natl. Acad. Sci. **13**, 419 (1927).
[7] Allison and Williams, Phys. Rev. **35**, 1476 (1930).
[8] S. K. Allison, Phys. Rev. **41**, 1 (1932); L. G. Barratt, Phys. Rev. **41**, 561 (1932); Mark and Von Susich, Zeits. f. Physik. **65**, 253 (1930); Kirkpatrick and Ross, Phys. Rev. **43**, 586 (1933). No attempt is made at an exhaustive list of this literature which is very extensive.
[9] Von Laue, Zeits. f. Physik. **72**, 472 (1931).

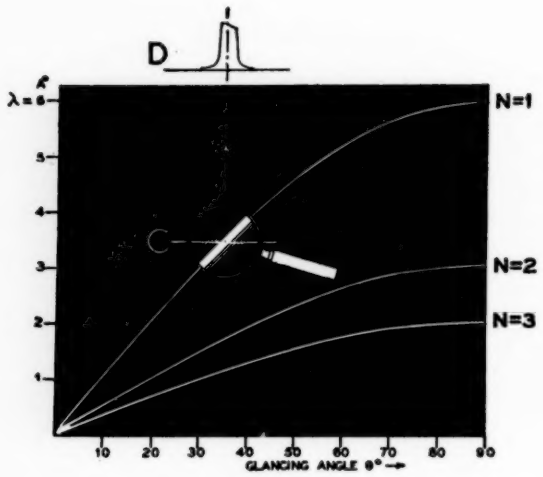

FIG. 1. Illustrating how the reflection properties of a crystal at various angles θ for various wave-lengths λ may be visualized as a function distributed over a plane cartesian coordinate system. The function will be nearly zero (black) save in regions close to the curved loci. As an aid to clarity we plot the regions of 100 percent reflection completely transparent and represent intermediate reflection coefficients with intermediate degrees of partial transparency. Such a graph we call a transparency graph. The striped effect seen in the magnifying glass is an effort to indicate the smooth gradation from almost complete transparency to opacity which cannot be otherwise indicated in a line drawing.

more refined *physical optics* of x-ray reflection teaches us that the connection between λ and θ is not quite rigid. For a given λ reflection at a crystal surface occurs over a small *range* of θ in the vicinity of the Bragg angle with varying degrees of intensity (diffraction pattern of the crystal) so that in a strict sense we must regard λ and θ as *independent variables*. The x-ray intensity reflected by the crystal is then to be thought of as a function of *both* λ and θ regarded as independent of each other. We must think now of a variable representing the intensity of reflection distributed all over the surface of the λ, θ plot of Fig. 1, but with values differing appreciably from zero only in the close vicinity of the lines on this plot. It will soon be apparent that the most helpful way to think of this intensity distribution over λ and θ is to represent it as a transparency. Regions of the plot where the reflecting power is unity are to be conceived as perfectly transparent while regions of zero reflecting power are opaque, with intermediate values grading between complete transparency and complete opacity. If then we examine a magnified cross section of one of the transparent traces along a line for which λ equals a constant as at C on our plot we would obtain the curve shown at D representing the transparency as a function of θ on this line. The shape of this curve is the diffraction pattern of the crystal for the wave-length and angle region indicated on the plot. We shall here make the assumption that a plot such as we have just described gives a *complete* description of the properties of a single crystal x-ray reflection.

This latter assumption is admittedly not rigorous. The author is well aware that more than two independent variables λ and θ are rigorously required to represent completely the intensity of reflection of a given crystal for a plane monochromatic beam of wave-length λ incident at angle θ_1 because the reflected beam may, in general, with reduced intensity, have a direction other than that required by geometrical optics so that a grazing angle θ_2 not necessarily equal to θ_1 and an azimuth ϕ measuring the departure of the plane of the angle of reflection from the plane of the angle of incidence are required. Thus strictly the intensity of reflection is a function of four independent variables, λ, θ_1, θ_2, and ϕ. In this paper however we are making the assumption that the one-to-one correspondences represented by the relations $\theta_1=\theta_2$ and $\phi=0$ are fulfilled so much more rigorously than is the one-to-one correspondence between λ and θ_1 represented by the Bragg Eq. (1) that the description in terms of λ and θ_1 alone is sufficient for our present purpose. All the conclusions of the present paper stand or fall according as this assumption is justified or unjustified. Of the two assumptions that of the one-to-one correspondence between θ_1 and θ_2 is by far the most important. There are good experimental reasons for hoping that this assumption is justified for good crystals of "perfect" type, chief among which is the extreme angular narrowness of the two crystal spectrometer rocking curves of good calcite in good accord with the theoretical predictions and their nearly triangular shape in cases where the single crystal diffraction pattern required by theory approximates a rectangle.

Case of Two Successive Reflections, Antiparallel Position

With this understanding then a transparency plot such as Fig. 1 gives a complete description of the intensity of a single crystal reflection for all possible values of λ and θ. Consider now for the same beam of x-rays two such reflections occurring successively at two crystal reflecting surfaces. There will exist two similar plots like Fig. 1 for these two reflections. (We shall discuss here only the case where all crystals have identical transparency graphs though this graphical method handles the case of crystals having *different* graphs with equal ease.) Referring to Fig. 2 the two successive crystal reflections are denoted by A and B. It is evident that with the crystals stationary in the antiparallel position here shown an *increase* of the angle θ_A corresponds to a *decrease* in the angle θ_B *of equal magnitude*. If the dihedral angle is ω between the faces of the two crystals then when $\theta_A=0$; $\theta_B=\omega$ and when $\theta_B=0$; $\theta_A=\omega$. Also the final intensity after two reflections is the product of the intensity of reflection at each one. With the two crystals at a fixed angle ω the bicrystalline reflection still involves only two variables λ and either θ_A or $\theta_B=\omega-\theta_A$. The entire situation can thus be represented by superposing the two transparency graphs with their θ coordinates mutually reversed and displaced so that where $\theta_A=0$; $\theta_B=\omega$ and where $\theta_B=0$, $\theta_A=\omega$. It is evident that with such a reversed superposition the two graphs together will be everywhere opaque save in the small quasi-quadrilateral regions where the transparent traces on the individual graphs mutually intersect. An attempt to illustrate this situation in these pages would result in a black rectangle with a few small, symmetrically disposed, isolated, white patches

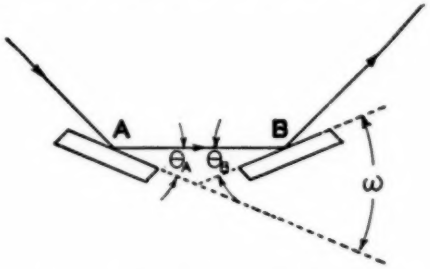

Fig. 2. Geometrical relationships in the two crystal spectrometer, antiparallel position.

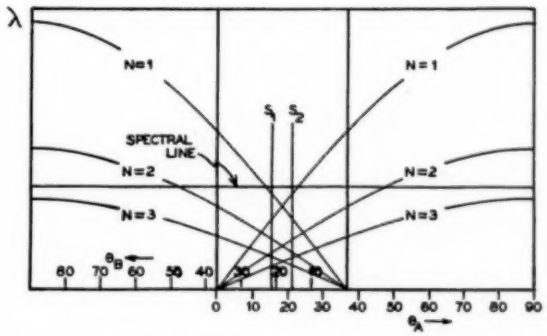

Fig. 3. Action of the two crystal spectrometer in the antiparallel position analyzed by the method of transparency graphs. The two systems of traces here shown in black lines must be imagined as if on two separate sheets of paper with the lines transparent and the background opaque so that light can only penetrate at the intersections of the transparent traces. A spectral line is represented as a horizontal line source of light immediately behind the charts at a height corresponding to its wavelength. Rocking the crystals corresponds to sliding one sheet over the other horizontally so that the "window" formed by an intersection moves vertically and explores the shape of the spectral line.

dotted about on its surface, so the reader is requested to accept, instead, the graph of Fig. 3 in which the entire set of traces on each of the two reversed superposed graphs appears as black lines. The reader should however mentally substitute for this figure the picture of the two reversed superposed transparency plots in which light can only be transmitted through the intersections of the transparent traces. It may be even helpful for the reader to construct two or more such plots and actually superpose them. It will then be apparent how the transparent intersections move up and down along the wavelength scale when the upper plot slides horizontally over the lower plot corresponding to variation of ω the dihedral angle between the crystals. This illustrates the action of the two crystal spectrometer when exploring a spectrum in the antiparallel position. A spectral line can be thought of as a uniform horizontal line source of light directly behind the two superposed graphs at a height on their vertical wave-length scale corresponding to the wave-length of the spectral line to be represented. Sliding one graph over the other then causes the small transparent intersection or window to travel vertically over the spectral line and by plotting the total transmitted intensity as a function of the displacement of the transparency graphs the "shape" of the

line is explored (the more faithfully the more restricted the window). What we may call rather freely the *area* of each window formed by the intersection of two graphs of order (n, m) is a measure of the total x-ray intensity which can be transmitted through the bicrystalline reflection in the (n, m) order. This "area" is in fact a surface integral of the product of the two intensity functions on the two superposed graphs since the quasi-quadrilateral transparent region in general has no sharp boundaries but fades off gradually on the sides into complete opacity. That such an integral really measures the total intensity transmitted through the bicrystalline reflection can be seen from the fact that on the graph it consists of weighted elements of extension $d\lambda$ in the vertical direction and of extension $d\theta$ in the horizontal direction and these on the two crystal spectrometer are precisely the elements that determine the total intensity since the solid angle under which the source can send radiation into the ion chamber is proportional to $d\theta$ and the spectral range which can be used in the source is proportional to $d\lambda$.

It is usual in the two crystal spectrometer to introduce lead stops so disposed as to place rough limitations on the horizontal angles of incidence and reflection at the two crystal surfaces. The effect of these can roughly be introduced into our superposed graph concept by including in the discussion only that part of the graph between the two vertical lines, such as S_1 and S_2 Fig. 3 which limit θ_A and θ_B in a way roughly similar to the lead stops. Two or more intersection points in the same vertical line however are thus active *simultaneously* in spite of this stop limitation. This superposition of the (2, 2) order spectrum upon the (1, 1) order is a pitfall which is well known and can be avoided usually by appropriate choice either of filters or of the voltage used to excite the x-rays so as to suppress the unwanted order.

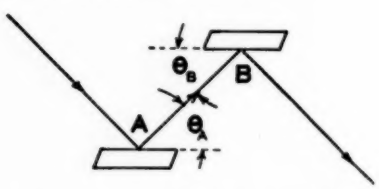

FIG. 4. Geometrical relationships in the two crystal spectrometer, parallel position.

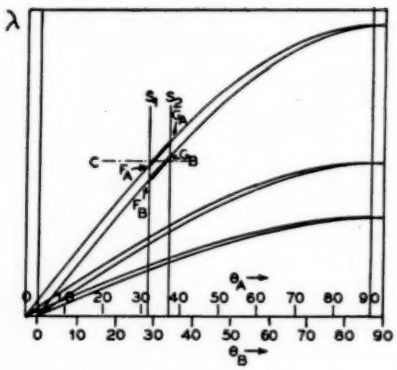

FIG. 5. Action of the two crystal spectrometer in the parallel position analyzed by the method of transparency graphs. The graphs are here shown mutually displaced from the position corresponding to complete parallelism so that they can be distinguished separately in a drawing.

Throughout the present paper the vertical divergence of the x-ray beam is supposed to be held constant and sufficiently small so that it need not be discussed.

CASE OF TWO SUCCESSIVE REFLECTIONS IN THE PARALLEL POSITION

In Fig. 4 two crystals are shown in the "parallel" position. It is evident here that with the crystals fixed at or near parallelism an increase of θ_A produces a corresponding equal increase in θ_B. It is therefore evident that we must superpose our transparency graphs with their θ scales increasing in the same sense (say from left to right). In Fig. 5 again we substitute a black line graph of the situation and request the reader either in imagination or in reality to construct the corresponding directly superposed transparency graphs. The use of lead stops and shields will again place a rough limitation on the angle θ indicated by the two vertical lines S_1 and S_2 so that only the narrow region on the plot between these limits will be under discussion. By the appropriate choice of voltage on the tube and the use of a target with strong emission lines whose wave-lengths are selectively reflected in the desired order (say the first) at angles included in the region between S_1 and S_2 the entire x-ray intensity can be restricted to one small region of say the first order branch of the transparent loci, such as the regions F_A, G_A and F_B, G_B in Fig. 5. Now if we slide the two transparency graphs horizontally until the arcs F_A, G_A and

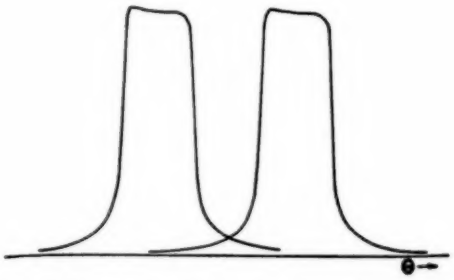

FIG. 6. Enlarged profile of the intensity of reflection taken along the horizontal line C in Fig. 5. where it cuts the two arcs F_AG_A and F_BG_B.

F_B, G_B coincide identically a maximum intensity can pass through the elongated window formed by the complete superposition of these transparent traces. All spectral lines and all of the continuous spectrum falling in the region traversed by the arc F, G can shine through the window whose "area" is seen to be far greater than the small quadrilateral areas of windows formed by intersections in the antiparallel position (Fig. 3).

Let us take a horizontal section as at C Fig. 5, and plot the transparency across each of the traces at this section. Fig. 6 shows these two cross sections or diffraction maxima from the two traces, the shape illustrated being the prediction of the theory of Prins for Mo K-radiation reflected in the first order on the cleavage planes of calcite.[10] Over the small range F, G, a horizontal cross section through the traces taken at any point whatever will have substantially the same shape as that shown in Fig. 6 since the shape of the diffraction pattern does not in general vary rapidly with wavelength. Therefore when the transparent graphs of Fig. 5 are displaced horizontally so that these graphs pass through complete coincidence (exact parallelism of the crystal reflecting planes) the behavior of the intensity transmitted through the graph as a function of the displacement can be readily inferred by displacing the profiles of Fig. 6 across each other and plotting the product integral over the two overlapping curves as a function of their displacement as indicated in the successive positions A, B, C, D and E, Fig. 7. The curve so obtained is the familiar rocking curve in the parallel position of the two crystal spectrometer and it is immediately apparent why, even with asymmetric single crystal diffraction profiles, the rocking curves are necessarily symmetrical since the paired configurations on either side of the coincidence point C are identical.

[10] The profile here shown is taken from Compton and Allison's book *X-Rays in Theory and Experiment*, page 386.

THE PRINCIPLE OF SHARPENING BY SLIGHTLY DISPLACED SUPERPOSITION OF DIFFRACTION PATTERNS

Suppose now that the transparency graphs of Fig. 5 are only *slightly* displaced away from the position of exact coincidence so that a horizontal cross section of the two transparency graphs looks like the case B or D of Fig. 7. The super-

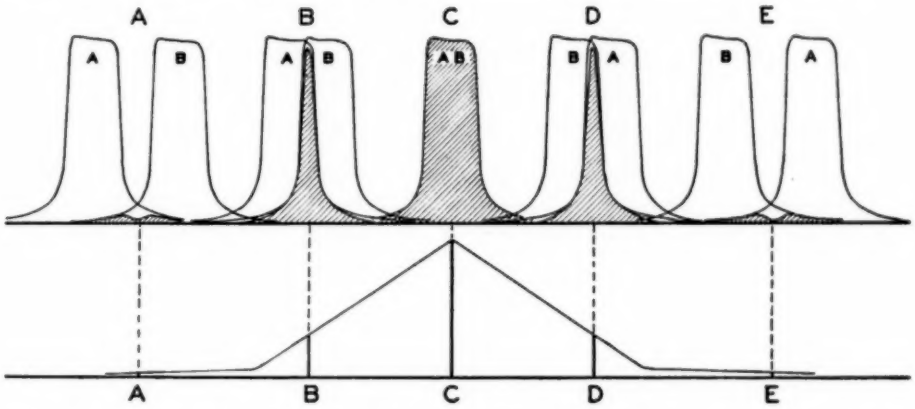

FIG. 7. Illustrating the variation of reflected intensity with various degrees of overlapping of the diffraction patterns of crystals A and B as the crystals are rocked through the parallel position. The values of the product integrals plotted as ordinates in the lower curve correspond to the total superposed transparency "area" available with different degrees of overlapping of the transparent traces F_AG_A and F_BG_B as the graphs of Fig. 5 slide over each other.

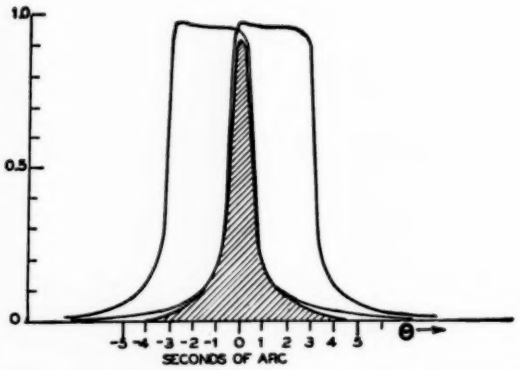

FIG. 8. The principle of "sharpening" by appropriate displaced superposition of diffraction patterns. The shaded profile is the product of multiplying the ordinates point by point on the two unshaded curves.

position of these two transparent traces in this fixed position will yield a composite trace whose horizontal profile we obtain by constructing the point by point *product* of the ordinates of the two slightly displaced curves to yield the heavy shaded profile shown in Fig. 8. If the displacement is judiciously chosen it is evident that this resultant product *will be a very much narrower curve* than either of the factors while retaining almost the original maximum height because the maximum heights of the Prins traces correspond nearly to unity. Thus under these conditions the beam of x-rays after two reflections, though it is neither monochromatic nor unidirectional *possesses a much sharper relationship between direction and wave-length* than did the beam after only one crystal reflection. *It may thus be regarded as a sharpened tool with which to explore the diffraction pattern of a third crystal.* This leads to the application of our transparency charts to the theory of the three crystal spectrometer for the study of the asymmetric diffraction patterns of Prins which up to the present have been thought to be undetectable.

Bollman and Bailey have found experimentally with three calcite crystals reflecting Mo K-radiation on their cleavage planes and have subsequently verified by graphical integration with the theoretical diffraction patterns of Prins that the simple application of the principle of displaced superposition of diffraction patterns is not enough to give a "tool" adequate satisfactorily to reveal the Prins diffraction pattern of a third crystal. When the core of the com-

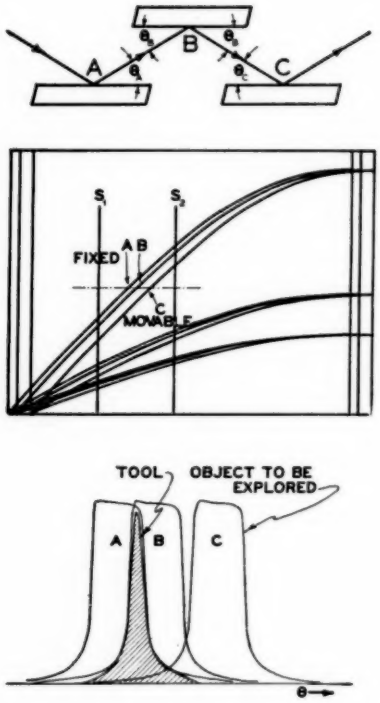

FIG. 9. Geometry of the three crystal spectrometer (parallel case), its triple transparency graph and the profiles of tool and object to be explored.

posite diffraction pattern of the two crystals constituting the tool has been narrowed down by displaced superposition the importance of the side fillets or wings is relatively so much increased as to necessitate a special procedure to remove their distorting effect. The details will be given in a paper describing the experimental results.

THE THREE CRYSTAL SPECTROMETER

Figure 9 shows the disposition of x-ray beams and crystals A, B, C to form the three crystal spectrometer. With these crystals in fixed relation to each other and with their reflecting planes very nearly in mutual parallelism it is evident that increasing the angle θ_A *increases* the angles θ_B and θ_C by exactly the same amount. Hence the transparency graphs for the three reflections must be superposed with their scales of θ all increasing in the same sense (say from left to right). If we displace crystal B say three seconds of arc away from strict parallelism with crystal A then transparency graphs A and B will be displaced from exact coincidence in such a way that the transparent trace formed by the super-

position of the two graphs will be much narrower than before. Crystals A and B are thenceforth held in fixed relation to each other and the beam which has been successively reflected from both of them now has the sharpened relationship between wave-length and direction represented by the narrower trace on the transparency graph. With this beam falling on the reflecting face of crystal C the latter is now rocked through a small angular range and the intensity after three reflections is plotted as a function of this rocking angle, a sufficient range being covered to completely explore the resultant pattern. This is equivalent to sliding the graph C over the fixed displaced pair of graphs A and B and because of the narrowness of the composite trace formed by A and B it becomes a sufficiently sharp tool to reveal with considerable fidelity the features of the horizontal profile of the trace on graph C. In this process reflections A and B furnish what may be described as the exploring tool while reflection C is the object studied. But it is immediately evident from the concept of the transparency graphs that *any* pair out of the three crystals may serve as the tool by giving this pair the appropriate displacement from parallelism and fixing its members in this displaced position while the third crystal is rocked and the intensity of the tricrystalline reflection is plotted as a function of this rocking angle. The pair of reflections constituting the "tool" need not be an adjacent pair since the total intensity depends simply on the product of the intensities of reflection on the three graphs and therefore obeys the commutative law of multiplication. Thus the three crystal spectrometer affords a ready method of studying the diffraction patterns *of all three* crystals separately with equal ease. True, the results are only *first approximations* to the true diffraction pattern since the sharpened tool in each case cannot be infinitely sharp and in practice will probably never be less than say one-tenth the width of the diffraction patterns themselves. However there is this immense advantage in getting these first approximations to the diffraction pattern shapes of all three crystals, namely that the approximate profiles of any pair used as a tool can now be applied to determine (by multiplying them together) the approximate shape of that tool. The approximate profile of the third crystal can then be *corrected* (by the solution of an integral equation) since the shape of the tool with which it was explored is known. This method would give a second approximation to the profile of each crystal and this can of course be obtained for all three profiles. It is easy to see therefore how by an iteration method it would be at least conceptually possible to get, through repeated approximations, an accurate, completely resolved profile for all three crystals. We are not yet in a position to say how practical such a scheme might turn out to be. The solution of integral equations with data of limited accuracy is frequently disappointing, but the conceptual possibility of an iteration process in the three crystal case is worth mentioning since it is quite impossible in the two crystal case.

It need scarcely be added that the rocking profile, obtained by rocking any one of the three crystals such as C with the other two crystals A and B in fixed slightly displaced nearly parallel relationship, should be studied for several degrees of displacement of the tool pair AB. If any asymmetry in the rocking profile appears then that displacement of AB which yields most

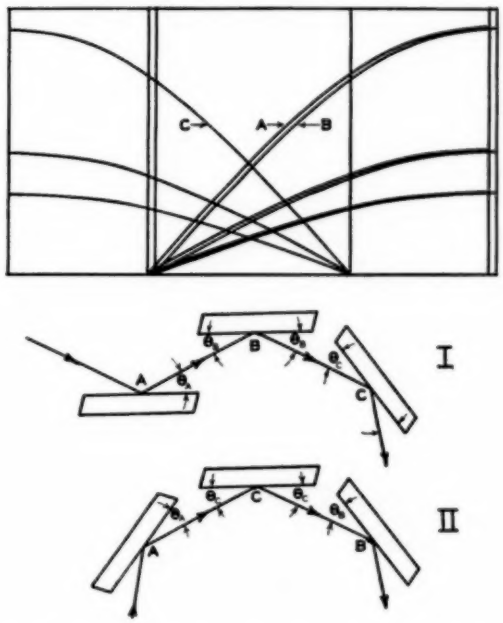

FIG. 10. Analysis of the other formal possibility in the three crystal spectrometer in which one of the transparency graphs is reversed with respect to the other two. Either of the geometrical dispositions of crystals and x-ray beams shown here falls in this class.

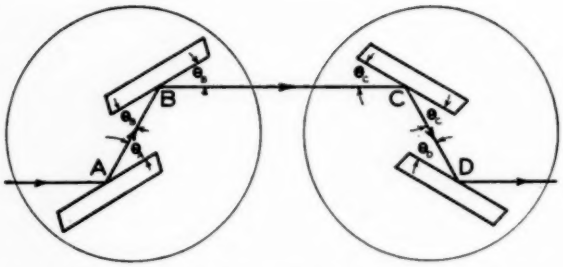

FIG. 11. The most interesting of several possible dispositions of crystals and reflections in the four crystal spectrometer.

pronounced asymmetry seems likely to be the most favorable one for use as a tool.

So much for the three crystal spectrometer with all three reflecting surfaces mutually parallel so as to call for transparency graphs with angle scales all increasing in the same sense. Much less interest attaches to any other possible three crystal configuration. Indeed the properties of the only other arrangement of three crystals which can be regarded as truly distinct from the foregoing one are obviously obtained by reversing the sense of the angle scale of one of the transparency graphs. This leads to a situation like the one shown in Fig. 10 for which the author can see no especially interesting application at present.[11]

Thus the three crystal spectrometer gives an improvement over the two crystal spectrometer in angular resolving power offering the possibility of studying the asymmetric diffraction patterns predicted by Prins but no great improvement in *spectral* resolving power can be expected from it. New and interesting possibilities however enter when we pass to the case of *four* successive crystal reflections.

[11] The equivalent configurations of crystals and beams I or II in Fig. 10 *do* offer the possibility of increasing the *wave-length resolving power* to a small extent over the best attainable in the two crystal spectrometer. Consider the case where all three crystals are used in the same order. Referring to the transparency graph of Fig. 10 it is easy to see that the vertical extension of the window formed by the intersection of the two partially overlapping traces A and B with the third trace C *can never be made less than half the vertical extension for two intersecting traces* no matter how thin the composite trace AB is made by the judicious choice of the displacement of its components. This limitation is however removed in the four crystal arrangement which we are about to discuss. It is possible that for special cases even this slightly increased wave-length resolving power which the three crystal arrangements of Fig. 10 afford coupled with the greater economy of x-ray intensity available with three reflections as compared to four may make this configuration of some utility.

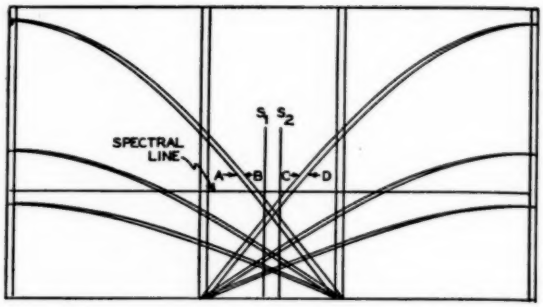

FIG. 12. Transparency graph for the four crystal case of Fig. 11.

THE FOUR CRYSTAL SPECTROMETER

Figure 11 shows the most interesting of several possible dispositions of crystals and reflections with four crystals A, B, C, and D. With all four crystals in fixed relationship it is apparent that increasing θ_A increases θ_B but decreases θ_C and θ_D. Hence the transparency graphs are to be superposed with one pair A, B having the angle scales of its members increasing in one sense while the remaining pair C, D has the angle scales of its members increasing in the opposite sense. Each pair, by the method of slightly displaced superposition already described, now can be made to constitute a sharpened tool. The members of each pair are therefore to be held in rigid mutual geometrical relationship but the pairs are rocked as a whole, the one with respect to the other, so that a spectrum can be explored. The result is easily understood in terms of the transparency graphs. The black lines of Fig. 12 are as before substituted for the transparent traces, the pairs of traces whose

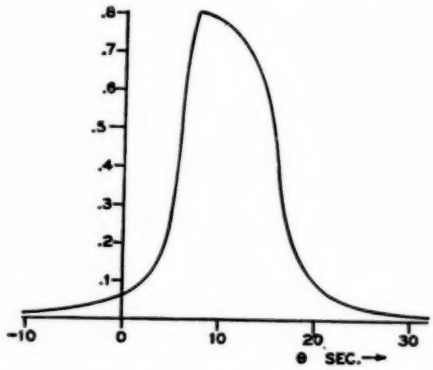

FIG. 13. Profile of the diffraction pattern of 2.3A x-rays, unpolarized, reflected from a calcite cleavage face as predicted by Prins theory. Taken from Compton and Allison *X-Rays in Theory and Experiment.*

members lie closely adjacent representing respectively the parallel pairs A, B, and C, D. The reader will understand of course that although the members of a pair of adjacent traces are shown in Fig. 12 as distinctly separated he is to think of them as superposed in the manner already described with only a very slight displacement of such amount that the total effect of this displaced pair is to give a much narrower transparent trace than either member alone would give.

The four crystal spectrometer is then in effect a two crystal spectrometer with pairs substituted for each of the two single crystals so that the result is the same as though two crystals with very much narrower diffraction patterns had been used. On the transparency graphs the narrow traces formed by the displaced pairs cross to form windows of much smaller dimension in the vertical (or wave-length) direction with a consequent increase of spectral resolving power.

The reduction in the size of the quadrilateral shaped window at the fourfold intersection on the transparency graph means a serious reduction in available x-ray intensity. It is unfortunate, but apparently unavoidable, that an n fold increase in resolving power by this method results in diminishing the available intensity through multiplication by a factor n^{-2}: An increase in resolving power is thus paid for rather dearly.

The Principle of "Sharpening" by Repeated Undisplaced Superposition of Diffraction Patterns

So far we have described only one method of sharpening or narrowing the traces on the transparency graph, that of displaced superposition of two traces. Now this method is most appropriate the nearer the horizontal profile section of a single trace approximates *a rectangular shape*. For traces like those in Fig. 6 which depart insignificantly from being rectangular by some asymmetry at the top and a little transition "fillet" on either side it is evident that a strong sharpening effect can be obtained by displaced superposition. On the other hand if the trace profile more nearly resembles the curve commonly known as the "witch," $y=(1+x^2/a^2)^{-1}$ the author has verified mathematically that no help can be expected from the use of displaced superposition of such profiles. In point of fact the Prins theory predicts that the trace profiles do indeed become more and more witch-like for longer wave-lengths, Fig. 13 being an example for the case of 2.3A units reflected from a cleavage face of calcite. When two equal witches with half-breadths, a (at half-maximum height), are superposed with increasing mutual displacement 2δ it turns out that when $\delta=a$ the product or resultant of the two curves just begins to manifest a double peak and is therefore thenceforth an undesirable exploring "tool" for most purposes. Restricting ourselves therefore to displacements $|\delta|<|a|$ it is easy to show that the resultant curve is always broader at half of its maximum height than is either one of the component curves at half of its maximum height. We must then in the case of such profiles fall back on another and perhaps somewhat less promising method of sharpening the trace. This consists in superposing, *in exact coincidence*, a number of similar witch-like profiles. The resultant curve will be narrowed simply because the wings of the curve have numerical values considerably less than unity for the intensity of reflection so that the product of multiplying many such factors will be relatively more strongly suppressed than will be regions of the

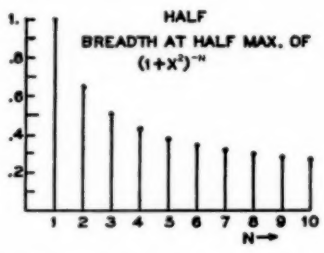

FIG. 14. Showing how raising the "witch" equation to higher and higher powers, n, progressively decreases the half-breadth at half-maximum height of the resultant curve.

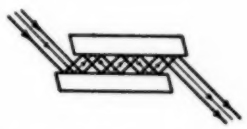

FIG. 15. A simple method of applying experimentally the principle of undisplaced superposition for sharpening the traces on the transparency graph.

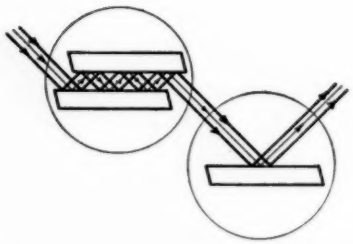

FIG. 16. Method of applying the principle of sharpening by undisplaced superposition to increase the angular resolving power in the three crystal spectrometer.

curve near the maximum where the values are more nearly unity. Fig. 14 is a graph showing how the half-breadth, a_n of a witch at half-maximum height diminishes as we raise the analytical expression for the curve to higher and higher powers, n. The process is one which yields rapidly diminishing returns in x-ray intensity because even the maximum of such witch-like profiles is not unity and the area under the profile therefore diminishes more rapidly than the breadth. Fig. 15 shows a simple way of realizing such a sharpening by repeated undisplaced superposition of the transparency traces. The crystals A and B must be of high quality absolutely free from mechanical strain so that the crystal planes will approach being mutually parallel over their entire reflecting surfaces to the highest degree. One plans beforehand how many successive reflections are desirable and knowing the Bragg angle to be investigated the appropriate separation between the reflecting faces can be computed to give this number of reflections. The transparency graphs for all these reflections evidently have their θ scales in the same sense. The state of parallelism of the two crystals can be determined of course directly by plotting the intensity of the x-ray beam after the n parallel reflections as a function of the rocking position of one of them with respect to the other. It is scarcely necessary to point out that this principle of sharpening can be applied to the three crystal combination for the study of diffraction patterns or to the four crystal arrangement for improving spectral resolution. Figs. 16 and 17 show the disposition of crystals and x-ray beams appropriate to these two applications.

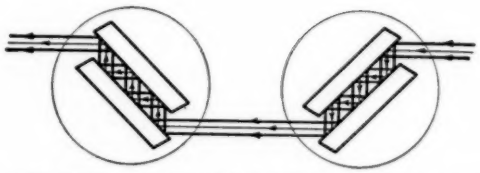

FIG. 17. Method of applying the principle of sharpening by undisplaced superposition to increase the spectral resolving power in the four crystal spectrometer.

NOMENCLATURE

It is regrettable that the choice of notations of Allison and Williams for the two crystal spectrometer does not stand the test of generalization to more than two successive reflections. If these authors had chosen the convention of algebraic signs so that, for example, working in the first order on both crystals in the anti-parallel position was denoted $\{1, -1\}$ instead of $(1, 1)$ (with $\{1, 1\}$ for the parallel position) then this notation could have been generalized very satisfactorily. It is clear that the prime requisites of a notation are: 1. that equivalent situations shall be denoted by equivalent symbols, and 2. that different situations shall be denoted by different symbols. Allison and Williams' notation only meets the second requirement. *It should be amply evident by now that the essential character of a given configuration of crystals and beams, both as to its properties for resolving wave-lengths and its angular resolution, turns uniquely on the type of trace intersection (or coincidence) required to represent that configuration on the transparency graph.* Hence a complete specification of the situation is given by stating the order number of each trace and assigning an algebraic sign to each order number representing whether the θ scale on the transparency graph for that particular trace increases from left to right or from right to left. Reversal of all signs in a given symbol in this notation leaves the situation unchanged so that the arbitrary convention of always writing the first-order number in the symbol positive can be retained. In this new convention the *sequence* in which the order numbers are written is immaterial for the complete description of the transparency graph. Thus the configurations I and II of Fig. 10 which for both angular and spectral resolution are entirely equivalent would in the new notation

be denoted $\{1, 1, -1\}$ and $\{1, -1, 1\}$, respectively. Their equivalence is thus immediately apparent in their symbols. To avoid confusion with the notation of Allison and Williams the author suggests the use of braces for the new notation.[12]

Other Possibilities

Some four years ago Paul Kirkpatrick suggested to the author the possibility of obtaining increased x-ray resolving power by the use of a number of similar crystals standing on an arc of a circle arranged in a succession like that indicated in Fig. 18, the crystals being so orientated that all the dihedral angles between any two adjacent crystals are equal. It was his idea to provide a mechanism so that this dihedral angle common to all adjacent pairs could be varied for all the crystals at once, their centers of rotation being simultaneously shifted so that the reflected beam would never leave the face of any crystal. In Fig. 18 two positions assumed by the arrangement as the angle is varied are shown.

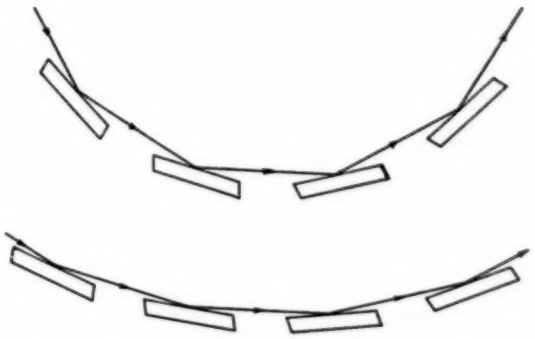

Fig. 18. Paul Kirkpatrick's suggested extension of the two crystal spectrometer.

Acknowledgments

At the time Kirkpatrick made this suggestion the author had not yet invented the convenient method of thinking about such problems with transparency graphs described in this paper. An analysis of Kirkpatrick's suggested arrangement by means of transparency graphs shows that for the case of three crystals it is identical to the case analyzed in our Fig. 10 and hence is without great interest. For the case of four crystals Kirkpatrick's arrangement is identical in its results to our four crystal arrangement pictured in Fig. 11 and analyzed in Fig. 12. It seems to the author to have the disadvantage of being mechanically somewhat more difficult to realize than the solutions here proposed but the author feels deeply indebted to Professor P. Kirkpatrick nevertheless because this suggestion of his involving the use of more than two successive crystal reflections started the entire train of thought which has led the author to the analysis and conclusions of the present paper.

At the present writing work is well advanced by V. L. Bollman and the author in preparation for an experimental test of the three crystal arrangement of Fig. 9 studying the diffraction pattern of calcite.

[12] To avoid all confusion we state below the rules for determining algebraic signs in Allison's notation and in our new proposed notation and a rule for transforming either notation into the other.

In Allison's notation the order number of the first reflection is always given the positive sign. As we proceed along the beam in the direction of propagation each succeeding reflection is called positive or negative according as the reflecting crystal is on the same side or the opposite side of the beam as is the first reflecting crystal.

In the new proposed notation the order number of the first reflection is always positive. As we proceed along the beam in the direction of propagation each succeeding reflection takes a sign opposite to its immediate predecessor if the crystal is on the *same* side of the beam as was the crystal in the immediately preceding reflection; or if the crystal is on the opposite side of the beam to its immediate predecessor its reflection takes the *same* sign as the immediately preceding reflection.

To transform either notation into the other reverse the signs of the second, fourth, sixth, etc. reflections and leave unchanged the signs of the first, third, fifth, etc. reflections.

LETTERS TO THE EDITOR

Prompt publication of brief reports of important discoveries in physics may be secured by addressing them to this department. Closing dates for this department are, for the first issue of the month, the eighteenth of the preceding month, for the second issue, the third of the month. Because of the late closing dates for the section no proof can be shown to authors. The Board of Editors does not hold itself responsible for the opinions expressed by the correspondents.

Communications should not in general exceed 600 words in length.

On the Generalization of the Notation for the Double Crystal X-Ray Spectrometer

In a paper elsewhere in this number of the *Physical Review* DuMond[1] has discussed the possible uses of an x-ray spectrometer in which successive reflections from more than two crystals are used. He has invented the device of "transparency graphs" which is of great assistance in the rapid estimate of the resolving power inherent in a postulated arrangement of the crystals. In endeavoring to devise a notation which will give unambiguously the relative positions of the crystals, and at the same time indicate some of the properties of the specified configuration, he reaches the conclusion that a straightforward generalization of the notation of Allison and Williams[2] is unsatisfactory. It is the purpose of this letter to discuss this conclusion, and to show that a generalization of the notation of Allison and Williams will give information about the possibilities of a configuration which may well be as important to the investigator as that which DuMond conveys in his revised notation.

The notation of Allison and Williams was invented for the double spectrometer, and was based upon the following formula, which arises naturally from the geometry of the instrument:

$$D \equiv d\beta/d\lambda = (n_A/2d\cos\theta_A) \pm (n_B/2d\cos\theta_B). \qquad (1)$$

In this formula, D is the dispersion of the instrument, expressed in terms of the angle $d\beta$ through which crystal B must be rotated to diffract a wave-length differing from that diffracted at a previous position by $d\lambda$. In describing the position of the instrument as (n_A, n_B), with the well-known[3] convention for the sign of n_B, we can deduce from the notation, in addition to an unambiguous description of the configuration of the crystals, the following information:

(1) The magnitude of the algebraic sum (n_A+n_B) gives approximately the dispersion of the instrument with respect to that of a single crystal spectrometer in the first order. (The approximation consists in setting $\cos\theta_A = \cos\theta_B = 1$.) Thus in the position Mo $K\alpha$ (1, 2) the angular separation of the alpha-doublet on the scale of the second crystal is approximately three times that on the scale of a single crystal instrument.

(2) The sign of the algebraic sum (n_A+n_B) gives the direction of rotation of crystal B with respect to crystal A. Thus, although the dispersion in the position Mo $K\alpha$ (1, −4) is approximately the same as that of the previous example, crystal B must be rotated in a sense opposite to that of A in passing from shorter to longer wave-lengths.

Let us now consider the extension to more than two crystals, where the general symbol is $(n_A, n_B, n_C \cdots)$. The Allison-Williams notation is suited to give the answer to the following question: given a configuration in which the spectrometer is set to diffract the wave-length λ, what rotation of crystals B, $C \cdots$ about their axes will set the spectrometer for wave-length $\lambda+d\lambda$? (It is assumed that the slits are wide enough so that A need not be turned.) Let $d\beta_B$, $d\beta_C$, etc., be the necessary rotations, and let $d\theta$ be the necessary rotation of a single crystal in the first order. Then

$$\begin{aligned} d\beta_B &\doteq (n_A+n_B)d\theta, \\ d\beta_C &\doteq \{(n_A+n_B)+(n_B+n_C)\}d\theta, \\ d\beta_D &\doteq d\beta_C+(n_C+n_D)d\theta, \end{aligned} \qquad (2)$$

etc.

Thus in the special cases of Fig. 1 we can deduce the following information. In configuration 1-I, the necessary rotation of crystal C is $4d\theta$; in 1-III crystal C must be moved $-2d\theta$ to pick up $\lambda+d\lambda$, in the opposite sense to the rotation of crystal A. In 1-IV, the necessary rotations are: B, O; C, $-2d\theta$; D, $-2d\theta$. In the configuration of Fig. 1-II, all the sums are zero, we have zero dispersion and zero wave-length resolving power.

DuMond's objection to the extension of the Allison-Williams notation is that the configurations of Fig. 1-I and 1-III, which his transparency graphs show can be manipulated in such a manner as to have the same resolving power, are not represented by simple permutations of the symbols {1, −1, 1}. He points out that the configuration of Fig. 1-II should have a set of symbols which cannot be permuted into the set representing any of the other three-crystal configurations, since the properties of this con-

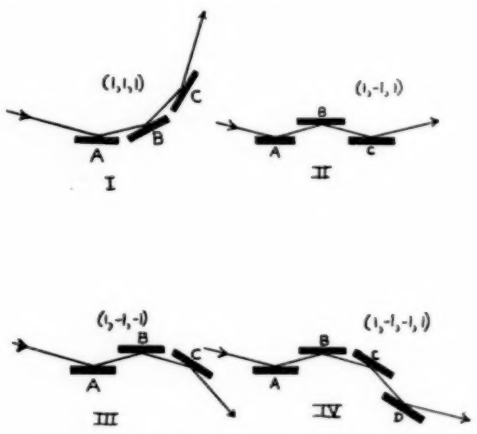

FIG. 1. Special cases of the multi-crystal spectrometer. The notation is a direct extension of the Allison-Williams notation for the double crystal spectrometer.

figuration are, in a sense, unique. The discussion presented here shows that an extension of the Allison-Williams notation, which conserves the relation with an extended dispersion formula similar to (1), gives the uniqueness of the configuration of Fig. 1-II by the property that it is the only three-crystal configuration for which the sums of Eq. (2) are all zero.

SAMUEL K. ALLISON

University of Chicago,
Chicago, Illinois,
June 4, 1937.

[1] J. W. DuMond, Phys. Rev. **52**, 872 (1937). The Editor of the Phys. Rev. kindly permitted me to read the manuscript.
[2] S. K. Allison and J. H. Williams, Phys. Rev. **35**, 149 (1930).
[3] Cf. A. H. Compton and S. K. Allison, *X-Rays in Theory and Experiment* (Van Nostrand, 1935), p. 718.

The Isotopic Constitution of Osmium

Aston[1] found osmium to consist of the isotopes 186, 187, 188, 189, 190 and 192. It is the purpose of this communication to show that in addition to the above isotopes an extremely rare isotope, Os^{184}, exists, present to about one part in 5700 in osmium.

A new high resolving, high intensity mass spectrometer especially designed for the detection of rare isotopes and the measurement of relative abundances was used in this investigation. A complete description of this new apparatus will appear in the November 1 *Physical Review*. For the time being it may be said that its operation is similar to that of the smaller apparatus previously described.[2] Positive ions are produced by the collision of electrons with the gas or vapor studied. The m/e analysis of the ions formed is accomplished by a 180° magnetic analyzer.

OsO_4 vapor was admitted to the apparatus through a capillary leak. $(OsO_4)^+$, $(OsO_3)^+$, $(OsO_2)^+$, $(OsO)^+$ and Os^+ ions were observed. Fig. 1 shows a typical mass spectrum obtained in the Os^+ region. In addition to the previously known isotopes may be seen the relatively weak peak in the 184 position. That this new peak really represents a new isotope may be concluded from the following:

(1) The peak corresponding to Os^{184} was observed not only in the Os^+ spectrum but also in the $(OsO_2)^+$, $(OsO_3)^+$ and $(OsO_4)^+$ spectra. In each case the relative abundance found agreed within the experimental errors. No study was made of the OsO^+ spectrum as $Os^{184}O^{16}$ would fall in the 200 position in coincidence with Hg^{200}, one of the strong isotopes of Hg. As very slight traces of Hg are sometimes found in the apparatus it was felt that the results here might not be reliable.

(2) The abundance ratio of Os^{186} to Os^{184} in the $(OsO_4)^+$ spectrum was studied over a threefold range of pressure,

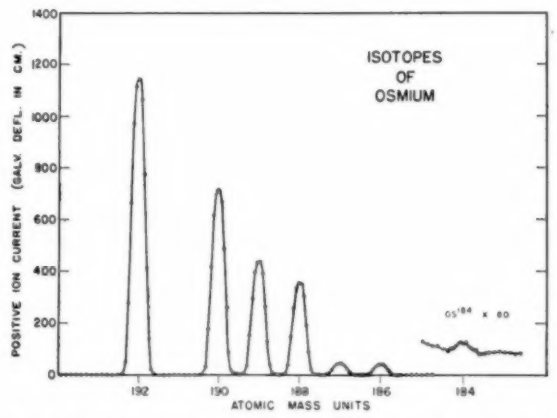

FIG. 1. Mass spectrum showing the isotopes of osmium. The region about Os^{184} is drawn to 80 times scale. Positive ion current is expressed in terms of centimeters deflection of galvanometer at its highest sensitivity. One centimeter represents about 2.5×10^{-15} amp.

TABLE I.

Mass number	192	190	189	188	187	186	184
Abundance	100	64.4	39.4	32.4	4.01	3.87	0.043
Aston's values	100	59.0	40.9	31.5	1.41	2.35	

and it was found to be constant within the limits of error. When the pressure was reduced by a large amount the rare peak completely disappeared in the background, as was to be expected if it was due to a rare isotope and not some residual impurity.

(3) Previous experience with the apparatus enables one to conclude that the peaks observed were not "ghosts."

Table I shows the isotopes along with their abundances relative to Os^{192}. Aston's values, converted from percentages, are included in the table for comparison. I believe that my abundances relative to Os^{192} are correct to one percent for Os^{190}, Os^{189} and Os^{188}. The values for Os^{187} and Os^{186} may be in error by three percent and the value for the new isotope Os^{184} may be correct to only 10 percent. When allowance is made for the packing fraction of -1 and the factor 1.000275 in going from the atomic to the chemical scale a chemical atomic weight of 190.21 is found for the above figures. Aston's values yield the weight 190.28. The present International Value, 191.5, lies outside of the errors possible in the mass-spectrographic method.

A search was made for other isotopes but none were detected. The following upper limits may be set for their existence relative to Os^{192}: Os^{194}, 1/10 000; Os^{193}, 1/6000; Os^{191}, 1/3700; Os^{185}, Os^{183} and Os^{182}, 1/14,000.

The present investigation definitely verifies the existence of the relatively rare isotope Os^{187}, which together with Re^{187} forms an isobaric pair of adjacent elements.

ALFRED O. NIER*

Harvard University,
Cambridge, Massachusetts,
September 28, 1937.

* National Research Fellow.
[1] Aston, *Mass Spectra and Isotopes*, p. 157.
[2] Nier, Phys. Rev. **50**, 1041 (1936).

Erratum: The Efficiency of Counters and Counter Circuits

On page 324 of the (Phys. Rev. **52**, 322 (1937)) above paper the sentence beginning in line 16 of the first column should be amended as follows:

"Thus the efficiency of the entire counting apparatus is given by Eq. (2), with τ_i in place of τ_r."

ARTHUR E. RUARK
FOREST E. BRAMMER

University of North Carolina,
Chapel Hill, North Carolina,
September 23, 1937.

On the Values of Fundamental Atomic Constants

In a Letter to the Editor of the *Physical Review*[1] R. T. Birge makes comments on my article "On the Values of Fundamental Atomic Constants."[2] Professor Birge states that the finally adopted values of that article do not satisfy the Bohr formula for the Rydberg constant, which has been used for the calculation of parts of the material upon which the values are based. Professor Birge inserts the values $e=(4.800\pm0.005)10^{-10}$ e.s.u. and $h=(6.610\pm0.015)10^{-27}$ erg·sec. in the formula and finds a value $e/m=1.766$ which value according to him is far outside my stated limits of error $(1.7585\pm0.002)10^{7}$ e.m.u./g. We must not forget, however, that limits of error were given for e and h as well, and that the value of e/m from the above-mentioned calculation ought to read 1.766 ± 0.010. This means that the Bohr formula is satisfied.

STEN VON FRIESEN

Research Institute for Physics,
Academy of Sciences,
Stockholm 50, Sweden,
September 20, 1937.

[1] R. T. Birge, Phys. Rev. **52**, 241 (1937).
[2] S. v. Friesen, Proc. Roy. Soc. **A160**, 424 (1937).

Comments on the Above Letter

If one admits the correctness of the Bohr formula for the Rydberg constant, then it appears to me quite illogical to advocate the adoption of a set of values of e, e/m and h that fails to satisfy that formula. This is the only point I desired to make in my earlier letter. Another possible formulation of the actual state of affairs is as follows. If one adopts $e=4.796\times10^{-10}$, which is close to von Friesen's *lower* limit of error for e, and $e/m=1.760\times10^{7}$, which is close to his *upper* limit of error for e/m, then the Bohr formula *requires* that $h=6.608\times10^{-27}$, which is close to von Friesen's adopted value of 6.610. This then is a possible, but on the basis of present facts, highly improbable set of values that *does* satisfy the Bohr formula.

R. T. BIRGE

Department of Physics,
University of California,
Berkeley, California,
September 29, 1937.

On a Letter of Wick's About Superconductivity

In a letter published in this journal G. C. Wick[1] has recently proposed an interpretation of the behavior of superconducting metals, which he fears to be "so natural that it might be considered as quite obvious." As, according to Wick, this interpretation seems to be supported by other physicists it might perhaps not be superfluous if I enumerate some points which seem to me far from being quite obvious.

1. Any statements about the dependence of free energy F upon magnetic induction B can, of course, never imply the phenomenon of conductivity. The magnetic field of the persistent currents, having a curl, requires the explicit introduction of the macroscopic current, at least if one wants to maintain Maxwell's theory.

2. If it be admitted that Wick's interpretation is incomplete, it can scarcely be seen how it could be completed with respect to the conductivity phenomenon, without encountering the notorious paradoxes which have up to now frustrated any interpretation of superconductivity as a limiting case of ordinary conductivity.

3. *A priori* the existence of two phases (the pure superconducting and the normal phase) and the appearance of the "transition" (mixed) state could be conditioned by a concave section of the free energy curve as proposed by Wick (and Peierls):

$$F=a+b|B|+cB^2+\cdots. \tag{1}$$

But if this were so, one should expect to find deviations from the "normal" value $F=\frac{1}{2}B^2$ in the normal state at least in the immediate neighborhood above the magnetic threshold value H_τ; i.e., the magnetic permeability $[\partial^2F/\partial B^2]^{-1}$ should depend on B for $B\gtrsim H_\tau$. But actually no such variations have so far been discovered.[2]—The analogy with the van der Waals equation, by which Wick apparently has been intrigued, is entirely misleading: There, in the gaseous state, the deviations from the ideal gas equation clearly indicate the proximity of a concave section of the free energy curve.—Also the fact that one can change continuously from the liquid into the gaseous state (by going round the critical point) has no analogy with the superconductor.

Thus I cannot see any ground for making use of such a general expression as (1) for the free energy, nor any reason for modifying the interpretation of superconductivity,[3] which gave the occasion to Wick's concept, but which in contrast to the latter implies *both* sides of the phenomenon, the diamagnetism as well as the superconductivity, and which moreover indicates a way of getting rid of the old difficulties.

F. LONDON

Institut Henri Poincaré,
Université de Paris,
September 23, 1937.

[1] G. C. Wick, Phys. Rev. **52**, 526 (1937).
[2] See e.g., K. Mendelssohn, Proc. Roy. Soc. **A155**, 558 (1936).
[3] F. London, Phys. Rev. **51**, 678 (1937); Physica **3**, 450 (1936).

Grain Orientation in Rolled Magnesium Alloys

The preferred orientation in rolled Mg and its alloys is usually of a simple type, in which the c axis is in the direction of the rolling plane normal. The scatter about this direction is less than 50°, and is slightly less in the cross rolling than in the rolling direction. This orientation has been reported by Schmid and Wasserman[1] and by Caglioti and Sachs.[2] Norton[3] gives a reproduction of an x-ray photogram of a specimen showing this type of orientation (Fig. 15*c*). He also gives such a reproduction for a markedly different specimen showing two fiber axes, lying about 15° to either side of the rolling plane normal in the rolling direction (Fig. 15*d*).

Experiments in this laboratory agree with the literature just cited in finding the simple type of orientation in nearly all rolling alloys independent of elements added, whether in large or small amounts (Al, Mn, O−4%), and independent of rolling treatment (hot or cold rolling at various percents reduction per pass). If a few tenths

percent of Ca is added to Mg, or to any of these alloys, however, the double orientation always shows up, irrespective of the type of treatment.

Two similar axes exist in rolled Zn also, as shown by Caglioti and Sachs,[2] and Fuller and Edmunds.[4] This is due to the reorientation by twinning which can take place when Zn is rolled. The close packed hexagonal structure of Mg, however, will not permit of twinning under the stresses present in rolling; that the structure has not changed in these alloys where Ca has been added was shown by back reflection photograms. The reported state diagrams of the Mg-Ca system[5, 6] show insoluble Mg_2Ca to be present, which would not change the lattice structure, in agreement with our results. Therefore, the double orientation in these alloys cannot be due to twinning.

It would seem, then, that the insoluble Mg_2Ca was in some way the cause of the observed effect, but any suggestion at this time as to the mechanism of the action would be pure speculation. It is hoped that further studies may shed light on the origin of the phenomenon.

I wish to thank Dr. J. D. Hanawalt, head of the X-Ray and Spectroscopy Laboratory, for his many suggestions, and the Dow Chemical Company for their permission to publish this letter.

JOHN C. MCDONALD

The Dow Chemical Company,
X-Ray and Spectroscopy Dept.,
Midland, Michigan,
September 20, 1937.

[1] E. Schmid and G. Wasserman, Metallwirtschaft **9**, 698 (1930).
[2] V. Caglioti and G. Sachs, Metallwirtschaft **11**, 1 (1932).
[3] Symposium on Radiography and X-Ray Diffraction (American Society for Testing Materials, Philadelphia, Pa., 1936) p. 321.
[4] M. L. Fuller and G. Edmunds, A. I. M. E., TP No. 524 (1934).
[5] J. L. Houghton, J. Inst. Met. **4**, 325 (1937).
[6] H. Vosskühler, Zeits. f. Metallkunde **3**, 29, 236 (1937).

Important Notice

THE American Institute of Physics will pay $2.00 per copy for each of the following issues of the *Physical Review:*

Volume 1, No. 6—June, 1913
Volume 2, No. 1—July, 1913
Volume 2, No. 2—August, 1913
Volume 2, No. 4—October, 1913
Volume 2, No. 5—November, 1913
Volume 7, No. 1—January, 1916
Volume 7, No. 2—February, 1916
Volume 7, No. 3—March, 1916
Volume 7, No. 4—April, 1916
Volume 7, No. 5—May, 1916
Volume 9, No. 2—February, 1917

Copies should be in good condition. They should be addressed to the Publications Manager, American Institute of Physics, 175 Fifth Avenue, New York, New York, with the name and address of sender and with a covering letter.